新 制
農
357
京大附図

APPLICATION OF IMMOBILIZED ENZYMES TO CLINICAL ANALYSIS AND FOOD MANUFACTURE USING CHROMATOGRAPHIC OPERATIONS

SHUJI ADACHI

1 9 8 2

APPLICATION OF IMMOBILIZED ENZYMES TO CLINICAL ANALYSIS AND FOOD MANUFACTURE USING CHROMATOGRAPHIC OPERATIONS

Contents

INTRODUCTION

From the standpoints of clinical analysis and food manufacture, enzymes have many properties which make them ideal catalysts. They can operate under extremely mild conditions of pH and temperature, can generally induce fast reaction rates, and are extremely specific in the types of reaction in which they are involved. This specificity gives them the capability of catalyzing many reactions not possible with ordinary chemical catalyst. In spite of this potential, enzymes have been used relatively little as commercial catalysts because of the serious drawbacks of high cost, instability, and the difficulty of separating the enzymes from the reaction products.

The immobilization of enzymes to artificial matrices, which was first tried by Grubhofer and Schleich,[1] offers exciting possibilities for the solution of problems of instability and high cost. Within the last twenty years, a new technology based on enzyme immobilization has rapidly emerged and has been developed to the points where immobilized enzyme processes are now in commercial operation for the resolution of amino acids,[2] the production of L-aspartic acid,[3] and the isomerization of glucose to fructose.[4,5]

A wide variety of enzymes have been immobilized, and the resulting enzyme adducts demonstrate some distinct advantages over their soluble counterparts. The first advantage is that the enzymes immobilized to matrices can be easily separated from the reaction

product. The ease of separation allows continued reuse, thus providing an economic advantage. The second is that immobilized enzyme processes can be in continuous operation. The continuity of processes can reduce the operating costs, especially personal expenditures. Another advantage which often, but not always, results from attachment of enzymes to solid surface is increased stability.

The modes in which enzymes are attached to solid matrices can be conveniently grouped into three categories;[6] adsorption of enzymes at solid interfaces, inclusion of enzymes in gel matrices, and covalent linkage of enzymes to solid surfaces. The reactions with immobilized enzymes, even if by any mode of attachment, are heterogeneous. Therefore, the reactions catalyzed by immobilized enzymes may be affected by the diffusion of substrates, the environment in gel matrices, and so on. In Part I, the factors affecting immobilized enzyme kinetics are investigated. The diffusion coefficients of saccharides and amino acids in dextran and acrylamide gels are measured in Chapter 1. Chapter 2 deals with the unsteady state effectiveness factor in a batch reactor including immobilized-enzyme particles. A few reports[7,8] have been published on the methods for estimating the kinetic parameters of the reaction catalyzed by an immobilized enzyme. It has been assumed in the reports that the gel-phase diffusivity of substrate is obvious. However, it is not explicitly found in many cases. Two methods for estimating diffusivity of substrate and kinetic parameters of

Michaelis-Menten equation simply and simultanuously are proposed in Chapter 3. There are some reports[9,10] that describe the effects of environment in gel matrices on immobilized-enzyme reactions. However, verly little is known about the effects of gel constituents on enzyme reactions. It is studied in Chapter 4 how the constituents of dextran gels, which are extensively used as supports for enzyme immobilization, influence on an enzyme-catalyed reaction. Immobilization of enzymes by ionic linkage offers an advantage of extreme simplicity. Adsorbed enzymes, however, do suffer the problem of desorption. In Chapter 5, stability of the enzyme immobilized by ionic linkage is mentioned.

The specificity of enzymes, and their ability to catalyze reactions of substrate at low concentrations, make them attractive as analytical reagents. Enzyme-catalyzed reactions have been used for analytical purposes for some time for the determination of substrates, activators, inhibitors, and enzymes. The use of immobilized enzymes for analytical purposes can increase the speed, ease, and reproducibility of assays utilizing enzymes. The enzyme electrodes[11] and enzyme thermistors[12] have been devised as the analytical tools including immobilized enzymes. Another type of the analytical technique utilizing immobilized enzymes is proposed in Part II. It is a pulse response technique using immobilized enzyme column. Chapter 6, 7, and 8 deal with the determination of substrates by the technique. The components in human serum are ana-

lyzed by the technique in Chapter 8. In Chapter 9, the technique is applied to determination of an enzyme in serum.

One industrially used enzyme is glucose isomerase which isomerizes glucose to fructose. Through the use of this enzyme the less sweet and cheaper glucose can be isomerized to obtain a sweeter mixture, a common type of fructose syrup, containing on dry basis about 50% glucose and 50% fructose. The fructose syrup can be used in place of sucrose in certain foods and beverages. Production of syrup with higher fructose content is desirable because of its sweetness and solubility at low temperature. Part III deals with the production of higher fructose syrup. Chromatographic separation of glucose and fructose from their mixture is a normally used technique, by which higher fructose syrup can be produced. The technique is described in Chapter 10. The more effective sepration is accomplished by using a simulated moving-bed adsorber and it is mentioned in Chapter 11. A new system for producing the higher fructose syrup is proposed in Chapter 12. The system consists of adsorption process and immobilized-enzyme reaction. In Chapter 13, the three processes for producing the higher fructose syrup, which are mentioned in Chapters 10, 11, and 12, are apprais-ed on the standpoint of the amount of desorbent used in the processes.

Literature Cited

1) N. Grubhöfer and L. Schleith, *Naturwissenshaften*, 40, 508 (1953).

2) I. Chibata, T. Tosa, T. Sato, T. Mori, and Y. Matsuo, *Proceedings of IVth International Fermentation Symposium: Fermentation Technology Today*, p.383, Society of Fermentation Technology, Japan, 1972.

3) T. Tosa, T. Sato, T. Mori, and I. Chibata, *Appl. Microbiol.*, 27, 886 (1974).

4) U.S. Patent, 3788945 (1974).

5) Japanese Patent, 51-20576 (1976).

6) R. D. Falb, *Biotechnol. Bioeng. Symp.*, No.3, 177 (1972).

7) P. S. Banting and K. J. Laidler, *Biochemistry*, 11, 4477 (1972).

8) T. Kobayashi and K. J. Laidler, *Biochim. Biophys. Acta*, 302, 1 (1973).

9) L. Goldstein, Y. Levin, and E. Katchlski, *Biochemistry*, 3, 1913 (1964).

10) C. W. Wharton, E. M. Crook, and K. Brocklehurst, *Eur. J. Biochem.*, 6, 572 (1968).

11) S. J. Updike and G. P. Hicks, *Nature*, 214, 986 (1966).

12) B. Danielsson, K. Gadd, B. Mattiasson, and K. Mosbach, *Anal. Lett.*, 9, 987 (1976).

PART I

FACTORS AFFECTING IMMOBILIZED-ENZYME KINETICS

PART I

FACTORS AFFECTING IMMOBILIZED-ENZYME KINETICS

Introduction

Practical application of enzymatic catalysis often requires that enzymes are immobilized, thereby permitting recovery and continuous use. Since enzymes are immobilized to water-insoluble matrices, the reactions catalyzed by immobilized enzymes are heterogeneous. It is important that the kinetics of immobilized enzymes are well understood to facilitate their utilization. In particular, it is necessary to acount for the effects of diffusional limitations and environment in gel matrices and to develop procedures which permit extraction of intrinsic kinetic parameters from observed reaction rates.[1,2] In other words, the kinetics of immobilized enzymes may be affected by such factors. The development of an immobilized-enzyme system also requires a thorough understanding of engineering parameters such as, activation energy, pH profile, and operational half-life of the immobilized enzyme. This part deals mainly with factors affecting the kinetics of immobilized enzymes and engineering parameters.

In Chapter 1, diffusion coefficients of low molecules in dextran and acrylamide gels, which are widely used as carriers for immobilizing enzymes, are measured. The unsteady state effectiveness factor in an isothermal batch reactor including immobilized-enzyme

particles is discussed in Chapter 2. Two procedures for estimating the diffusion coefficient of substrate and extracting intrinsic kinetic parameters from observed reaction rates are proposed in Chapter 3. Chapter 4 deals with the effects of gel constituents on an enzyme-catalyzed reaction and with kinetic properties of enzyme immobilized by ionic linkage. Operational stability of immobilized enzyme by ionic linkage is discussed in Chapter 5.

Literature Cited

1) I. Chibata,"*Immobilized Enzymes*," Chapters 3 and 5, Kodansha, Tokyo, 1975.

2) R. D. Falb, *Biotechnol. Bioeng. Symp.*, No.3, 177 (1972).

Chapter 1

Diffusion Coefficients of Low Molecules in Gels

1. 1. Introduction

In recent years cross-linked polymers such as dextran gels and acrylamide gels have been extensively utilized as support for immobilized enzymes and in gel chromatography. The reaction rate of an immobilized enzyme is frequently found restricted by the diffusional velocity of substrates within particles.[1] Similarly, the column efficiency in gel chromatography is appreciably influenced by the gel phase diffusion.[2,3] Information on diffusion coefficient in gels is therefore very important.

Diffusivity in gels is considered to be lower than that in solution because of the interaction between diffusing substances and gel components and of the steric hindrance. However, only a few works have been reported on diffusion in gels in comparison with those on gaseous diffusion in solid catalysts.[4] Nelson[5] compared the diffusion coefficient in an ion-exchange resin with that in a model electrolyte solution. Horowitz and Fenichel[6] measured diffusion coefficients of molecules of a molecular weight less than 100 in a dextran gel (Sephadex G-34). They pointed out that the ratio of the diffusion coefficient in the gel to that in aqueous solution was in the 0.6 ~ 0.7 range regardless of the size, chemical grouping and temperature of solutes. Ackers and Steere[7]

studied diffusion of proteins through agar-gel membranes and explained the decrease of the diffusion coefficients by a theoretical equation of Renkin.[8]

In regard to diffusion of amino acids and saccharides in polymer solutions such as dextran and its derivatives, Namikawa *et al.*[9] reported their observation that the diffusion coefficient decreased with the increase in polymer concentration. The lowering degree of the diffusion coefficient could be well explained by a model in which a direct interaction (hydrogen bond) between diffusing substances and polymer was taken into consideration.

In the present study, we measured the diffusional velocity of relatively low molecular weight substances such as saccharides and amino acids in dextran gels, acrylamide gels and photo-crosslinkable resins[10,11] of different gel concentrations or various degrees of crosslinkage. For this purpose, spherical beads of dextran gels and acrylamide gels or a plane sheet of the photo-crosslinkable resins were prepared. Comparison of the diffusion coefficients in the gels with those in the polymer solutions indicated that diffusion in gels was restricted not only by the interaction between gel components and diffusing substances but also by the steric hindrance. An attempt was made to correlate the decrease of diffusion coefficients in gels with the diffusion coefficients in polymer solutions and the distribution coefficient which represents the partition of solutes between the gel phase and the space outside the gel particle.

1. 2. Materials and Methods

Materials. All chemicals used in this study were of analytical grade. Dextran T-40 (mol. wt. 4×10^4) was purchased from Pharmacia Fine Chemicals. Acrylamide, N,N'-methylenebisacrylamide (BIS), N,N,N',N'-tetramethylethylenediamine (TEMED), ammonium persulfate, epichlorohydrin, D-glucose, maltose, glycine, L-β-alanine, L-valine and L-arginine were obtained from Wako Pure Chemical Industries, maltotriose from Hayashibara Biochemical Inc., glucoamylase (pure grade) from Seikagaku Kogyo Co., and Sorbitan sesqioleate from Tokyo Kasei Co.

Preparation of dextran gel beads. Dextran gel beads were prepared by a modification of the pearl polymerization method.[12] Ten grams of dextran was suspended in 4 ml of distilled water and dissolved by adding 6 ml of 5 mol/l sodium hydroxide solution, and the solution was allowed to stand overnight in a vacuum to eliminate air bubbles. To this alkaline dextran solution, 1 - 6 ml of epichlorohydrin was added in order to vary the degree of crosslinkage of the gel. The mixture became viscous after 10 - 20 min of slow stirring at 40°C with a glass stick. At this stage, this solution was immediately poured into liquid parafin which had been incubated at 50°C in a 250 ml beaker under vigorous stirring, accomplished with an agitator.

The polymerization reaction was allowed to proceed for 20 hr at 50°C. The gel produced was washed with *n*-hexane and acetone, and

then with water till it became neutral. The shape of the gel was found to be quite spherical by photographic observation, and the water regain was in the range of 3.8 - 24.0 g/g-dry gel. The gel beads having a diameter of 2 - 4 mm were used in the experiment.

Preparation of acrylamide gel beads. Acrylamide monomer and a cross-linking agent, BIS, were dissolved in distilled water to the prescribed concentration. The final volume was adjusted to 5 ml. To this solution was added a catalyst system consisting of 1 ml of ammonium persulfate (5%) and 0.1 ml of TEMED. The final concentration of the total monomer (acrylamide plus BIS) was varied from 10 to 40%(w/v), with the BIS content, in terms of percentage (w/w) of the total amount of monomer, kept at 9.1%. The BIS content was varied from 5 to 25% at a fixed total monomer concentration of 22%.

This mixture was poured with an injector into a measuring cylinder containing 600 ml of an organic phase (toluene-chloroform; 435/165) and 0.5 ml of an emulsion stabilizing agent, Sorbitan sesquioleate. During polymerization, the organic phase was kept under nitrogen atmosphere at room temperature. The polymerization was completed before the bead reached the bottom of the cylinder. The gel bead was washed with toluene to remove chloroform and then with a large amount of distilled water.

Preparation of photo-crosslinkable resins. A 1-mm thick plane

sheet of photo-crosslinkable resins was prepared by the same method as previously reported,[10,11] and a piece of the original sheet of 3 X 4 cm was used in the experiment. The photo-crosslinkable resin named ENT 1000[11] is basically composed of polyethylene glycol.

Measurement of diffusion coefficient. Diffusion coefficients in dextran or acrylamide gels were measured by a method similar to that by Horowitz and Fenichel.[6] A single swollen gel bead was transferred to an excess of the sample solution at the prescribed concentration (glucose 1 mol/l, maltose 0.5 mol/l, maltotriose 0.33 mol/l, glycine 1.4 mol/l, L-β-alanine 1.0 mol/l, L-valine 0.3 mol/l, L-arginine 0.5 mol/l), and allowed to be equilibrated for 24 hr at room temperature under shaking.

Then, the bead was removed from the solution, blotted with a piece of filter paper to eliminate excess liquid on the surface, and put in a holder made of stailess steel wire. This holder was immersed successively at appropriate time intervals (1 - 10 min) in a test tube (I.D. 22 mm), in which 5 ml of distilled water or 1.0 mol/l acetate buffer (pH 4.5) in case of L-arginine as a diffusing substance had been pipetted beforehand. Mixting of solution in the tube was accomplished with a magnetically rotated bar at the bottom. The temperature was controlled at 25 $\pm$ 0.1°C.

In most runs, eight tubes were used. Each transfer was accomplished in 3 - 5 seconds, and this loss of time could be ignored compared with the experimental time. The bead was allowed to re-

main in the final test tube for 2 - 6 hr to recover all remaining solute. The concentration of glucose in a wash-out solution in each tube was determined by the glucose oxidase method,[13] and that of amino acids by the ninhydrin reaction. Maltose and maltotriose were completely hydrolyzed into glucose with glucoamylase, and the amount of glucose produced was determined by the above descrived method.

To photo-crosslinkable resins was applied the following method. A swollen resin sheet equilibrated with a diffusing substance (glucose) was put into a beaker filled with 150 ml of distilled water which was kept well stirred with a magnetically rotated bar. At appropriate time intervals, 0.5 ml of the sample solution was taken, and the concentration of glucose was determined by the glucose oxidase method.

Analysis of the experimental data. In case of dextran and acrylamide gels, the relative average concentration of solute in the bead at any time, $C_g(t_j)/C_0$ is given by

$$C_g(t_j)/C_0 = \sum_{i=j+1}^{N} C_s(t_i) / \sum_{i=1}^{N} C_s(t_i) \qquad (1\text{-}1)$$

where C_0 represents the initial concentration of solute in the bead, $C_s(t_i)$ the concentration of each wash-out solution, N the total number of test tubes and t the time. In the experiment with the photo-crosslinkable resin, $C_g(t_j)/C_0$ was calculated from the

concentration of the sample solution as $C_g(t_j)/C_0 = 1 - C_s(t_j)/C_e$, where $C_s(t_j)$ represents the concentration of the sample solution at time t_j and C_e the concentration of the sample solution after all the solute in the resin sheet has been eluted.

The relations of $C_g(t_j)/C_0$ with the time for a spherical bead and a plane sheet are easily derived by Eqs. (1-2) and (1-3),[14] respectively, on the basis of the assumptions: (1) the concentration of solute in a bulk solution outside a bead is negligibly low and (2) the dependency of diffusion coefficient on the concentration is negligible.

$$C_g(t_j)/C_0 = (6/\pi^2) \sum_{n=1}^{N} (1/n^2) \exp(-D_e n^2 \pi^2 t_j / r^2)$$

for spherical bead (1-2)

$$C_g(t_j)/C_0 = (8/\pi^2) \sum_{n=1}^{N} (1/n^2) \exp(-D_e n^2 \pi^2 t_j / l^2)$$

for plane sheet (1-3)

where D_e is the diffusion coefficient in the gel, r the radius of a bead and l the half thickness of a sheet. The diffusion coefficient was so determined as to achieve the maximum consistency between the experimental data and the calculated results by Eq. (1-2) or (1-3). In most experimental runs, $C_g(t_j)/C_0$ was in the range of 0.2 to 1.0. The radius of a bead and the thickness of a sheet were measured with a profile projector (Nippon Kogaku K.K. Model 8C).

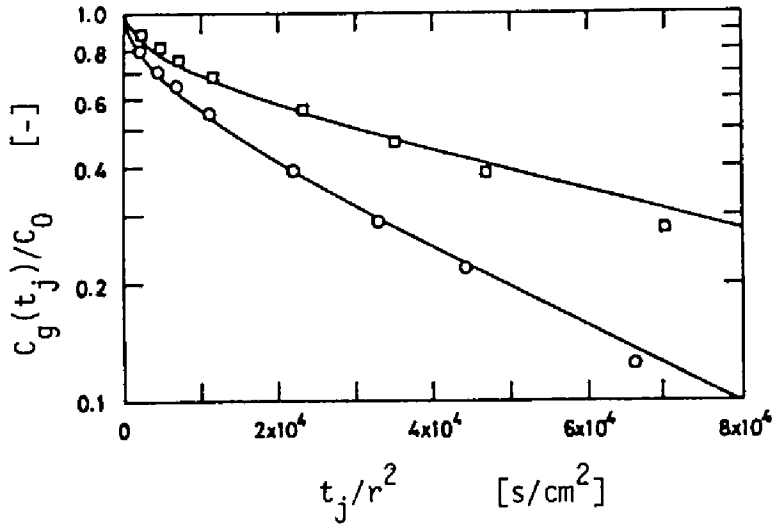

Fig. 1-1. Theoretical and experimental relations between $C_g(t_j)/C_0$ and t_j/r^2 for dextran gels. Diffusing substances; ○, glucose; □, maltotriose. The gel concentration was evaluated at 20.6%(w/v). The solid curves show the calculated results by Eq.(1-2), with 0.23×10^{-5} and 0.10×10^{-5} cm^2/s used as D_e for glucose and maltotriose, respectively.

Figure 1-1 shows a comparison between the experimental and calculated results obtained for a dextran gel, in which $C_g(t_j)/C_0$ was plotted against t_j/r^2. A fairly good agreement was observed between them. Thus, a reasonable diffusion coefficient might be obtained by the method described above.

Distribution coefficient. For evaluation of distibution coefficients of the solutes for dextran gels, the correlation derived by Ogston[15] was available. He proposed the following formula:

$$K = \exp[-\pi L(r_s + r_r)^2] \qquad (1\text{-}4)$$

where L is the concentration of rods (dextran molecules), expressed in cm rod/cm^3, r_s the equivalent radius of a solute molecule and r_r the radius of the rod. Laurent and Killander[16] experimentally determined r_r to be 7 A. They also gave the relationship between L and dextran concentration; *i.e.*, in a dextran gel L had a value of 4 X 10^{12} cm/cm^3 for the concentration of 0.1 g/ml. The values of r_s were estimated from the diffusion coefficient in a dilute solution (D) by Stoke's law[8] or the radius of a sphere of

Table 1-1 Estimated Molecular Dimensions

Substances	D at 25°C [cm^2/s X 10^5]	Molecular radius [A]
Glucose	0.68[17]	3.6
Maltose	0.50[18]	4.9
Maltotriose	0.43[a]	6.4
Glycine	1.06[19]	2.3
L-β-Alanine	0.93[19]	2.6
L-Valine	-	3.4[b]
L-Arginine	0.52[c]	4.1

a) The value for raffinose was used.[19]

b) The radius of a sphere of equal weight and density was calculated.[8] As the value of ρ, 1.23 was used.[19]

c) Measured for 0.5 mol/l L-arginine in 1.0 mol/l acetate buffer pH 4.5.[9]

equal weight and density (ρ) as shown in Table I.

The distribution coefficients of saccharides for acrylamide gels and photo-crosslinkable resines were determined experimentally, since no theory for these gels has yet been established. A single gel bead or sheet was equilibrated in the saccharide solutions of the same concentration as used in the diffusion experiment. Then, the gel was removed from the solution, blotted to eliminate excess liquid on the surface and placed in a test tube until all the solute was eluted. The test tube was filled with 25 ml of distilled water. The distribution coefficient was calculated by equation $K = 25 \cdot C_e/(C_0 V_g)$, where C_0 represents the initial concentration of the saccharide solution, C_e the final concentration of a solution in the test tube and V_g the volume of a gel bead or a sheet.

Gel concentration. Since the cross-linked polymers used in this study swelled in water or some aqueous solutions, the gel concentration was calculated on the basis of the water regain and the partial specific volume of the gel component, *i.e.*, 0.61 for dextran gels,[20] 0.89 for acrylamide gels[21] and 0.91 for the photo-crosslinkable resin (polyethylene glycol).[21]

Diffusion coefficient in solution (D_0). Diffusion coefficients of maltotriose, glycine, L-β-alanine, L-valine, L-arginine in the absence of gel matrix were determined by the height area

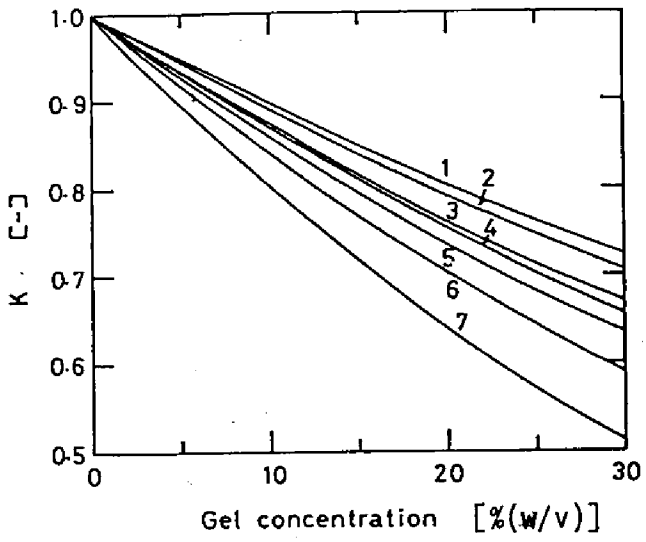

Fig. 1-2. Theoretical relations between K and gel concentrations for various saccharides and amino acids in dextran gels. The solid curves represent the calculated results by Eq. (1-4). See the text for details. Curve 1, glycine; curve 2, L-β-alanine; curve 3, L-valine; curve 4, glucose; curve 5, L-arginine; curve 6, moltose; curve 7, maltotriose.

method with the Schlieren optical apparatus.[9] The values for glucose and maltose were cited from the literature.[17,18]

1. 3. Results

Distribution coefficient. Figure 1-2 shows a plot of the calculated values of the distribution coefficients of saccharides and amino acids *versus* gel concentrations for dextran gels. Figure 1-3a shows a plot of the experimental data of the distribution coefficients of saccharides *versus* gel concentrations for acrylamide

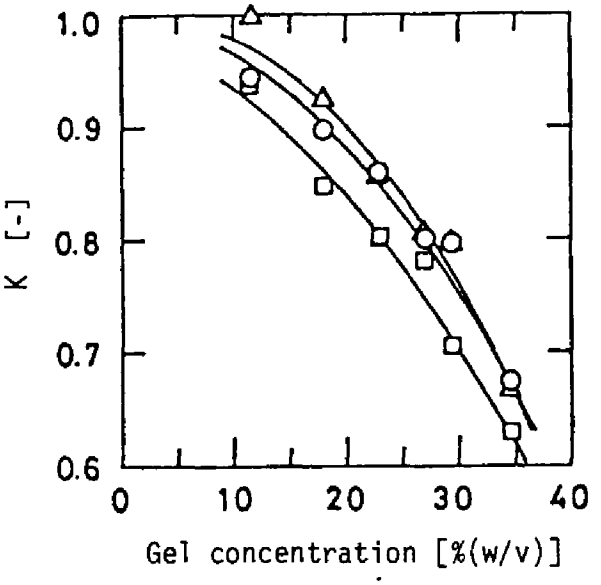

Fig. 1-3a. Experimental relations between K and gel concentrations for various saccharides in acrylamide gels. ○, glucose; △, maltose; □, maltotriose. BIS content was fixed at 9.1%.

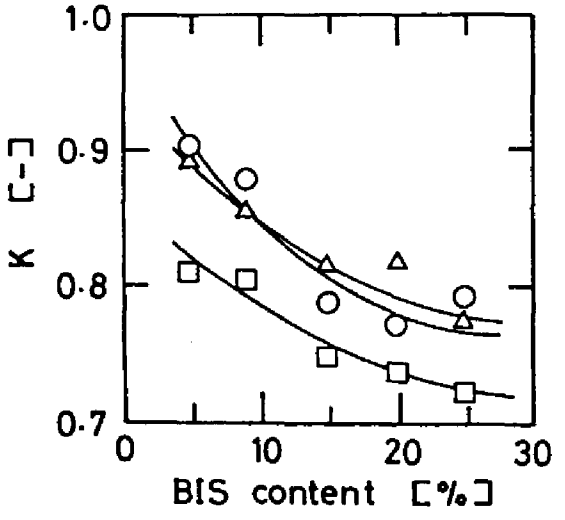

Fig. 1-3b. Relations between K and BIS content for various saccharides in acrylamide gels. Total monomer concentration was fixed at 22%. The symbols are shown in Fig. 1-3a.

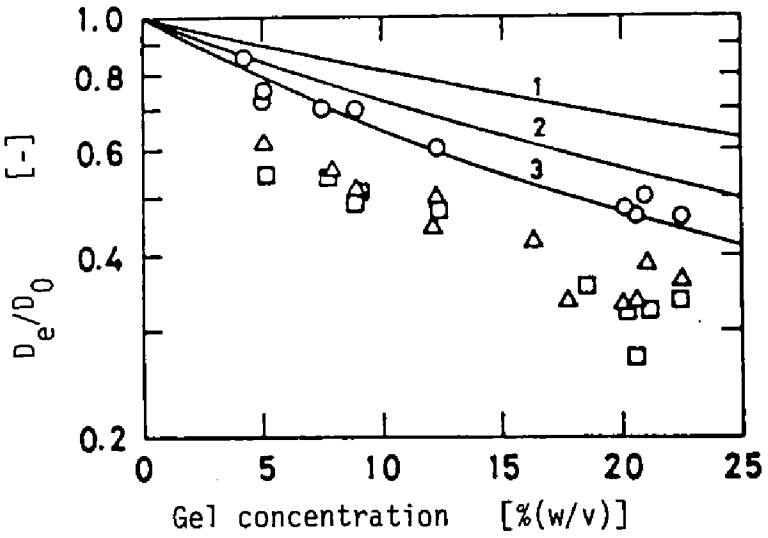

Fig. 1-4a. Diffusion coefficients of various saccharides in dextran gels and in dextran solutions. The symbols show the experimental data of D_e/D_0. The solid curves represent the theoretical results of D_p/D_0. ○ and curve 1, glucose; △ and curve 2, maltose, □ and curve 3, maltotriose. As the values of D_0, 0.5 X 10^{-5}, 0.45 X 10^{-5} and 0.37 X 10^{-5} cm^2/s were employed for glucose,[17] maltose[18] and maltotriose, respectively.

gels at a constant BIS content (9.1%). In Fig. 1-3b, K is plotted against BIS content at a constant monomer concentration (22%).

Diffusion coefficient of saccharides and amino acids in dextran gels. The observed values of relative diffusion coefficients D_e/D_0 of saccharides and amino acids in dextran gels against gel concentrations are shown in Figs. 1-4a and 1-4b, respectively. On the diffusion of saccharides and amino acids in dextran solution, Namikawa *et al.*[9] pointed out that the decrease of diffusion coef-

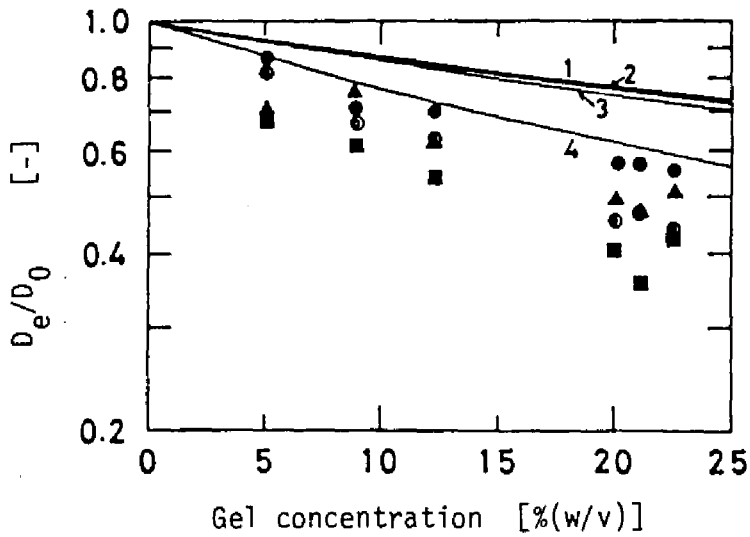

Fig. 1-4b. Diffusion coefficients of various amino acids in dextran gels and in dextran solutions. The symbols show the experimental data of D_e/D_0. The solid curves represent the theoretical results of D_p/D_0. ● and curve 1, glycine; ◎ and curve 2, L-β-alanine; ▲ and curve 3, L-valine; ■ and curve 4, L-arginine. As the values of D_0, 0.79×10^{-5}, 0.80×10^{-5}, 0.71×10^{-5} and 0.52×10^{-5} cm^2/s were used for glycine, L-β-alanine, L-valine and L-arginine, respectively.[9)]

ficient was ascribable to a direct interaction (hydrogen bond) between diffusing substances and dextran molecules. The solid curves in Figs. 1-4a and 1-4b represent the theoretical results of the ratio of diffusion coefficient in dextran solution D_p to D_0, which were in good agreement with the experimental ones.

As seen in Figs. 1-4a and 1-4b, D_e/D_0 was appreciably lower than D_p/D_0 and the degree of the lowering depended on both the gel con-

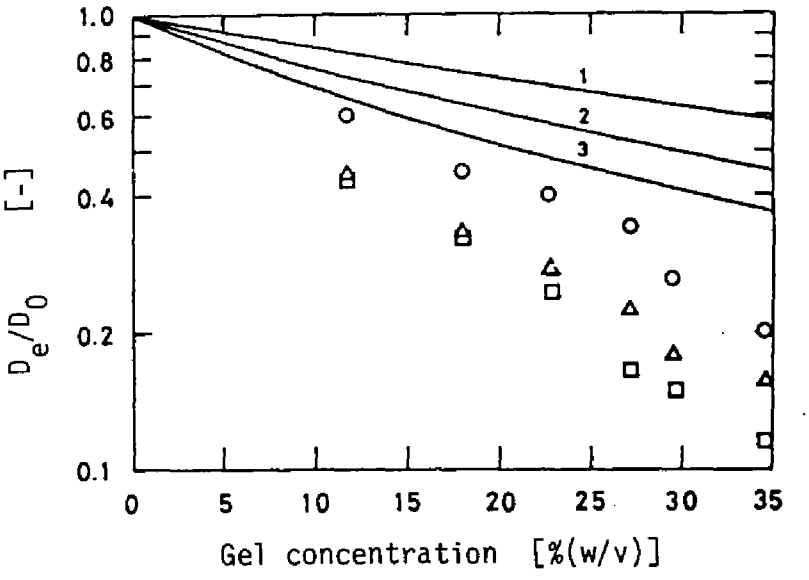

Fig. 1-5a. Diffusion coefficients of various saccharides in acrylamide gels and in polyacrylamide solutions. The symbols show the experimental data of D_e/D_0. BIS content was kept at 9.1%. The solid curves represent the theoretical results of D_p/D_0. See the Appendix for details. Curve 1, glucose; curve 2, maltose; curve 3, maltotriose. The symbols are the same as shown in Fig. 1-4a.

centration and the size of diffusing substances. This implies that diffusion in gels is restricted not only by the interaction between diffusing substances and the gel component (dextran) but also by the steric hindrance of gel matrix.

Diffusion coefficient of saccharides in acrylamide gels. The diffusion coefficients of saccharides in acrylamide gels are shown in Figs. 1-5a and 1-5b. Figure 1-5a shows a plot of D_e/D_0 *versus*

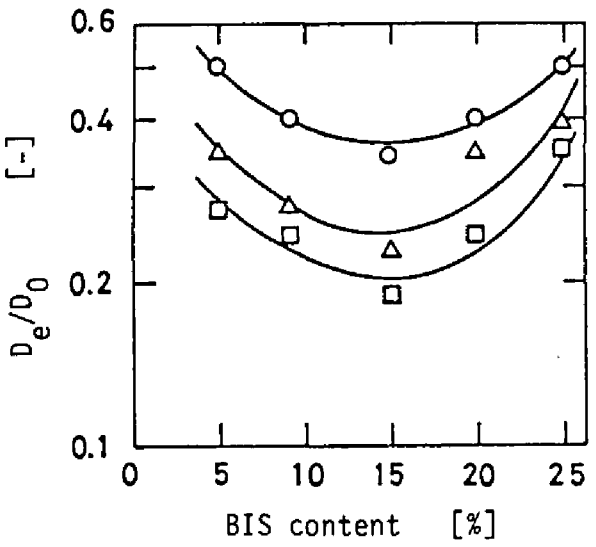

Fig. 1-5b. Effect of BIS content on D_e/D_0 for various saccharides in acrylamide gels. Total monomer concentration was kept at 22%. The symbols are the same as shown in Figs. 1-4a and 1-5a.

gel concentrations at a constant BIS content (9.1%), in which the theoretical results of D_p/D_0 in acrylamide polymer solution are also drawn in solid lines. Details of the calculation are described in the Appendix. The values of D_e/D_0 in acrylamide gels were much lower than D_p/D_0 in the same way as observed in dextran gels.

In Fig. 1-5b, D_e/D_0 is plotted against BIS content at a total monomer concentration of 22%. The minimum D_e/D_0 was observed at a BIS content of about 15%. This striking and unexpected feature of the permeability of acrylamide gels was also founded in the studies so far reported. Hjertén *et al.*[22] observed a marked increase in gel permeability for proteins at a higher BIS content

above 15%. Degani and Miron[23] also observed in the sdudy of acrylamide-entrapped cholinesterase that the entrapping efficiency strongly depended on BIS content and reached its maximum at 5%.

Diffusion coefficient of glucose in photo-crosslinkable resins.

The diffusion coefficient of glucose was also measured in the photo-crosslinkable resins to be compared with that in dextran and acrylamide gels. As shown in Table 1-2, the values of D_e/D_0 were larger than those for dextran and acrylamide gels at the same gel concentrations. On the other hand, the distribution coefficients of glucose were much smaller than those for dextran and acrylamide gels, and were nearly equal to D_e/D_0. This might mean that the diffusion in the photo-crosslinkable resin was restricted only by

Table 1-2 Diffusion Coefficient and Distribution Coefficient of Glucose in a Photo-Crosslinkable Resin.

Gel concentration [%(w/v)]	19.7		27.4	
	D_e/D_0	K	D_e/D_0	K
Photo-crosslinkable resin (ENT 1000)	0.62	0.54	0.40	0.35
Dextran gel[a)]	0.48	0.76	0.40	0.68
Acrylamide gel[a)]	0.44	0.89	0.33	0.80

a) The values of D_e/D_0 and K for dextran and acrylamide gels were estimated by interpolating or extrapolating the experimental data shown in Figs. 1-2, 1-3a, 1-4a, and 1-5a.

the steric hindrance of gel matrix and that the interaction between glucose and the resin was negligible. As a matter of fact, the possibility of hydrogen bond formation with polyethylene glycol is considered to be very small,[9,24] since it contains only ether-like oxygen.

1. 4. Discussion

Various models[4,25] have been proposed for establishment of relations between the diffusion coefficient in porous matrix such as ion-exchange resins[25] and solid catalysts[4] and that in the absence of such matrix. In most of the previous approaches,[4] the ratio D_e/D_0 was expressed as a function of a void fraction in porous materials ε and tortuosity factor τ which accounts for both tortuosity and varying pore cross section, *i.e.*, $D_e/D_0 = \varepsilon/\tau$. In these treatments, however, neither the interaction between solutes and pore wall (gel component) nor the effect of solute size was taken into consideration.

The experimental results obtained in the present study showed that diffusion in gels might be restricted not only by the interaction between solute and gel component but also by the steric hindrance of gel matrix. Thus, D_e should be expressed as $D_e = D_p(K/\tau)$. K was employed in place of ε to account for the effect of the size of diffusing substances. In Fig. 1-6, D_e measured in dextran gels are plotted against KD_p in a log-log coordinate. As seen in

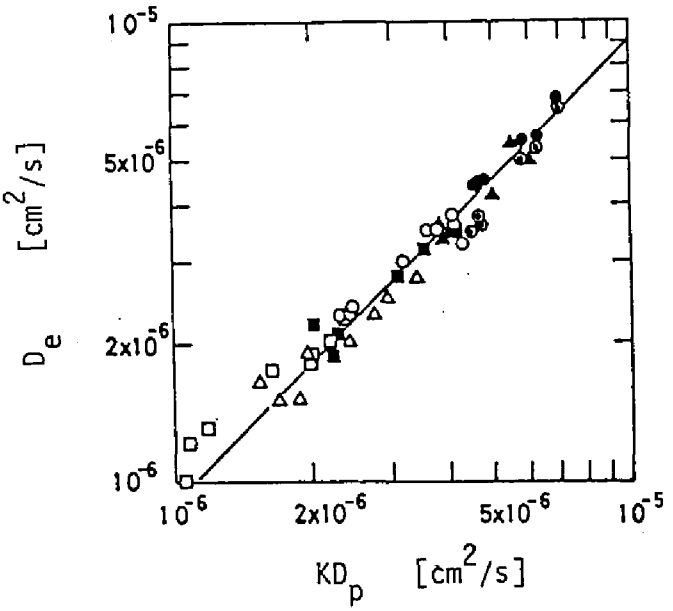

Fig. 1-6. Experimental relations between D_e and KD_p for various saccharides and amino acids in dextran gels. The solid line shows $D_e = D_p(K/\tau)$, in which τ is specific as 1.1. Diffusing substances; ○, glucose; △, maltose; □, maltotriose; ●, glycine; ◎, L-β-alanine; ▲, L-valine; ■, L-arginine.

the figure, the plot of D_e *versus* KD_p gave a straight line with a slope of unity and τ was evaluated as 1.1.

Figure 1-7 shows a plot of D_e *versus* KD_p for acrylamide gels. The experimental data gave a nearly straight line, but the slope was higher than unity. This means that diffusion coefficient in acrylamide gels cannot be correlated with $D_e = D_p(K/\tau)$, probably owing to the heterogeneous structure of acrylamide gels. According to recent studies with a scanning electron microscope,[26,27] acrylamide gels have a cellular structure, that is, the gel is composed

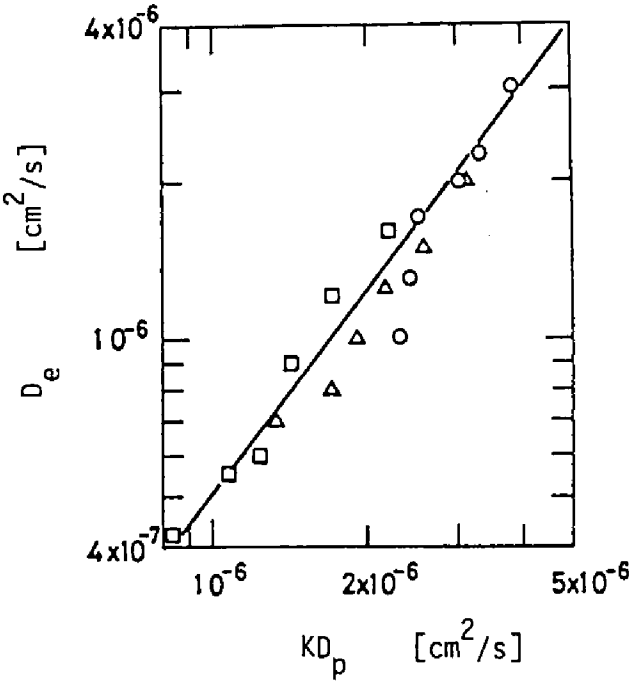

Fig. 1-7. Experimental relations between D_e and KD_p for various saccharides in acrylamide gels. The experimental data shown in Fig. 1-5a were employed. The solid line had a slope larger than unity, and the application of $D_e = D_p(K/\tau)$ to the experimental data failed. See the text for details. Diffusing substances; ○, glucose; △, maltose; □, maltotriose.

of a closed space (a small cell) with a diameter of a few microns and a cell wall, and is extremely different from a homogeneous structure presumed for dextran gels. In such a heterogeneous structure of the acrylamide gel, the structure of the cell wall may be strongly responsible for the overall permeability. The distribution coefficient in the wall may be much smaller than the observed value. Similarly, an unusual dependency of D_e on BIS

content shown in Fig. 1-5b might be explained by the change of the cell wall structure with BIS content.[27] On the other hand, in the photo-crosslinkable resine, D_e/D_0 was nearly equal to K as described previously.

The findings obtained above presented the following information on the permeability of cross-linked polymers: The diffusional velocity in the gel was restricted not only by the interaction between diffusing substances and gel components but also by the steric hindrance of gel matrix. The photo-crosslinkable resin showed the highest permeability, where the interaction between the diffusing substance and the resin component was considered negligible. The diffusion coefficients in dextran gels were well correlated with $D_e=D_p(K/\tau)$, in which both the interaction and the obstruction by the gel matrix were considered. However, with acrylamide gels, an attempt to correlate the experimental data with $D_e = D_p(K/\tau)$ failed. It was pointed out as the reason for this failure that the structure of the acrylamide gels was heterogeneous and different from that of dextran gels. Further studies on the structure of pore matrix must lead to a better understanding on the permeability in gels.

1. 5. Summary

Diffusion coefficients of saccharides and amino acids were measured in cross-linked polymers such as dextran gels, acrylamide gels

and photo-crosslinkable resins of different gel concentrations or various degrees of crosslinkage. Comparison of diffusion coefficients in gels with those in polymer solutions indicated that the diffusional velocity in gels was restricted not only by the interaction between diffusing substances and gel components but also by the steric hindrance of gel matrix. The diffusion coefficients in dextran gels and acrylamide gels were appreciably lower than those in polymer solutions, and the degree of lowering depended on both the gel concentration and the size of diffusing substances. The photo-crosslinkable resins basically composed of polyethylene glycol showed a higher permeability than dextran and acrylamide gels on account of a weak interaction between diffusing substances and resin component. Furthermore, an attempt was made to correlate the decrease of diffusion coefficients in gels with the diffusion coefficients in polymer solutions and the distribution coefficient of the diffusing substances.

Appendix

Since the acrylamide gel has two atoms per one monomer molecule which can form hydrogen bond, a model proposed by Namikawa *et al.*[9] might be applied to the evaluation of D_p/D_0. Thus, D_p/D_0 is expressed as

$$D_p/D_0 = \frac{1}{2}\left[1 + \frac{K_H - nC_{dt} + nC_{At}}{(B^2 + 4nC_{At}K_H)^{1/2}}\right] \tag{1-5}$$

where

$$B = K_H + n(C_{dt} - C_{At}) \qquad (1\text{-}6)$$

In these equations, C_{dt} represents the polymer concentration based on monomer unit, C_{At} the concentration of a diffusing substance, K_H the dissociation constant of hydrogen bonding (= 29 mol/l)[9] and n the number of atoms which can form hydrogen bond in the diffusing substance.

Nomenclature

C_e	final concentration of a solution in the test tube	[mol/l]
C_g	average concentration of solute in the bead	[mol/l]
C_s	concentration of wash-out solution	[mol/l]
C_0	initial concentration of solute in the bead	[mol/l]
D_e	diffusion coefficient in the gel	[cm^2/s]
D_p	diffusion coefficient in polymer solution	[cm^2/s]
D_0	diffusion coefficient in solution	[cm^2/s]
K	distribution coefficient	[-]
L	concentration of rods	[cm rod/cm^3]
l	half thickness of a sheet	[cm]
N	total number of test tube	[-]
r	radius of a bead	[cm]
r_r	radius of the rod	[cm]
r_s	equivalent radius of a solute molecule	[cm]

t	time	[s]
V_g	volume of a gel or a sheet	[cm^3]
ϵ	void fraction in porous materials	[-]
ρ	density	[g/cm^3]
τ	tortuosity factor	[-]

Literature Cited

1) I. Chibata,"*Immobilized Enzymes*," Chapters 3 and 5, Kodansha, Tokyo, 1975.

2) T. Takeuchi and S. Mori, " *Gel Chromatography: Fundamentals*," Chapter 2, Kodansha, Tokyo, 1975.

3) K. Nakanishi, S. Yamamoto, R. Matsuno, and T. Kamikubo, *Agric. Biol. Chem.*, 41, 1465 (1977).

4) C. N. Satterfield, "*Mass Trasfer in Heterogeneous Catalysis*," Chapter I, MIT Press, 1970.

5) F. Nelson, *J. Polymer Sci.*, 40, 563 (1959).

6) S. B. Horowitz and I. R. Fenichel, *J. Phys. Chem.*, 68, 3378 (1964).

7) G. K. Ackers and R. L. Steere, *Biochim. Biophys. Acta*, 59, 137 (1962).

8) E. M. Renkin, *J. Gen. Physiol.*, 38, 225 (1955).

9) R. Namikawa, H. Okazaki, K. Nakanishi, R. Matsuno, and T. Kamikubo, *Agric. Biol. Chem.*, 41, 1003 (1977).

10) S. Fukui, A. Tanaka, T. Iida, and E. Hasegawa, *FEBS Lett.*, 66, 179 (1976).

11) A. Tanaka, S. Yasuhara, M. Osumi, and S. Fukui, *Eur. J. Biochem.*, 80, 193 (1977).

12) M. Morishita, M. Fukushima, and Y. Inaba, "*Microencapsulation: Process and Application*," ed. by J. E. Vandagaer, Plenum Publishing Co., New York, p.115.

13) E. C. Toren, Jr., *J. Chem. Educ.*, 44, 173 (1967).

14) J. Crank, "*Mathematics of Diffusion*," Oxford Univ. Press, 1956, p.47, 86.

15) A. G. Ogston, *Trans. Faraday Soc.*, 54, 1754 (1958).

16) T. C. Laurent and J. Killander, *J. Chromatogr.*, 14, 317 (1964).

17) J. K. Gladden and M. Dole, *J. Am. Chem. Soc.*, 75, 3900 (1953).

18) "*International Critical Table*," Volume V, McGraw-Hill, New York, 1929, p.71.

19) "*Hand Book of Biochemistry and Physics*," 47th ed., ed. by C. D. Hodgman, Chemical Rubber Publishing, Cleveland, 1966, F-43.

20) K. H. Granth, *J. Colloid Sci.*, 13, 308 (1958).

21) "*The Merck Index*," 8th ed., Merk & Co., Inc., Rahway, 1968, p.17, 434.

22) S. Hjertén, S. Jerstedt, and A. Tiselius, *Anal. Biochem.*, 27, 108 (1969).

23) Y. Degani and T. Miron, *Biochim. Biophys. Acta*, 212, 362 (1970).

24) J. B. Hendricken, D. J. Cram, and G. S. Hammond, "*Organic Chemistry*," 3rd ed., McGraw-Hill, New York, 1962, p.302.

25) F. Helfferich, "*Ion Exchanger*," Chapter 6, McGraw-Hill, New York, 1962.

26) Z. Blank and A. C. Reimshuessel, *J. Material Sci.*, 9, 1815 (1974).

27) R. Rückel and M. Brager, *Anal. Biochem.*, 68, 415 (1975).

Chapter 2

Effectiveness Factor in a Batch Reactor Including Immobilized-Enzyme Particles

2. 1. Introduction

It is experimentally convenient to study the kinetics of an immobilized-enzyme reaction in an isothermal batch reactor. Such a reactor is often used for estimating the kinetics of the immobilized-enzyme reaction. The reaction catalyzed by the immobilized enzyme is heterogeneous. For heterogeneous reactions, the transient diffusional phenomena sometimes complicate the interpretation of the data taken from such a reactor.

The purpose of this chapter is to discuss on the unsteady state effectiveness factor in the heterogeneous reactor including immobilized-enzyme particles. We consider only the case where an enzyme reaction is represented by Michaelis-Menten equation. The discussion will give the critical time taken to satisfy the pseudo-steady state assumption.

Some investigators have reported on the unsteady state effectiveness factor in a batch reactor where a first-order reaction is allowed to proceed. Villandsen and Stewart[1] considered the unsteady state effectiveness factor in a batch reactor with an infinite volume of reactant. Lewis and Paynter[2] discussed on the unsteady state effectiveness factor for a finite volume of reactant.

There are some discussions[3,4] dealt with the steady state ef-

fectiveness factor for a reaction catalyzed by an immobilized enzyme. Some investigators[5-7] have presented approximate correlations between the steady state effectiveness factor and the general modulus proposed by Bischoff.[8]

2. 2. Problem Formulation

The Michaelis-Menten type of kinetics is considered for an immobilized-enzyme catalyzed reaction. The immobilized-enzyme particles with interior void fraction, ε, which is containing initially diluent, are immersed into a volume, V_0, of reactant. For simplicity, the following assumptions are made: i) the reaction is allowed to proceed under an isothermal condition, ii) the enzyme is homogeneously distributed into the particles, and iii) the effect of film diffusion of substrate on the reaction rate can be ignored.

The problem can be stated by the following partial differential equation and its associated boundary conditions.

$$\frac{\partial y}{\partial \theta} = \left(\frac{\partial^2 y}{\partial \xi^2} + \frac{2}{\xi}\frac{\partial y}{\partial \xi}\right) - 9\phi^2 \nu_0 \frac{y}{y + \nu_0} \tag{2-1}$$

$$\text{at } \xi = 1, \quad \theta > 0, \quad \partial y_s/\partial \xi = -\alpha(\partial y/\partial \xi) \tag{2-2}$$

$$\text{at } \xi = 0, \quad \theta > 0, \quad \partial y/\partial \xi = 0 \tag{2-3}$$

$$\text{at } \xi = 1, \quad \theta = 0, \quad y = 1 \tag{2-4}$$

$$\text{at } 0 \leq \xi < 1,\ \theta = 0, \qquad y = 0 \tag{2-5}$$

where the dimensionless variables and parameters are defined by

$$y = C_{AR}/C_{AS0} \tag{2-6a}$$

$$y_S = C_{AS}/C_{AS0} \tag{2-6b}$$

$$\theta = D_{eA}t/(R^2) \tag{2-6c}$$

$$\xi = r/R \tag{2-6d}$$

$$\phi = (R/3)[Vm/(Km\ D_{eA})]^{1/2} \tag{2-6e}$$

$$\nu_0 = Km/C_{A0} \tag{2-6f}$$

$$\alpha = 3W\varepsilon/(V_0\rho_p) \tag{2-6g}$$

Unfortunately, Eq.(2-1) can not be solved analytically. Hence, numerical solution of Eq.(2-1) is obtained.

However, when the substrate concentration is much less than Km, that is, $y << \nu_0$, the reaction term in Eq.(2-1) can be approximated by Eq.(2-7).

$$9\phi^2\nu_0 \frac{y}{y + \nu_0} \simeq 9\phi^2 y \tag{2-7}$$

In such a case, the analytical solution of Eq.(2-1) can be obtained.

$$y = \frac{2\alpha k_i'^2 \exp[-(9\phi^2 - k_i'^2)\theta]}{\alpha k_i'^2(2+\alpha) - (9\phi^2 - k_i'^2)(9\phi^2 - k_i'^2 + \alpha)} \cdot \frac{1}{\xi} \cdot \frac{\sinh(k_i'\xi)}{\sinh(k_i')}$$

$$+ \sum_{n=1}^{\infty} \frac{2\alpha k_n^2 \exp[-9(\phi^2 + k_n^2)\theta]}{\alpha k_n^2(2+\alpha) + (9\phi^2 + k_n^2)(9\phi^2 + k_n^2 + \alpha)} \cdot \frac{1}{\xi} \cdot \frac{\sin(k_n\xi)}{\sin(k_n)} \tag{2-8}$$

where k_i' and k_n are given by the following equations.

$$\tanh(k_i') = \alpha k_i'/(9\phi^2 - k_i'^2 + \alpha) \tag{2-9}$$

$$\tan(k_n) = \alpha k_n/(9\phi^2 + k_n^2 + \alpha) \tag{2-10}$$

The dimensionless concentration of substrate at the surface of immobilized-enzyme particles can be obtained by setting $\xi = 1$ at Eq. (2-8).

Lewis and Paynter[2] have defined the effectiveness factor in a batch reactor as follows:

$$E_{f\theta} = \frac{\int_0^1 (4\pi\xi^2)[y/(y+\nu_0)]d\xi}{(4\pi/3)[y_s/(y_s+\nu_0)]} \tag{2-11}$$

or

$$\eta_\theta = \frac{1}{3\phi^2} \cdot \frac{(\partial y/\partial \xi|_{\xi=1})/V}{\{\nu_0[y_s/(y_s+\nu_0)]\}/V_0} \tag{2-12}$$

where V and V_0 are related by Eq. (2-13)

$$V = V_0 + \varepsilon V_c \tag{2-13}$$

The effectiveness factor defined by Eq. (2-11), $E_{f\theta}$, is different from that defined by Eq. (2-12), η_θ. There is the following relation between them.

$$E_{f\theta} = (V/V_0)\eta_\theta$$

$$= [1 + \varepsilon(V_c/V_0)]\eta_\theta \qquad (2\text{-}14)$$

In this work, the effectiveness factor defined by Eq.(2-11) is discussed. When Michaelis-Menten kinetics can be approximated to the first-order reaction due to low substrate concentration, the unsteady state effectiveness factor is easily calculated from Eq. (2-8). However, Eq.(2-1), which includes the Michaelis-Menten kinetics, cannot be solved. Therefore, Eq.(2-1) is solved numerically by Crank-Nicolson method. The integration of the resulting concentration profile in the particle by Simpson's method gives the unsteady state effectiveness factor, $E_{f\theta}$.

2. 3. Computational Results

The steady state effectiveness factor $E_{f\infty}$ can be obtained when the left-hand side of Eq.(2-1) = 0. First, we considered the first-order reaction. Figure 2-1 shows the time dependency of $E_{f\theta}/E_{f\infty}$ value for various values of $E_{f\infty}$ and α. As shown in Fig. 2-1, the effect of the parameter α on the $E_{f\theta}/E_{f\infty}$ is negligible. Figure 2-2 illustrates the relation between $E_{f\theta}/E_{f\infty}$ and θ for Michaelis-Menten kinetics under various ν_0 values. In Fig. 2-2, the α value is fixed to be 0.1. When the value of $E_{f\theta}/E_{f\infty}$ reaches 0.98, we consider a pseudo-steady state to be achieved. The critical time is represented by θ_c. Figure 2-3 illustrates the relation between θ_c and $E_{f\infty}$ using ν_0 as a parameter. When $\nu_0 = \infty$, the reaction is of first-order. On the other hand, the case where ν_0

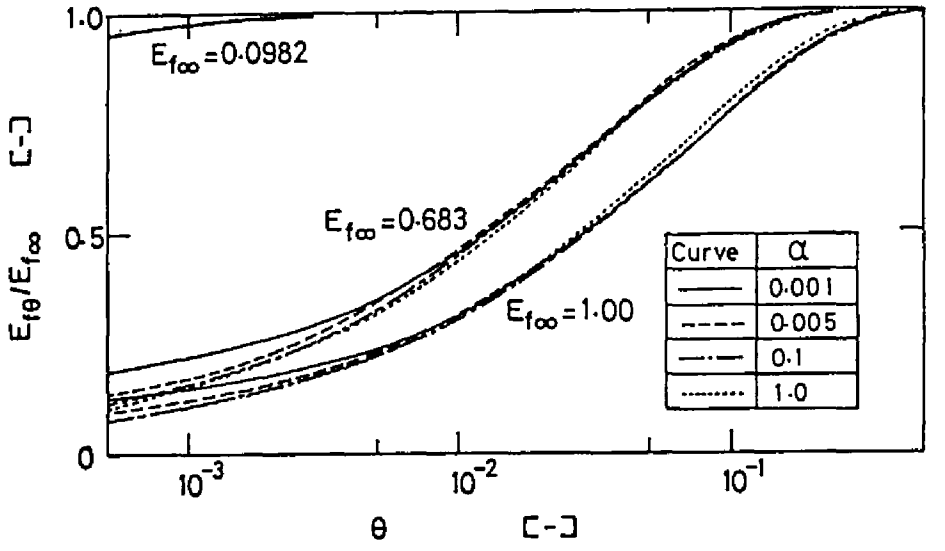

Fig. 2-1. Time dependency of $E_{f\theta}/E_{f\infty}$ value for various $E_{f\infty}$ and α values when an enzymatic reaction can be approximated to be of first-order.

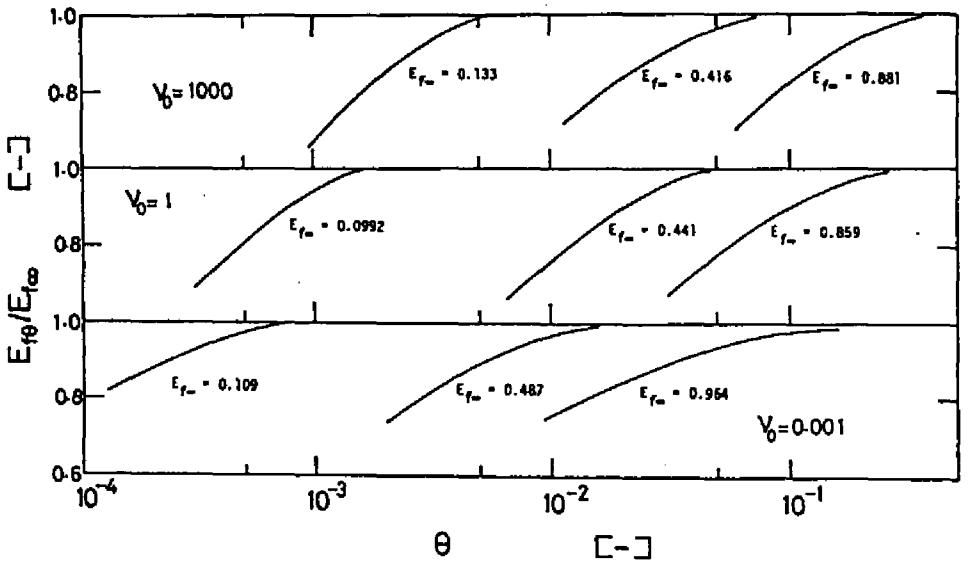

Fig. 2-2. Relation between $E_{f\theta}/E_{f\infty}$ and θ for Michaelis-Menten kinetics.

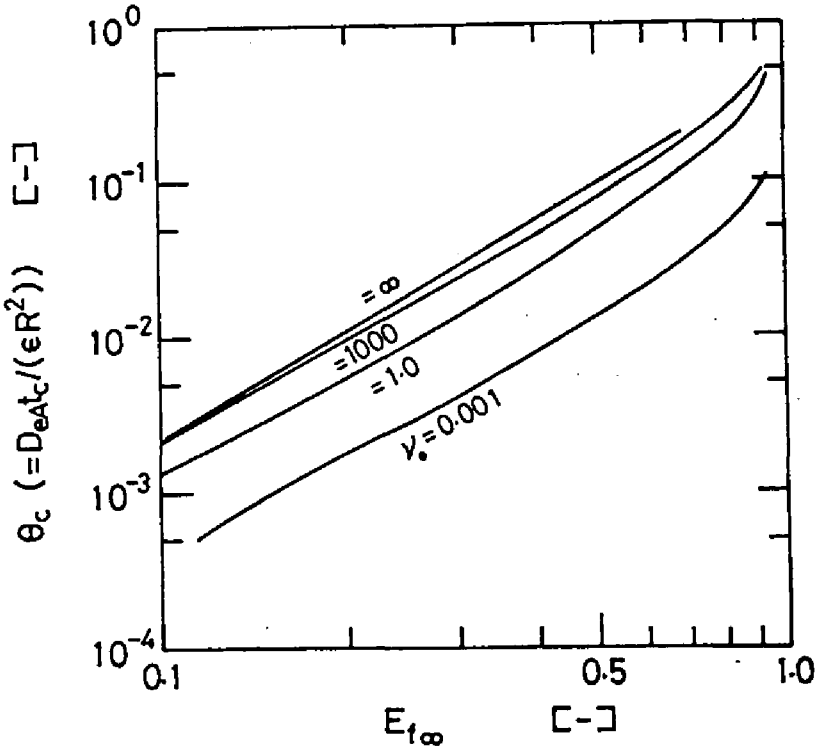

Fig. 2-3. Relation between $E_{f\infty}$ and critical time θ_c required to establish the pseudo-steady state.

value is equal to 0.001 corresponds to the case where Michaelis-Menten equation is approximated to zeroth-order reaction.

The θ_c is a function of $E_{f\infty}$, ϕ, ν_0 and α values. However, the effect of α value on the θ_c value is negligibly small. The effect of ϕ on θ_c is included in $E_{f\infty}$ because $E_{f\infty}$ is a function of ϕ. From Fig. 2-3, an actual time taken to achieve the pseudo-steady state after the start of reaction in the batch reactor is calculated under the following typical conditions. The pseudo-steady state is achieved within 10 - 20 s under the conditions that $E_{f\infty}$ = 0.8, ϵ = 0.5, R = 0.025 cm, and D_{eA} value is in the order of

10^{-6} cm^2/s. This result shows that the pseudo-steady state is achieved in a relatively short time in the batch reactor including immobilized-enzyme particles except for extreme operating conditions. In conclusion the steady state effectiveness factor can be used through the course of reaction.

2. 4. Summary

The unsteady state effectiveness factor in an isothermal batch reactor including immobilized-enzyme particles was discussed. The critical time when we can approximate a pseudo-steady state to be achieved was presented graphically as a function of the steady state effectiveness factor for various ν_0 (= Km/C_{A0}) values. The discussion had led to a conclusion that the pseudo-steady state is achieved within 10 - 20 s under usual operating conditions.

Nomenclature

C_{AR}	concentration of component A at stationary phase	[mol/cm^3]
C_{AS}	concentration of component A in bulk solution	[mol/cm^3]
D_{eA}	effective diffusion coefficient	[cm^2/s]
$E_{f\theta}$	unsteady state effectiveness factor defined by Eq.(2-11)	[-]
$E_{f\infty}$	steady state effectiveness factor	[-]
Km	Michaelis constant	[mol/cm^3]
R	radius of the bead	[cm]

r	radial distance	[cm]
t	time	[s]
V_c	volume of gel phase	[cm^3]
Vm	maximum reaction rate	[$mol/cm^3 \cdot s$]
V_0	volume of reactant	[cm^3]
W	weight	[g]
y	$= C_{AR}/C_{AS0}$	[-]
y_S	$= C_{AS}/C_{AS0}$	[-]
α	$= 3W\varepsilon/(V_0\rho_p)$	[-]
ε	= interior void fraction	[-]
η_θ	unsteady state effectiveness factor defined by Eq. (2-12)	[-]
θ	$= D_{eA}t/(\varepsilon R^2)$	[-]
ξ	$= r/R$	[-]
ν_0	$= Km/C_{A0}$	[-]
ρ_p	apparent density	[-]
ϕ	$= (R/3)[Vm/(Km \cdot D_{eA})]^{1/2}$	[-]

Literature Cited

1) J. V. Villadsen and W. E. Stewart, *Chem. Eng. Sci.*, 22, 1483 (1967).

2) W. E. Lewis and J. D. Paynter, *Chem. Eng. Sci.*, 26, 1357 (1971).

3) G. W. Roberts and C. N. Satterfield, *Ind. Eng. Chem. Fundamentals*, 4, 288 (1965).

4) M. Moo-Young and T. Kobayashi, *Can. J. Chem. Eng.*, 50, 162 (1972).

5) T. Kobayashi, K. Ohmiya, and S. Shimidzu, *J. Ferment. Technol.*, 54, 260 (1976).

6) B. Atokinson and I. J. Davis, *Trans. Instn Chem. Engrs*, 52, 248 (1974).

7) S. Gondo, S. Isayama, and K. Kusunoki, *J. Chem. Eng. Jpn*, 7, 64 (1974).

8) K. B. Bischoff, *AIChE J.*, 11, 351 (1965).

Chapter 3

Simultaneous Estimation of Diffusivity of Substrate and Kinetic Parameters of Michaelis-Menten Equation

3. 1. Introduction

A knowledge of diffusion coefficient of substrate and kinetic parameters of an immobilized enzyme is required for design of a reactor including the immobilized enzyme. The kinetic parameters, Km and Vmax, of any immobilized enzyme are ussually estimated from the reaction rate observed in an isothermal batch reactor or from the conversion of substrate observed in an isothermal tubular reactor. When the diffusional rate of substrate into the immobilized-enzyme support is rate-limiting, the parameters are estimated by using immobilized-enzyme particles which are crushed and reduced their diameter. The use of crushed particles is complicated and does not always give the correct parameters because the crushing of immobilized-enzyme particles is in danger of deactivation of the enzyme.

Kobayashi and Laidler[1)] have proposed a method to estimate the kinetic parameters, Km and Vmax, of Michaelis-Menten equation. Their method is limited to the case where the effective diffusion coefficient of substrate, D_{eA}, is known. The D_{eA} value, however, is often unknown. Therefore, their method requires the separate determination of D_{eA}.

In this chapter, we propose two new methods to estimate Km,

Vmax, and D_{eA} simultaneously from the time course of substrate concentration observed in an isothermal batch reactor. One method is based on analysis of time courses of substrate concentrations observed by using two kinds of immobilized-enzyme particles different in diameter at the same initial substrate concentration. In another method, the initial substrate concentrations are varied using immobilized-enzyme particles with an given diameter. The kinetic parameters of hydrolysis of N-glutaryl-L-phenylalanine *p*-nitroanilide (GPNA) by α-chymotrypsin immobilized into acrylamide gel and crushed-firebrick particles, and the effective diffusivity of GPNA, were estimated by the two methods. Appropriateness of parameters estimated was verified by the following facts: the time course of substrate concentration calculated by using the parameters fitted to the experimental data, and the conversion of substrate, which was obtained in the packed column, coincided with the conversion calculated by using the parameters estimated.

4. 2. Materials and Methods

Materials α-Chymotrysin, bovine serum albumin (BSA), glutaraldehyde, and N-glutaryl-L-phenylalanine *p*-nitroanilide (GPNA) were purchased from Sigma. Firebrick LBP-13, which was obtained from Isoraito Kogyo, was crushed and sieved to desired size. The particles were washed with 0.01 mol/l potassium phosphate buffer

(pH 7.4) and distilled water, and then dried. Acrylamide monomer (AAm), N,N'-methylenebisacrylamide (BIS), N,N,N',N'-tetramethylethylenediamine (TEMED), ammonium persulfate, and Sorbitan were purchased from Nakarai Chemicals. Other reagents were of analytical grade.

Immobilization of α-chymotrypsin into crushed-firebrick particles Firebrick was crushed and sieved to particles with various mean diameters (0.0505, 0.0775, 0.1090, 0.1545, and 0.2190 cm). Fourty ml of 2.5%(w/v) α-chymotrypsin, 40 ml of 20%(w/v) BSA, and 40 ml of 2%(v/v) glutaraldehyde, which were dissolved in 0.04 mol/l potassium phosphate buffer (pH 7.4), were mixed. Firebrick particles of a given mean diameter (200 g) were added to the mixture and immediately stirred. The suspension was kept freezed at -20°C over one day. It was then melt at 4°C and dehydrated. The immobilized-α-chymotrypsin particles were washed with the buffer until the absorbance of wash at 280 nm became below 0.02. They were successively washed with distilled water and dried at 4°C. The resulting immobilized-enzyme particles were stored at 4°C in refrigerator before use.

Entrapment of α-chymotrypsin in acrylamide gel The method for entrapping α-chymotrypsin in acrylamide gel was essentially the same as that reported by Ohmiya *et al.*[2] except for irradiation by a fluorescent light. Bovin serum albumin was added to α-

chymotrypsin solution to prevent the deactivation of the enzyme during the immobilization. Leakage of α-chymotrypsin from the acrylamide gel was avoided by covalent binding of the enzyme to amino group of the enzyme, BSA, or acrylamide with glutaraldehyde.

Four ml of 5%(w/v) ammonium persulfate and 4 ml of 2.5%(v/v) glutaraldehyde were simultaneously added to a mixture of 6 ml of 8%(w/v) α-chymotrypsin, 6 ml of 3.2%(w/v) BSA, and 40 ml of AAm-BIS solution (BIS content: 5%). The mixture was immediately poured into 200 ml of organic solvent (toluene/chloroform = 144/56 (v/v)), which contained 0.3 - 0.5 ml of Sorbitan and 0.64 ml of TEMED, and was emulsified by magnetic stirring in a nitrogen atmosphere. The water phase was kept at pH 8.0 with 0.05 mol/l sodium phosphate buffer. The polymerization was performed at 0 - 4°C for 20 min. The resulting immobilized-α-chymotrypsin beads were filtered on a glass filter. The beads were washed with 100 ml of chilled toluene, with chilled sodium phosphate buffer, and successively with a large amount of chilled 0.05 mol/l Tris-HCl buffer (pH 8.0) containing 1.0 mol/l NaCl and 0.05 mol/l $CaCl_2$. The beads were sieved to obtain the desired size. They were suspended in the Tris-HCl buffer and stored in a refrigerator before use. The remaining activity of α-chymotrypsin after immobilization was about 60%. No loss of the activity was observed over 30 hr at 30°C.

Assay of α-chymotrypsin activity The hydrolysis of GPNA by immobilized α-chymotrypsin was allowed to run at pH 8.0 and 30°C.

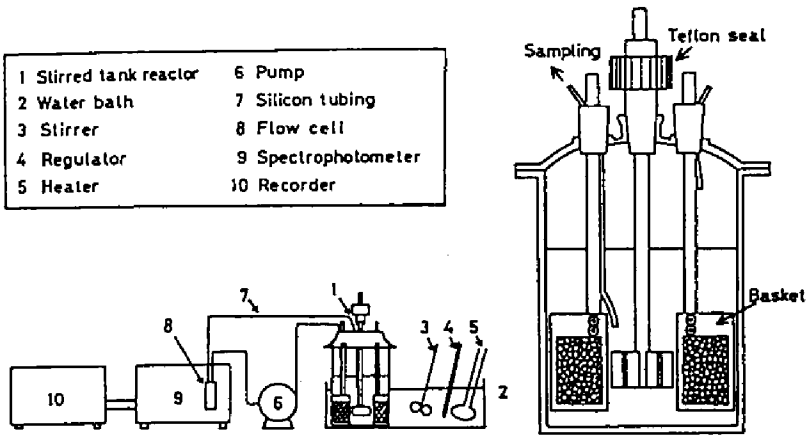

Fig. 3-1. Schematic representation of isothermal batch reactor including immobilized-α-chymotrypsin particles.

The concentration of the product, *p*-nitroaniline, was followed by measuring the absorbance of the bulk solution at 410 nm, where the absorbance due to GPNA is negligible.

Batch reactor Figure 3-1 shows the experimental apparatus. The firebrick particles (5 g) to which α-chymotrypsin was immobilized were put into four stainless steel baskets. The baskets were placed near baffles. The reaction was carried out at pH 8.0 with 0.05 mol/l Tris-HCl buffer containing 2.0 mol/l NaCl and at 30°C. The volume of substrate solution was 1000 cm^3. The agitator with six paddles was revolved at 700 - 800 r.p.m. where the film mass transfer resistance was confirmed to be negligible. The initial concentration of GPNA was 8.8×10^{-5} or 3.52×10^{-4} mol/l. The concentration of the product was continuously monitored by

passing the bulk solution through a spectrophotometer (Shimadzu, Spectronic 88).

Some alterations of procedures were made in the experiments using α-chymotrypsin entrapped into acrylamide gel as a catalyst. The gels (0.7 - 3 g) were held into one or two stainless steel baskets. The volume of GPNA solution was 275 - 700 ml. The solution was agitated by a magnetic stirrer. The bulk solution was sampled at appropriate intervals and its absorbance at 410 nm was measured. The solution sampled was returned into the reaction vessel after measurement of absorbance.

Tubular reactor The appropriateness of the parameters (Km, Vmax, and D_{eA}) estimated by proposed methods was verified by comparing the concentration profile of GPNA observed experimentally in a tubular reactor with that calculated by using the parameters.

Figure 3-2 is a diagram of experimental apparatus. Immobilized α-chymotrypsin firebrick particles (5 g) were packed in each column. The inner diameter of the column, 2.0 cm, was larger than the diameter of particles, so that the effect of wall on mass transfer could be ignored. The columns were kept at 30°C by circulating thermostatic water through jackets. The inactive firebrick particles with the same diameter as the active ones were packed above and below the active particle zone to preheat the substrate solution and to keep the flow pattern constant. The substrate solution was introduced upwards into the reactor by

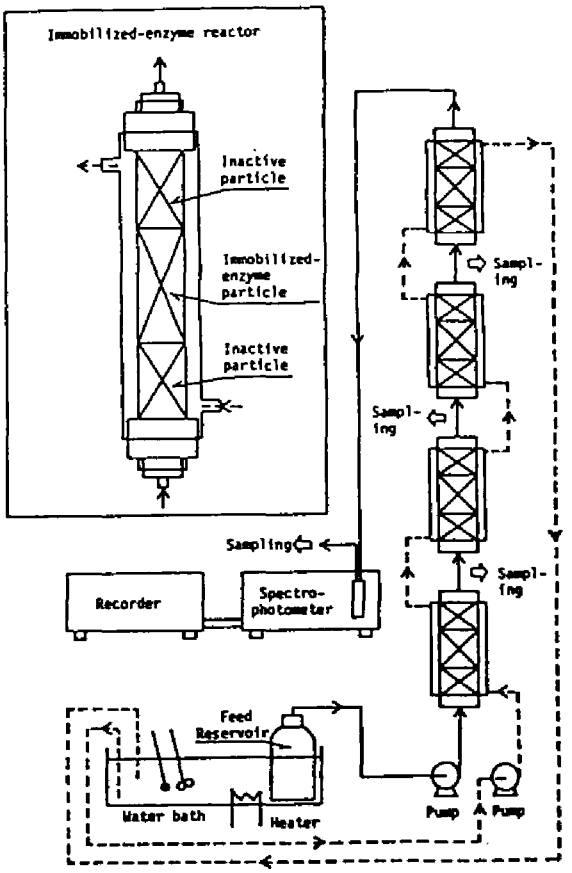

Fig. 3-2. Schematic diagram of tubular reactor.

a constant-feeding pump. The absorbance of eluate at 410 nm was continuously measured at the outlet of the last column. After establishment of steady state was confirmed, the concentration of the product sampled at the outlet of each column was measured.

When α-chymotrypsin entrapped into acrylamide gel was used as a catalyst, we used an apparatus of small scale and omitted the preheating zone of inactive gels.

The concentration profile of the substrate in the tubular reac-

tor was calculated from Eq.(3-1), or Eqs.(3-2) and (3-3), which were solved numerically by Runge-Kutta-Gill method. When film mass transfer resistance can be ignored, the design equation of the reactor is given by Eq.(3-1).

$$\frac{dC_A}{dz} = -\frac{(1-\varepsilon_b)}{u_0} \cdot E_{f\infty}(C_A) \cdot \frac{Vmax \cdot C_A}{Km + C_A} \tag{3-1}$$

When the rate of film mass transfer of substrate is not fast enough, the following equations must be solved.

$$\frac{dC_A}{dz} = -\frac{3(1-\varepsilon_b)}{u_0 R} \cdot k_L \cdot (C_A - C_{Ai}) \tag{3-2}$$

$$k_L \cdot (C_A - C_{Ai}) = (R/3) \cdot E_{f\infty}(C_A) \cdot \frac{Vmax \cdot C_{Ai}}{Km + C_{Ai}} \tag{3-3}$$

The boundary condition is given as follows:

$$\text{at } z = 0, \qquad C_A = C_{A0} \tag{3-4}$$

where C_A and C_{Ai} denote the substrate concentration in mobile phase and that at the surface of catalyst, respectively. R is the radius of a bead, z the axial distance, ε_b the void fraction of the bed, u_0 the superficial velocity, and k_L the film mass transfer coefficient. The value of k_L was evaluated from the correlation proposed by Kataoka *et al.*[3] under the assumption that the molecular diffusivity of GPNA was 1.0×10^{-5} cm^2/s. In calcula-

tion of $E_{f\infty}$, the approximate expression proposed by Kobayashi *et al.*[4] was used.

Estimation of kinetic parameters The diameter of acrylamide gels can be reduced easily by grinding them. The intrinsic kinetic parameters of immobilized α-chymotrypsin free from intraparticle diffusional resistance can be obtained by using the ground α-chymotrypsin.

About 0.1 g of ground enzyme-gels were accurately weighed in Erlenmeyer flask. Addition of 25 ml of GPNA solution initiated the reaction under magnetic stirring at 30°C. At appropriate intervals, the solution was sampled through a glass filter to prevent contamination of ground gels and the *p*-nitroaniline concentration was measured. The initial reaction rates based on the unit volume of immobilized-enzyme gels were observed for various GPNA concentrations. The Michaelis constant Km and maximum reaction rate Vmax were estimated from Linewever-Burk plot.

Estimation of diffusivity of GPNA in acrylamide gel The diffusion coefficient of GPNA in the acrylamide gel was observed by the following three methods.

(a) *Leakage method:* In active acrylamide gel beads with large diameter (*ca.* 2 cm) were prepared. Some beads were immersed into GPNA solution over 24 hr at room temperature. The beads were removed from the solution and blotted with a piece of paper to elim-

inate excess liquid on the surface. They were put into 25 ml of Tris-HCl buffer. An increase in absorbance of the buffer solution at 317 nm was measured. The solution was mixed under magnetic stirring. The temperature was controlled at 30°C.

A fraction of GPNA remaining within beads at any time, M_L, is expressed by the following equation.

$$M_L \equiv \frac{C_{A\infty} - C_A}{C_A} = (1 + 1/\alpha) \sum_{n=1}^{\infty} \frac{\exp(-q_n^2 D_{eA} t/R^2)}{(3/2)(1+\alpha) + (q_n^2/6\alpha)} \qquad (3\text{-}5)$$

where

$$\alpha = W/(V\rho_p) \qquad (3\text{-}6)$$

and q_n is the *n*th root of the following equation.

$$q = 3\alpha[(q/\tan q) - 1] \qquad (3\text{-}7)$$

W and ρ_p are the weight and the apparent density of beads, respectively. V is the volume of the buffer solution. C_A and $C_{A\infty}$ represent the concentrations of GPNA at any time and at equilibrium. In our experimental conditions, α was 0.0846.

(b) *Penetration method:* Some particles with large diameter were poured into 24 ml of GPNA solution. A decrease of GPNA concentration in bulk solution was measured. Other procedures were the same as leakage method.

An exact solution for the fraction of solute penetrated at any

time, M_p, has presented by Crank.[5] Carman and Haul[6] have reported an approximate solution for M_p. In this study, diffusion coefficient of GPNA in acrylamide gel was evaluated by using the approximate solution given in Eq.(3-8).

$$M_P \equiv \frac{C_{A0} - C_A}{C_{A0} - C_{A\infty}} = (1 - 1/\alpha)[1 - \frac{\gamma_1}{\gamma_1+\gamma_2} eerfc\{3\alpha\gamma_1(D_{eA}t/R^2)^{1/2}\} - \frac{\gamma_2}{\gamma_1+\gamma_2} eerfc\{-3\alpha\gamma_2(D_{eA}t/R^2)^{1/2}\}] \quad (3\text{-}8)$$

where

$$\gamma_1 = (1/2)[\{1 + 4/(3\alpha)\}^{1/2}] \quad (3\text{-}9a)$$

$$\gamma_2 = \gamma_1 - 1 \quad (3\text{-}9b)$$

and $$eerfc\ z \equiv \exp z^2 \cdot erfc\ z \quad (3\text{-}10)$$

C_{A0} represents the initial concentration of solute. The value of α was 0.162 in our experiment.

(c) *Moment analysis of elution profile of solute in fixed bed :*

A moment analysis of the elution curve of a solute from the column, where inactive acrylamide gel beads are packed, can be utilized to estimate the diffusion coefficient of the solute within the particles.

The inactive beads were packed into a column equipped with a water jacket (30°C). 0.5 mℓ of 2.6 X 10^{-6} mol/l GPNA solution

was introduced to the top of the bed as a pulse and eluted with 0.05 mol/l Tris-HCl buffer containing 1.0 mol/l NaCl and 0.05 mol/l $CaCl_2$. The absorbance of the eluate at 317 nm was continuously measured by using a micro-flow cell equipment. The details of experimental procedures and analysis of the curve will be described in Part II.

3. 3. Theoretical Considerations

Some investigators[4,10-12] have presented approximate expressions of effectiveness factor for Michaelis-Menten rate equation at pseudo-steady state. These expressions are functions of the generalized Thiele modulus m proposed by Bischoff[13] and the ratio of Michaelis constant to substrate concentration ν ($= Km/C_A$). The generalized Thiele modulus is defined as

$$m = \frac{\phi}{\sqrt{2}} \frac{1}{1+\nu} \left[\frac{1}{\nu} + \ln\left(1 + \frac{1}{\nu}\right)\right]^{1/2} \tag{3-11}$$

where

$$\phi = (V_p/S_p)\,[Vmax/(Km \cdot D_{eA})]^{1/2} \tag{3-12}$$

Kobayashi *et al.*[4] have presented the following approximate expression for effectiveness factor.

$$E_{f\infty} = \frac{E_0 + aE_1}{1+a} \qquad (a = 2.6\nu^{0.8}) \tag{3-13}$$

for sphere

$$E_0 = \begin{cases} 1 & (m < 1/\sqrt{3}) \\ 1 - [1/2 + \cos\{(\Psi+4\pi)/3\}]^3 & (m > 1/\sqrt{3}) \end{cases} \quad (3\text{-}16)$$

$$\Psi = \cos^{-1}[(2/3m^2) - 1] \quad (3\text{-}17)$$

$$E_1 = (1/m)[1/\tanh(3m) - 1/3m] \quad (3\text{-}18)$$

Using the effectiveness factor at pseudo-steady state $E_{f\infty}$, a decrease of substrate concentration in an isothermal batch reactor is expressed by the following equation.

$$-\frac{dC_A}{dt} = \frac{W}{V\rho_p} \cdot E_{f\infty} \cdot \frac{Vmax \cdot C_A}{Km + C_A} \quad (3\text{-}19)$$

Then, an overall reaction rate r_{obs} is given by

$$r_{obs} = -\frac{V\rho_p}{W} \cdot \frac{dC_A}{dt} = E_{f\infty} \cdot \frac{Vmax \cdot C_A}{Km + C_A} \quad (3\text{-}20)$$

Rearrengement of Eq. (3-20) gives the following equations.

$$E_{f\infty} \cdot \frac{C_A}{r_{obs}} = \frac{Km}{Vmax} + \frac{1}{Vmax} \cdot C_A \quad (3\text{-}21)$$

$$\frac{C_A}{r_{obs}} = \frac{1}{E_{f\infty}} \left\{ \frac{Km}{Vmax} + \frac{1}{Vmax} \cdot C_A \right\} \quad (3\text{-}22)$$

Method I Time courses of substrate concentrations in bulk

solution are separately observed by using immobilized enzymes with two different particle radii, R_1 and R_2. The initial substrate concentrations are the same. The dC_A/dt values at the same substrate concentration are evaluated by the graphical differentiation, and the overall reaction rates, r_{obs1} and r_{obs2}, are calculated from Eq.(3-20). Since $\nu_1 = \nu_2$, Eq.(3-11) gives the following equation.

$$m_1/m_2 = \phi_1/\phi_2 = R_1/R_2 \tag{3-23}$$

The ratio $E_{f\infty 1}$ to $E_{f\infty 2}$ is given by the following equation from Eq. (3-20).

$$E_{f\infty 1}/E_{f\infty 2} = r_{obs1}/r_{obs\,2} \tag{3-24}$$

Kinetic parameters, Km and Vmax, and effective diffusivity of substrate D_{eA} are estimated by the following procedures:

(1) Assume Km' value. The Km value of free enzyme can be conveniently used as the Km' value of immobilized enzyme.

(2) Assume m_1 for each C_A.

(3) Calculate m_2 by using Eq.(3-23), and evaluate $E_{f\infty 2}$ from Eq. (3-13).

(4) Calculate $E_{f\infty 1}$ by substituting m_1 into Eq.(3-13) and obtain $E_{f\infty 2}'$ from Eq.(3-24).

(5) Compare $E_{f\infty 2}$ with $E_{f\infty 2}'$. If the difference between $E_{f\infty 2}$ and $E_{f\infty 2}'$ is not within a permissible error ε_E, assume m_1

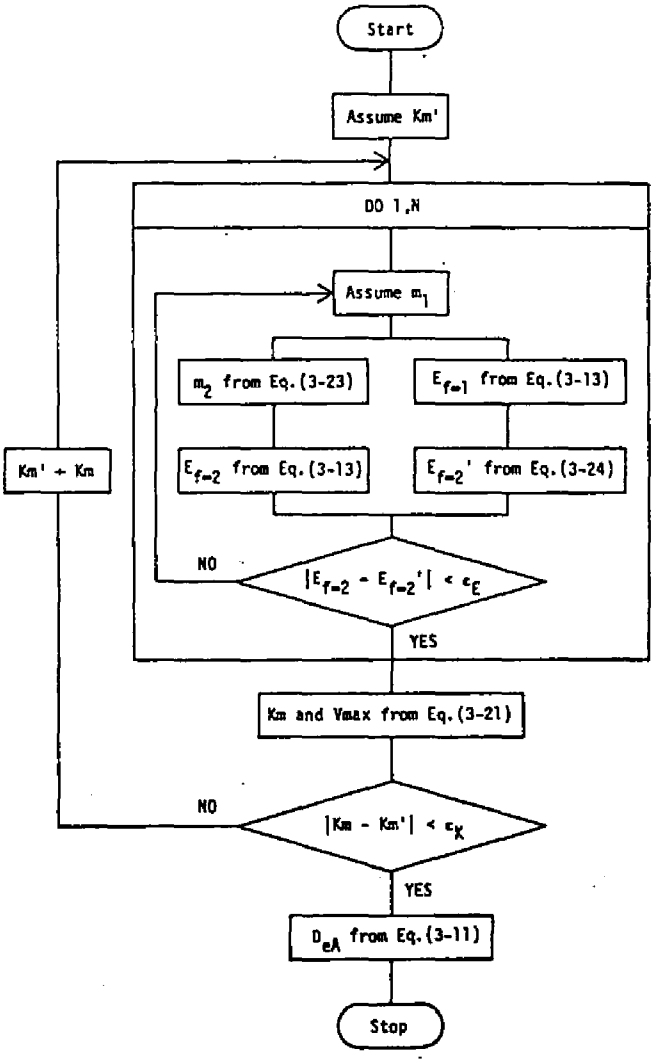

Fig. 3-3. Flow chart for estmating Km, Vmax, and D_{eA} values by method I.

again.

The calculations are repeated until the difference between $E_{f\infty 2}$ and $E_{f\infty 2}'$ becomes smaller than the permissible error. These calculations give the m_1, m_2, $E_{f\infty 1}$, and $E_{f\infty 2}$ values for each C_A. By performing the same calculations for various C_A values, $E_{f\infty}$ and m

values are estimated as a function of C_A. Since the relation between $E_{f\infty} \cdot C_A / r_{obs}$ and C_A has been given by Eq. (3-21), Km value is estimated by using the least square method. The Km value is compared with the Km' value. If the Km value does not coincide with the Km' within a permissible error ε_K, the Km value is substituted into the Km' value and the calculations mentioned above are repeated until the difference between Km and Km' becomes within the error ε_K. The Km and Vmax values are estimated by these calculations and hence D_{eA} value is also calculated by using Eq. (3-11). The flow chart of the method is illustrated in Fig. 3-3.

Method II Although the method described here requires essentially no change of initial substrate concentration, it may be desirable to estimate accurately kinetic parameters, Km and Vmax, and effective diffusivity of substrate D_{eA} by using two different initial concentration of substrate. Assuming that there is no change of $E_{f\infty}$ value within a relatively narrow range of substrate concentrations, the relation between C_A / r_{obs} and C_A in Eq. (3-22) are assumed to be linear and Km' value is evaluated. The ratio of $E_{f\infty 1}$ to $E_{f\infty 2}$ is represented by the following equation from Eq. (3-20). $E_{f\infty 1}$ and $E_{f\infty 2}$ are the effectiveness factors for two different substrate concentrations, C_{A1} and C_{A2}, respectively.

$$E_{f\infty 1} / E_{f\infty 2} = [(1 + \nu_1)/(1 + \nu_2)] \cdot (r_{obs1} / r_{obs2}) \qquad (3\text{-}25)$$

Since the radius of immobilized-enzyme particles used for C_{A1} is the same as that for C_{A2} and hence $\phi_1 = \phi_2$, Eq.(3-11) gives the following equation.

$$\frac{m_1}{m_2} = \frac{1 + \nu_1}{1 + \nu_2} \cdot \frac{[1/\nu_2 - \ln(1 + 1/\nu_2)]^{1/2}}{[1/\nu_1 - \ln(1 + 1/\nu_1)]^{1/2}} \qquad (3\text{-}26)$$

Kinetic parameters and effective diffusivity of substrate are estimated by the following procedures.

(1) Assume m_1.

(2) Calculate m_2 from Eq.(3-26) and evaluate $E_{f\infty 2}$ by using Eq. (3-13).

(3) Calculate $E_{f\infty 1}$ from Eq.(3-11) and then obtain $E_{f\infty 2}'$ from Eq.(3-25).

(4) Compare $E_{f\infty 2}$ with $E_{f\infty 2}'$. If the difference between $E_{f\infty 2}$ and $E_{f\infty 2}'$ is over a permissible error ε_E, assume m_1 again.

(5) The m_1, m_2, $E_{f\infty 1}$, and $E_{f\infty 2}$ values are determined when the difference between $E_{f\infty 2}$ and $E_{f\infty 2}'$ becomes smaller than the error ε_E. By substituting $E_{f\infty}$ values into Eq.(3-22), Vmax is evaluated. Substitution of m, Vmax, and Km values into Eq.(3-11) gives D_{eA} value.

(6) $E_{f\infty} \cdot C_A / r_{obs}$ values are plotted against C_A values by using Eq.(3-21) and then Km and Vmax values are obtained. Compare Km value with Km' value. When the difference between Km' and Km values is over a permissible error ε_K, Km value

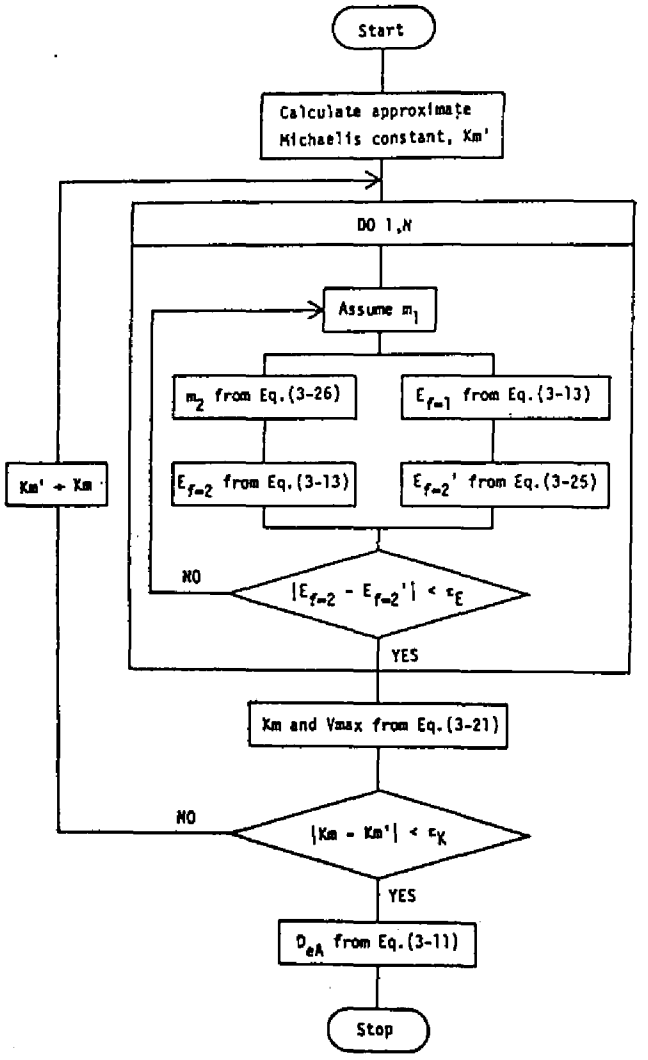

Fig. 3-4. Flow chart for estimating Km, Vmax, and D_{eA} values by method II.

is substituted into Km' value and the above calculations are repeated.

Figure 3-4 shows the flow chart for method II.

3. 4. Results and Discussion

Table 3-1 shows the kinetic parameters of α-chymotrypsin immobilized onto firebrick particles and the effective diffusivity of GPNA. The values are estimated by method I and by approximating the shape of particle to be spherical. The values estimated may be reasonable because of the Km value of the free enzyme (1.81 X 10^{-4} mol/l), of the molecular diffusivity of GPNA (in a order of 10^{-5} cm^2/s), of the tortuosity factor of the particle (in a range of 3 - 5), and of the porosity of the particle (about 0.5). Figure 3-5 illustrates a comparison of experimental data with the

Table 3-1. Kinetic Parameters of α-Chymotrypsin Immobilized onto Firebrick Particles and Effective Diffusivity of GPNA Estimated by Using Method I.

$d_{p,ave}$ [cm]	$E_{f\infty,ave}$ [-]	Km [mol/l]	Vm [mol/l·s]	D_{eA} [cm^2/s]
0.0505	0.945	1.12 X 10^{-4}	3.33 X 10^{-6}	2.18 X 10^{-6}
0.0775	0.873			
0.0505	0.915	1.74 X 10^{-4}	3.90 X 10^{-6}	2.13 X 10^{-6}
0.1095	0.679			
0.0505	0.932	2.93 X 10^{-4}	4.93 X 10^{-6}	3.43 X 10^{-6}
0.1545	0.601			
0.0775	0.899	0.50 X 10^{-4}	2.70 X 10^{-6}	2.18 X 10^{-6}
0.1545	0.601			
0.1095	0.870	2.49 X 10^{-4}	3.55 X 10^{-6}	6.43 X 10^{-6}
0.1545	0.765			

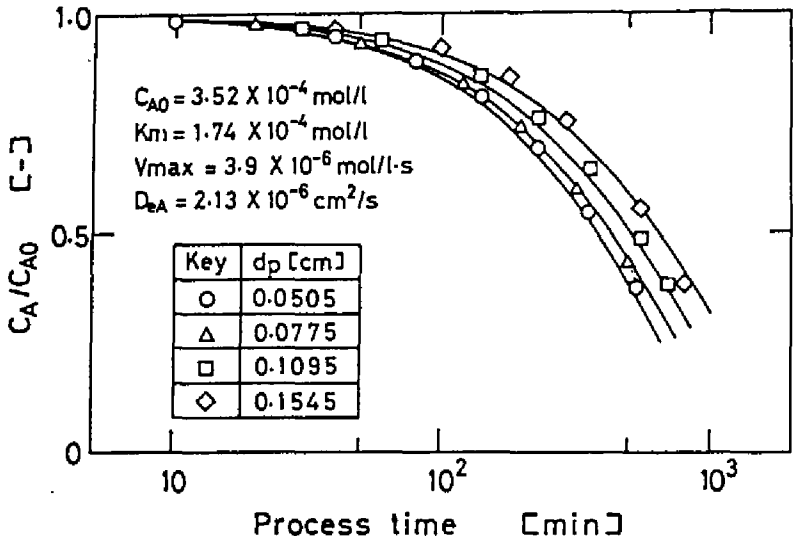

Fig. 3-5. Comparison of experimental data with the curves calculated by using the parameters estimated by method I. The values of parameters used in calculation are listed in the figure. α-Chymotrypsin was immobilized onto firebrick particles.

curves calculated from Eq. (3-19) by using the Km, Vmax, and D_{eA} values estimated by method I. As shown in the figure, the calculated curves coincide well with experimental data. The curves calculated by using the values estimated for a certain set of radii, however, do not always express the experimental data for another set of radii. This discordance may be due to that the distribution of the enzyme in firebrick particle is different for various radii.

Table 3-2 shows the kinetic parameters of α-chymotrypsin immobilized onto firebrick particles, which were estimated by method

Table 3-2. Kinetic Parameters of α-Chymotrypsin Immobilized onto Firebrick Particles and Effective Diffusivity of GPNA Estimated by Using Method II.

$d_{p,ave}$ [cm]	C_{A0} [mol/l]	Km [mol/l]	Vmax [mol/l·s]	D_{eA} [cm^2/s]
0.0505	3.52×10^{-4}	2.91×10^{-4}	4.87×10^{-6}	7.07×10^{-6}
	0.88×10^{-4}		5.48×10^{-6}	8.05×10^{-6}
0.0775	3.52×10^{-4}	3.62×10^{-4}	5.68×10^{-6}	5.85×10^{-6}
	0.88×10^{-4}		6.12×10^{-6}	6.98×10^{-6}
0.1095	3.52×10^{-4}	0.98×10^{-4}	2.78×10^{-6}	3.78×10^{-6}
	0.88×10^{-4}		3.77×10^{-6}	5.10×10^{-6}

II. Figure 3-6 illustrates the time courses of substrate concentration, which were calculated by using the values estimated for the particle with a diameter of 0.0505 cm. The curves calculated by using the parameters estimated for a low substrate concentration are over the experimental data. This may be due to that the Vmax and D_{eA} values estimated are larger than the intrinsic values.

Table 3-3 shows the kinetic parameters of α-chymotrypsin entrapped into acrylamide gel and the effective diffusivity of GPNA. The values are estimated by method II. Vmax and D_{eA} values listed in the table are mean values of those estimated for high and low substrate concentrations. The Km and Vmax values obtained by using the granulated immobilized α-chymotrypsin and D_{eA} values estimated by three different procedures are also listed in Table 3-3. Figure 3-7 shows the curve calculated by using the parame-

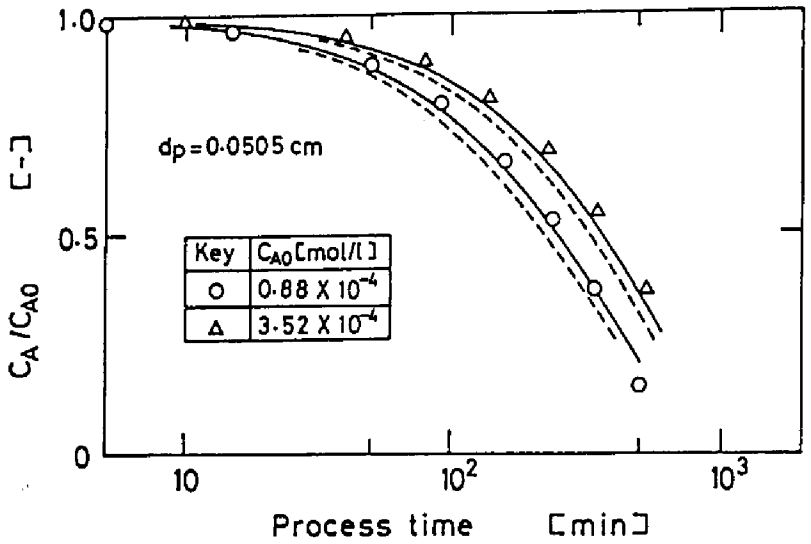

Fig. 3-6. Comparison of experimental data with the curves calculated by using the parameters estimated by method II. α-Chymotrypsin immobilized onto firebrick particles was used as a catalyst. The solid and broken curves were calculated by using the parameters estimated when C_{A0} = 3.52 X 10^{-4} mol/l and when C_{A0} = 0.88 X 10^{-4} mol/l, respectively.

ters estimated when d_p = 0.0538 cm. The solid curve is calculated by using the parameters estimated by method II. On the other hand, the broken curve is obtained by using the Km and Vmax values estimated by using granulated immobilized enzyme and the D_{eA} value estimated by moment analysis of elution curves of GPNA in a column packed with acrylamide gel containing no enzyme. Both the solid and broken curves coincide fairly well with the experimental data in Fig. 3-7.

Figures 3-8 and 3-9 show the concentration profiles in tubular

Table 3-3. Kinetic Parameters of Acrylamide Gel Entropped α-Chymotrypsin and Diffusion Coefficient of GPNA Estimated by Using Method II and Granulated Gel and Physical Methods.

Run No.	Method	Km [mol/l]	Vmax [mol/l·s]	D_{eA} [cm^2/s]
1*	Method II	3.86×10^{-4}	2.89×10^{-6}	3.54×10^{-6}
2	Method II	4.23×10^{-4}	6.45×10^{-6}	5.82×10^{-6}
3	Method II	3.42×10^{-4}	2.27×10^{-6}	7.15×10^{-6}
	Granulated	3.29×10^{-4}	4.20×10^{-6}	-
4	Method II	1.76×10^{-4}	2.34×10^{-6}	14.4×10^{-6}
	Granulated	2.20×10^{-4}	6.40×10^{-6}	-
5	Method II	3.23×10^{-4}	3.77×10^{-6}	4.38×10^{-6}
	Granulated	3.70×10^{-4}	5.49×10^{-6}	-
6	Method II	0.94×10^{-4}	22.2×10^{-6}	0.88×10^{-6}
	Granulated	2.25×10^{-4}	2.67×10^{-6}	-
Leakage method				0.82×10^{-6}
Penetration method				1.90×10^{-6}
Moment analysis				2.48×10^{-6}

* The amount of enzyme entrapped was a half of that in other runs.

reactors packed with α-chymotrypsin immobilized onto firebrick particles. The profiles were observed at various flow rates. The curves in Figs. 3-8 and 3-9 were calculated from the Km, Vmax, and D_{eA} values estimated by methods I and II, respectively. In Fig. 3-9, the solid and broken curves represent the result calculated with and without consideration of film mass transfer resistance. Under the experimental conditions, the film mass transfer resist-

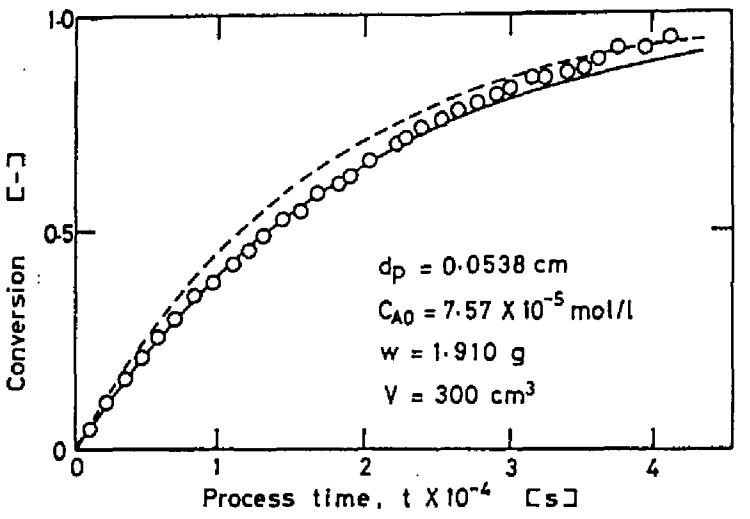

Fig. 3-7. Comparison of experimental data observed in run 5 of Table 3-3 with the calculated curves. α-Chymotrypsin was entrapped into acrylamide gel. The solid curve was calculated by using the parameters estimated by method II. The broken curve was obtained by utilizing the kinetic parameters estimated by using granulated immobilized enzyme and the D_{eA} value estimated by moment analysis.

ance is not significant. Figures 3-8 and 3-9 show that the parameters estimated by both methods I and II using an isothermal batch reactor can be conveniently utilized for designing a tubular immobilized-enzyme reactor.

The two methods proposed here can estimate conveniently the Km and Vmax values of immobilized enzyme and the diffusivity of substrate by using experimental data observed in a batch reactor. The methods, however, possess some limitations. Both methods I and II can not be utilized when the reaction catalyzed by immo-

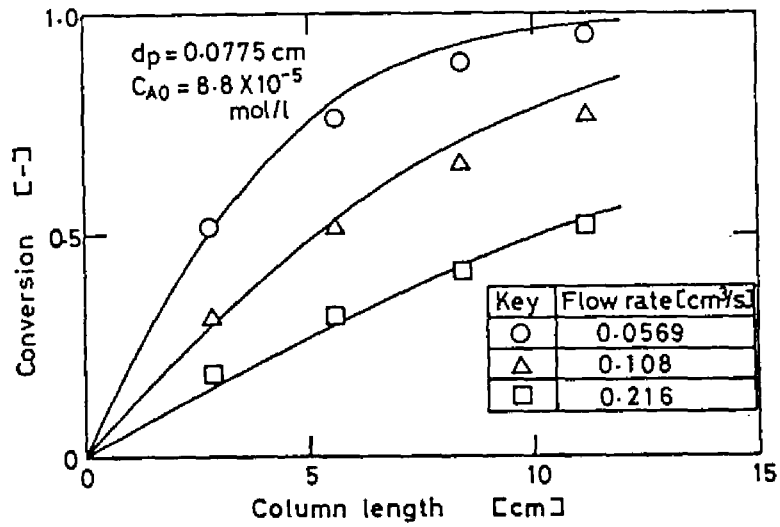

Fig. 3-8. Concentration profiles in tubular immobilized-α-chymotrypsin reactor. The curves were calculated by using the parameters estimated from method I.

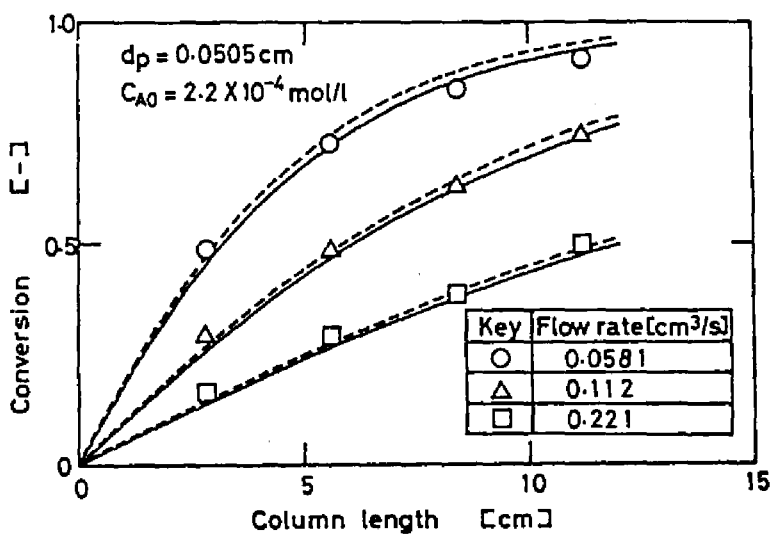

Fig. 3-9. Comparison of experimentally obtained concentration profiles in tubular reactor with profiles predicted by using the parameters estimated by method II. The solid and broken curves were calculated with and without consideration of film mass transfer resistance.

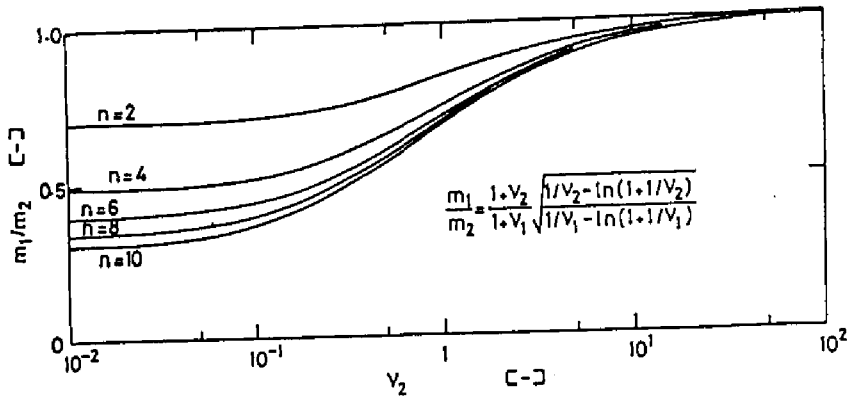

Fig. 3-10. Relation between ν_2 and m_1/m_2 when $C_{A1} = n \cdot C_{A2}$ $(n > 1)$.

bilized enzyme is within reaction- and diffusion controllings. The methods are effectively used in a range between reaction- and diffusion controllings. Method I can not be utilized when the radii of two particles are close each other and the ratio of dC_A/dt value for R_1 to that for R_2 falls within the margin of error of graphical differentiation. In method II, the initial substrate concentrations must be changed with a certain range. When C_{A1} and C_{A2} are chosen as two different substrate concentrations and $C_{A1} = n \cdot C_{A2}$ $(n > 1)$, the relation between ν_2 $(= Km/C_{A2})$ and m_1/m_2 are obtained from Eq. (3-26) as shown in Fig. 3-10. When Michaelis-Menten equation can be approximated to be of first-order, that is, $C_{A2} << Km$, m_1/m_2 approaches to 1.0. When $C_{A2} >> Km$, $E_{f\infty 1}/E_{f\infty 2} \rightarrow 1.0$. Therefore, both methods can not be utilized in such regions.

When we use immobilized enzymes as industrial catalysts, large amounts of enzymes may be, in many cases, immobilized and apparent

half-lifes of the catalysts are elongated. The reaction catalyzed by any enzyme prepared under such conditions may be between reaction- and diffusion controllings. When the reaction is in such a region, it is important to estimate kinetic parameters of the immobilized enzyme and the effective diffusivity of substrate. The usual procedure to estimate the parameters by using granulated immobilized-enzyme is complicated and does not always give the intrinsic kinetic parameters because of denaturation of the enzyme during granulation. There have been no methods to estimate the effective diffusivity of substrate through immobilized-enzyme particles. From above discussion the proposed methods may be excellent methods to estimate kinetic parameters, Km and Vmax, and effective diffusivity D_{eA} simultaneously, although they possess some limitations.

3. 5. Summary

Two methods for simultaneous estimation of kinetic parameters of any immobilized enzyme, Km and Vmax, and the effective diffusivity of substrate D_{eA} were proposed. The methods were applied to estimation of the Km and Vmax values of α-chymotrypsin immobilized into firebrick particles and acrylamide gels and the D_{eA} value of the substrate. The time courses calculated by using the parameters estimated by both methods successfully represented the experimental data. The tubular immobilized-α-chymotrypsin reac-

tor could also exhibit the performance predicted by using the parameters estimated.

Nomenclature

C_A	concentration of component A in mobile phase	[mol/l]
C_{Ai}	concentration of component A at the surface of catalyst.	[mol/l]
D_{eA}	effective diffusion coefficient	[cm^2/s]
d_p	diameter of the particle	[cm]
$E_{f\infty}$	steady state effectiveness factor	[-]
Km	Michaelis constant	[mol/l]
k_L	film mass transfer coefficient	[cm/s]
m	generalized Thiele modulus	[-]
R	radius of the bead	[cm]
r_{obs}	overall reaction rate	[mol/l·s]
S_p	surface area of a particle	[cm^2]
t	time	[s]
u_0	superficial linear velocity	[cm/s]
V	volume of the solution	[cm^3]
Vmax	maximum reaction rate	[mol/l·s]
V_p	volume of a particle	[cm^3]
W	weight of the beads	[g]
z	axial distance	[cm]

α	$= W/(V\rho_p)$	[-]
ε_b	void fraction of the bed	[-]
ν	$= Km/C_A$	[-]
ρ_p	apparent density	[g/cm^3]
ϕ	$= (V_p/S_p)[Vmax/(Km \cdot D_{eA})]^{1/2}$	[-]

Literature Cited

1) T. Kobayashi and K. J. Laidler, *Biochim. Biophys. Acta*, 302, 1 (1973).

2) K. Ohmiya, C. Terao, S. Shimizu, and T. Kobayashi, *Agric. Biol. Chem.*, 39, 491 (1975).

3) T. Kataoka, H. Yoshida, and K. Ueyama, *J. Chem. Eng. Jpn*, 5, 132 (1972).

4) T. Kobayashi, K. Ohmiya, and S. Shimizu, *J. Ferment. Technol.*, 54, 260 (1976).

5) J. Crank, "*Mathematics of Diffusion*," Oxford Univ. Press, 1956, p.88.

6) P. C. Carman and R. A. Haul, *Proc. Roy. Soc.*, 222-A, 109 (1954).

7) M. Kubin, *Collect. Czech. Chem. Commun.*, 30, 1104 (1965).

8) M. Suzuki, *Seisankenkyu*, 24, 187 (1972).

9) K. Nakanishi, S. Yamamoto, R. Matsuno, and T. Kamikubo, *Agric. Biol. Chem.*, 41, 1465 (1977).

10) B. Atkinson and I. J. Davis, *Trans. Instn Chem. Engrs*, 54,

248 (1974).

11) M. Moo-Young and T. Kobayashi, *Can. J. Chem. Eng.*, 50, 162 (1972).

12) S. Gondo, S. Isayama, and K. Kusunoki, *J. Chem. Eng. Jpn*, 7, 64 (1974).

13) K. B. Bischoff, *AIChE J.*, 11, 351 (1965).

Chapter 4

Effects of Gel Constituents on Immobilized-Enzyme Reaction

4. 1. Introduction

It is known well that immobilization of enzymes often causes some changes of kinetic properties of the enzymes. These changes have been ascribed to (1) ununiform distribution of substrate in outer and inner phase of immobilized enzyme caused by finite diffusion velocity of the substrate,[1] (2) the difference of electrostatic potential between outer and inner phases due to the charge of carrier[2] and (3) chemical modification of enzyme due to covalent attachment to carrier.[3] In these explanations, a premise is implied that the presence of carrier constituents in a high concentration does not affect the intrinsic kinetic properties in inner phase of the immobilized enzyme.

It is very difficult to investigate the interaction between an enzyme and its carrier using the immobilized enzyme itself. One alternative way to overcome this difficulty may replace an immobilized enzyme reaction system with the model system, in which the enzyme reaction runs in a medium containing a polymer, the component of carrier.

Laurent[4] and Mattiasson *et al.*[5] examined enzymic reactions in polymer media. They explained the change of the Michaelis constant by the exclusion effect and that of the maximum reaction

rate by the sieving effect when the molecular weight of substrate was high.

In this chapter an attempt is made to investigate the interactions between glucoamylase and a neutral polymer, dextran or a negatively charged polymer, dextran sulfate, which are the components of supports extensively used for immobilization of enzymes. Since glucoamylase is positively charged[6] under the reaction conditions, the effect of electrostatic attraction of dextran sulfate can be expected. The interactions were studied in terms of the change of kinetic properties of the enzyme reaction with maltose in the presence and absence of dextran and dextran sulfate.

Characteristics of immobilized enzyme by ionic linkage was also studied using glucoamylase onto SP-Sephadex C-25 and C-50 as model system. Experimental as well as theoretical considerations were made on the pH profiles of the rate constant k_0(app) and the Michaelis constant Km(app).

4. 2. Materials and Methods

Materials. Glucoamylase was purchased from Seikagaku Kogyo Co. To check the contamination with α-amylase in the enzyme preparation, the relationship between the decrease in blue value (percentage of absorbance of iodine color to that of initial one) and the increase in reducing value (percentage of glucosidic linkage cleaved) was studied by the same method as described by

Tsujisaka.[6] Amylose (the degree of polymerization = 600) was used as a substrate for the enzyme reaction. The plot of blue value *versus* reducing value gave a linear line having a negative slope represented by an equation, blue value (%) = 100 - reducing value (%). Since this means that the enzyme was free from α-amylase,[6] the enzyme was used without further purification. The enzyme concentration was determined spectrophotometrically using the molecular weight of the enzyme, 56,000 and the absorption coefficient, $E_{280}^{1\%}$ 13.6 cm^{-1}.[7]

Maltose was purchased from Wako Pure Chemical Industries Ltd. The preparation was used without further purification since the amount of glucose and maltotriose contained as impurities were so small that they did no hindrance in our experiments.

Dextran and dextran sulfate (sulphur content = 17 ± 1%) were obtained from Pharmacia Fine Chemicals Ltd. and their weight-average molecular weights were 70,000 and 500,000, respectively. The dextran sulfate included two or three sulfate groups per glucose residue.

SP-Sephadex C-25 and C-50 were also obtained from Pharmacia Fine Chemicals Ltd. Both ion exchangers have the capacity of 2.3 ± 0.3 meq./g. SP-Sephadex C-25 has a higher degree of cross-linkage than C-50.

Enzymic reaction in dextran or dextran sulfate solution The

reaction was allowed to run in most case at pH 4.5 with 0.05 mol/l acetate buffer at 25°C in a test tube immersed in a thermostatically controlled water bath. Britton-Robinson buffer (0.029 mol/l)[8] was used for measurement of pH dependency of the enzyme activity. The effect of dextran sulfate on the kinetic parameters was examined with 0.01 mol/l acetate buffer.

Two ml of the enzyme solution was added to the mixture of 4 ml of maltose and 6 ml of buffer, dextran or dextran sulfate solution. Dextran or dextran sulfate was dissolved in the same buffer as maltose and enzyme. The maltose concentration was in the range of 0.28 to 4.16 mmol/l. At appropriate time intervals (usually 1 min), 1 ml of the reaction mixture was removed from the reaction vessel and put into 1 ml of 0.5 mol/l NaOH solution to stop the reaction. Scores of minutes later, 1 ml of 0.5 mol/l acetic acid and 1 mol/l phosphate buffer were added to the sampled solution and the pH of the solution was adjusted to 6.5. The amount of glucose produced was determined by Glucostat method.[9]

Fluorescence measurements. Fluorescence measurements were performed in 0.05 mol/l acetate buffer (pH 4.5) at 25°C with a spectrofluorometer (Union Giken Ltd. High Sens. Spectrofluorometer FS 401). The fluorescence spectra of glucoamylase in the presence and absence of dextran were measured at the wavelength of excitation, 280 nm. The wavelength of emission was scanned from

300 nm to 400 nm. If the fluorescence intensity of an enzyme changed by binding of a ligand to the specific site of the enzyme, the dissociation constant of the enzyme-ligand complex can be estimated by measuring the change in fluorescence intensity of the enzyme solution due to the change in the ligand concentration. This method is generally called the fluorescence titration.[10)]

The fluorescence titration of glucoamylase with dextran was carried out at constant concentration of the enzyme by the successive dilution method,[10)] as follows: a definite amount of glucoamylase-dextran mixture was withdrawn from a cuvette after the first measurement had been made, and the same volume of the enzyme solution was added to the cuvette to give a lower concentration of dextran. The wavelength of excitation and emission for fluorescence titration experiment were 285 nm and 340 nm, respectively. The enzyme solution was used as a standard to correct for instrumental signal drift with time.

Measurement of dielectric constant. The dielectric constant of dextran solution of various concentrations were measured on TC-1C Ratio Arm Transformer Bridge (Ando Denki Co.) at 25°C in the frequency range of 0.1 to 1.0 MHz.[11)]

The dielectric constants for methanol solution were estimated by interpolating from the published values.[12)]

Immobilization of glucoamylase. Glucoamylase was immobilized to SP-Sephadex C-25 and C-50 by ionic linkage. The ion exchangers were adequately equilibrated with an acetate buffer and lyophilized. Approximately 0.03 g of the lyophilized SP-Sephadex was accurately weighed and swollen for two days with 5 ml of the buffer in a test tube (I.D. 22 mm). Twenty ml of glucoamylase solution of appropriate concentration was added and equilibrated under magnetical stirring at 25°C. After adsorption reached equilibrium, 5 ml of the outer solution was taken to determine the enzyme activity in it with maltose as substrate. The amount of glucoamylase immobilized to SP-Sephadex was estimated from the difference between the initial amount and that in the outer solution.

Determination of kinetic parameters of immobilized glucoamylase. By addition of 5 ml of maltose to 20 ml of an immobilized glucoamylase suspension, the reaction was allowed to run under conditions where the intraparticle and film diffusion resistances of the substrate were ignored. At appropriate time intervals, 0.5 ml of the outer solution was sampled from the suspension through a pipette equipped with a glass filter (Top G-2), and the amount of glucose produced was determined by Glucostat method.[9] The time course usually included eight points. To estimate the reaction velocity of the immobilized enzyme, increase of the enzyme concentration resulting from decrease in volume of the outer solution

due to sampling was corrected. The reaction velocity of the immobilized glucoamylase was determined by subracting the activity due to the enzyme in the outer solution from that of the immobilized enzyme suspension. The initial concentration of maltose was in the range of 0.5 mmol/l to 10 mmol/l. The apparent Michaelis constant Km(app) and the apparent rate constant of degradation of maltose k_0(app) of immobilized glucoamylase were estimated by Hofstee plot. The pH and ionic strength of acetate buffer were varied, and Km(app) and k_0(app) were obtained.

Water regain. The SP-Sephadex swollen adequately in a buffer was filtered through a glass filter (Top 4G-2). The water regain of the ion exchangers was calculated from the difference between the wet weight and the dry weight.

4. 3. Theoretical Considerations

Estimation of pH in ion exchanger. To predict the kinetic parameters of immobilized enzymes, the pH in ion exchangers must be known. The following assumptions were made to estimate pH in ion exchangers theoretically; (1) Donnan's equilibrium is established between the phase of ion exchanger and that of the outer solution,[2] (2) the effect of charge of glucoamylase on the equilibrium is negligible since the amount of the enzyme loaded to the ion exchanger is small and (3) the activity coefficients of

ions in the ion exchanger phase are the same as those in the outer solution phase. The difference between the electrostatic potential in the ion exchanger phase and that in the outer solution phase, $\Delta\phi$, is expressed by the following equations with regard to the component i of acetate buffer.

$$\Delta\phi = RT\ln(C_{H^+}/\bar{C}_{H^+}) - \Pi V_{H^+} \tag{4-1}$$

$$\Delta\phi = RT\ln(C_{Na^+}/\bar{C}_{Na^+}) - \Pi V_{Na^+} \tag{4-2}$$

$$\Delta\phi = RT\ln(\bar{C}_{CH_3COO^-}/C_{CH_3COO^-}) + \Pi V_{CH_3COO^-} \tag{4-3}$$

$$\Delta\phi = RT\ln(\bar{C}_{OH^-}/C_{OH^-}) + \Pi V_{OH^-} \tag{4-4}$$

where R is the gas constant, T the absolute temperature, Π the swelling pressure and V_i the partial molar volume. C and $\bar{C}$ denote the concentrations in outer solution phase and in ion exchanger phase, respectively. Since the electroneutrality must be held in the ion exchanger,

$$\bar{C}_{R^-} + \bar{C}_{CH_3COO^-} + \bar{C}_{OH^-} = \bar{C}_{Na^+} + \bar{C}_{H^+} \tag{4-5}$$

where $\bar{C}_{R^-}$ is the concentration of ionogenic sulfopropyl group in the ion exchanger and can be calculated from the exchange capacity, the density and the water regain of the ion exchanger. The pressure term ΠV_i can be ignored because the V_i values are small. From Eqs. (4-1) - (4-5), the concentration of hydrogen ion in the ion exchanger $\bar{C}_{H^+}$ is given by Eq. (4-7)

$$\bar{C}_{H^+} = \frac{\bar{C}_{R^-} + [\bar{C}_{R^-}{}^2 + 4(C_{H^+} + C_{Na^+})(C_{CH_3COO^-})]^{1/2}}{2[1 + (C_{Na^+}/C_{H^+})]} \qquad (4\text{-}6)$$

Thus, the pH in the ion exchanger can be calculated from the concentration of each component in the outer solution.

4. 4. Results and Disdussion

Reactions in dextran solution. In order to examine the effect of dextran on the glucoamylase-catalyzed reaction, the Michaelis constant Km and the rate constant k_0 during the course of degradation of the enzyme-substrate complex were determined in dextran solutions of various concentrations. The Hoffstee plots are shown in Fig. 4-1. As shown in Fig. 4-1, the Km value is constant, while the k_0 value decreases with the increasing dextran concentrations. These results suggest that dextran is apparently a noncompetitive inhibitor of glucoamylase.

Then, the ratio of the maximum velocity in the presence of dextran Vm^D to that in the absence of dextran Vm is given by

$$Vm/Vm^D = 1 + C_I/Ki \qquad (4\text{-}7)$$

where C_I and Ki are the inhibitor concentration and the inhibitor constant, respectively. Figure 4-2 shows the linear relationship between Vm/Vm^D and C_I. The Ki value was calculated as 34%(w/v).

Since the noncompetitive inhibition of dextran seemed some-

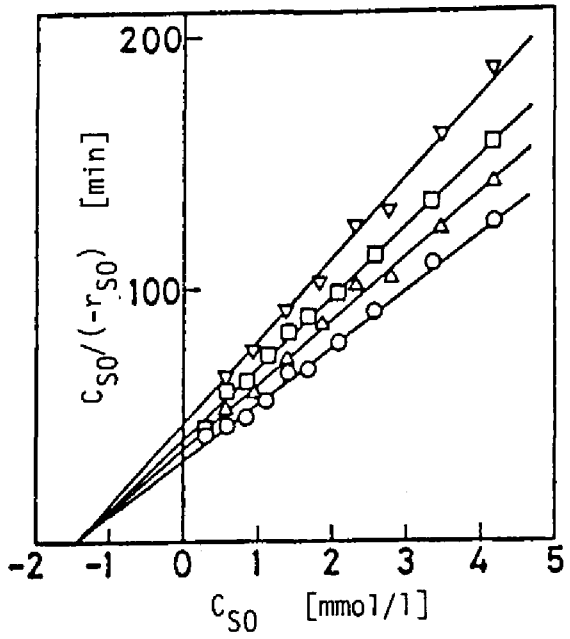

Fig. 4-1. Hofstee plots for the hydrolysis of maltose by glucoamylase in dextran solutions. The reaction was allowed to run at pH 4.5 with 0.05 mol/l acetate buffer at 25°C in 0%(○), 5%(△), 10%(□) and 15%(▽) dextran solutions. The enzyme concentration was 5×10^{-7} mol/l.

what peculiar, other factors by which this phenomenon could be explained were sought for. Ono *et al.*[13] reported that in a bacterial α-amylase-catalyzed reaction the k_0 value decreased with the decrease of the dielectric constant of the solution, while the Km value was kept constant. According to Moriyama *et al.*,[11] the dielectric constant of dextran solution decreased with the increase of dextran concentration. A well established theory[14] about the influence of dielectric constant on the enzyme reaction suggests a linear relationship between Km value and the re-

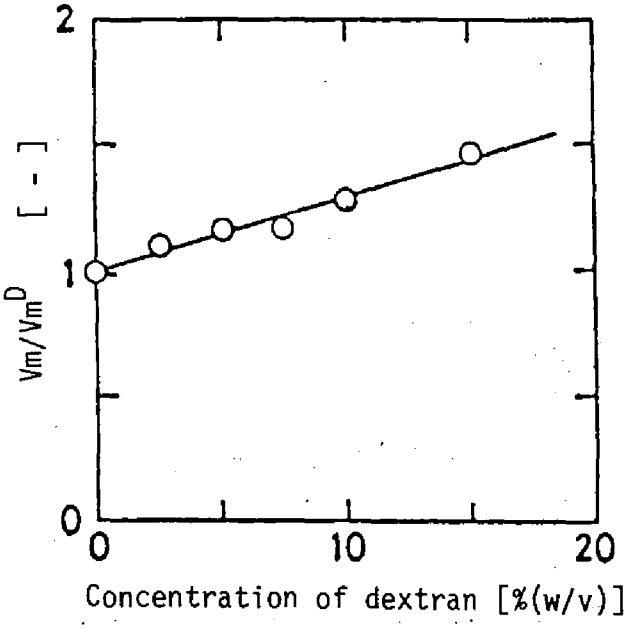

Fig. 4-2. Plot of Vm/Vm^D *versus* concentration of dextran. The intercept of ordinate gives the Ki value 34 %(w/v).

ciprocal of dielectric constant ε and that between k_0 value and $1/\varepsilon$. Figure 4-3 shows plots of the logarithms of k_0 and Km values obtained in dextran solutions *versus* $1/\varepsilon$. In Fig. 4-3, the same plots obtained in methanol solutions of various concentrations are also shown to be compared with those in dextran solutions. Although the straight lines were obtained, the tendency of the k_0 value in dextran solution was different from that in methanol solution. Accordingly, it is concluded that the decrease of the k_0 value in the presence of dextran can not be explained by the change of dielectric constant of the solution.

The exclusion and sieving effects were also rejected since the

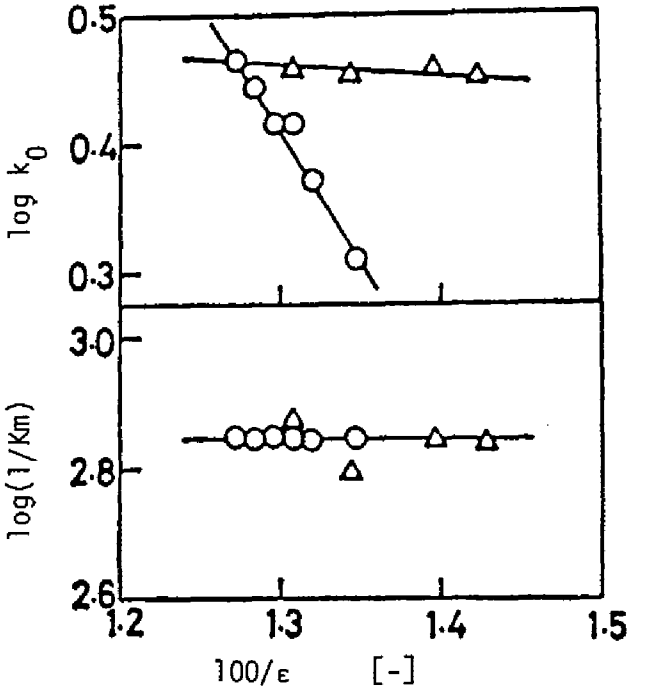

Fig. 4-3. Plots of log(I/Km) and log k_0 *versus* the reciprocal of the dielectric constant of dextran (○) and methanol (△) solution.

Km value did not change with dextran concentrations. The binding of dextran to glucoamylase was confirmed by fluorescence titration of the enzyme with dextran as shown later.

Reactions in dextran sulfate solution. In order to examine the effect of ployelectrolyte on the glucoamylase-catalyzed reaction, the Km and k_0 values were estimated in dextran sulfate solution at pH 4.5, 4.0 and 3.5 with 0.01 mol/l acetate buffer. The results are shown in Fig. 4-4. The dependency of the Km and k_0 values on dextran sulfate concentration is not observed at pH 4.5

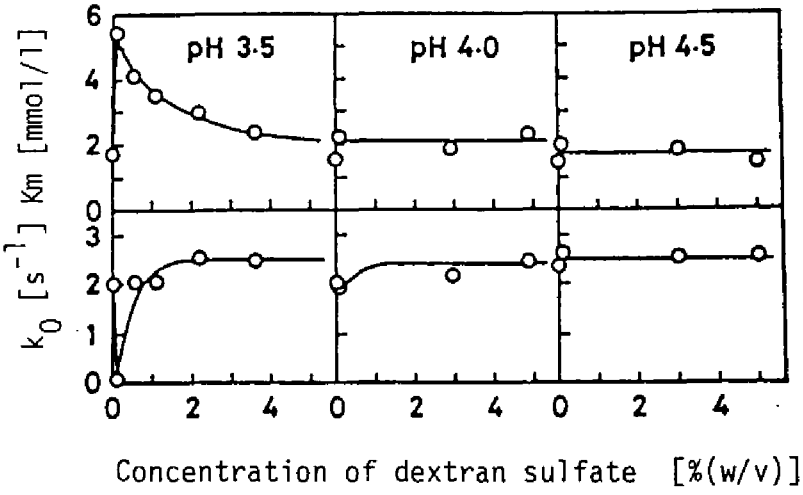

Fig. 4-4. Dependency of kinetic parameters on concentration of dextran sulfate at pH 3.5, 4.0 and 4.5 in 0.01 mol/l acetate buffer at 25°C.

and 4.0. At pH 3.5, however, the kinetic parameters depended remarkably on dextran sulfate concentration. As shown before, the k_0 value decreased in dextran solution at pH 4.5. These findings suggest some interaction between the enzyme and negatively charged dextran sulfate.

pH-activity curves. Figure 4-5 shows the pH-activity curves in the hydrolysis of maltose with glucoamylase obtained in 0.029 mol/l Britton-Robinson buffer, dextran and dextran sulfate solution. There is not a large difference between the curves obtained in the buffer and dextran solution, while the pH optimum in dextran sulfate solution shifts slightly to an alkaline pH. The decrease of the activity in dextran sulfate solution below pH 4.0

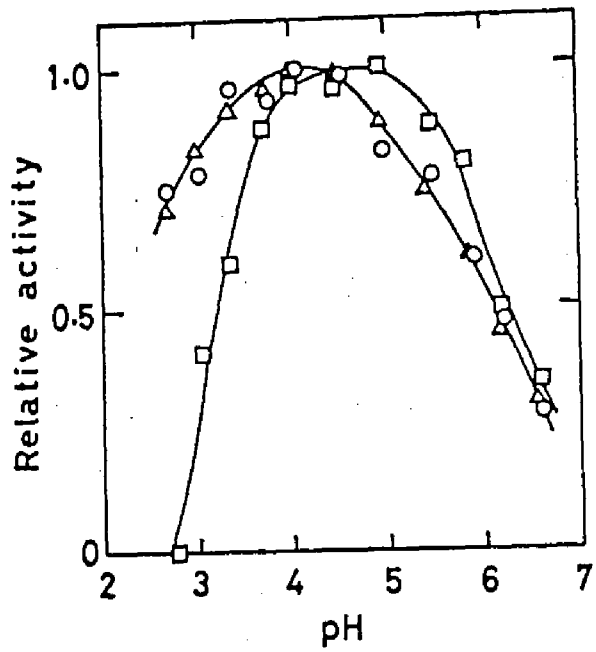

Fig. 4-5. pH-activity curves in the hydrolysis of maltose by glucoamylase. The enzyme and maltose concentrations were 5 X 10^{-7} mol/l and 1.11 X 10^{-2} mol/l, respectively. ○, 0.029 mol/l Britton-Robinson buffer; △, 10% dextran; □, 0.5% dextran sulfate.

is considerably great as compared with that obtained in the buffer solution. These results also indicate that there might be some interactions between the enzyme and dextran sulfate.

Spectrofluorometry. The fluorescence spectra of glucoamylase in 0.05 mol/l acetate buffer and dextran solution are shown in Fig. 4-6. The peak of fluorescence intensity appeared near 350 nm in both cases. The relative fluorescence intensity clearly decreased by the addition of dextran. The fluorescence peak near

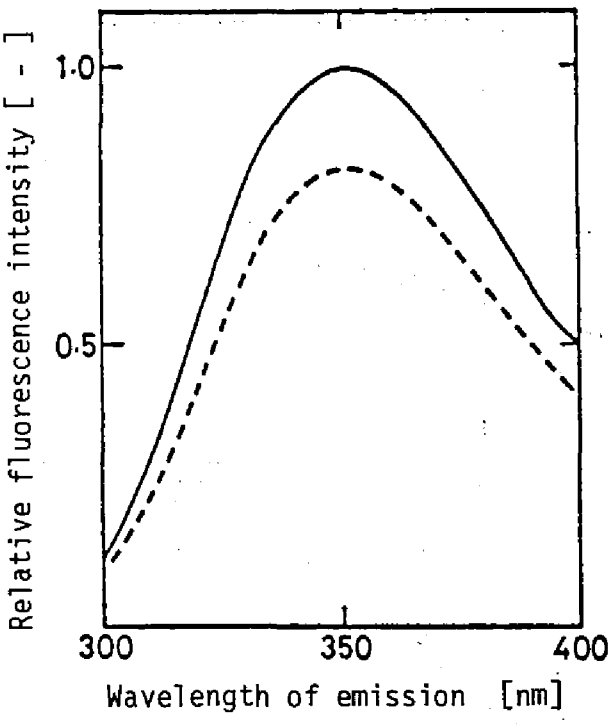

Fig. 4-6. Fluorescence spectra of glucoamylase in 0.05 mol/l acetate buffer (pH 4.5) at 25°C. The glucoamylase concentration was 1.31 X 10^{-6} mol/l. Samples were excited at 280 nm in acetate buffer (——) and 8.4%(w/v) dextran (----) solution.

350 nm may be due to tryptophan residure, which is located at the first subsite of the enzyme.[15)]

Supposing the binding of dextran to glucoamylase, the fluorescence titration of the enzyme with dextran was performed. Binding equilibrium between free enzyme E and dextran D is

$$E + D \underset{}{\overset{Kd}{\rightleftharpoons}} ED \qquad (4\text{-}8)$$

where Kd and ED represent the dissociation constant and the gluco-

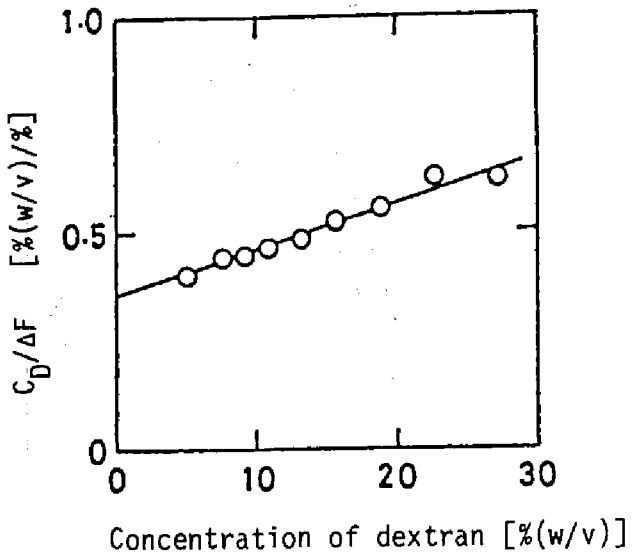

Fig. 4-7. Plot of $C_D/\Delta F$ *versus* Concentration of dextran for fluorescence titration of glucoamylase with dextran at pH 4.5 and 25°C. Glucoamylase concentration, 1.33×10^{-6} mol/l; wavelength of excitation, 285 nm; wavelength of emission, 340 nm.

amylase-dextran complex, respectively. Then, the difference of the fluorescence intensities in the presence and absence of dextran, ΔF, is expressed by Eq. (4-9) as a function of the total enzyme concentration C_{E0} (free plus bound) and dextran concentration C_D.

$$C_D/\Delta F = C_D/(f \cdot C_{E0}) + Kd/(f \cdot C_{E0}) \qquad (4\text{-}9)$$

where f is the difference between the molar fluorescence intensities of the enzyme E and bound enzyme ED. The nonspecific decrease of fluorescence intensity with increase of the concentration of

dextran might be included in the results of titration. L-Tryptophan ethyl ester is considered as model compound of the first subsite of glucoamylase, and considering the nonspecific decrease evaluated from the decrease of fluorescence intensity of L-tryptophan ethyl ester in dextran solution, the results of titration experiment were corrected.

As shown in Fig. 4-7, $C_D/\Delta F$ is proportional to C_D and the Kd value is calculated as 34%(w/v). This value coincides with the Ki value obtained by the inhibition experiment. Thus, the binding was again confirmed.

Fluorescence spectra seem to indicate that the binding of dextran occurs at the first subsite of glucoamylase which is the subsite adjacent to the catalytic site. This finding suggests a competitive inhibition of dextran, whereas the kinetic experiments clearly showed a noncompetitive inhibition. This conflict is resolved by applying the subsite theory.[16] The details are shown in Appendix.

The effect of dextran on the glucoamylase-catalyzed maltose hydrolysis appeared as the decrease of maximum reaction rate. This effect could be explained neither by exclusion and sieving effects nor by the decrease of dielectric constant of solution, but it could be understood by the noncompetitive binding between glucoamylase and dextran. The concentration of dextran, the carrier component, is about 10%(w/v) when Sephadex G-100 is used as a car-

rier of immobilized glucoamylase. The lowering of the reaction rate is at most 30%.

The significant change of kinetic parameters in dextran sulfate solution may be due to the electrostatic effect. Thus, the apparent kinetic parameters of glucoamylase immobilized on a cation exchanger may be influenced not only by the change of pH inside the carrier but also by the electrostatic interaction between charge of the enzyme and that of carrier.

Kinetic parameters of immobilized glucoamylase. The rate constant of degradation of maltose k_0(app) and the Michaelis constant Km(app) of glucoamylase immobilized onto SP-Sephadex C-25 and C-50 were estimated at various pH values using 0.01 mol/l and 0.05 mol/l acetate buffer. The k_0(app) and Km(app) are shown in Fig. 4-8 against pH of the outer solution together with k_0 and Km of free glucoamylase. Since the k_0 and Km of free glucoamylase did not depend on the ionic strength of the buffer, the k_0 and Km in this study were determined using 0.01 mol/l acetate buffer. The k_0(app) and Km(app) are considered to be true kinetic parameters for the immobilized glucoamylase, because the reaction was allowed to run under the conditions where the intraparticle and film diffusion resistances of the substrate could be ignored.

It has been presented that the effect of the constituent of SP-Sephadex on the kinetic parameters is negligible. The shift of pH dependency of k_0(app) to alkaline pH was observed and there

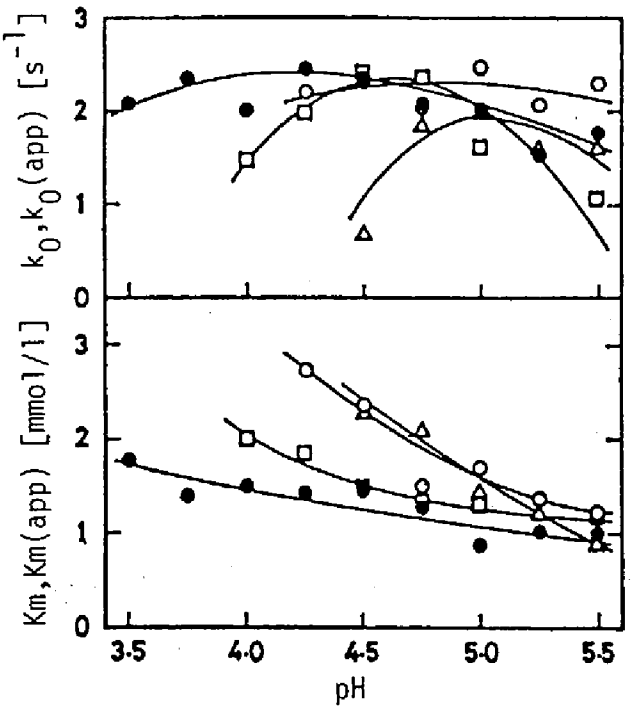

Fig. 4-8. Plots of the kinetic parameters of free and immobilized glucoamylase *versus* pH in outer solution at 25°C. ●, free glucoamylase; ○, immobilized to SP-Sephadex C-50 in 0.01 mol/l acetate buffer; □, to C-50 in 0.05 mol/l and △, to C-25 in 0.01 mol/l.

was a considerable difference between Km and Km(app). As many investigators[2,17,18] have pointed out, these results seem to be due to a difference between pH in the ion exchanger and that in the outer solution. We tried to estimate pH theoretically in the ion exchanger and to replot these results against the estimated inner pH. The water regain Wr of SP-Sephadex C-25 and C-50 was measured at various ionic strengths. In Fig. 4-9, Wr is plotted against the concentration of sodium ion. The highly cross-linked SP-Sephadex C-25 gave a lower water regain than C-50. In Fig. 4-10, the

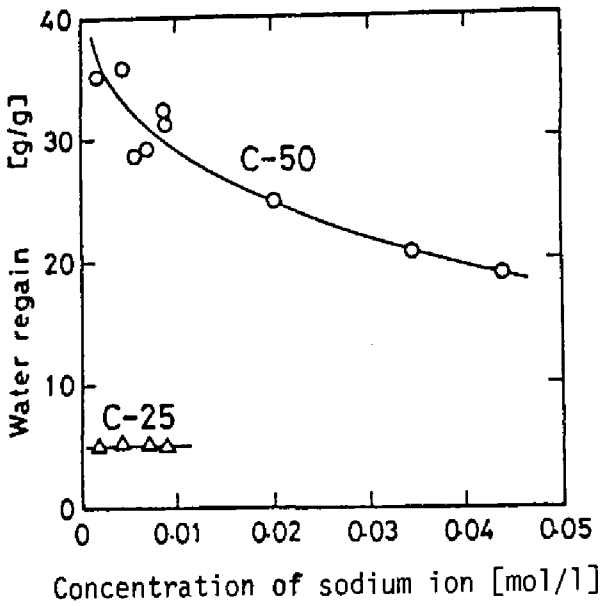

Fig. 4-9. Water regain of SP-Sephadex C-25 and C-50. The acetate buffer with various pH values was used.

kinetic parameters of the immobilized glucoamylase are replotted against pH in the ion exchanger, which was estimated using Eq. (4-6). The relation of kinetic parameters of the immobilized glucoamylase to pH in the ion exchanger is in a fairly good agreement with that of kinetic parameters of the free enzyme to pH in the outer solution. This implies the appropriateness of application of Eq.(4-6) in estimating the pH in the ion exchanger.

From a view point of industrial application of the immobilized glucoamylase, the experimental results obtained were summarized in relation to a fraction Y of glucoamylase adsorbed and a fractional retention of the enzyme η, which are defined as the ratio of the amount of the enzyme adsorbed to SP-Sephadex to the initial amount

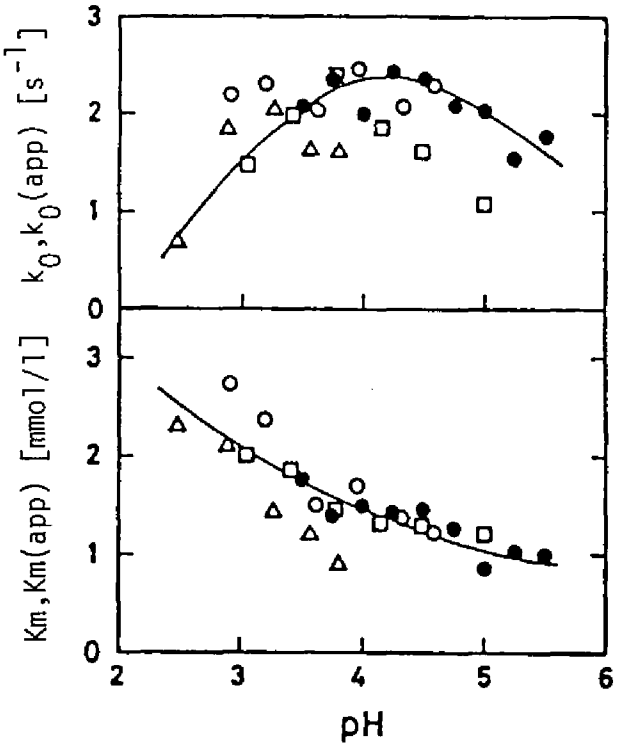

Fig. 4-10 Plots of the kinetic parameters of immobilized glucoamylase *versus* pH in SP-Sephadex. The pH in the ion exchanger was evaluated by Eq. (4-6). The symbols are the same as used in Fig. 4-8.

of the enzyme and the ratio of $Y(k_0(app)/Km(app))$ value of the immobilized glucoamylase to (k_0/Km) value of the free enzyme obtained at optimum pH 4.5, respectively. η is slightly different from "true" fractional retention of the enzyme activity, $Y(k_0(app)/k_0)$ defined by Yamane.[19] In Fig. 4-11, Y and η are plotted against pH in the outer solution. Figure 4-11 shows that the operations are the most advantageous at pH 5.5, 5.0 and 4.5 in the SP-Sephadex C-25∿0.01 mol/l acetate buffer system, in C-50∿0.01 mol/l sys-

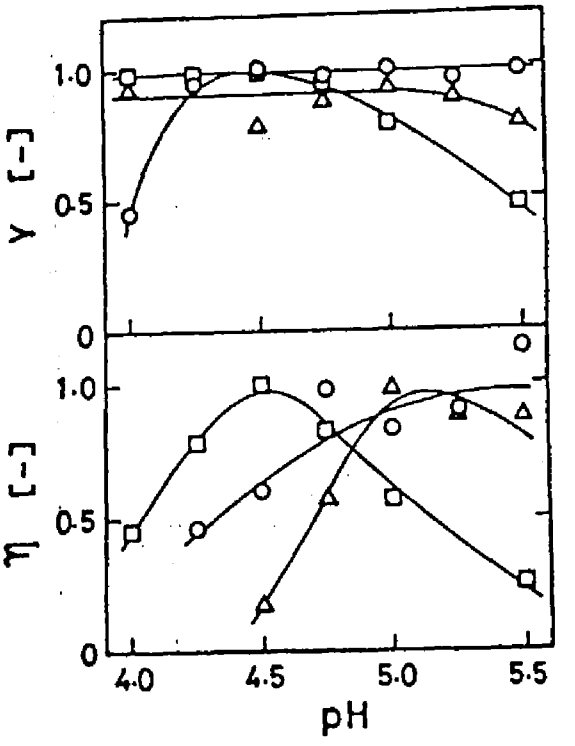

Fig. 4-11. Relations of Y and η to pH in outer solution. The Y and η were defined in the text. The symbols are the same as used in Fig. 4-8.

tem and in C-50∿0.05 mol/l system, respectively.

4. 5. Summary

The hydrolysis of maltose by glucoamylase (EC 3.2.1.3 from *Rhizopus niveus*) was carried out in the presence and absence of dextran and dextran sulfate, which are the components of supports of immobilized enzymes. The interaction between dextran and the enzyme was observed by the fluorescence spectrophotometry. The kinetic and fluorescence experiments indicated that dextran bound

to glucoamylase and was apparently a noncompetitive inhibitor of the enzyme. The dissociation constant of the enzyme-dextran complex was estimated to be 34%(w/v). The reaction rate was hardly affected at pH 4.0 and 4.5 by addition of dextran sulfate, while the kinetic parameters depended considerably on the concentration of dextran sulfate at pH 3.5. These findings indicated that there might exist some interactions between the enzyme and dextran sulfate.

Glucoamylase was immobilized to SP-Sephadex C-25 and C-50 by ionic linkage. The kinetic properties of the immobilized glucoamylase were quantitatively investigated using maltose as substrate. The change of kinetic parameters, k_0 and Km, due to immobilization was explaned in terms of decrease of pH in the ion exchanger, which was estimated from Donnan's equilibrium.

Appendix

According to the subsite theory,[16] glucoamylase has seven subsites and the subsite affinities of the first subsite to the seventh one are 0.00, 4.85, 1.59, 0.43, 0.22, 0.11 and 0.10 kcal/mol, respectively. The catalytic site is located between the first and the second subsites.

The reaction scheme is as follows: (1) Dextran binds specifically to the first subsite as suggested by fluorescence spectrum. (2) Maltose binds to the enzyme in productive and nonproductive

modes. (3) When dextran occupies the first subsite, maltose can bind to the enzyme only nonproductively. This scheme is expressed in Eqs.(4-10) to (4-13).

$$E + S \overset{Km}{\rightleftharpoons} ES_1 \xrightarrow{k_0} E + P \tag{4-10}$$

$$E + S \overset{Km'}{\rightleftharpoons} ES_2 \quad \text{(nonproductive)} \tag{4-11}$$

$$E + D \overset{Ki}{\rightleftharpoons} ED \tag{4-12}$$

$$ED + S \overset{Km'}{\rightleftharpoons} EDS \quad \text{(nonproductive)} \tag{4-13}$$

where Km, Km' and Ki represent the dissociation constants of ES_1, ES_2 or EDS, and ED complexes, respectively. It is pointed out that these equations do not include noncompetitive inhibition scheme but possess competitive one potentially when maltose was used as a substrate. Then, the reaction rate r_S is given by

$$-r_S = \frac{k_0 \cdot C_{E0} \cdot C_S}{Km(1 + C_S/Km + C_S/Km' + C_I/Ki + C_I \cdot C_S/Ki \cdot Km')} \tag{4-14}$$

The Km and Km' values can be calculated using the above subsite affinities. Since the calculated Km value is far greater than the calculated Km' value, the C_S/Km term in the denominator of Eq.(4-14) can be neglected as compared with the C_S/Km' term. Then, the reaction rate is approximated by Eq.(4-15).

$$-r_S = \frac{k_0 \cdot Km' \cdot C_{E0} \cdot C_S}{Km(Km' + C_S)(1 + C_I/Ki)} \tag{4-15}$$

This equation clearly shows the noncompetitive inhibition scheme. If the substrate is higher oligomer than maltose, the Km value is the same order as the Km' value. Then, noncompetitive inhibition may not appear.

Nomenclature

C	concentration in outer solution phase	[mol/l], [%(w/v)]
$\bar{C}$	concentration in ion exchanger phase	[mol/l]
F	fluorescence intensity	[-]
f	difference between the molar fluorescence intensities of the free enzyme and bound enzyme	[l/mol]
Kd	dissociation constant	[%(w/v)]
Ki	inhibitor constant	[%(w/v)]
Km	Michaelis constant	[mol/l]
k_0	rate constant	[s^{-1}]
R	gas constant	[J/K·mol]
r	reaction rate	[mol/l·s]
T	absolute temperature	[K]
Vm	maximum reaction rate	[mol/l·s]
V	partial molar volume	[l/mol]
Wr	water regain	[g/g-gel]
Y	fraction of the enzyme adsorbed	[-]
ε	dielectric constant	[$C^2/N \cdot m^2$]

η	dielectric constant	$[C^2/N \cdot m^2]$
Π	swelling presure	[atm]
ϕ	electrostatic potential	[V]

Subscripts

D	dextran
E	enzyme
I	inhibitor
S	substrate
0	initial

Literature Cited

1) M. D. Lilly and A. K. Sharp, *Chem. Eng. (London)*, 46, CE-12 (1968).

2) L. Goldstein, Y. Levin, and E. Katchalski, *Biochemistry*, 3, 1913 (1964).

3) E. Katchalski, *Proc. IV IFS: Ferment. Technol. Today*, 1972, p.353.

4) T. C. Laurent, *Eur. J. Biochem.*, 21, 498 (1971).

5) B. Mattiasson, A. C. Johansson, and K. Mosbach, *Eur. J. Biochem.*, 46, 341 (1974).

6) Y. Tsujisaka, *Bulletin of the Osaka Municipal Technical Research Institute*, 23, 15, 20 (1960).

7) M. Ohnishi, T. Yamashita, and K. Hiromi, *J. Biochem. (Tokyo)*, 79, 1007 (1976).

8) H. T. Britton and R. A. Robinson, *J. Chem. Soc.*, 1931, 1456.

9) E. C. Toren, Jr., *J. Chem. Educ.*, 44, 172 (1967).

10) A. J. Pescen, C.-G. Rosén, and T. L. Pasby, "*Fluorescence Spectoscopy*," Marcel Dekker Inc., New York, 1971, p.203.

11) S. Moriyama, R. Matsuno, and T. Kamikubo, *Agric. Biol. Chem.*, 41, 1985 (1977).

12) R. Davis and T. Jones, *Phil. Mag.*, 28, 307 (1939).

13) S. Ono, K. Hiromi, and Y. Sano, *Bull. Chem. Soc. Jpn*, 36, 431 (1963).

14) K. Hiromi, *Bull. Chem. Soc. Jpn*, 33, 1251, 1264 (1960).

15) M. Ohnishi, H. Kegai, and K. Hiromi, *J. Biochem. (Tokyo)*, 77, 695 (1975).

16) K. Hiromi, *Biochem. Biophys. Res. Commun.*, 40, 1 (1970).

17) "*Immobilized Enzymes*," ed. by I. Chibata, Chapters 3 and 5, Kodansha, Tokyo, 1975.

18) C. W. Wharton, E. M. Crook, and K. Brocklehurst, *Eur. J. Biochem.*, 6, 572 (1968).

19) T. Yamane, *Biotechnol. Bioeng.*, 19, 749 (1977).

Chapter 5

Stability of Enzyme Immobilized by Ionic Linkage

5. 1. Introduction

Binding affinity of enzymes to ion exchangers by ionic linkage is relatively weak and affected by ionic strength of solutions. This property is considered to be a defect of enzyme immobilization by ionic linkage. This defect, however, can be compensated by many advantages, *i.e.*, simpleness of immobilization process, easiness of regeneration, retention of high enzyme activity as well as substrate specificity after immobilization. These merits suggest usefulness of immobilization of enzymes by ionic linkage for industrial purposes. Actually, application of immobilized enzyme by ionic linkage to industrial process led to a great success.[1)]

During the last twenty years, extensive studies have been done on immobilization techniques of enzymes and properties of the immobilized enzymes. Some workers elucidated general properties of immobilized enzymes such as the effect of mass transfer on kinetic parameters.[2-4)] In previous chapter, we also have reported on the effect of dextrans, constituents of carrier for immobilization on glucoamylase-catalyzed reaction.

In this chapter, characteristics of immobilized enzyme by ionic linkage were studied using glucoamylase immobilized onto SP-Sephadex C-25 and C-50 as model system. Distribution coefficients of

glucoamylase between the ion exchangers and liquid phase and diffusion coefficients of the enzyme in the ion exchanger were obtained. A theoretical equation to predict the half-life of activity of immobilized enzymes caused by desorption of enzymes was proposed in terms of the distribution coefficient, the diffusion coefficient and the operational variables of continuous reaction.

5. 2. Materials and Methods

Materials. Glucoamylase (EC 3.2.1.3, pure grade, from *Rhizopus niveus*) was purchased from Seikagaku Kogyo. The enzyme was used without further purification. The enzyme concentration was determined spectrophotometrically using an absorption coefficient, $E_{280}^{1\%}$ 13.6 cm^{-1} and the molecular weight, 56,000.[5] SP-Sephadex C-25 and C-50 were obtained from Pharmacia Fine Chemicals. Both ion exchangers have the capacity of 2.3 $\pm$ 0.3 meq./g. SP-Sephadex C-25 has a higher degree of cross-linkage than C-50. Other reagents were purchased from Wako Pure Chemical Industries and Nakarai Chemicals. Every chemical was of analytical grade.

Distribution coefficient. Approximately 0.01 g of lyophilized SP-Sephadex exactly weighed was adequately swollen in 5 ml of acetate buffer (pH 5.0). After addition to it of 20 ml of glucoamylase solution of known concentration, the mixture was equilibrated under shaking at 25°C. Then, the enzyme concentration remaining in the outer solution, C_{le} was determined in terms of the

enzyme activity using maltose as substrate. The amount of the enzyme adsorbed on the ion exchanger was calculated from the difference between the initial amount and that in the outer solution at the adsorption equilibrium. The amount of the enzyme adsorbed on the ion exchanger was converted into molar concentration, C_{2e}, using the water regain and the density of the ion exchanger (C-25; 1.54g/cm^3, C-50; 1.86 g/cm^3). At lower C_{1e}, C_{2e} is related to C_{1e} by the following equation as discussed in Theoretical Considerations.

$$C_{2e} = K \cdot C_{1e} \tag{5-1}$$

where K is the distribution coefficient. The enzyme concentration in the ion exchanger was obtained for various concentrations C_{1e}. They were plotted in a log-log co-ordinate and K value was evaluated.

Diffusion coefficient of glucoamylase in SP-Sephadex. Diffusion coefficients of glucoamylase in SP-Sephadex were determined by analyzing the non-steady state of adsorption process. An appropriate amount of lyophilized SP-Sephadex was swollen in 100 ml of acetate buffer (pH 5.0). Then, 100 ml of glucoamylase solution of known concentration was added to it. Mixing of solution was accomplished with a magnetically rotated bar. At appropriate time intervals, 0.5 ml of the outer solution was pipetted through a glass filter. The concentration C_1 was estimated from the activity. A fraction M of the enzyme adsorbed at any time t is defined by

Eq.(5-2)

$$M = (C_{10} - C_1)/(C_{10} - C_{1e}) \tag{5-2}$$

where C_{10} and C_{1e} are the enzyme concentrations at t = 0 and at the adsorption equilibrium, respectively. The diffusion coefficient in the ion exchanger D_e was determined so that M calculated by the following equation[6] would fit with the experimental M.

$$M = 1 - \sum_{k=1}^{\infty} \frac{\exp(-\lambda_k^2 D_e t/R^2)}{(3\alpha/2) + \lambda_k^2/6(1+\alpha)} \tag{5-3}$$

where

$$\alpha = KW/\varepsilon V\rho \tag{5-4}$$

and λ_k is the kth root of λ in Eq.(5-5).

$$\lambda^2 = 3\alpha[(\lambda/\tan\lambda) - 1] \tag{5-5}$$

V represents the volume of the bath of solution, ε the void fraction of the bath, W the weight, R the radius and ρ the density of the swollen ion exchanger. R was measured by an optical mirography (Nikon S-Ke). When $(D_e t/R^2)^{1/2} < 0.1$, Eq.(5-3) is approximated to the following equation.[7]

$$M = (1 + \frac{1}{\alpha})[1 + \frac{\gamma_1}{\gamma_1+\gamma_2} e\,\mathrm{erfc}\{3\alpha\gamma_1 (D_e t/R^2)^{1/2}\}$$

$$- \frac{\gamma_2}{\gamma_1 + 2} \text{eerfc}\{-3\alpha\gamma_2 (D_e t/R^2)^{1/2}\}] \qquad (5\text{-}6)$$

where

$$\gamma_1 = (1/2)[\{1 + (4/3\alpha)\}^{1/2} + 1] \qquad (5\text{-}7a)$$

$$\gamma_2 = \gamma_1 - 1 \qquad (5\text{-}7b)$$

and $$\text{eerfc}(x) \equiv \exp(x^2) \cdot \text{erfc}(x) \qquad (5\text{-}8)$$

Following assumption are included in the derivation of the above equation; (1) adsorption equilibrium is instantaneously attained at the surface of the ion exchanger[8] and (2) effect of mass transfer through the stagnant film adjacent to the surface of the ion exchanger is negligible. The diffusion coefficient D_e determined here is the apparent one in the ion exchanger as discussed in Theoretical Considerations.

5. 3. Theoretical Considerations.

Distribution coefficient. When the equilibrium concentration of enzyme is sufficiently low, an approximate equation for the distribution coefficient K is derived using Donnan's equilibrium and the condition of electroneutrality.

$$K = (C_{R^-2}/C_{Na^+1})^Z \exp(-\Pi V_E/RT) \qquad (5\text{-}9)$$

where C_{R^-2} is the concentration of ionogenic sulfopropyl group in

the ion exchanger, Z the number of charge of glucoamylase, Π the swelling pressure, V_E the partial molar volume of glucoamylase, R the gas constant, and T the absolute temperature.

Leakage of enzyme from ion exchanger. Since the ionic linkage between enzymes and ion exchangers is reversible, the leakage of the enzymes is inevitable during the continuous reaction. A theoretical equation to represent the desorption process in the continuous reaction was proposed. The same assumptions as those in the estimation of diffusion coefficient were introduced. A mass balance equation of enzyme in ion exchanger is expressed by Eq.(5-10).

$$\frac{\partial C_2}{\partial t} = D_e \left(\frac{\partial^2 C_2}{\partial r^2} + \frac{2}{r} \cdot \frac{\partial C_2}{\partial r} \right) \tag{5-10}$$

where r is the radial distance and C_2 is the enzyme concentration defined as moles of the bound plus free enzymes per unit volume of the ion exchanger. As in the case of physical adsorption such as gas adsorption onto activated charcoal, there may exist two phases in the ion exchanger, *i.e.*, in one phase enzyme is in bound state and in the other in free state. However, in the case of adsorption by ionic linkage it is very difficult to distinguish these two phases. Therefore the C_2 defined above was used in the mass balance equation for simplicity. Thus, the diffusion coeffi-

cient D_e used in Eq.(5-10) is the apparent one. A mass balance equation of the enzyme in the outer solution for a continuous stirred tank reactor (CSTR) gives the following equation.

$$\frac{\partial C_1}{\partial t} = -(F/\varepsilon V)C_1 + \frac{3(1-\varepsilon)}{\varepsilon R}\left(-D_e\frac{\partial C_2}{\partial r}\right)\Bigg|_{r=R} \tag{5-11}$$

where F is the flow rate. The initial and boundary conditions are given as

$$\text{at } t = 0, \qquad C_1 = C_{10}, \quad C_2 = C_{20} \tag{5-12a}$$

$$\text{at } r = R, \qquad C_2 = K \cdot C_1 \tag{5-12b}$$

$$\text{at } r = 0, \qquad \partial C_2/\partial r = 0 \tag{5-12c}$$

These equations were solved in terms of the normalized outer concentration $C^*_1 = C_1/C_{10}$ and the normalized mean inner concentration $\overline{C}^*_2$ through Laplace transform method.

$$C^*_1 = \sum_{k=1}^{\infty} \frac{2B\exp(-A\xi_k^2\theta)}{A\xi_k^4 + (3AB + AB^2 - 2)\xi_k^2 + (1/A) - B} \tag{5-13}$$

$$\overline{C}^*_2 = 3\int_0^1 r^{*2}C^*_2\,dr^*$$

$$= \sum_{k=1}^{\infty} \frac{6\{(1/A\xi_k^2) - 1\}\exp(-A\xi_k^2\theta)}{A\xi_k^4 + (3AB + AB^2 - 2)\xi_k^2 + (1/A) - B} \tag{5-14}$$

where r^* is the normalized radial distance ($r^* = r/R$), C^*_2 the nor-

malized inner concentration ($C_2^* = C_2/C_{20}$), θ the normalized time ($\theta = t/(\varepsilon V/F)$) and

$$A = \varepsilon V D_e/FR^2 \tag{5-15a}$$

$$B = 3(1 - \varepsilon)K/\varepsilon \tag{5-15b}$$

ξ_k is the kth root of ξ in the following equation.

$$-A\xi^2 + 1 + AB[(\xi/\tan \xi) - 1] = 0 \tag{5-16}$$

The time course of leakage of the enzyme was computed by FACOM-M 190 at the data proceeding center, Kyoto University. The half-life of the immobilized enzyme caused by the leakage was estimated by varing A and B as parameters.

5. 4. Results and Discussion

Distribution coefficient. The distribution coefficient of glucoamylase to SP-Sephadex was estimated at 25°C, pH 5.0. In Fig. 5-1, the logarithm of C_{2e}, which is an equilibrium concentration of the enzyme in the ion exchanger, is plotted against that of C_{1e}. Each plot gave a straight line with a slope of unity over a wide range of the enzyme concentration and the K value calculated from each plot is summarized in Table 5-1. Dependency of K values obtained on ionic strength and type of ion exchanger can be well understood qualitatively by the theoretical equation Eq. (5-9). The difference between K value for SP-Sephadex C-50 $\sim$ 0.01

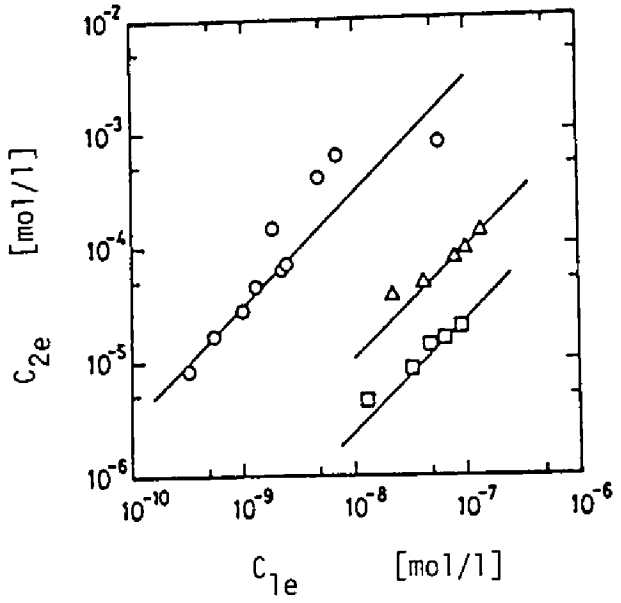

Fig. 5-1. Relation between C_{2e} and C_{1e} at pH 5.0 and 25°C. The C_{1e} and C_{2e} are the equilibrium glucoamylase concentration in outer solution and that in SP-Sephadex. ○, SP-Sephadex C-50 in 0.01 mol/l acetate buffer; □, C-50 in 0.05 mol/l and △, C-25 in 0.01 mol/l.

mol/l acetate buffer system and that for C-50 ∿ 0.05 mol/l acetate buffer system is ascribable to the effect of ionic strength. The difference between K value for C-50 and that for C-25 is ascribable to the difference of a swelling pressure, *i.e.*, swelling pressure of C-25 is higher than that of C-50.

Diffusion coefficient. Diffusion coefficients of enzymes in ion exchangers are important in view of preparation of the immobilized enzymes and leakage of the enzymes from the ion exchangers during continuous operation. The diffusion coefficient of gluco-

Table 5-1. Distribution and Diffusion Coefficients of Glucoamylase (25°C and pH 5.0).

Ion exchanger	Acetate buffer [mol/l]	R^a [cm]	Wr [g/g]	K [-]	D_e [cm^2/s]	$K \cdot D_e$ [cm^2/s]
SP-Sephadex C-50	0.01	1.1×10^{-2}	31.2	3.0×10^{4}	7×10^{-11}	2×10^{-6}
	0.05	9.5×10^{-3}	20.6	2.5×10^{2}	2×10^{-9}	0.5×10^{-6}
SP-Sephadex C-25	0.01	6.0×10^{-3}	5.0	1.0×10^{3}	1×10^{-9}	1×10^{-6}

a Surface mean diameter.

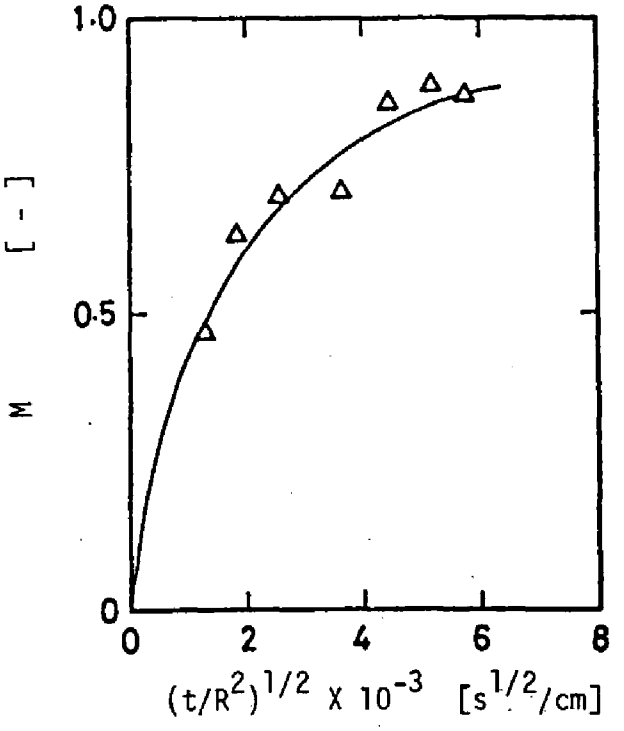

Fig. 5-2. Relation between M and $(t/R^2)^{1/2}$ for SP-Sephadex C-25 at 25°C. The buffer solution was 0.01 mol/l acetate buffer with pH 5.0. The M in an ordinate is defined in Eq. (5-2). The solid line was calculated from Eq. (5-6) using 1×10^{-9} cm^2/s as diffusion coefficient.

amylase in SP-Sephadex was estimated at 25°C, pH 5.0. Figure 5-2 shows a relation between a fraction of the enzyme adsorbed, M and $(t/R^2)^{1/2}$ for SP-Sephadex C-25 at pH 5.0 with 0.01 mol/l acetate buffer. The solid line in Fig. 5-2, which was calculated from Eq. (5-6) using 1 X 10^{-9} cm^2/s as D_e, shows a fairly good agreement with the experimental data under consideration of experimental errors. The diffusion coefficients in the ion exchangers are extremely low as compared with that of the enzyme in an acetate buffer solution (1.26 X 10^{-6} cm^2/s), which was measured with the Schlieren optical apparatus.[9] These low diffusion coefficients can not be ascribable to the steric hindrance of gel matrix but to the binding of the enzyme to the ionogenic group, *i.e.*, the bound enzyme cannot diffuse on the surface of the solid phase but the free enzyme can diffuse in the ion exchanger. The ratio of the amount of the enzyme bound to the solid phase to that of the free enzyme in the ion exchanger might be approximately expressed by the distribution coefficient K. Accordingly, the product of K and D_e represents a diffusion coefficient of the enzyme in acetate buffer solution and is shown in Table 5-1. $K \cdot D_e$ resembles the diffusion coefficient in the buffer solution in each case. Such a concept was applied to estimation of diffusion coefficients of amino acids in polyelectrolyte solutions and a fairly good agreement was observed between the theory and the experiment.[9] Thus, the diffusion coefficient of enzyme in ion exchanger can be rough-

ly expressed by D/K, where D is the diffusion coefficient of enzyme in buffer solution.

Leakage of enzyme from ion exchanger. It is significant for continuous operation of immobilized enzymes to estimate the half-life. When enzymes are immobilized to ion exchangers, the desorption of the enzymes from the ion exchangers during continuous operation can not be avoided.[1] The time dependency of the enzyme concentration in the outer solution and that in the ion exchanger can be calculated by Eqs.(5-13) to (5-16). In Eqs.(5-13) and (5-14), C_1^* and $\bar{C}_2^*$ can be calculated using A and B as parameters. Since C_1 is usually negligibly low, the half-life of activity of the immobilized enzyme due to leakage is evaluated from the time course of $\bar{C}_2^*$. Figure 5-3 shows the plot of $\bar{C}_2^*$ against the normalized time θ varying the A value with a constant B value ($B = 10^3$). The θ value at $\bar{C}_2^* = 0.5$ is the normalized half-life of an immobilized enzyme $\theta_{1/2}$. The larger A value the shorter $\theta_{1/2}$. This means that the larger space velocity (SV = F/V) reduces the half-life. The $\theta_{1/2}$ value was calculated for various A and B values. In Fig. 5-4, the relation of $\theta_{1/2}$ to A is shown in a log-log coordinate using B as a parameter. When glucoamylase is immobilized to SP-Sephadex C-50 at pH 5.0 with 0.01 mol/l acetate buffer and the reaction of the immobilized enzyme is allowed to run on CSTR at $\varepsilon = 0.34$ and SV = 2.0 hr^{-1}, the half-life is calculated to be 281 days from Fig. 5-4 using K, R and D_e shown in Table 5-1.

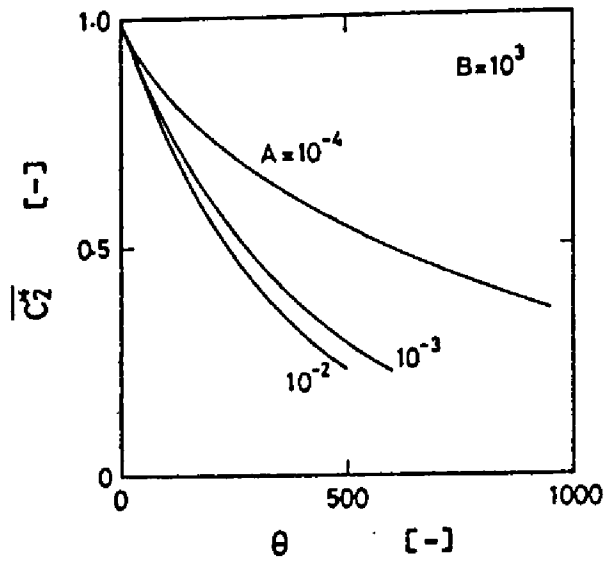

Fig. 5-3. Time courses of leakage of enzyme from an ion exchanger. Solid curves are calculated by Eq. (5-14) for various A values at constant B value. $\bar{C}_2^*$ and θ are defineed in the text.

When the diffusion resistance in ion exchangers can be ignored (almost $A \cdot B > 10$), the half-life may be calculated more easily. In this case, a mass balance equation for the enzyme in CSTR is expressed as follows:

$$-\partial C_2/\partial t = [F/(1 - \varepsilon)V] \cdot C_1 \qquad (5\text{-}17)$$

$$C_2 = K \cdot C_1 \qquad (5\text{-}18)$$

The initial condition is given as $C_2 = C_{20}$ at $t = 0$. The normalized enzyme concentration in the ion exchanger C_2^* is expressed by Eq. (5-19).

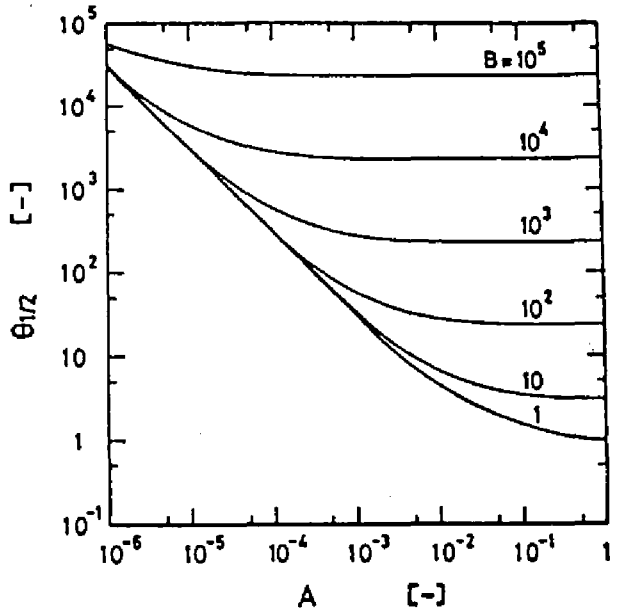

Fig. 5-4. Relation of the normalized half-life to parameters A and B. The $\theta_{1/2}$ value was evaluated using Eq. (5-14). The $\theta_{1/2}$, A and B are defined in the text.

$$C_2^* = \exp(-3\theta/B) \tag{5-19}$$

where both θ and B are the same as those defined previously. The normalized half-life $\theta_{1/2}$ and the actual half-life $t_{1/2}$ are given by the following equations.

$$\theta_{1/2} = 0.231 \cdot B \tag{5-20a}$$

$$t_{1/2} = 0.231(\varepsilon V/F) \cdot B \tag{5-20b}$$

The $\theta_{1/2}$ calculated from Eq.(5-20a) corresponds to the plateau region in Fig. 5-4.

The present treatment is applicable only to continuous stirred

tank reactor. In a plug flow reactor, the half-life may be longer than the present result, because the enzyme desorbed at the upper part of the reactor may reduce the desorption rate of the enzyme. Therefore, the present equation may be useful for practical purposes. It is difficult to estimate the diffusion coefficients of enzymes in ion exchanger. The utilization of the value obtained by dividing the diffusion coefficients of the enzymes in buffer solutions by the distribution coefficient as the diffusion coefficients of the enzymes in the ion exchangers may be advisable for practical purposes.

The distribution coefficient between glucoamylase and the ion exchanger was found to depend greatly on the ionic strength of buffer solution and the type of ion exchanger. The diffusion coefficient of the enzyme in the ion exchanger was much lower than that in buffer solution. This low diffusion coefficient was considered to be due to the binding of the enzyme to the ionogenic group. The theoretical equation was proposed to predict the half-life of activity of immobilized enzymes due to leakage of the enzymes. In the equation, denaturation of enzymes was not taken into account. Denaturation of immobilized enzymes may not be ignored when a reactor is operated for a long period. Detailed studies on the denaturation of enzymes will enable us to predict the half-life with a more accuracy. Finally, it should be noted that cation exchanger has been used for immobilization of gluco-

amylase from *Rhizopus niveus* by ionic linkage[3] as used in the present study, while anion exchanger for glucoamylase from *Aspergillus niger*.[10-12]

5. 5. Summary

Glucoamylase (from *Rhizopus niveus*) was immobilized to SP-Sephadex C-25 and C-50 by ionic linkage. The physical properties of the immobilized glucoamylase were quantitatively investigated. Binding equilibrium between the enzyme and the ion exchanger was investigated. A linear relationship between the concentrations of enzymes in the ion exchanger and in the outer solution phase was observed over a wide range of enzyme concentrations. Distribution coefficients were obtained, by which the amount of the enzyme immobilized can be calculated. Diffusion coefficients of the enzyme in the ion exchangers were also estimated from analysis of the adsorption process. A theoretical equation to predict the half-life of the activity of immobilized enzymes caused by desorption of the enzymes was proposed in terms of the distribution coefficient, the diffusion coefficient and the operational variables of a continuous reaction.

Nomenclature

$A = \varepsilon V D_e / (F R^2)$ [-]

$B = 3(1 - \varepsilon) K / \varepsilon$ [-]

C	concentration	[mol/l]
C_1^*	normalized outer concentration	[-]
$\bar{C}_2^*$	normalized mean inner concentration	[-]
D	diffusion coefficient in buffer solution	[cm^2/s]
D_e	diffusion coefficient in the ion exchanger	[cm^2/s]
F	volumetric flow rate	[cm^3/s]
K	distribution coefficient	[-]
M	fraction of enzyme adsorbed	[-]
R	radius of particle	[cm]
R	gas constant	[J/K·mol]
r	radial distance	[cm]
SV	space velocity	[hr^{-1}]
T	absolute temperature	[K]
t	time	[s]
V	volume of the bath of solution	[cm^3]
V	partial molar volume	[cm^3/mol]
W	weight	[g]
Z	number of charge of the enzyme	[-]
α	$= KW/(\varepsilon V\rho)$	[-]
ε	void fraction of the bath	[-]
θ	$= t/(\varepsilon V/F)$	[-]
Π	swelling pressure	[atm]
ρ	density of the swollen ion exchanger	[g/cm^3]

Subscript

e	equilibrium
0	initial
1	outer solution phase
2	ion exchanger phase

Literature Cited

1) I. Chibata, T. Tosa, T. Sato, T. Mori, and Y. Matsuo, *Proceedings of the IVth International Fermentation Symposium: Fermentation Technology Today*, p.383, Society of Fermentation Technology, Japan, 1972.

2) M. Moo-Young and T. Kobayashi, *Can. J. Chem. Eng.*, 50, 162 (1972).

3) K. Miyamoto, T. Fuji, N. Tamaoki, M. Okazaki, and Y. Miura, *J. Ferment. Technol.*, 51, 566 (1973).

4) "*Immobilized Enzymes*," ed. by I. Chibata, Chapters 3 and 5, Kodansha, Tokyo, 1975.

5) M. Ohnishi, T. Yamashita, and K. Hiromi, *J. Biochem. (Tokyo)*, 79, 1007 (1976).

6) J. Crank, "*Mathematics of Diffusion*," Oxford Univ. Press, 1956, p.88.

7) P. C. Carman and R. A. Haul, *Roc. Roy. Soc.*, 222-A, 109 (1954).

8) F. Helfferich, "*Ion Exchanger*," McGraw-Hill, New York, 1964, p.95, 251.

9) R. Namikawa, H. Okazaki, K. Nakanishi, R. Matsuno, and T. Kamikubo, *Agric. Biol. Chem.*, 41, 1003 (1977).

10) R. J. H. Wilson and M. D. Lilly, *Biotechnol. Bioeng.*, 11, 349 (1969).

11) M. J. Bachler, G. W. Strandberg, and K. L. Smiley, *Biotechnol. Bioeng.*, 12, 85 (1970).

12) Y. K. Park, *J. Ferment. Technol.*, 52, 140 (1974).

PART II

PULSE RESPONSE IN IMMOBILIZED-ENZYME COLUMN

PART II

PULSE RESPONSE IN IMMOBILIZED-ENZYME COLUMN

Introduction

Because of the high specificity and the high catalytic activity of enzyme reactions under non-extreme conditions, enzymatic analysis is meritorious compared to chemical analysis using acids, bases, etc. The high cost of the enzyme may be reduced by its immobilization. With the explosive increase of samples for clinical and food analysis in recent years, much attention has been paid to the utilization of immobilized enzymes for analytical purposes as well as for the mass conversion of materials. Analytical instruments using immobilized enzymes, such as enzyme thermisters [1-4] and enzyme electrodes,[5-9] have been devised. An analytical method using an immobilized-enzyme column can be based on chromatographic techniques.

As shown in Figure II-1, a substrate solution of unknown concentration is applied to the inlet of the column as a pulse. Since the substrate is undetectable in its original form, it is converted to a product of detectable form by an enzyme reaction in the column, or else a coupling coenzyme of undetectable form is converted to a detectable form. The elution curve of the product or of the coenzyme at the outlet of the column is followed continuously by a suitable analytical instrument, such as a spectrophoto-

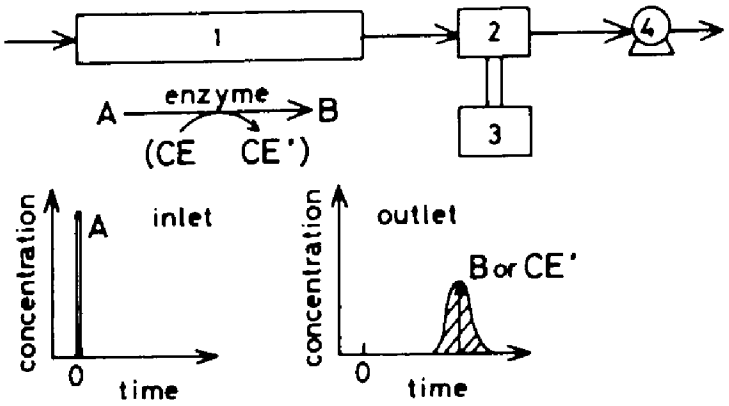

Fig. II-1. Schematic representation of analysis based on a pulse response in an immobilized-enzyme column. A denotes the substrate, which is undetectable in its original form and the concentration of which is unknown, and B is the detectable product. CE is a coenzyme of undetectable form and CE' is one of detectable form. Concentration of the substrate A is determined from the intensity of the elution profile, such as the peak height or the area under the curve of product or CE'. 1, Immobilized-enzyme column; 2, detector; 3, recorder; 4, constant-feeding pump.

meter. The concentration of the original substrate solution is determined from the intensity of the elution curve, including the peak height and the area under the curve.

For a linear relationship between the substrate concentration and the intensity of the elution curve, the substrate concentration must be less than the Michaelis constant Km, so that the reaction is first-order. This condition is often satisfied because substrate concentrations are usually low in clinical analysis. To

perform a rapid analysis, a large amount of enzyme is immobilized on the carrier, and a short column is used with a high flow rate. Under such conditions, the mass transfer of the substrate might easily affect the elution profile. For effective analysis, the effect of the physical properties of the immobilized enzyme and the substrate and the effect of operational variables on the elution profiles must be known. A theoretical method for predicting the elution curve of the product is here proposed on the mass balance model extensively used in gel chromatography. The validity of the theory was confirmed in a column that was filled with spherical acrylamide-gel-entrapped invertase. The theory was extended to systems of reversible and consecutive reactions and to determination of an enzyme using an immobilized-indicator enzyme.

In Chapter 6, a theoretical method for predicting the elution curve of the product is proposed on the mass balance model. The validity of the theory is experimentally confirmed in an acrylamide-gel-entrapped-invertase column. The theory is extended to systems of reversible and consecutive reactions.

In clinical and food analyses, a substrate which is not easy to analyze by the usual methods is converted to a readily detectable product by reversible or consecutive reactions. A theoretical method for predicting the elution profiles of the product, which is extended to such sysyems in Chapter 6, is confirmed experimentally in Chapter 7.

In Chapter 8, it is shown that pyruvate and L-lactate in human serum are successfully analzed by the pulse response technique using an immobilized-lactate dehydrogenase column.

It is important in clinical chemistry to analyze an enzyme activity in serum. In Chapter 9, the pulse response technique can be applied to determination of the enzyme by using a column in which the beads immobilizing an indicator enzyme are packed.

Literature Cited

1) K. Mosbach, B. Danielsson, A. Borgerud, and M. Scott, *Biochim. Biophys. Acta*, 403, 256 (1975).

2) B. Mattiasson, *FEBS Lett.*, 77, 107 (1977).

3) B. Danielsson, K. Gadd, B. Mattiasson, and K. Mosbach, *Clin. Chim. Acta*, 81, 163 (1977).

4) B. Mattiasson, B. Danielsson, and K. Mosbach, *Anal. Lett.*, 9, 217 (1976).

5) G. P. Hicks and S. J. Updike, *Nature*, 214, 986 (1967).

6) L. B. Wingard, Jr., C. C. Liu, and N. L. Nagda, *Biotechnol. Bioeng.*, 13, 629 (1971).

7) G. G. Guilbault and J. G. Montalvo, *J. Am. Chem. Soc.*, 92, 2533 (1970).

8) S. Suzuki, I. Karube, and I. Satoh, "*Biochemical Application of Immobilized Enzymes and Proteins*," ed. by T. M. S. Chang, Plenum, New York, 1977, Vol. 2, p.177.

9) I. Satoh, I. Karube, and S. Suzuki, *Biotechnol. Bioeng.*, 19, 1095 (1977).

Chapter 6

Theoretical Method for Predicting Elution Curves

6. 1. Introduction

The pulse response technique using an immobilized-enzyme column is promising as an analytical method for determining the concentration of specific substances in food, serum, etc., because of the high specificity and high activity of enzyme reaction.

In this chapter, a theoretical method for predicting the elution curve of the product is proposed on the mass balance model extensively used in gel chromatography. The validity of the theory is confirmed in a column that is filled with spherical acrylamide-gel-entrapped invertase. The theory is extended to system of reversible and consecutive reactions.

6. 2. Materials and Methods

Materials. Yeast invertase was purchased from Wako Pure Chemical industries. The protein content of the enzyme preparation was found to be 3.65 mg/ml, using bovine serum albumin (BSA) as a standard. Acrylamide monomer (AAm), N,N'-methylenebisacrylamide (BIS), N,N,N',N'-tetramethylethylenediamine (TEMED), and ammonium persulfate were also obtained from Wako Pure Chemical Industries. Arlacel C (sorbitan sesquioleate) was purchased from Tokyo Kasei Kogyo. Blue Dextran was purchased from Pharmacia. Sucrose and glucose were obtained from Wako Pure Chemical Indus-

tries and Nakarai Chemicals, respectively. All other reagents were of analytical grade.

Preparation of immobilized invertase. The method for entrapping invertase in acrylamide gel was essentially the same as that reported by Ohmiya *et al.*[1] except for irradiation by a fluorescent light. One ml of 5%(w/v) ammonium persulfate was added to a mixture of 7 ml of appropriately diluted invertase solution and 7 ml of 40%(w/v) AAm-BIS solution; the BIS content was 5%. The mixture was immediately poured into 200 ml of organic solvent (toluene/chloroform = 144/56) which contained Arlacel C and 0.16 ml of TEMED, and was emulsified by magnetic stirring in a nitrogen atmosphere. All reagents were dissolved in 0.05 mol/l acetate buffer (pH 5.0). The size of the acrylamide beads was regulated by controlling the amount of detergent and the stirring speed of the magnetic bar. The polymerization was performed at 0 - 4°C for 20 min. The prepared immobilized-invertase gels were separated from the organic solvent with a glass filter, then washed with 100 ml of chilled toluene and with a large amount of chilled acetate buffer. The gels were sieved to obtain the desired size. They were suspended in buffer and stored in a refrigerator before use.

Assay of free invertase activity. The hydrolysis of sucrose by invertase was allowed to run at pH 5.0 with 0.05 mol/l acetate buffer at 25°C. The sucrose concentrations were in the range of

0.01 to 1.4 mol/l. The initial reaction rate was estimated from the increase of glucose concentration, which was assayed by the glucostat method.[2)]

Estimation of kinetic parameters of immobilized invertase.

The immobilized-invertase characteristics were estimated using a batch reactor and a continuous-stirred-tank reactor (CSTR). In the former case, about 0.2 - 0.3 g (wet weight) immobilized invertase beads was accurately weighed. After the addition of 20 ml of sucrose solution, the reaction mixture was shaken for 4 hr at 25°C. The amount of glucose produced was assayed by the method described above. The conversion was less than 10%.

The effective volume of the CSTR was 50 ml, and about 3.1 g of immobilized-enzyme beads were loaded onto it. After about five times the residence time had passed, the glucose produced was determined at the outlet.

An invertase-catalyzed reaction is inhibited by a high concentration of substrate,[3)] and the reaction rate equation is

$$-r_A = \frac{k_0 \cdot C_{E0} \cdot C_A}{Km + C_A + C_A^2/Ki} \qquad (6\text{-}1)$$

where r_A is the formation rate of substrate, k_0 the rate constant, C_{E0} the total enzyme concentration, C_A the substrate concentration, and Ki is the inhibition constant. Equation (6-1) can be reduced

to Michaelis-Menten equation when C_A is much lower than Ki. In that case, the Lineweaver-Burk plot gives the values of Km and Vmax (= $k_0 \cdot C_{E0}$). When C_A >> Km, Eq.(6-1) becomes:

$$-r_A = \frac{k_0 \cdot C_{E0}}{1 + C_A/ki} \qquad (6\text{-}2)$$

The Ki value can be estmated from the plot of $1/(-r_A)$ *versus* C_A.

The kinetic parameters (Km and Vmax) of the immobilized invertase employed for pulse experiments were estimated using a packed-bed reactor, when the effect of intraparticle diffusion resistance was negligible because of a low Vmax and a small gel radius. When the effect of diffusional resistance was significant owing to a high Vmax and a large gel radius, the immobilized-invertase beads were granulated to reduce the gel radius, and the activity was assayed in a batch reactor.

Pulse response experiments. The immobilized-invertase beads were packed in a column equipped with a water jacket. Substrate solution (0.5 ml) was carefully added to the top of the bed, and the flow was started. The moment the sucrose solution disappeared, the eluent was added by a constant-feeding pump (Tokyo Rikakikai Co., MP-B). The eluent was 0.05 mol/l acetate buffer (pH 5.0), and the bed was kept at 25°C. At appropriate intervals, the eluate was collected at the bottom of the bed. The eluate was divided into halves. One half was used to assay the glucose produced

by the invertase-catalyzed reaction. By adding an invertase solution to the other, the unreacted substrate was completely hydrolyzed and the glucose concentration was determined. The sucrose concentration of the eluate was estimated from the difference between these glucose concentrations.

Determination of particle size. Acrylamide-gel-entrapped invertase particles were confirmed to be spherical by observation wit an optical microscope (Nikon S-Ke). The diameters of more than 250 particles were measured, and the square mean value was calculated.

Determination of physical properties of substrate. The values of the axial dispersion coefficient (D_z), the gel phase diffusion coefficients (D_s), the distribution coefficients (K) of both substrate and product, and the void fraction (ε) of the bed were determined by moment analysis[4-6] of elution profiles of the substrate and the product, using an immobilized-invertase column denatured by heating. The first-order normalized statistical moment (μ_1'), *i.e.*, the average residence time, and the second-order normalized central moment (μ_2), *i.e.*, the variance of elution profiles, were related to D_z, D_s, K, and ε by Eqs(6-3) and (6-4), respectively.

$$\mu_1' = (Z/u_0)[\varepsilon + (1 - \varepsilon)K] \qquad (6\text{-}3)$$

$$\mu_2 = (2Z/u)[(D_z/u^2)(1 + HK)^2 + HKR^2/(15D_s)] \qquad (6\text{-}4)$$

where Z is the height of the bed, u_0 the linear superficial velocity, u the linear interstitial velocity, R the particle radius, and $H = (1 - \varepsilon)/\varepsilon$. By comparing the experimental μ_1' and μ_2 with Eqs. (6-3) and (6-4), D_z, D_s, K, and ε were determined. The experimental method was the same as that of Nakanishi *et al.*[6] The concentration of the eluate was analyzed by the method described above.

6. 3. Theoretical Considerations.

A method for predicting the elution curve of the product has been proposed based on the mass balance model extensively used in gel chromatography. The first-order enzyme reaction in the gel phase was added to the mass balance equation as well as axial dispersion in the mobile phase and gel-phase diffusion of the solute. Let us consider the irreversible first-order reaction shown in Eq. (6-5) with rate constant k, where k = Vmax/Km:

$$A \xrightarrow{k\ (= Vmax/Km)} B \qquad (6\text{-}5)$$

Km and Vmax are the Michaelis constant and the maximum reaction rate, respectively. The Michaelis-Menten rate equation can be reduced to a first-order one when the substrate concentration is lower than Km. Mass balance equations referring to substrate concentrations at the mobile phase C_A and the gel phase C_{AS} are given

by

$$\frac{\partial C_A}{\partial t} = D_z \frac{\partial^2 C_A}{\partial z^2} - u\frac{\partial C_A}{\partial z} - \frac{3(1-\varepsilon)k_f}{\varepsilon R}(C_A - C_A|_{r=R}) \qquad (6\text{-}6)$$

$$\frac{\partial C_{AS}}{\partial t} = D_s\left(\frac{\partial^2 C_{AS}}{\partial r^2} + \frac{2}{r}\cdot\frac{\partial C_{AS}}{\partial r}\right) - kC_{AS} \qquad (6\text{-}7)$$

where t is time, k_f the mass transfer coefficient, and r the radial distance variable. The third term on the right-hand side of Eq.(6-7) represents the decrease in C_{AS} by the enzyme reaction.

These equations are basically the same as those employed by Marrazzo *et al.*[7] They analyzed the characteristics of the hydrolysis of sucrose by invertase immobilized onto porous glass particles at steady state, taking account axial dispersion as well as intraparticle substrate diffusion. In the same way, mass balance equations for the product B are written thus:

$$\frac{\partial C_B}{\partial t} = D_z \frac{\partial^2 C_B}{\partial z^2} - u\frac{\partial C_B}{\partial z} - \frac{3(1-\varepsilon)k_f}{\varepsilon R}(C_B - C_B|_{r=R}) \qquad (6\text{-}8)$$

$$\frac{\partial C_{BS}}{\partial t} = D_s\left(\frac{\partial^2 C_{BS}}{\partial r^2} + \frac{2}{r}\cdot\frac{\partial C_{BS}}{\partial r}\right) + kC_{AS} \qquad (6\text{-}9)$$

Initial and boundary conditions are given as follows:

$$t = 0, \quad z \geq 0, \quad C_A = C_{AS} = 0 \qquad (6\text{-}10a)$$

$$C_B = C_{BS} = 0 \qquad (6\text{-}10b)$$

$t > 0,\quad r = R,\quad C_{AS} = K \cdot C_A \qquad (6\text{-}10c)$

$$C_{BS} = K \cdot C_B \qquad (6\text{-}10d)$$

$t > 0,\quad r = 0,\quad \partial C_{AS}/\partial r = 0 \qquad (6\text{-}10e)$

$$\partial C_{BS}/\partial r = 0 \qquad (6\text{-}10f)$$

$0 \leq t \leq t_0,\quad z = 0,\quad C_A = C_{A0} \qquad (6\text{-}10g)$

$t > t_0,\quad z = 0,\quad C_A = 0 \qquad (6\text{-}10h)$

$t > 0,\quad z = 0,\quad C_B = 0 \qquad (6\text{-}10i)$

$$k_f(C_A - C_A|_{r=R}) = D_s(\partial C_{AS}/\partial r)|_{r=R} \qquad (6\text{-}10j)$$

$$k_f(C_B - C_B|_{r=R}) = D_s(\partial C_{BS}/\partial r)|_{r=R} \qquad (6\text{-}10k)$$

where t_0 is the sample injection time. The condition of a pulse is represented by Eqs.(6-10g) and (6-10h). For simplicity, a common K and D_s for both substrate and product are assumed.

An analytical solution for C_A has been reported by Wakao *et al.*[8] However, the solution is quite complex, because roots of a multivalued function must be obtained, and the series summation must be calculated twice. Furthermore, their solution cannot be applied exactly to our experimental system. Therefore, a numerical method was adopted. By applying the Laplace transform to these differential equations, solutions of C_A and C_B in the Laplace domain were obtained in the dimensionless forms of y_A and y_B, which are defined as C_A/C_{A0} and C_B/C_{B0}, respectively. $\bar{y}_A$ and $\bar{y}_B$ represent the solutions in the Laplace domain and are the function of the complex number *s*.

$$\bar{y}_A = \frac{1-e^{-s\theta_0}}{s} \exp\left[\frac{-s-3HK\lambda_1/(\phi'^2\lambda_1+\phi^2)}{1/2+\{1/4+(1/\delta)[s+3HK\lambda_1/(\phi'^2\lambda_1+\phi^2)]\}^{1/2}}\right] \tag{6-11}$$

$$\bar{y}_B = \frac{1-e^{-s\theta_0}}{s}\left[\exp\left[\frac{-s-3HK\lambda_0/(\phi'^2\lambda_0+\phi^2)}{1/2+\{1/4+(1/\delta)[s+3HK\lambda_0/(\phi'^2\lambda_0+\phi^2)]\}^{1/2}}\right] - \exp\left[\frac{-s-3HK\lambda_1/(\phi'^2\lambda_1+\phi^2)}{1/2+\{1/4+(1/\delta)[s+3HK\lambda_1/(\phi'^2\lambda_1+\phi^2)]\}^{1/2}}\right]\right] \tag{6-12}$$

where

$$\lambda_0 = (s\phi^2)^{1/2}\coth(s\phi^2)^{1/2} - 1 \tag{6-13a}$$

$$\lambda_1 = (s\phi^2+\phi_M^2)^{1/2}\coth(s\phi^2+\phi_M^2)^{1/2} - 1 \tag{6-13b}$$

$$\phi_M = R(k/D_s)^{1/2} \tag{6-14a}$$

$$\phi = R[1/(D_s\tau)]^{1/2} \tag{6-14b}$$

$$\phi' = R[K/(k_f R\tau)]^{1/2} \tag{6-14c}$$

$$\delta = Z/(D_z/u) \tag{6-14d}$$

$$HK = (1 - \varepsilon)K/\varepsilon \tag{6-14e}$$

and τ is the average residence time with respect to void volume of the column. When the volume of substrate solution applied is much smaller than the void volume of the bed, *i.e.*, when the input can be considered to be a pulse, the term $[1 - \exp(-s\theta_0)]/s$ in Eqs. (6-11) and (6-12) can be approximated by θ_0. $\bar{y}_A$ and $\bar{y}_B$ are the

functions of the nondimensional parameters composed of physical properties of immobilized enzyme and the substrate, and of operational variables, as shown in Eqs.(6-14).

To obtain the solutions in the time domain, the numerical inversion of the soltions in the Laplace domain is performed by the numerical integration of the complex function of Eq.(6-15) or by the Fourier series approximation of Eq.(6-16).[9,10]

$$y_i = \frac{1}{2\pi i} \lim_{\beta\to\infty} \int_{\alpha-i\beta}^{\alpha+i\beta} e^{s\theta} \bar{y}_i(s)\, ds \tag{6-15}$$

$$y_i = \frac{e^{\alpha\theta}}{T}\left[\frac{1}{2}\bar{y}_i(\alpha) + \sum_{k=1}^{\infty}\{Re[\bar{y}_i(\alpha + \frac{k\pi i}{T})]\cos(\frac{k\pi i}{T}) - Im[\bar{y}_i(\alpha + \frac{k\pi i}{T})]\sin(\frac{k\pi i}{T})\}\right] \tag{6-16}$$

where θ is the dimensionless time ($= t/\tau$). *Re* and *Im* indicate the real and imaginary parts of $\bar{y}_i$, respectively. T is an arbitray constant. The inversion by Eq.(6-16) is accomplished in a shorter time than that by Eq.(6-15).

The elution curves are calculated as the function of θ under various values of the dimensionless parameters shown in Eqs.(6-14). The calculation was performed using a FACOM M-190 or M-240 computer at the Data-Processing Center of Kyoto University. $\bar{y}_A$ and $\bar{y}_B$ in the case where the enzyme is immobilized onto non-porous support can be easily obtained. The mass balance model can be ex-

tended to the system of reversible as well as consecutive reactions. The solutions in the Laplace domain for these cases are shown in the Appendix. The solutions in the time domain are calculated by the methods described above.

6. 4. Results and Discussion

Kinetic parameters of free and immobilized invertase. The kinetic parameters (k_0, Km, and Ki) of immobilized invertase were estimated in 0.05 mol/l acetate buffer (pH 5.0) at 25°C. The k_0, Km, and Ki values of the free enzyme were obtained under the same conditions. The double reciprocal plots are shown in Fig. 6-1. The k_0 and Km values were evaluated from these plots. Figure 6-2 shows the plots of $C_{E0}/(-r_A)$ *versus* C_A for free and immobilized invertase. The Ki values were determined. The kinetic parameters of the immobilized enzyme are taken to be free from the effect of diffusional resistance, because the reaction was allowed to run under conditions where intraparticle and film diffusional resistance of the substrate could be ignored. The k_0, Km, and Ki values of the free and immobilized invertase are summarized in Table 6-1. Changes in Km and Ki values due to immobilization were not observed. Sixty-eight percent of the enzyme activity was maintained after immobilization. Although details of the data are not shown here, enzyme leakage from the gel matrix was not observed and the inactivation rate of the immobilized enzyme during con-

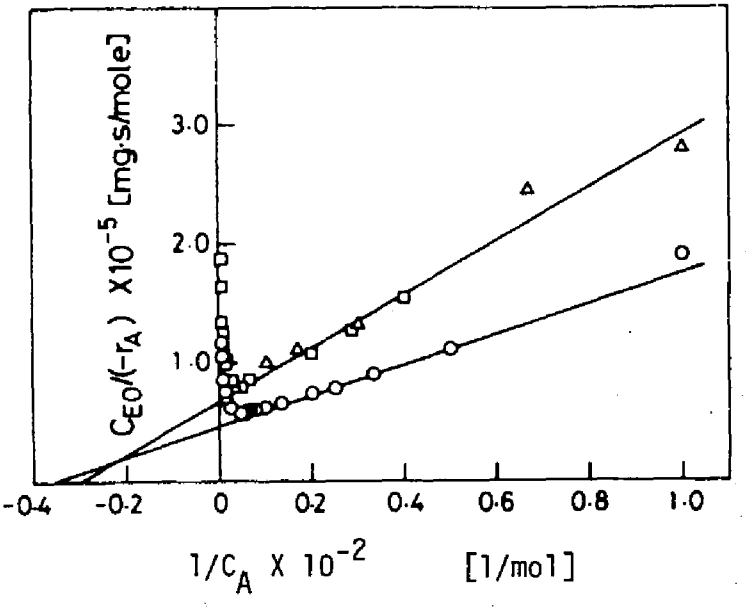

Fig. 6-1. Double reciprocal plots for estimating Km and k_0 values for free and immobilized invertase. Reaction was run with 0.05 mol/l acetate buffer (pH 5.0) at 25°C. Total enzyme concentration C_{E0} of the immobilized enzyme was calculated by assuming that the enzyme laoded for immobilization was wholly entrapped. (○) Soluble invertase; immobilized invertase: (□) batch reactor and (△) CSTR.

Table 6-1. Kinetic Parameters of Free and Immobilized Invertase at pH 5.0 and 25°C.

	Km [mol/l]	Ki [mol/l]	k_0 [mol/mg·s]
Free	0.028	1.1	2.17×10^{-5}
Immobilized	0.033	1.3	1.47×10^{-5}

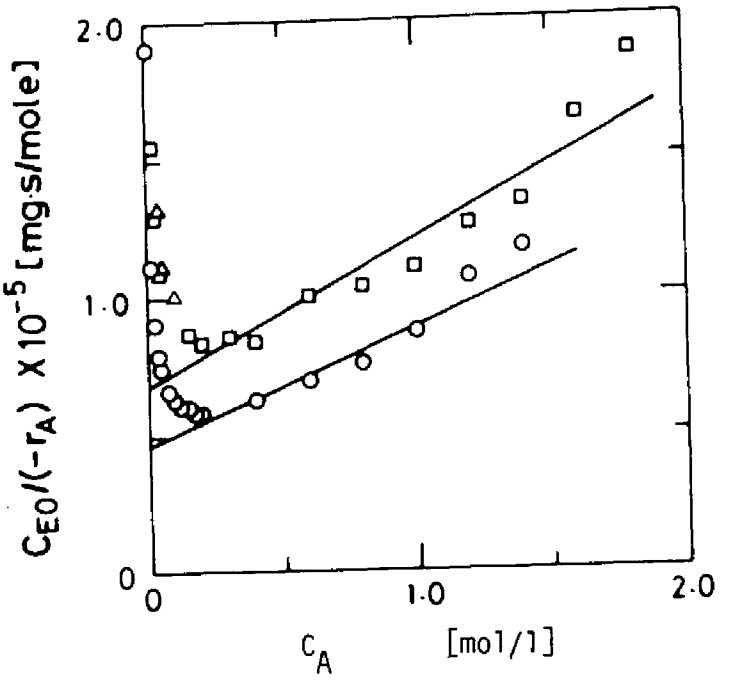

Fig. 6-2. Plots of $C_{E0}/(-r_A)$ *versus* C_A for free and immobilized invertase. Conditions and symbols are the same as shown for Fig. 6-1.

tinuous operation in a packed-bed-type reactor was very slow under the conditions used. The use of acrylamide-gel-entrapped invertase was found to be suitable for an experimental test of the validity of our proposed theory.

Determination of ε, K, D_z *and* D_s. The values of the void fraction ε of a bed and the distribution coefficients K of sucrose and glucose were determined from the first-order statistical moment of the elution curves for Blue Dextran and for saccharides, respectively. The data obtained experimentally are shown in Fig. 6-3, where μ_1' was plotted against Z/u_0 on a logarithmic scale.

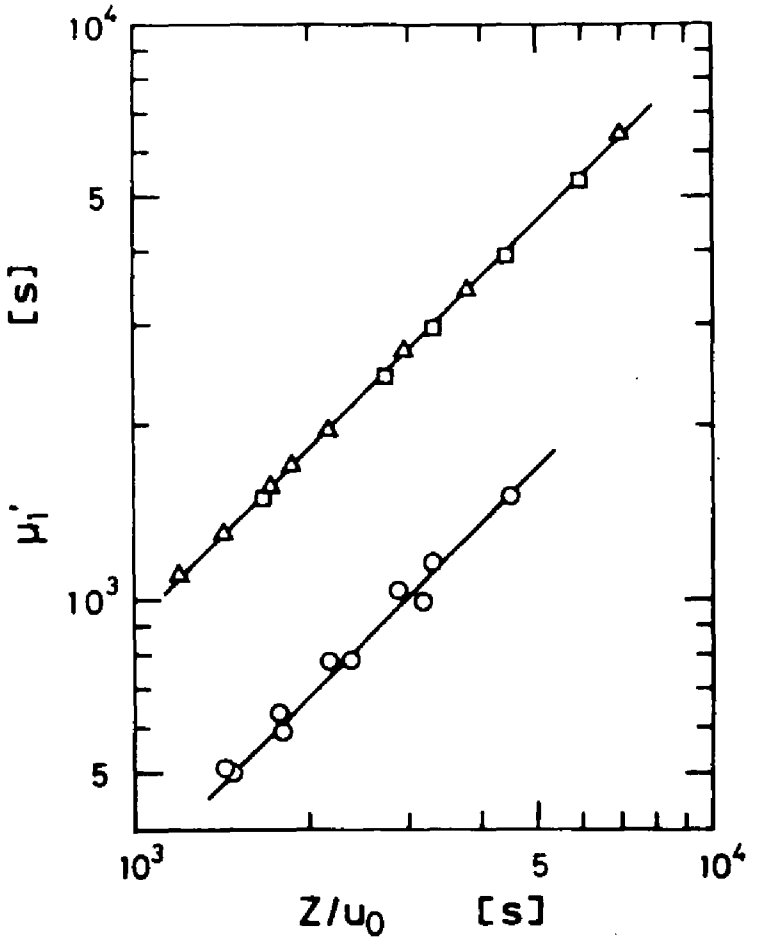

Fig. 6-3. Experimental relations between first-order statistical moment and Z/u_0. Column size = 15.4 mmϕ X 383 mm. Sample volume applied was 0.5 ml. (○) 0.3% Blue Dextran; (□) 0.01 mol/l sucrose; (△) 0.01 mol/l glucose.

The values of the axial dispersion coefficient and of the gel-phase diffusion coefficients were estimated from Eq.(6-4). Plots of $\mu_2/(2Z/u)$ *versus* $1/u$ are shown in Fig. 6-4. In the calculation of μ_1' and μ_2, integrations were carried out numerically by Simpson's rule. The values of D_z/u and D_s were calculated from the

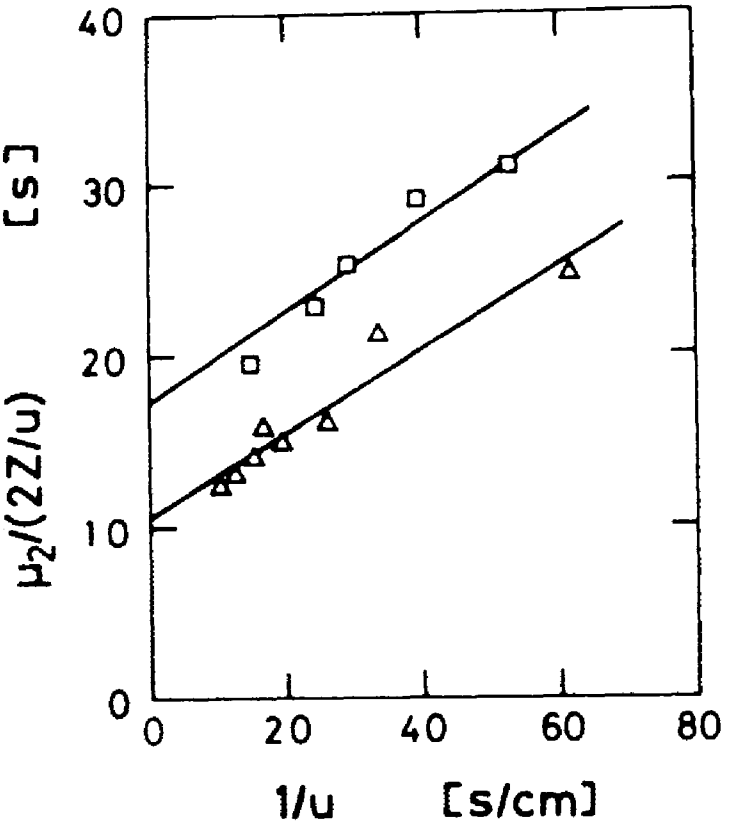

Fig. 6-4. Experimental relations between second-order central moment and 1/u. (□) 0.01 mol/l sucrose; (△) 0.01 mol/l glucose.

slope and the intercept, respectively. The values of ε, K, D_z/u, and D_s (which were estimated for the gel used in the pulse test shown in Fig. 6-5) are illustrate in Table 6-2. The value of D_z/u was about 1.3 times the mean diameter of the gel, and this was reasonable considering the range of the Reynolds number.[11] The distribution coefficients for sucrose and glucose were similar to those estimated for a single bead of acrylamide gel, while the D_s values of the saccharides were somewhat smaller than those estmat-

Table 6-2. Values Determined for the Parameters for a Column[a] of Immobilized-Invertase Beads at 25°C.

	ε [-]	R^b [cm]	K [-]	D_z/u [cm]	D_s [cm^2/s]
Glucose	0.34	0.0133	0.88	0.0330	1.91×10^{-6}
Sucrose			0.88	0.0355	1.17×10^{-6}
Average	-	-	0.88	0.0343	1.54×10^{-6}

a Column size = 15.4 mmϕ X 383 mm.

b Surface mean radius.

ed for a single bead using maltose and glucose as a solute in Chapter 1. The same tendency was observed in gel chromatography of an NaCl-Sephadex bead system.[6] The values of ε, K, and D_s by Marrazzo *et al.*[7] were similar to those measured in this study. Owing to the high Reynolds number, their Peclet number (= $2Ru/D_z$) was larger than our value.

Pulse response experiments. Two series of experiments were performed and the experimental conditions are summarized in Table 6-3. In the first series, the effect of diffusional resistance was negligible because of a low Vmax and a small gel radius. In the second series, the effect of diffusional resistance was significant because of a high Vmax and a large R. In both series of experiments, the substrate concentration was made 5 or 10 mmol/l smaller than the Michaelis constant (30 mmol/l) to make the reaction first-order. Figure 6-5 shows the results for the first se-

Table 6-3. Experimental Conditions for Pulse Tests.

Parameter	1st series	2nd series
Km [mmol/l]	30	30
Vmax [mmol/l·min]	0.573	8.66
R [cm]	0.0133	0.0544
Column dimension	15 mmϕ X 389 mm	12 mmϕ X 119 mm
Flow rate	1.0 - 3.0 cm^3/min	
Effect of diffusional resistance	negligible	significant
Substrate	5 or 10 mmol/l	
Eluent	0.05 mol/l acetate buffer (pH 5.0)	

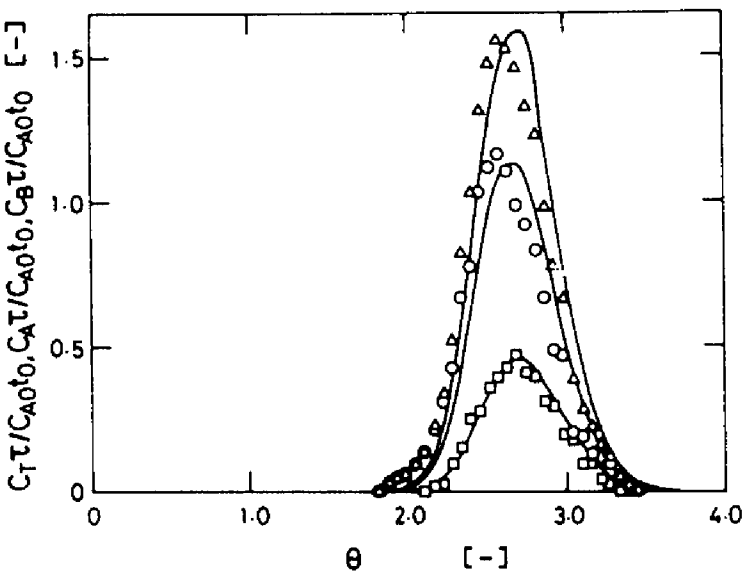

Fig. 6-5. Elution profiles of substrate and product in first series. Column dimension = 15 mmϕ X 389 mm; R = 0.0133 cm. (——) Calculated according to the theory using the values of the dimensionless parameters. C_{A0} = 0.01 mol/l; τ = 544 s; ϕ_M = 0.191; ϕ = 0.473; ϕ' = 0; HK = 1.71; δ = 1130. (△) C_T, sucrose plus glucose; (○) C_A, sucrose; (□) C_B, glucose.

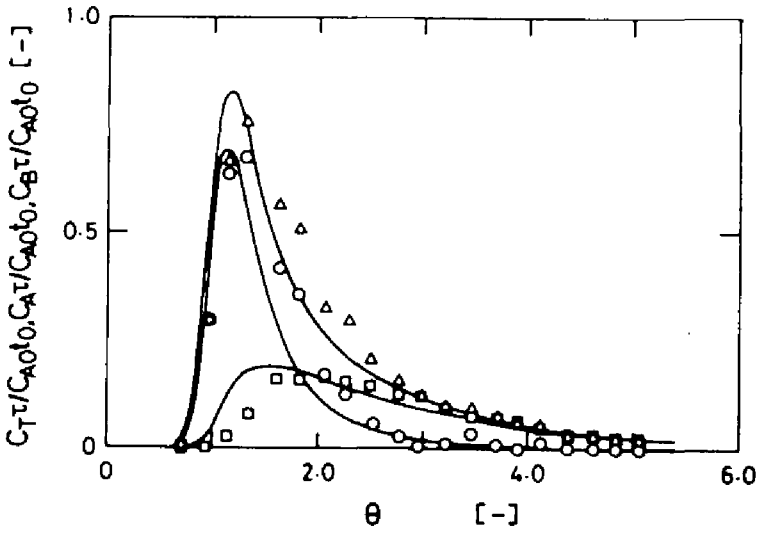

Fig. 6-6. Elution profiles of substrate and product in second series. Keys are shown in Fig. 6-5. C_{A0} = 0.01 mol/l; τ = 130 s; ϕ_M = 3.04; ϕ = 3.84; ϕ' = 0.576; HK = 1.08; δ = 110. Column dimension: 12 mmϕ X 119 mm; R = 0.0544 cm.

ries. The abscissa is time, θ, and the coordinate is the concentration, which are both dimensionless. The elution profiles of the substrate and of the product are symmetrical. Theoretical elution profiles (represented here by solid curves) coincide fairly well with the experimental ones. In the calculation of the theoretical curves, the mass transfer coefficient k_f was taken to be infinite (*i.e.*, $\phi' = 0$). The results of the second series are shown in Fig. 6-6. Asymmetrical elution profiles having long tails were obtained. The tails may reflect the influence of diffusional resistance in the gel phase. The elution profiles of the substrate and the product intersect each other at about θ = 2.0.

Moreover, the elution curve of the product is very broad and the peak position is not clear. This elution profile is unsuitable for analytical purposes. These phenomena were well reproduced by the theoretical elution profiles. The k_f value was estimated from the correlation proposed by Wilson and Geankoplis.[12)]

Theoretical elution profiles in reversible and consecutive reactions. Since it was proved that the mass balance model was applicable to the prediction of elution profiles in an irreversible reaction, the theory was extended to the system of reversible and consecutive reactions. For consecutive reactions, two cases are considered. The first is that two enzymes are coimmobilized in a carrier and the second is that two enzymes are immobilized independently in different carriers and then mixed.

The solutions for C_i (i = A, B, and C) in the Laplace domain in reversible reactions and consecutive reactions are shown in the Appendix. In the calculatation of elution profiles, it was assumed that the value of D_z/u was equal to the gel diameter, and the k_f value was taken to be infinite.

Figure 6-7 shows the elution profiles of a product produced by a reversible reaction under two extreme conditions. The curve R-1, which has a sharp peak, shows the elution profile when the effect of diffusional resistance is negligible. The curve R-2 is obtained when the effect of diffusional resistance is significant. The upper figure shows the distribution of the degree of close-

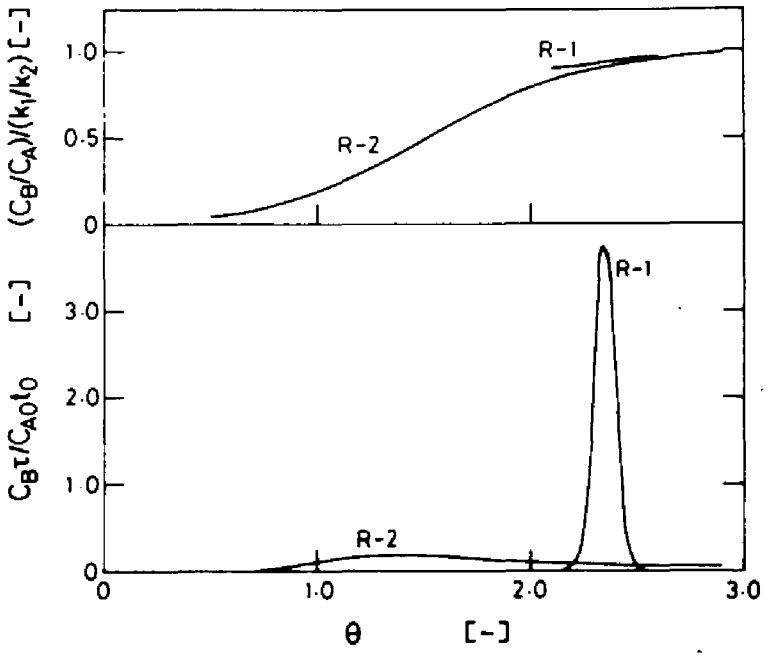

Fig. 6-7. Theoretical elution profiles of product and distribution of degree of closeness to equilibrium. Curve R-1 is obtained when the effect of diffusional resistence is negligible, while R-2 is obtained when the effect is significant. Upper figure shows the distribution of the degree to equilibrium with time. R-1: ϕ_{M1} = 0.05; ϕ_{M2} = 0.05; ϕ = 0.0447; ϕ' = 0; HK = 1.35; δ = 5000. R-2: ϕ_{M1} = 5.00; ϕ_{M2} = 5.00; ϕ = 4.47; ϕ' = 0; HK = 1.35; δ = 50.

ness to equilibrium with time. When the diffusional resistance is insignificant, not only is the peak of the elution profile very sharp but also the distribution is uniform.

Figure 6-8 shows the elution profiles of the final product of consecutive reactions in both coimmobilized- and mixed-enzyme columns. The symbols CI refers to a coimmobilized- and M to a mixed-

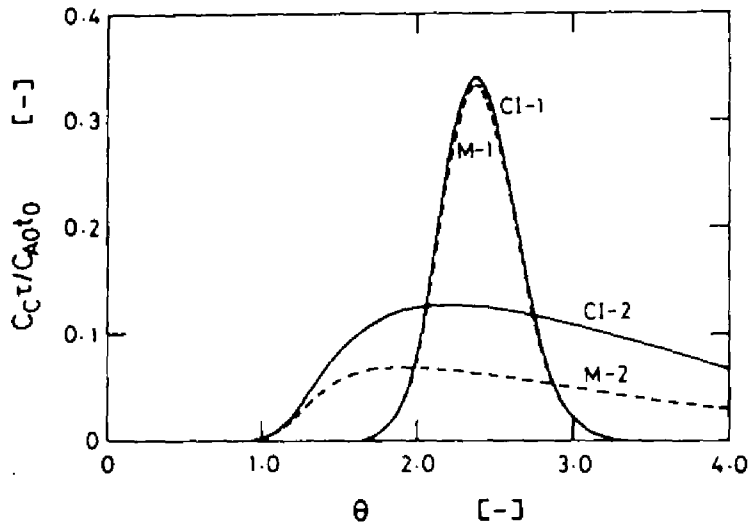

Fig. 6-8. Theoretical elution profiles of final product of consecutive reactions in coimmobilized- and mixed-type enzyme columns. Symbol CI represents the coimmobilized type and M the mixed-type enzyme column. k_f value was taken to be infinite. CI-1 (M-1 values in parentheses): ϕ_{M1} = 0.354 (0.500); ϕ_{M2} = 0.351 (0.497); ϕ ($\phi_1 = \phi_2$) = 0.447; ϕ' ($\phi_1' = \phi_2'$) = 0; HK = 1.35; δ = 500. CI-2 (M-2 values in parentheses): ϕ_{M1} = 3.54 (5.00); ϕ_{M2} = 3.51 (4.97); ϕ ($\phi_1 = \phi_2$) = 3.16; ϕ' ($\phi_1' = \phi_2'$) = 0; HK = 1.35; δ =250.

type enzyme column. The curves CI-1 and M-1 show profiles for when the effect of diffusional resistance in the gel phase is small, and the curves CI-2 and M-2 for when the effect of diffusional resistance is significant. In both cases, the coimmobilized-type column shows high conversion. Moreover, diffusional resistance promotes this tendency.

6. 5. Summary

A theoretical method for predicting the elution profile of a pulse response in an immobilized-enzyme column is proposed. The method is based on a mass balance model, which is extensively used in gel chromatography. To test the method, a pulse of sucrose solution was applied to a column of spherical acrylamide gel in which was entrapped invertase from yeast, and it was eluted with 0.05 mol/l acetate buffer at pH 5.0. The elution curves of the substrate and the product were in fairly good agreement with the theoretically calculated ones. The method was extended to the system of reversible as well as consecutive reactions.

Appendix

Irreversible reaction. The solutions of y_A and y_B in the Laplace domain have been presented when an enzyme is immobilized to a porous support. Here, we consider the solutions of y_A and y_B in the Laplace domain in the case where the enzyme is attached onto a non-porous support.

The mass balance equations for the substrate A and the product B are given by the following equations under the assumption that the mass transfer through the film around the particle is very fast.

$$\frac{\partial C_A}{\partial t} = D_z \frac{\partial^2 C_A}{\partial z^2} - u\frac{\partial C_A}{\partial z} - \frac{1-\varepsilon}{\varepsilon}\frac{3}{R}kC_A \qquad (6\text{-}17)$$

$$\frac{\partial C_B}{\partial t} = D_z \frac{\partial^2 C_B}{\partial z} - u\frac{\partial C_B}{\partial z} + \frac{1-\varepsilon}{\varepsilon}\cdot 3\cdot\frac{1}{R}\cdot kC_A \tag{6-18}$$

The initial and boundary conditions are given as follows:

$$t = 0, \quad z \geq 0, \quad C_A = 0 \tag{6-19a}$$

$$C_B = 0 \tag{6-19b}$$

$$0 \leq t \leq t_0, \quad z = 0, \quad C_A = C_{A0} \tag{6-19c}$$

$$t > t_0, \quad z = 0, \quad C_A = 0 \tag{6-19d}$$

$$t > 0, \quad z = 0, \quad C_B = 0 \tag{6-19e}$$

The solutions of C_A and C_B in the Laplace domain are given in the dimensionless form by Eqs. (6-20) and (6-21).

$$\bar{y}_A = \frac{1 - e^{-s\theta_0}}{s} \exp\left[\frac{-s - \eta H}{1/2 + \{1/4 + (1/\delta)(s+\eta H)\}^{1/2}}\right] \tag{6-20}$$

$$\bar{y}_B = \frac{1 - e^{-s\theta_0}}{s} \left[\exp\left[\frac{-s}{1/2 + \{1/4 + s(1/\delta)\}^{1/2}}\right] - \exp\left[\frac{-s - \eta H}{1/2 + \{1/4 + (1/\delta)(s+\eta H)\}^{1/2}}\right]\right] \tag{6-21}$$

where

$$\eta = 3k\tau/R \tag{6-22}$$

The solutions in the time domain are obtained by the numerical inversion of $\bar{y}_A$ and $\bar{y}_B$ according to Eqs. (6-15) or (6-16).

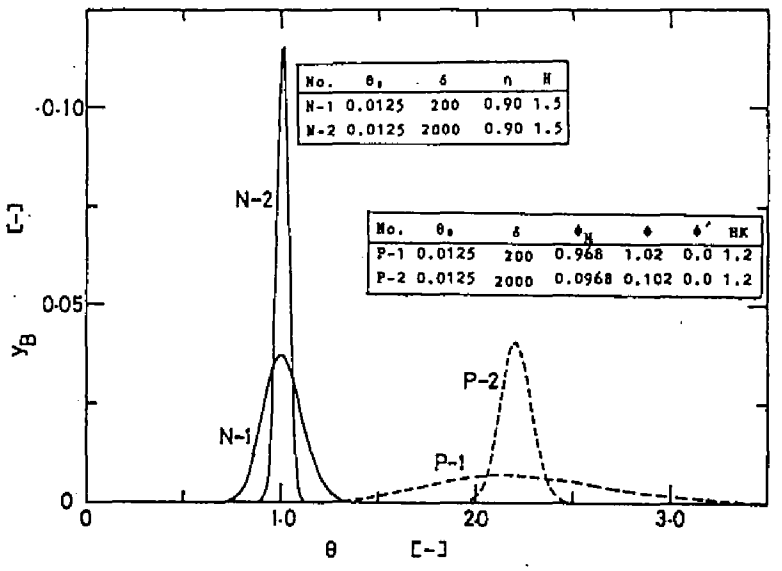

Fig. 6-9. Theoretical elution profiles of product of irreversible reaction in columns packed with enzymes immobilized to non-porous and porous supports. Symbol N represents the non-porous support and P the porous one. The non-dimensional parameters used in the calculation are listed in the figure.

The elution curves of pulse inputs in immobilized-enzyme column with an irreversible reaction were calculated theoretically for two cases. The first case is that the enzyme was immobilized into a porous carrier. The second is that the enzyme is attached onto a non-porous support. Figure 6-9 shows the elution curves, where P and N denote the porous and non-porous carriers, respectively. The following conditions are adopted in calculation. The size of column is 8 mmϕ X 200 mm. The void fraction of the bed is 0.4 for both the carriers. The common distribution coefficients for

substrate and product are used to be 0.8. The gel phase diffusion coefficient for substrate is 2 X 10^{-6} cm^2/s and is identical to that for product. The average residence time based on the void volume of the bed is 5 min in each calculation. The rate constant is set to make the conversion 0.7. Two different diameters of particles are considered to be 50 μ and 500 μ. The values of non-dimensional parameters used in calculation are listed in the figure. The figure indicates that the use of non-porous support is superior to that of porous support as long as the enzyme immobilized onto non-porous support exhibits a high activity.

Reversible reactions. Let us consider the reaction scheme which follows:

$$A \underset{k_2}{\overset{k_1}{\rightleftharpoons}} B \tag{6-23}$$

where k_1 and k_2 are the first-order rate constants of forward and backward reactions.

(i) *Porous support.* When the enzyme is immobilized into a porous support, the mass balance equations for A and B are expressed in the same way as Eqs. (6-6) to (6-9) for irreversible first-order reaction. The solutions for y_A and y_B in the Laplace domain are given by

$$\bar{y}_A = [\{1 - \exp(-s\theta_0)\}/s][\beta_1 \exp(\xi_1) - \beta_1 \exp(\xi_2)] \tag{6-24}$$

$$\bar{y}_B = [\{1 - \exp(-s\theta_0)\}/s] \cdot \beta_1 \cdot [\exp(\xi_2) - \exp(\xi_1)] \qquad (6\text{-}25)$$

where

$$\xi_1 = \frac{-s - 3HK\lambda_1/(\phi'^2\lambda_1+\phi^2)}{1/2+\{1/4+(1/\delta)[s+3HK\lambda_1/(\phi'^2\lambda_1+\phi^2)]\}^{1/2}} \qquad (6\text{-}26a)$$

$$\xi_2 = \frac{-s - 3HK\lambda_0/(\phi'^2\lambda_0+\phi^2)}{1/2+\{1/4+(1/\delta)[s+3HK\lambda_0/(\phi'^2\lambda_0+\phi^2)]\}^{1/2}} \qquad (6\text{-}26b)$$

$$\lambda_0 = (s\phi^2)^{1/2}\coth(s\phi^2)^{1/2} - 1 \qquad (6\text{-}27a)$$

$$\lambda_1 = (s\phi^2+\phi_{M1}^2+\phi_{M2}^2)^{1/2}\coth(s\phi^2+\phi_{M1}^2+\phi_{M2}^2)^{1/2} - 1 \qquad (6\text{-}27b)$$

$$\beta_1 = \phi_{M1}^2/(\phi_{M1}^2+\phi_{M2}^2) \qquad (6\text{-}27c)$$

$$\beta_2 = \phi_{M2}^2/(\phi_{M1}^2+\phi_{M2}^2) \qquad (6\text{-}27d)$$

and

$$\phi_{M1} = R(k_1/D_s)^{1/2} \qquad (6\text{-}28a)$$

$$\phi_{M2} = R(k_2/D_s)^{1/2} \qquad (6\text{-}28b)$$

To simplify, the distribution coefficients and diffusion coefficients of components A and B are assumed to be identical. The inverse Laplace transform can be achieved numerically by Eqs. (6-15) or (6-16). The above solutions are applicable when the film diffusional resistance cannot be ignored. When the k_f value is assumed to be infinite, the solutions become simpler.

(ii) *Non-porous support.* Considering the reverse reaction, the mass balance equations for A and B are expressed in the same way as Eqs. (6-17) and (6-18) for irreversible first-order reaction. The solutions of y_A and y_B in Laplace domain are given by

$$\bar{y}_A = [\{1-\exp(-s\theta_0)\}/s][\{\eta_1/(\eta_1+\eta_2)\}\exp(\xi_3) + \{\eta_2/(\eta_1+\eta_2)\}\exp(\xi_4)] \quad (6\text{-}29)$$

$$\bar{y}_B = [\{1-\exp(-s\theta_0)\}/s][\eta_1/(\eta_1+\eta_2)][\exp(\xi_4)-\exp(\xi_3)] \quad (6\text{-}30)$$

where

$$\xi_3 = \frac{-s - (\eta_1+\eta_2)H}{1/2+\{1/4+(1/\delta)[s+(\eta_1+\eta_2)H]\}^{1/2}} \quad (6\text{-}31a)$$

$$\xi_4 = \frac{-s}{1/2+[1/4+s(1/\delta)]^{1/2}} \quad (6\text{-}31b)$$

and

$$\eta_1 = 3k_1\tau/R \quad (6\text{-}32a)$$

$$\eta_2 = 3k_2\tau/R \quad (6\text{-}32b)$$

Consecutive reactions. The reaction scheme is given by Eq. (6-33) where a reactant A is converted into an intermediate B by an enzyme E_1, and B is changed to the final product C by another enzyme E_2. Each step is considered to be a first-order reaction.

$$A \xrightarrow[(E_1)]{k_1} B \xrightarrow[(E_2)]{k_2} C \tag{6-33}$$

For consecutive reactions, two cases are considered. The first (denoted by CI) is where two enzymes (E_1 and E_2) are coimmobilized in a carrier. The second (denoted by M) is where E_1 and E_2 are immobilized independently in different carriers and then mixed.

(1) *Coimmobilized system.* Two kinds of supports, porous and non-porous supports, are considered.

(i) *Porous support.* The mass balance equations for A, B, and C are described by Eqs. (6-6) to (6-9) except for the reaction terms in the gel phase. The solutions of y_A and y_B in the Laplace domain are given by

$$\bar{y}_A = [\{1-\exp(-s\theta_0)\}/s]\exp(\omega_1) \tag{6-34}$$

$$\bar{y}_B = [\{1-\exp(-s\theta_0)\}/s]\cdot[\phi_{M1}^2/(\phi_{M1}^2+\phi_{M2}^2)] \cdot[\exp(\omega_2)-\exp(\omega_1)] \tag{6-35}$$

where

$$\omega_1 = \frac{-s - 3HK\lambda_1/(\phi'^2\lambda_1+\phi^2)}{1/2+\{1/4+(1/\delta)[s+3HK\lambda_1/(\phi'^2\lambda_1+\phi^2)]\}^{1/2}} \tag{6-36a}$$

$$\omega_2 = \frac{-s - 3HK\lambda_2/(\phi'^2\lambda_2+\phi^2)}{1/2+\{1/4+(1/\delta)[s+3HK\lambda_1/(\phi'^2\lambda_1+\phi^2)]\}^{1/2}} \tag{6-36b}$$

and

$$\lambda_1 = (s\phi^2+\phi_{M1}^2)^{1/2}\coth(s\phi^2+\phi_{M1}^2)^{1/2} - 1 \qquad (6\text{-}37a)$$

$$\lambda_2 = (s\phi^2+\phi_{M2}^2)^{1/2}\coth(s\phi^2+\phi_{M2}^2)^{1/2} - 1 \qquad (6\text{-}37b)$$

The solutions for y_C in the Laplace domain is expressed by Eq. (6-38) using the $\bar{y}_0$ that is the solution for y_A in the Laplace domain with no reaction.

$$\bar{y}_C = \bar{y}_0 - \bar{y}_A - \bar{y}_B \qquad (6\text{-}38)$$

$$\bar{y}_0 = \frac{1-e^{-s\theta_0}}{s}\exp\left[\frac{-s - 3HK\lambda_0/(\phi'^2\lambda_0+\phi^2)}{1/2+\{1/4+(1/\delta)[s+3HK\lambda_0/(\phi'^2\lambda_0+\phi^2)]\}^{1/2}}\right] \qquad (6\text{-}39)$$

where

$$\lambda_0 = (s\phi^2)^{1/2}\coth(s\phi^2)^{1/2} - 1 \qquad (6\text{-}40)$$

(ii) *Non-porous support.* The solutions of y_A, y_B, and y_C in the Laplace domain are expressed by the following equations.

$$\bar{y}_A = [\{1-\exp(-s\theta_0)\}/s]\cdot\exp(\omega_4) \qquad (6\text{-}41)$$

$$\bar{y}_B = [\{1-\exp(-s\theta_0)\}/s]\cdot[\eta_1/(\eta_1-\eta_2)] \cdot[\exp(\omega_5)-\exp(\omega_4)] \qquad (6\text{-}42)$$

$$\bar{y}_C = [\{1-\exp(-s\theta_0)\}/s]\cdot[\exp(\omega_3)+\{\eta_2/(\eta_1-\eta_2)\}\exp(\omega_4) -\{\eta_1/(\eta_1-\eta_2)\}\exp(\omega_5)] \qquad (6\text{-}43)$$

where

$$\omega_3 = \frac{-s}{1/2+[1/4+s(1/\delta)]^{1/2}} \tag{6-44a}$$

$$\omega_4 = \frac{-s - \eta_1 H}{1/2+[1/4+(1/\delta)(s+\eta_1 H)]^{1/2}} \tag{6-44b}$$

$$\omega_5 = \frac{-s - \eta_2 H}{1/2+[1/4+(1/\delta)(s+\eta_2 H)]^{1/2}} \tag{6-44c}$$

(2) *Mixed ststem.* The enzyme E_1 (which catalyzes the reaction $A \longrightarrow B$) is immobilized to a gel with a radius R_1, and another enzyme E_2 to a gel with a radius R_2. The volumetric fraction of gel with R_1 (R_2) to the total volume occupied by the gel is represented by γ_1 (γ_2).

(i) *Porous support.* Equations (6-45) and (6-46) show the solutions for y_A and y_B in the Laplace domain.

$$\bar{y}_A = [\{1-\exp(-s\theta_0)\}/s]\cdot\exp(\nu_1) \tag{6-45}$$

$$\bar{y}_B = \frac{1-e^{-s\theta_0}}{s}\cdot\frac{(\xi_1/\phi_1^2)(\lambda_1-\lambda_3)}{(\xi_1/\phi_1^2)(\lambda_1-\lambda_3)+(\xi_2/\phi_2^2)(\lambda_4-\lambda_2)} \cdot[\exp(\nu_2)-\exp(\nu_1)] \tag{6-46}$$

where

$$\nu_1 = \frac{-s-3\xi_1\lambda_3/\phi_1^2-3\xi_2\lambda_2/\phi_2^2}{1/2+[1/4+(1/\delta)(s+3\xi_1\lambda_3/\phi_1^2+3\xi_2\lambda_2/\phi_2^2)]^{1/2}} \tag{6-47a}$$

$$\nu_2 = \frac{-s-3\xi_1\lambda_1/\phi_1^2-3\xi_2\lambda_2/\phi_2^2}{1/2+[1/4+(1/\delta)(s+3\xi_1\lambda_1/\phi_1^2+3\xi_2\lambda_4/\phi_2^2)]^{1/2}} \tag{6-47b}$$

and

$$\lambda_1 = (s\phi_1^2)^{1/2}\coth(s\phi_1^2)^{1/2} - 1 \tag{6-48a}$$

$$\lambda_2 = (s\phi_2^2)^{1/2}\coth(s\phi_2^2)^{1/2} - 1 \tag{6-48b}$$

$$\lambda_3 = (s\phi_1^2+\phi_{M1}^2)^{1/2}\coth(s\phi_1^2+\phi_{M1}^2)^{1/2} - 1 \tag{6-48c}$$

$$\lambda_4 = (s\phi_2^2+\phi_{M2}^2)^{1/2}\coth(s\phi_2^2+\phi_{M2}^2)^{1/2} - 1 \tag{6-48d}$$

The solution for the final product in the Laplace domain is expressed by Eq.(6-49) according to the linearity of the Laplace transformation:

$$\bar{y}_C = \bar{y}_0 - \bar{y}_A - \bar{y}_B \tag{6-49}$$

$$\bar{y}_0 = \frac{1-e^{-s\theta_0}}{s}\exp\left[\frac{-s-3\xi_1\lambda_1/\phi_1^2-3\xi_2\lambda_2/\phi_2^2}{1/2+\{1/4+(1/\delta)(s+3\xi_1\lambda_1/\phi_1^2+3\xi_2\lambda_2/\phi_2^2)\}^{1/2}}\right] \tag{6-50}$$

and

$$\phi_{M1} = R_1(k_1/D_s)^{1/2} \tag{6-51a}$$

$$\phi_{M2} = R_2(k_2/D_s)^{1/2} \tag{6-51b}$$

$$\phi_1 = R_1[1/(D_s\tau)]^{1/2} \tag{6-51c}$$

$$\phi_2 = R_2[1/(D_s\tau)]^{1/2} \tag{6-51d}$$

$$\xi_1 = (1 - \varepsilon)\gamma_1 K/\varepsilon \tag{6-51e}$$

$$\xi_2 = (1 - \varepsilon)\gamma_2 K/\varepsilon \tag{6-51b}$$

Altough solutions can be found where the k_f value is finite, they become much more complex. The solutions shown here are obtained by ignoring the resistance of film diffusion.

(ii) *Non-porous support.* The solutions for y_A, y_B, and y_C in the Laplace domain are expressed by the following equations.

$$\bar{y}_A = [\{1-\exp(-s\theta_0)\}/s]\cdot\exp(\nu_4) \tag{6-52}$$

$$\bar{y}_B = [\{1-\exp(-s\theta_0)\}/s]\cdot[\eta_1/(\eta_1-\eta_2)] \cdot[\exp(\nu_5)-\exp(\nu_4)] \tag{6-53}$$

$$\bar{y}_C = [\{1-\exp(-s\theta_0)\}/s]\cdot[\exp(\nu_3)+\{\eta_2/(\eta_1-\eta_2)\}\exp(\nu_4) -\{\eta_1/(\eta_1-\eta_2)\}\exp(\nu_5)] \tag{6-54}$$

where

$$\nu_3 = \frac{-s}{1/2+[1/4+s(1/\delta)]^{1/2}} \tag{6-55a}$$

$$\nu_4 = \frac{-s - \eta_1 H}{1/2+[1/4+(1/\delta)(s+\eta_1 H)]^{1/2}} \tag{6-55b}$$

$$\nu_5 = \frac{-s - \eta_2 H}{1/2+[1/4+(1/\delta)(s+\eta_2 H)]^{1/2}} \tag{6-55c}$$

and

$$\eta_1 = 3k_1\gamma_1\tau/R_1 \qquad (6\text{-}56a)$$

$$\eta_2 = 3k_2\gamma_2\tau/R_2 \qquad (6\text{-}56b)$$

Nomenclature

C_{E0}	total enzyme concentration	[mg-protein/l]
C_i	concentration of component i at mobile phase (i = A, B, and C)	[mol/l]
C_{iS}	concentration of i at gel phase	[mol/l]
D_s	gel-phase diffusion coefficient	[cm^2/s]
D_z	axial dispersion coefficient	[cm^2/s]
H	= (1 - ε)/ε	[-]
K	distribution coefficient	[-]
Ki	inhibition constant	[mol/l]
Km	Michaelis constant	[mol/l]
k	first-order rate constant	[s^{-1}]
k_0	molecular activity	[mol/mg-protein·s]
k_f	mass transfer coefficient	[cm/s]
R	particle radius	[cm]
r	radial distance	[cm]
r_A	formation rate of substrate	[mol/l·s]
s	Laplace transform variable (complex number)	[-]
t	time	[s]

u	linear interstitial velocity	[cm/s]
u_0	linear superficial velocity	[cm/s]
Vmax	maximum reaction rate	[mol/l·s]
y_i	$= C_i/C_{A0}$	[-]
$\bar{y}_i$	solution of y_i in Laplace domain	[-]
Z	bed height	[cm]
z	axial distance	[cm]
γ_i	volumetric fraction of gel with R_i to total gel	[-]
δ	$= Z/(D_z/u)$	[-]
ϵ	void fraction of the bed	[-]
θ	$= t/\tau$	[-]
μ_1'	first-order normalized statistical moment	[s]
μ_2	second-order normalized central moment	[s^2]
ξ_i	$= (1 - \epsilon)\gamma_i K/\epsilon$	[-]
τ	average residence time	[s]
ϕ	$= R[1/(D_s\tau)]^{1/2}$	[-]
ϕ'	$= R[1/(Rk_f\tau)]^{1/2}$	[-]
ϕ_M	$= R(k/D_s)^{1/2}$	[-]

Literature Cited

1) K. Ohmiya, C. Terao, S. Shimizu, and T. Kobayashi, *Agric. Biol. Chem.*, 39, 491 (1975).

2) E. C. Toren, Jr., *J. Chem. Educ.*, 44, 172 (1967).

3) M. Dixon and E. C. Webb, "*Enzymes*," Academic Press, New York, 1958, p.73.

4) M. Kubin, *Collect. Czech. Chem. Commun.*, 30, 1104 (1965).

5) M. Suzuki, *J. Chem. Eng. Jpn*, 7, 262 (1974).

6) K. Nakanishi, S. Yamamoto, R. Matsuno, and T. Kamikubo, *Agric. Biol. Chem.*, 41, 1465 (1977).

7) W. N. Marrazo, R. L. Merson, and B. J. McCoy, *Biotechnol. Bioeng.*, 17, 1515 (1975).

8) N. Wakao, K. Tanaka, and D. S. Scott, *J. Chem. Eng. Jpn*, 6, 547 (1973).

9) K. S. Crump, *J. ACM*, 23, 89 (1976).

10) S. Yamamoto, K. Nakanishi, R. Matsuno, and T. Kamikubo, *Agric. Biol. Chem.*, 43, 2499 (1979).

11) O. Levenspiel, "*Chemical Reaction Engineering*," Wiley, New York, 1972, p.282.

12) E. J. Wilson and C. J. Geankoplis, *Ind. Eng. Chem. Fundamentals*, 5, 9 (1966).

Chapter 7

Elution Profiles in Reversible and Consecutive Reactions.

7. 1. Introduction

In Chapter 6, a theoretical method for predicting the elution profile of a pulse input in an immobilized-enzyme column was presented, and its validity was confirmed experimentally with a first-order irreversible invertase reaction.

In clinical and food analysis, a substrate not easy to analyze is frequently converted to a readily detectable product by reversible or consecutive reactions. A theoretical method for predicting the elution profile of the product was easily extended to such systems in Chapter 6, although it has not been verified experimentally. In this chapter, the method will be confirmed experimentally for such systems, and the effect of the properties of the substrate and the immobilized enzyme and of the operational variables on the elution curves will be examined theoretically.

As model systems of reversible and consecutive reactions catalyzed by enzymes, we adopted the isomerization of glucose, and the hydrolysis of sucrose, and oxidation of glucose shown in Eqs. (7-1) and (7-2).

$$\text{glucose} \underset{k_2}{\overset{\text{glucose isomerase},\ k_1}{\rightleftharpoons}} \text{fructose} \qquad (7\text{-}1)$$

$$\text{sucrose} \xrightarrow[k_1]{\text{invertase}} \text{glucose} \xrightarrow[k_2]{\text{glucose oxidase}} \text{gluconic acid} \qquad (7\text{-}2)$$

For the consecutive reactions, two cases are considered. The first is where invertase and glucose oxidase are co-immobilized in a carrier; the second is where they are immobilized independently in different carriers and then mixed. The former is called a co-immobilized system and the latter a mixed-type system.

3. 2. Materials and Methods

Materials. The immobilized glucose isomerase (commercial name, Swetase; Nagase Sangyo) was, strictly speaking, an immobilezed microorganism, that is, *Streptomyces phaeochromogenes* was linked by an ionic bond to diatomaceous earth which adsorbed the quaternary pyridine compound. Invertase and glucose oxidase were purchased from Sigma. Blue Dextran was obtained from Pharmacia. Acrylamide monomer (AAm), N,N'-methylenebisacrylamide (BIS), L-cysteine, N,N,N',N'-tetramethylethylenediamine (TEMED), sorbitan, sucrose, glucose, and fructose were purchased from Nakarai Chemicals. All other reagents were of analytical grade.

Immobilization of invertase and glucose oxidase. The method for immobilizing the invertase and glucose oxidase in acrylamide gels was the same as that mentioned in Chapter 6 except for the addition of L-cystein to protect the glucose oxidase activity.[1)]

Co-immobilization of the two enzymes were carried out as follows with the independent immobilization of the enzymes is given in parentheses: Six ml of 0.04%(w/v) invertase, 4 ml of 0.25%(w/v) glucose oxidase (8 ml of 0.025%(w/v) invertase or 0.25%(w/v) glucose oxidase) and 6 ml (8 ml) of 3%(w/v) L-cystene were mixed with 40 ml of 33%(w/v) AAm-BIS solution, the BIS content of which was 5%. After addition of 4 ml of 5%(w/v) ammonium persulfate to the mixture, the aqueous solution was quickly poured into 300 ml of toluene-chloroform (18/7) solvent containing 0.5 ml of sorbitan and 0.96 ml of TEMED. The enzymes and other reagents were dissolved in 0.01 mol/l acetate buffer with pH 5.0. The polymerization was performed at 0 - 4°C for 20 min under a nitrogen atmosphere, with magnetic stirring (200 - 220 r.p.m.). The gels were separated from the organic solvent by filtration, washed with chilled distilled water, and sieved to regulate the size. They were suspended in the buffer and stored in a refrigerator until use.

Using buffer solution instead of the enzyme solution, inactive acrylamide gels containing no enzymes were prepared by the same procedure described above.

Reaction rate constants of immobilized enzymes. The reaction rate constants of immobilized enzymes were estimated using immobilized-enzyme gel granulated to reduce the gel radius (less than 100 μm) and to remove intraparticle diffusional residence (Theile

modulus ϕ_M < 0.62). The Michaelis constants and maximum reaction rates of immobilized glucose isomerase for forward and reverse reactions were determined as follows: about 0.8 - 0.9 g (wet weight) of granulated immobilized-enzyme gel was weighed accurately. By addition of 40 ml of glucose (or fructose) solution, the reaction was allowed to run with 0.05 mol/l Tris-HCl buffer (pH 8.0) containing 0.01 mol/l magnesium sulfate at 50°C with magnetic stirring. Considering from stirring speed, particle size, and diffusivity of the substrate, it was confirmed that the effect of film diffusional resistance can be ignored. At appropriate intervals, 0.1 ml of the reaction mixture was sampled and the amount of fructose (or glucose) produced was analyzed by the cysteine-carbazole-H_2SO_4 method[2] (or the glucostat method[3]). The time course usually included five points. The initial concentrations of the substrate were in the range of 0.15 to 1.50 mol/l. Conversion was less than 5%. The Michaelis constants and maximum reaction rates for the forward and reverse reactions were estimated by Lineweaver-Burk plots.

The Michaelis constants of free invertase and glucose oxidase at 25°C and pH 5.0 (0.05 mol/l acetate buffer) were 0.030 mol/l and 0.029 mol/l, respectively. The substrate inhibition constant of free invertase was 0.8 mol/l. The rate constants of the first-order reactions catalyzed by immobilized invertase and glucose oxdase were estimated from the conversion *versus* reaction time plot

where the substrate (sucrose or glucose) concentration was much less than the Michaelis constant. Under these conditions, the effect of substrate inhibition of invertase on estimating the rate constant could be ignored entirely. The reaction was started by the addition of 40 ml of sucrose (or glucose) solution to about 2 g of the granulated immobilized-enzyme gel, which had been weighed accurately in an Erlenmeyer flask. The decrease of the substrate concentration was observed at intervals. The amount of sucrose and glucose were analyzed by a high-performance liquid chromatography (Shimadzu LC-3A) equipped with a separation column (Shimadzu SCR-101) and a differential refractometer (Showa Denko Shodex RI SE-11) and by the glucostat method, respectively. The substrate concentrations were 3.0×10^{-4} mol/l and 5.0×10^{-4} mol/l for sucrose and glucose.

Physical properties of the immobilized-enzyme column and substrate. The physical properties of the substrate and product for the two reaction systems were assumed to be the same as those of glucose. The values of the axial dispersion coefficient, the gel phase diffusion coefficient, the distribution coefficient of glucose, and the void fraction of the bed were determined by moment analysis[4-6] of elution profiles of glucose and Blue Dextran. The immobilized-glucose isomerase gel denatured by heating or an inactive acrylamide gel was packed into a column. The pulse of a glucose solution was eluted at 50°C or at 25°C with 0.05 mol/l

Tris-HCl buffer (pH 8.0) containing 0.01 mol/l magnesium sulfate, or with 0.01 mol/l acetate buffer (pH 5.0). The concentration of the eluate was analyzed by the glucostat method or by a differential refractometer. The diameters of the gels were measured with an optical microscope (Olympus Optical). The mean value of the gel radius was calculated according to Nakanishi *et al.*[7] The details of the experimental and analytical methods are described in Chapter 6 and Ref. 6.

Pulse Response Experiments. The immobilized-glucose isomerase gel was packed into a column equipped with a water jacket. Glucose (0.5 ml) (or fructose) solution was carefully added to the top of the bed, and the flow was started. After the substrate solution disappeared, the eluent (0.05 mol/l Tris-HCl buffer containing 0.01 mol/l magnesium sulfate) was added by a constant-feeding pump (Tokyo Rikakikai MP-101). The bed was kept at 50°C. The glucose and fructose concentrations in the eluate collected at the bottom of the bed were analyzed by the glucostat method and the cysteine-carbazol-H_2SO_4 method, respectively.

For the consecutive reactions catalyzed by immobilized invertase and glucose oxidase, the acrylamide gel where the two enzymes were co-immobilized was packed into a column. But, for the mixed-type system, the immobilized-invertase gel was mixed with the immobilized-glucose oxidase gel at the ratio of 0.433/0.567 on the basis of wet weight. Then the mixed gel was packed. The volume of suc-

rose solution applied to the column was 0.5 or 3.0 ml. The eluent was 0.01 mol/l acetate buffer (pH 5.0) and the bed was kept at 25 °C. The experimental methods were the same as those described above. The sucrose and glucose concentrations in the eluate were determined by high-performance liquid chromatography (HPLC). The gluconic acid concentration could not be analyzed, because the elution volume of gluconic acid in HPLC was equivalent to that of the acetate buffer solution and because ordinary chemical analysis was useless in low concentrations.

Prediction of elution curves. When the reactions catalyzed by immobilized enzymes are taken to be a first-order reversible reaction and first-order consecutive reactions, the methods for predicting the elution profiles of substrate, intermediate, and product are described in Chapter 6.

7. 3. Results and Discussion

Kinetic parameters of immobilized glucose isomerase. The Michaelis constants and maximum reaction rates for forward and reverse reactions catalyzed by immobilized glucose isomerase were estimated at 50°C. The values of the kinetic parameters are shown in Table 7-1. These values are considered to be intrinsic, because of the small radius, the rapid magnetic stirring, and the coincidence with the Michaelis constants of free glucose isomerase.

Table 7-1. Kinetic Parameters of Immobilized Glucose Isomerase at pH 8.0 and 50°C.

	Km [mol/l]	Vmax X 10^3 [mol/l·s]
Forward reaction	0.259	1.29
Reverse reaction	0.262	1.30

The first-order reaction rate constants for forward and reverse reactions were calculated from the parameters to be 4.98 X 10^{-3} and 4.96 X 10^{-3} s^{-1}, respectively.

Physical properties of immobilized glucose isomerase and glucose. The immobilized glucose isomerase was denatured by heating and packed in a column. The values of the axial dispersion coefficient, the gel phase diffusion coefficient, and the distribution coefficient of glucose were estimated by moment analysis of elution curves of glucose. The void fraction of the bed was determined from the elution profiles of Blue Dextran, which could not permeate into the gel matrix due to its high molecular size.

Table 7-2. Parameters of Immobilized-Glucose Isomerase Column and Glucose at 50°C.

d_p [cm]	ε [-]	K [-]	D_z/u [cm]	D_s [cm^2/s]
0.0862	0.407	0.626	0.339	1.29 X 10^{-6}

The values estimated are listed in Table 7-2. Since the values of the distribution coefficient and the gel phase diffusion coefficient are relatively small, the gel structure of immobilized glucose isomerase can be inferred to be dense.

Pulse response in an immobilized-glucose isomerase column.

A pulse of glucose or fructose solution was applied to an immobilized-glucose isomerase column, and the glucose and fructose concentrations in the eluate were determined. The experimental conditions are summarized in Table 7-3. The glucose concentration applied to the column in run 2 was half of that in run 1. As substrate solution, a fructose solution was applied in run 3. In run 4, the flow rate of the eluent was increased as compared with other runs. The elution profiles of glucose and fructose at the

Table 7-3. Experimental Conditions for Pulse Response in an Immobilized-Glucose Isomerase Column.

Run No.	1	2	3	4
Column size	1.47 cmϕ X 23.3 cm			
Substrate	glucose		fructose	glucose
C_{A0} [mol/l]	$3.00X10^{-2}$	$1.50X10^{-2}$	$3.00X10^{-2}$	$3.00X10^{-2}$
Injection volume [cm^3]	0.5			
Flow rate [cm^3/s]	5.78×10^{-2}			$9.27X10^{-2}$
k_1 [s^{-1}]	4.98×10^{-3}			
k_2 [s^{-1}]	4.96×10^{-3}			
Eluent	0.05 mol/l Tris-HCl buffer (including 0.01 mol/l $MgSO_4$, pH 8.0)			

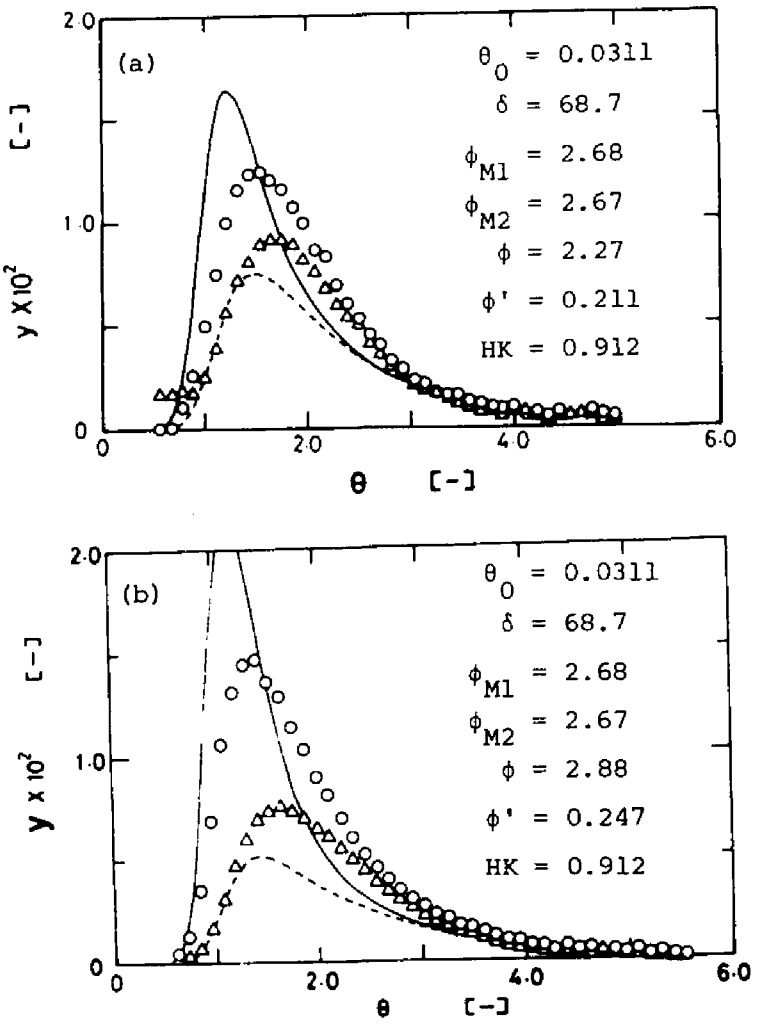

Fig. 7-1. (a) Elution profiles of glucose and fructose in an immobilized-glucose isomerase column in run 2. The symbols (○) and (△) correspond to glucose and fructose, respectively. The solid and broken curves were calculated for glucose and fructose according to the theory using the values of the dimensionless parameters listed in the figure. (b) Elution profiles of glucose and fructose obtained for run 4. The symbols are as shown in (a). The dimensionless parameters used for calculating the theoretical curves are listed in the figure.

outlet of the column, which were obtained for run 2, are shown in Fig. 7-1(a). The abscissa and the coordinate are the time and the concentration, which are both normalized by the residence time based on the void volume of the bed and the substrate concentration applied to the column as a pulse, respectively. Theoretical elution profiles represented by the solid and broken curves coincide fairly well with the experimental ones. In the calculation of the theoretical curves, the mass transfer coefficient was estimated from the correlation proposed by Wilson and Geankoplis.[10] The elution curve of glucose and fructose broadened by increasing the flow rate of the eluent. They were obtained in run 4 and are shown in Fig. 7-1(b). Theoretical elution curves are representative of the peak broading. The experimental elution curves of other runs which are not illustrated here were in agreement with the theoretical ones in the same degree of coincidence as runs 2 and 4.

Physical properties of the acrylamide gel column and glucose.

Acrylamide gel containing no enzymes was packed into a column. The values of the axial dispersion coefficient, the gel phase diffusion coefficient, and the distribution coefficient of glucose were obtained for three different gel diameters. The AAm-BIS concentration and the BIS content were the same as those when the enzymes were immobilized. Results obtained are listed in Table 7-4. The Peclet number for axial dispersion in a fixed bed (=

Table 7-4. Parameters of Acrylamide Gel Column and Glucose at 25°C.

d_p [cm]	ε [-]	K [-]	D_z/u [cm]	D_s [cm^2/s]
0.0651	0.433	0.927	0.144	2.57×10^{-6}
0.0856	0.446	0.895	0.283	2.72×10^{-6}
0.1001	0.471	0.879	0.319	2.68×10^{-6}
Average	-	0.900	-	2.66×10^{-6}

ud_p/D_z) is reported to be 1/3 to 1/2 in low Reynolds numbers.[11] In this study, the value of D_z/u is considered to be approximately twice the gel diameter. The values of the distribution coefficient and the gel phase diffusion coefficient are similar to those reported in Chapters 1 and 6.

Pulse response in co-immobilized and mixed-type systems. Two series of experiments were performed on the pulse response in an immobilized-enzyme column in which consecutive reactions were allowed to run. In the first series, invertase and glucose oxidase were co-immobilized into a carrier and called a co-immobilized system. In the second series, the two enzymes were immobilized independently in different carriers and mixed; a system of this kind is called a mixed-type system. Experimental conditions for the two series are summarized in Table 7-5. At runs 5, 6, 8, and 9 the input of sucrose solution was regarded as a pulse one, since the volume applied to the column was much smaller than the void

Table 7-5. Experimental Conditions for Pulse Response in an Immobilized-Invertase and Glucose Oxidase Column.

System	Co-immobilized			Mixed-type		
Run No.	5	6	7	8	9	10
Column size	1.485 cmϕ X 10.75 cm			1.485 cmϕ X 11.40 cm		
C_{A0} [mol/l]	1.50×10^{-2}					
Injection volume [cm^3]	0.5		3.0	0.5		3.0
Flow rate [cm^3/s]	0.0124	0.0175		0.0125	0.0175	
R_1 R R_2 [cm]	0.0293			0.0270 0.0270		
ε	0.471			0.466		
γ_1	-			0.433		
γ_2	-			0.567		
k_1 [s^{-1}]	1.91×10^{-3}			1.21×10^{-3}		
k_2 [s^{-1}]	8.85×10^{-4}			2.02×10^{-3}		
Eluent	0.01 mol/l acetate buffer (pH 5.0)					

volume of the column. To examine the effect of sample volume on elution profiles, 3 ml of sucrose solution was applied to the column at runs 7 and 10. As shown later, the inputs were no longer pulse inputs but had to be considered to be rectangular. The results for run 5 (co-immobilized type) are illustrated in Fig. 7-2, where the sucrose and glucose concentrations normalized by the sucrose concentration applied to the column are plotted against dimensionless time. The final product, gluconic acid, in the consecutive reactions could not be determined due to the absence of an adequate analytical method. The solid, broken, and dotted

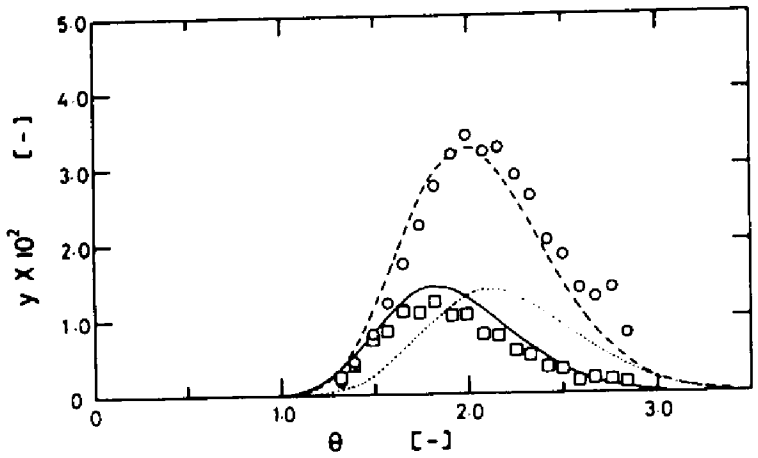

Fig. 7-2. Elution profiles of sucrose in a co-immobilized-invertase and glucose oxidase column. The symbols (□) and (○) correspomd to sucrose and glucose. The solid, broken, and dotted curves represent the theoretical curves for sucrose, glucose, and gluconic acid, respectively. Column dimension = 1.485 cmϕ X 10.75 cm. The theoretical curves were calculated using the values θ_0 = 0.057, δ = 91.72, ϕ_{M1} = 0.862, ϕ_{M2} = 0.502, ϕ = 0.674, ϕ' = 0.0, and HK = 1.07.

curves in Fig. 7-2 are theoretical curves for sucrose, glucose, and gluconic acid. The solid and broken curves coincide well with the experimental ones of sucrose and glucose. Figures 7-3 and 7-4 show the results for runs 9 and 10 (mixed-type). The curves in Fig. 7-3 are expressed in the same manner as in Fig. 7-2. In Fig. 7-4, the thicker solid, the broken, and dotted curves (1, 2, and 3) were calculated regarding the input of the sucrose solution as rectangular. Assuming that the input was a pulse, the calculated curves are shown by the thin curves (1', 2', and 3'). The thin curves are not close to the experimental results, including that

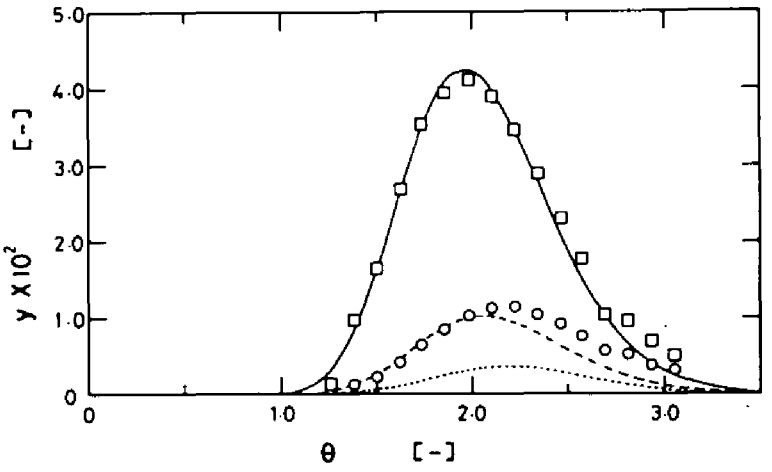

Fig. 7-3. Elution profiles of sucrose and glucose for a mixed-type system. Symbols and curves are shown in Fig. 7-2. The dimensionless parameters were as follows: θ_0 = 0.0543, δ = 105.6, ϕ_{M1} = 0.575, ϕ_{M2} = 0.743, ϕ_1 = 0.720, ϕ_2 = 0.720, ξ_1 = 0.471, and ξ_2 = 0.617. Column dimension = 1.485 cmϕ X 11.4 cm.

the input of substrate solution cannot be treated as a pulse when a large volume is applied to the column. The experimental elution curves of glucose are slightly higher than the theoretical ones in the latter part of curves in all runs. This might be due that the amount of oxygen dissolved in the eluent was equivalent to that of glucose produced by invertase-catalyzed reaction in the column.

Effects of parameters on elution profiles. Since it was proved that the mass balance model was applicable to the prediction of elution profiles in reversible and consecutive reactions,

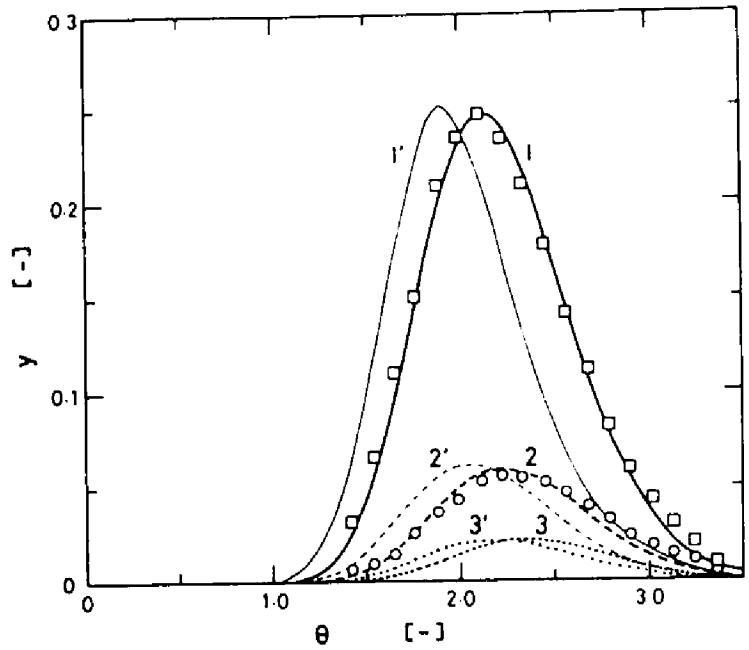

Fig. 7-4. Elution profiles of sucrose and glucose in run 10. The definitions of symbols and curves are shown in Fig. 7-2. The curves 1, 2, and 3 were calculated regarding the input of the sucrose solution as rectangular. The curves 1', 2', and 3' were obtained by assuming that the input was a pulse. In the calculation of the curves $\theta_0 = 0.3257$. The values of other parameters were the same as those in Fig. 7-3.

the effects of the dimensionless parameters on elution profiles were then examined from the theoretical calculations. Figures 7-5, 7-6, and 7-7 show the effects of the δ, ϕ, and θ_0 values on the elution profiles of the product in a reversible reaction at two HK values. δ [$= Z/(D_z/u)$] indicates the ratio of column length to the distance of the mixing of flow inside a column. ϕ ($= R[1/(D_s\tau)]^{1/2}$) is the square root of the ratio of the diffu-

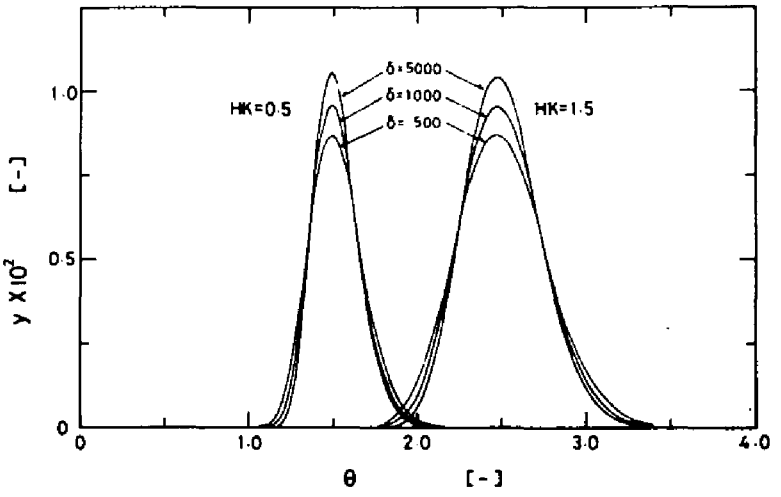

Fig. 7-5. Effect of the δ value on the elution profiles of the product in a reversible reaction. The values of the parameters used in the calculation were θ_Q = 0.01, ϕ_{M1} = 0.5, ϕ_{M2} = 0.354, ϕ = 0.5, and ϕ' = 0.0.

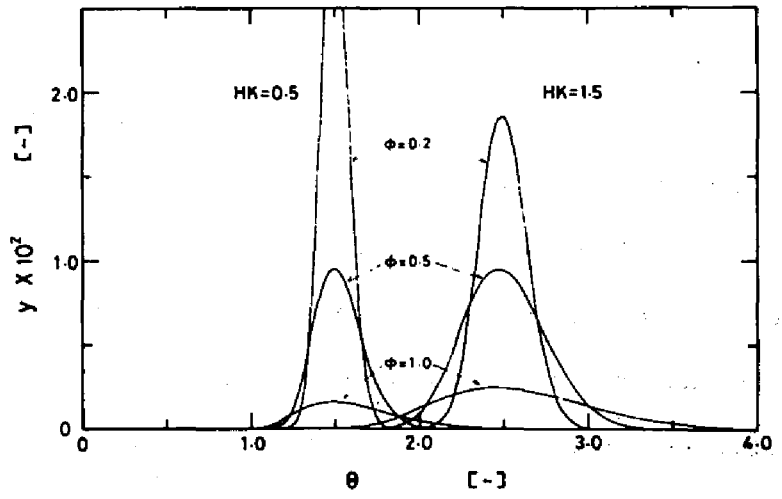

Fig. 7-6. Effect of the ϕ value on the elution profiles of the product in a reversible reaction. θ_0 = 0.01, ϕ_{M1} = 0.5, ϕ_{M2} = 0.354, ϕ' = 0.0, and δ = 1000.

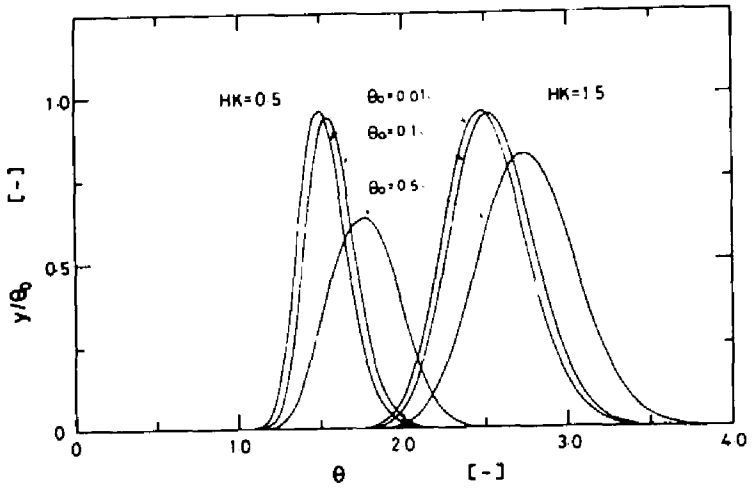

Fig. 7-7. Effect of sample volume on the elution profiles of the product in a reversible reaction. The curves are obtained under conditions where $\phi_{M1} = 0.5$, $\phi_{M2} = 0.354$, $\phi = 0.5$, $\phi' = 0.0$, and $\delta = 1000$.

sional time in the gel to the residence time in the void volume of a column. θ_0 ($= t_0/\tau$) is the ratio of the sample volume applied to a column to the void volume of a column. HK [$= (1 - \varepsilon)K/\varepsilon$] represents the ratio of the effective gel phase volume for a solute to the void volume of a column. The effects of these parameters on the elution curves were examined under conditions where the reaction was free from film mass transfer resistance. As shown in Fig. 7-5, the δ value does not affect the peak position and symmetry of elution curves but relates the width of the curves. When the ϕ value increases, that is, when the gel phase diffusional resistance is significant or the residence time is short, the elution curve broadens (Fig. 7-6). Although not shown in Fig.

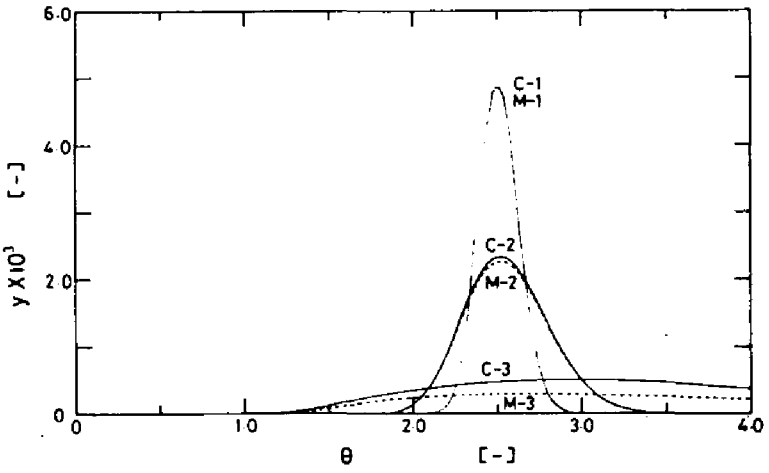

Fig. 7-8. Theoretical elution profiles of the final product of consecutive reactions in co-immobilized and mixed-tpye enzyme columns. The product of each reaction rate constant and the residence time is kept the same. Symbols C and M represent the co-immobilized and the mixed-type system, respectively. The values of θ_0 and δ were set to be 0.01 and 1000 for both systems. The HK value was 1.5. The values of ξ_1 and ξ_2 were both 0.75. The ϕ' value for the co-immobilized system was 0.0. The values of ϕ, ϕ_1, and ϕ_2 were 0.1 for C-1 and M-1, 0.5 for C-2 and M-2, and 2.5 for C-3 and M-3. The ϕ_{M1} and ϕ_{M2} values were 0.0708 and 0.0636 for C-1, 0.354 and 0.318 for C-2, 1.77 and 1.59 for C-3, 0.10 and 0.09 for M-1, 0.5 and 0.45 for M-2, and 2.50 and 2.25 for M-3. Curves C-1 and M-1 are added together.

7-6, the increase of the ϕ value results in the early appearance of a peak and in the asymmetry of the elution curve of the substrate. Figure 7-7 shows the effect of sample volume on elution curves. When the sample volume is less than 5% of the void volume

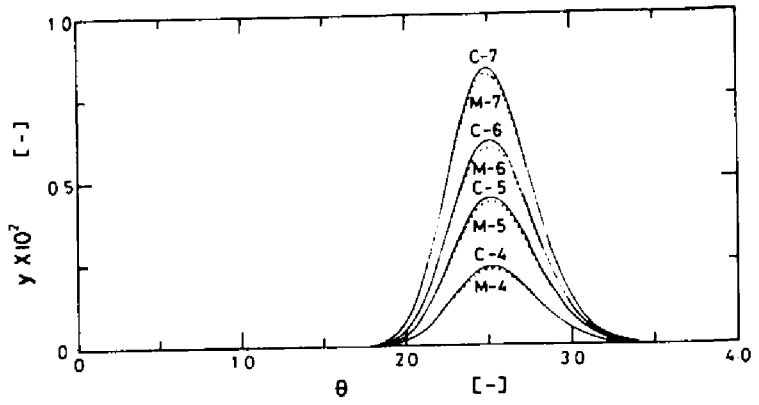

Fig. 7-9. Effect of the ratio of the rate constant of a first-step reaction to that of a second-step reaction on the elution curves of the final product in consecutive reactions with low ϕ and ϕ_{M1} values. Symbols are shown in Fig. 7-8. The curves were calculated under conditions where $\theta_0 = 0.01$, $\delta = 100$, ϕ_{M1} for C-4 to C-7 = 0.354, ϕ_{M1} for M-4 to M-7 = 0.50, $\phi = \phi_1 = \phi_2 = 0.5$, $\phi' = 0.0$, HK = 1.5, $\xi_1 = \xi_2 = 0.75$, ϕ_{M2} for C-4 = 0.317, ϕ_{M2} for C-5 = 0.500, ϕ_{M2} for C-6 = 0.708, ϕ_{M2} for C-7 = 3.54, ϕ_{M2} for M-4 = 0.477, ϕ_{M2} for M-5 = 0.707, ϕ_{M2} for M-6 = 1.00, and ϕ_{M2} for M-7 = 5.00.

of a bed, the sample volume effect is not observed and the elution curve coincides with that obtained by pulse approximation. However, when the sample volume is over 5% of the void volume, the elution curve retreats and broadens. This tendency is promoted by decreasing HK values.

Figures 7-8 to 7-10 show the elution profiles of the final product in consecutive reactions. In Fig. 7-8, the reaction rate constants of consecutive reactions are varied keeping constant the

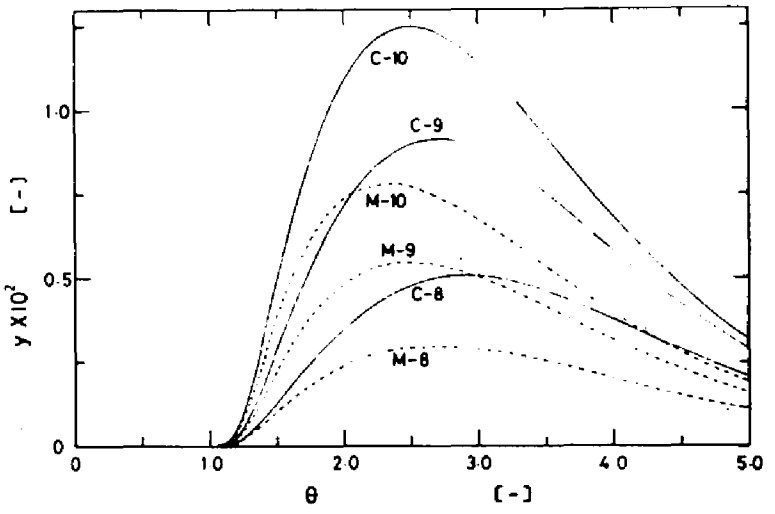

Fig. 7-10. Theoretical elution profiles of the final product of consecutive reactions at high ϕ and ϕ_{M1} values. The values of θ_0, δ, and ϕ ($\phi_1 = \phi_2$) were 0.01, 1000, and 2.50, respectively, for all curves. The ϕ' value was 0.0. The HK value was 1.5, and $\phi_1 = \phi_2 = 0.75$. The ϕ_{M1} value for the co-immobilized system was 1.77, and that for the mixed-type one was 2.50. The ϕ_{M2} values for C-8, C-9, and C-10 were 1.60, 2.50, and 3.54, respectively. The ϕ_{M2} values for M-8, M-9, and M-10 were 2.25, 3.53, and 5.00.

product of each rate constant and the residence time. The conversion in the first-order reaction is provided only the value of the product. The reaction rate constant is the largest and the residence time is the shortest in C-3 and M-3. As this figure shows, a long tail appears and a clear peak is not obtained when immobilized enzymes of high activities are prepared and the residence time shortened for a rapid analysis. The ratio of the reaction rate constant of the first step to that of the second step is vari-

ed in Figs. 7-9 and 7-10 with constant ϕ values. The small ϕ value corresponds to the small gel radius or the long residence time. The elution curves are symmetrical and there is little difference between the co-immobilized system and the mixed-type one in Fig. 7-9, since the ϕ and ϕ_{Ml} values are set to be small. On the other hand, Figure 7-10 shows that asymmetrical curves are obtained when ϕ and ϕ_{Ml} are large. These conditions are unfavorable for analysis.

7. 4. Summary

A pulse of substrate solution was applied to an immobilized-enzyme column, in which the substrate was then converted by reversible or consecutive reactions. Immobilized glucose isomerase was used for the reversible reaction, and immobilized invertase and glucose oxidase for the consecutive reactions. The elution profiles of substrate and product were determined experimentally. These profiles were in good agreement with the ones predicted theoretically. The effect of some parameters on the elution profiles for reversible and consecutive reactions was discussed.

Nomenclature

C_i	concentration of component i in mobile phase	[mol/l]
C_{A0}	concentration of substrate applied to a column	[mol/l]
D_s	gel phase diffusion coefficient	[cm^2/s]

D_z	axial dispersion coefficient	[cm^2/s]
d_p	particle diameter	[cm]
H	$= (1 - \varepsilon)/\varepsilon$	[-]
K	distribution coefficient	[-]
k_1	first-order rate constant for forward or first step reaction of reversible or consecutive reactions.	[s^{-1}]
k_2	first-order rate constant for reverse or second step reaction of reversible or consecutive reactions.	[s^{-1}]
k_f	mass transfer coefficient	[cm/s]
R	particle radius	[cm]
t	time	[s]
t_0	sample injection time	[s]
u	linear interstitial velocity	[cm/s]
y_i	$= C_i/C_{A0}$	[-]
Z	bed height	[cm]
γ_i	volumetric fraction of gel with R_i to total gel	[-]
δ	$= Z/(D_z/u)$	[-]
ε	void fraction of bed	[-]
θ	$= t/\tau$	[-]
θ_0	$= t_0/\tau$	[-]
ξ_i	$= (1 - \varepsilon)\gamma_i K/\varepsilon$	[-]

τ average residence time based on the void volume of bed [s]

$\phi = R[1/(D_s\tau)]^{1/2}$ [-]

$\phi' = R[1/(k_f R\tau)]^{1/2}$ [-]

$\phi_M = R(k/D_s)^{1/2}$ [-]

Literature Cited

1) A. Dahlqvist, B. Mattiasson, and K. Mosbach, *Biotechnol. Bioeng.*, 15, 395 (1973).

2) R. O. Marshall and E. R. Kooi, *Science*, 125, 648(1957).

3) E. C. Toren, Jr., *J. Chem. Educ.*, 44, 172 (1967).

4) M. Kubin, *Collect. Czech. Chem. Commun.*, 30, 1104 (1965).

5) M. Suzuki, *J. Chem. Eng. Jpn*, 7, 262 (1974).

6) K. Nakanishi, S. Yamamoto, R. Matsuno, and T. Kamikubo, *Agric. Biol. Chem.*, 41, 1465 (1977).

7) K. Nakanishi, S. Yamamoto, R. Matsuno, and T. Kamikubo, *Agric. Biol. Chem.*, 42, 1943 (1978).

8) K. S. Crump, *J. ACM*, 23, 89 (1976).

9) S. Yamamoto, K. Nakanishi, R. Matsuno, and T. Kamikubo, *Agric. Biol. Chem.*, 43, 2499 (1979).

10) E. J. Wilson and C. J. Geankoplis, *Ind. Eng. Chem. Fundam.*, 5, 9 (1966).

11) O. Levenspiel, "*Chemical Reaction Engineering*," Wiley, New York, 1972, p.282.

Chapter 8

Determination of Pyruvate and L-Lactate in Human Serum by Pulse Response Technique

8. 1. Introduction

The theoretical method for predicting elution curves was represented and its validity was experimentally confirmed with an irreversible invertase reaction in Chapter 6, and with a reversible glucose isomerase reaction and a consecutive invertase-glucose oxdase reaction in Chapter 7. In this chapter, the pulse response technique using an immobilized-lactate dehydrogenase (LDH) column is applied to determination of pyruvate and L-lactate in human serum. The concentrations of pyruvate and L-lactate loaded were analyzed from the elution curve of NADH, which was involved in the reaction system and has a specific absorption at 340 nm. According to the theoretical considerations mentioned in Chapter 6, LDH was immobilized onto non-porous support with small diameter to obtain the sharp elution curve at the short retention time.

Here we describe the reaction systems and the operating conditions which were used in the analysis of each of the two substances (pyruvate and L-lactate). The following reaction is the key reaction in analysis of these two substances.

$$\text{pyruvate} + \text{NADH} + \text{H}^+ \overset{\text{LDH}}{\rightleftharpoons} \text{L-lactate} + \text{NAD}^+ \qquad (8\text{-}1)$$

This reaction is reversible and its equilibrium point depends on the pH of the buffer solution used.

At pH 7.4, the equilibrium constant is so large (10^4) that the reaction from the left- to the right-hand side predominates, and the reaction can be approximately treated as an irreversible one. From the stoichiometric relationship shown in Eq.(8-1), the change in the concentration of pyruvate can be evaluated by measuring the decrease in the concentration of NADH.

When we measure the concentration of L-lactate, we must adjust the reaction conditions so that the equilibrium in Eq.(8-1) will shift to the left-hand side, *i.e.*, so that the reverse reaction in Eq.(8-1) may proceed. To realize this situation, the utilization of glycine-hydrazine buffer (pH 9.4) is effective. As shown in Eqs.(8-2) and (8-3), pyruvate formed through the reaction in Eq.(8-2) is removed from the LDH-catalyzed reaction system using the reaction in Eq.(8-3).

$$\text{L-lactate} + \text{NAD}^+ \xrightarrow{\text{LDH}} \text{pyruvate} + \text{NADH} + \text{H}^+ \qquad (8\text{-}2)$$

$$\text{pyruvate} + \text{hydrazine} \longrightarrow \text{hydrazone} \qquad (8\text{-}3)$$

8. 2. Materials and Methods

Reagents. Lactate hehydrogenase from pig heart was purchased from Toyobo. The kit reagents for analyzing pyruvate and L-lactate (Pyruvate Test and Lactate Test) were obtained from Boehriger-

Mannheim. NAD and NAD^+ were products of Kohjin. Non-porous glass beads were sieved to be less than 400 mesh. All other reagents were of analytical grade.

Immobilization of LDH onto non-porous glass beads. The procedure for immobilizing LDH onto non-porous glass beads *via* diazo-coupling was essentially the same as that described in papers[1,2] except for some modifications. Glass beads (30 g) were allowed to reflux in a 10%(v/v) solution of 3-aminopropyltriethoxysilane in dry toluene for 10 hr. The beads were washed with toulene and then dried in vacuum. The beads were suspended in 40 ml of 50% (v/v) N,N-dimethylformamide (DMF). After the addition of a saturated solution of *p*-nitrobenzoylazide in a mixture of 40 ml of DMF and 60 ml of 0.2 mol/l borate buffer (pH 9.3) to the suspension, the beads were stirred for 3 hr at room temperature. After the beads were washed with 150 ml of 50%(v/v) DMF and then with 150 ml of water, the nitro group was reduced to amino group by stirring the beads in 100 ml of a mixture of 0.5 mol/l $NaHCO_3$ and 0.1 mol/l dithionite (pH 8.5) at 37°C for 1 hr. The beads were then washed with 300 ml of water. Diazotization of the *p*-amino group was achieved by stirring the beads in 100 ml of chilled 0.1 mol/l $NaNO_2$ in 0.5 mol/l HCl. The resulting *p*-diazotized beads were successively washed with 150 ml of water, 50 ml of 1%(w/v) sulfamic acid, and 150 ml of water. The beads were incubated overnight at 4°C with 50 ml of LDH in sodium phosphate buffer (pH 8.3). After

being filtered on a glass filter, the beads were treated for one day at 4°C with 150 ml of 0.1%(w/v) bovine serum albumin (BSA) in the phosphate buffer to cover the *p*-diazo group uncoupled with LDH. The immobilized-LDH beads were filtered and washed with 200 ml of 0.5 mol/l NaCl and with 150 ml of potassium phosphate buffer (pH 7.4) or glycine-hydrazine sulfate buffer (pH 9.4). The immobilized LDH had high activity and good stability (data not shown).

Pretreatment of serum. Two ml of 0.6 mol/l $HClO_3$ were added to 1 ml of human serum. The mixture was kept at 0°C for 1 hr, and then centrifuged at 2500 r.p.m. for 15 min. 1.5 ml of the supernatant was pipetted into a test tube. 0.2 ml of 1.0 mol/l triethanolamine hydrochloride and 0.125 ml of 5.0 mol/l K_2CO_3 were added to it. The mixture was settled at 0°C. The supernatant was used for determining pyruvate and L-lactate concentrations.

Experimental apparatus. Figure 8-1 is a diagram of the experimental apparatus. The micropump (KHD-26), damper (KD-1), pressure gauge (KPG-250L), and sample injector (KHP-UI-130) are products of Kyowa Seimitsu. The size of the stainless steel column is 8 mmϕ X 200 mm. The immobilized-LDH column was kept at 25°C by circulating thermostatic water through a jacket. This apparatus is similar to that for high-performance liquid chromatography. The absorbance of eluate at 340 nm was monitored by a spectrophotometer (Shimadzu, SPD-2A). All instruments were connected by using

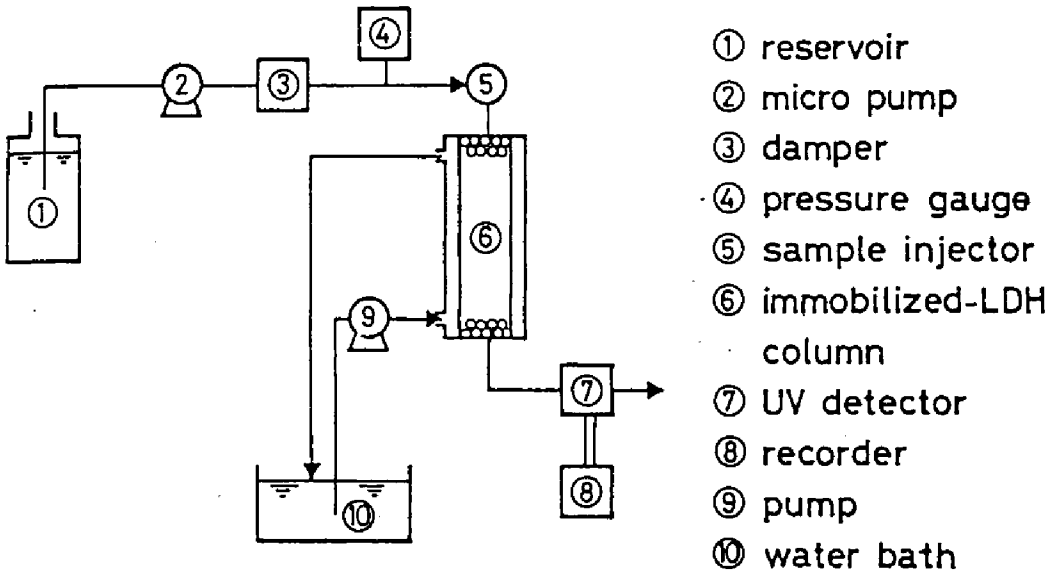

Fig. 8-1. Schematic diagram of experimental apparatus.

stainless steel tubing (I.D. 0.5 mm).

Determination of pyruvate. A pyruvate solution (100 µl), which included NADH at the same concentration as the eluent, was applied to the immobilized-LDH column through the sample injector and eluted with 8.88 X 10^{-5} mol/l NADH in 0.1 mol/l potassium phosphate buffer (pH 7.4). The flow rate was 0.894 ml/min. The absorbance of eluate at 340 nm was measured by a spectrophotometer and recorded. By applying pyruvate solution of known concentration, a standard curve relating the decrease in absorbance at 340 nm, $-\Delta A_{340}$, to pyruvate concentration was prepared. 100 µl of the pretreated serum was injected into the column and the value of $-\Delta A_{340}$ was observed. The concentration of pyruvate in serum was

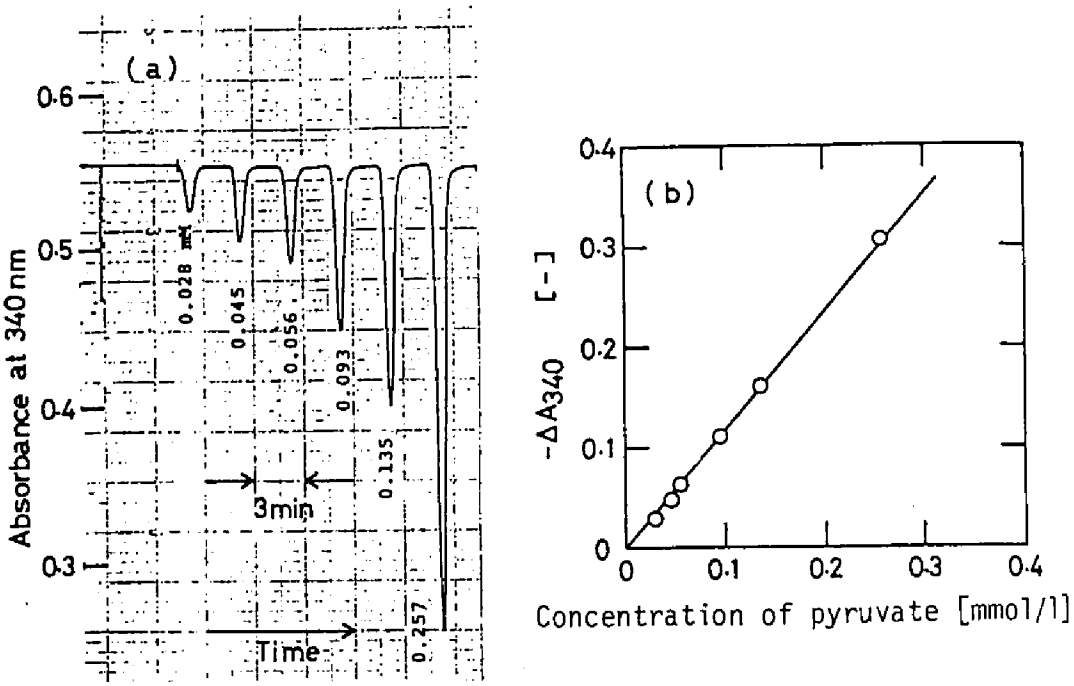

Fig. 8-2. Pulse response of pyruvate of known concentration. (a) Elution profiles of pulse inputs of pyruvate. (b) Plot of $-\Delta A_{340}$ against the concentration of pyruvate injected.

also analyzed by the procedure given in the manual enclosed with the Pyruvate Test.

Determination of L-lactate. As an eluent, 1.36×10^{-3} mol/l NAD^+ in glycine-hydrozine sulfate buffer (pH 9.4) was used. The flow rate was 0.948 ml/min. The increase in absorbance of the eluate at 340 nm, ΔA_{340}, caused by the formation of NADH during the reaction, was measured. The sample volume injected into the immobilized-LDH column was 100 µl. The concentration of L-lactate

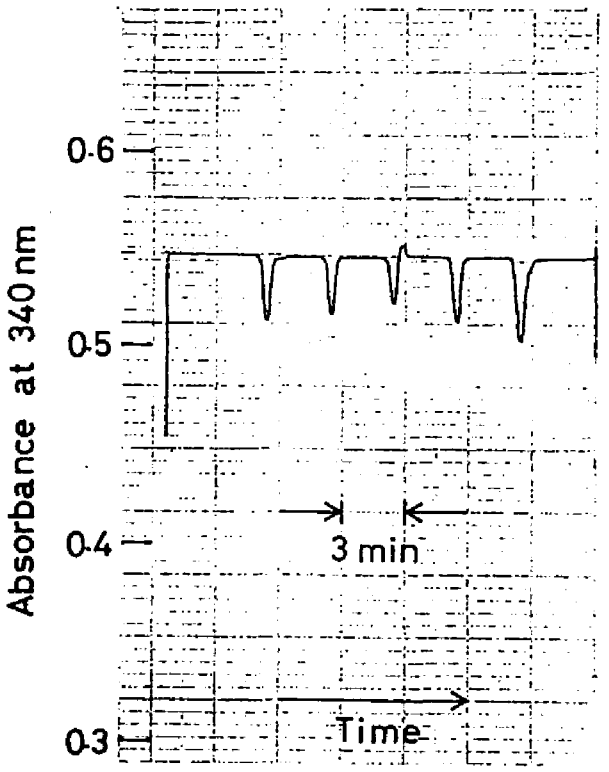

Fig. 8-3. Elution profiles of pulse inputs of the pre-treated human serum. Details are described in text.

in serum was determined by both the pulse response technique and the usual Lactate Test. L-Lactate solutions of known concentrations were prepared by diluting the standard 1 mol/l L-lactate solution obtained from Boehringer-Mannheim.

8. 3. Results and Discussion

Determination of pyruvate. Figure 8-2(a) shows the elution profiles of pulse inputs of pyruvate, the concentration of which were known. The elution profiles are sharp and symmetrical in

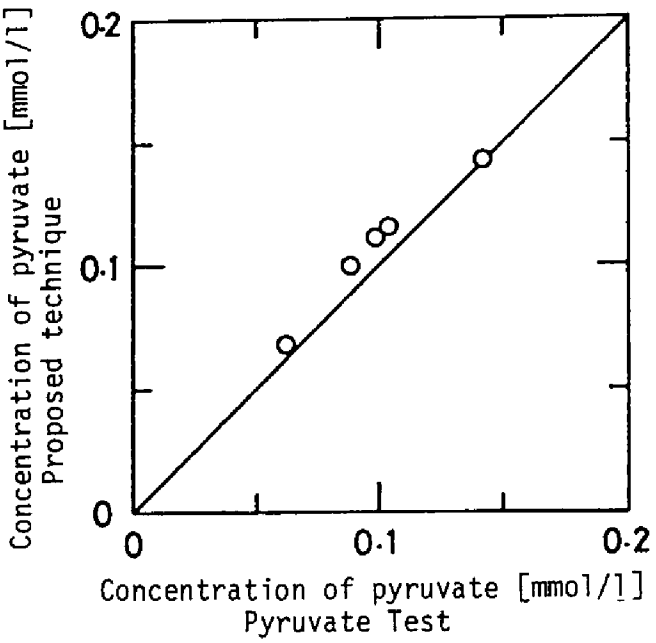

Fig. 8-4. Comparison of proposed technique with the ordinary one for determination of pyruvate.

shape. The width of peak is less than 2 min. Therefore, a sample was injected every 3 min. In Fig. 8-2(b), the maximum decrease in absorbance at 340 nm, $-\Delta A_{340}$, is plotted against the concentration of pyruvate applied. Under the experimental conditions, good linearity was observed between them. Figure 8-3 shows the elution curves of pulse inputs of the pretreated human serum. By using the standard curve in Fig. 8-2(b), the concentration of pyruvate in the serum was calculated from the maximum decrease in absorbance at 340 nm. As shown in Fig. 8-4, a good correlation was obtained between the concentration of pyruvate in serum determined by the pulse response technique and that determined by the usual

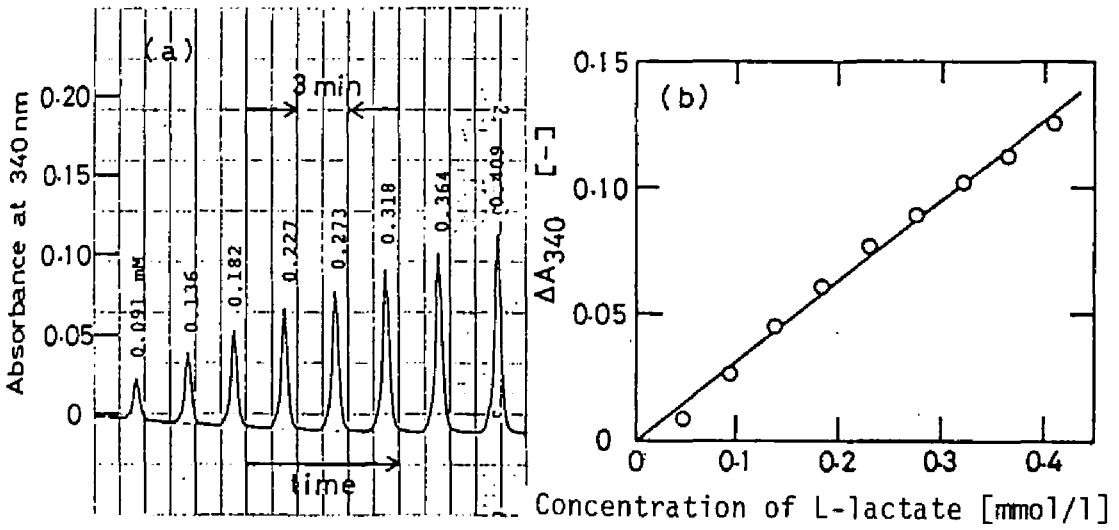

Fig. 8-5. Pulse response of L-lactate on known concentration. (a) Elution curves of pulse inputs of L-lactate. (b) Plot of ΔA_{340} against the concentration of L-lactate injected.

Pyruvate Test.

Determination of L-lactate. A pulse of L-lactate solution applied to the immobilized-LDH column was eluted with glycine-hydrazine buffer (pH 9.4) containing NAD^+. The absorbance of the eluate at 340 nm was recorded. Figure 8-5(a) shows the elution profiles of pulse inputs of L-lactate solution, the concentrations of which were known. In Fig. 8-5(b), the peak height of the elution profiles, ΔA_{340}, are plotted against the L-lactate concentrations. A linear relationship was observed between them. The concentrations of L-lactate in human serums were analyzed using the pulse response technique, although the elution curves are not

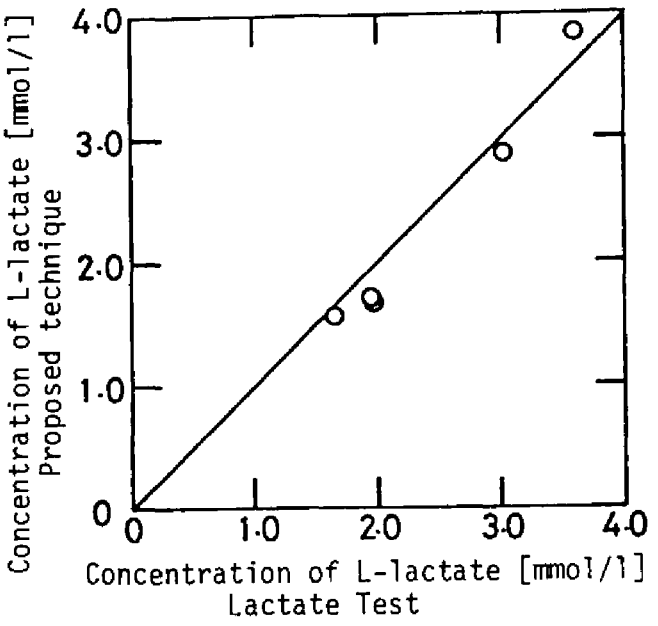

Fig. 8-6. Comparison of proposed technique with the ordinary one for analysis of L-lactate in human serum.

shown. Figure 8-6 illustrate that there is a good correlation between the concentration of L-lactate in serum determined by this technique and that analyzed by the usual Lactate Test.

Discussion. The immobilization of an enzyme onto non-porous particles with small diameter reduces the spreading of the elution curve, because the degree of axial dispersion is proportional to the particle diameter[3] and there is no spreading due to diffusion of the substrate into the particle. Therefore, in this study, LDH was immobilized onto non-porous beads of small diameter.

The pulse response technique has the following merits; the sample volume is very small, the time required for a sample is

Table 8-1. Comparison of Proposed Technique with Ordinary One for Determination of Pyruvate and L-Lactate.

component	Proposed technique		Ordinary technique	
	sample volume [ml]	time [min]	sample volume [ml]	time [min]
pyruvate	0.1	1.5	2	5
L-lactate	0.1	1.5	2	60[a]

a end point method.

short, and the handling is easy. Table 8-1 illustrates the comparison of the technique proposed with the ordinary one for pyruvate and L-lactate determinations. As shown in Table 8-1, the merits described above are evident.

8. 4. Summary

The pulse response technique using an immobilized-lactate dehydrogenase column was utilized to determine the concentrations of pyruvate and L-lactate. Lactate dehydrogenase was immobilized onto non-porous glass beads. The beads were packed in a column. A hundred microliter of sample was applied to the column and eluted with an adequate buffer solution containing NADH or NAD^+. The absorbance of the eluate at 340 nm was continuously measured. The peak height was found to be proportional to the concentration of the sample loaded. This technique was applied to determination

of pyruvate and L-lactate in human serum. There were good correlations between the concentrations of these components determined by this technique and those determined by the usual method.

Literature Cited

1) F. E. Stolzenbach and N. O. Kaplan, *Methods in Enzymology*, 44, 929 (1976).

2) T. L. Newirth, M. A. Diegel, E. K. Pye, and R. G. Kallen, *Biotechnol. Bioeng.*, 15, 1089 (1973).

3) K. Nakanishi, S. Yamamoto, R. Matsuno, and T. Kamikubo, *Agric. Biol. Chem.*, 41, 1465 (1977).

Chapter 9

Application of Pulse Response Technique to Determination of Enzyme

9. 1. Introduction

Former studies on application of immobilized enzymes to analysis[1-6] are mainly concerned with determination of substrates. Determination of enzyme activity also, however, is important in clinical chemistry.

In this chapter, it is shown that the pulse response technique can be utilized for determining an enzyme in serum. Glutamic pyruvic transaminase (GPT, EC 2.6.1.2) was selected as the enzyme whose concentration should be determined. This selection was based on the facts that lactate dehydrogenase (LDH), which could be immobilized onto non-porous glass beads in a previous chapter, is an indicator enzyme for analyzing GPT, the determination of GPT concentration is important in clinical analysis, and the elution profile of NADH is easily obtained by monitoring the absorbance at 340 nm.

The concentration of GPT is determined batchwise using the following reaction system:

$$\text{L-alanine} + \alpha\text{-ketoglutarate} \xrightarrow{\text{GPT}} \text{pyruvate} + \text{L-glutamate} \qquad (9\text{-}1)$$

$$\text{pyruvate} + \text{NADH} + \text{H}^{+} \xrightarrow{\text{LDH}} \text{L-lactate} + \text{NAD}^{+} \qquad (9\text{-}2)$$

Although soluble LDH is used in the usual method, use of immobilized LDH will make the operation easy and reduce its cost.

9. 2. Materials and Methods

Reagents. Lactate dehydrogenase and glutamic pyruvic transaminase were both from pig heart and were purchased from Toyobo and Boehringer-Mannheim, respectively. The kit reagent for analyzing GPT (GPT Test) was obtained from Boehringer-Mannheim. NAD^+ was a product of Kohjin. Non-porous glass beads had a diameter of *ca.* 400 mesh. All other reagents were of analytical grade.

Immobilization of LDH. LDH was immobilized onto non-porous glass beads *via* diazo-coupling. The procedures of immobilization were the same as those described in Chapter 8.

Experimental apparatus. The experimental apparatus used in this chapter was the same as that utilized in Chapter 8.

Elution profile of pulse input of GPT solution. The eluent was 0.1 mol/l potassium phosphate buffer, in which 8.72×10^{-5} mol/l NADH, 6.71×10^{-3} mol/l α-ketoglutarate, 3.22×10^{-2} mol/l DL-alanine, and 0.1%(w/v) bovine serum albumin (BSA) were included. The GPT solution applied to the immobilized-LDH column included NADH and α-ketoglutarate at the same concentrations as in the eluent. 100 μl of GPT solution were injected into the top of the column and eluted at the flow rate of 0.954 ml/min. The absorb-

ance of the eluate at 340 nm was recorded. The concentration of GPT solution applied was determined by the GPT Test. The relationship between the variation of absorbance at 340 nm, $-\Delta A_{340}$, and the concentration of GPT solution was examined.

9. 3. Theoretical Considerations.

A method for predicting elution curves of the components concerned with the determination of an enzyme is presented here based on the mass balance model used in Chapter 6. The basic partial differential equations are transformed to the Laplace domain and the solutions in the domain are obtained. The solutions are obtained by ignoring the resistance of film diffusion. The solutions in the time domin are numerically calculated by Eqs.(6-15) or (6-16).

The reaction system utilized in determination of GPT is considered. Two cases are discussed depending on the kinds of supports. The first is where LDH is attached to non-porous support. The second is where LDH is immobilized to porous carrier. The pore size of the porous carrier is small and GPT cannot penetrate into the carrier. We assume that the formation rate of pyruvate is proportional to the GPT concentration and is independent on the concentrations of L-alanine and α-ketoglutarate, that the formation rate of NAD^+ is linear to the pyruvate concentration, and that the GPT- and LDH-catalyzed reactions are both irreversible.

Non-porous support. Mass balance equations referring to the concentrations of GPT, pyruvate, and NAD^+ are given by

$$\frac{\partial C_E}{\partial t} = D_z \frac{\partial^2 C_E}{\partial z^2} - u\frac{\partial C_E}{\partial z} \tag{9-3}$$

$$\frac{\partial C_P}{\partial t} = D_z \frac{\partial^2 C_P}{\partial z^2} - u\frac{\partial C_P}{\partial z} + k_1 C_E - \frac{1-\varepsilon}{\varepsilon}\cdot\frac{3}{R} k_2 C_P \tag{9-4}$$

$$\frac{\partial C_N}{\partial t} = D_z \frac{\partial^2 C_N}{\partial z^2} - u\frac{\partial C_N}{\partial z} + \frac{1-\varepsilon}{\varepsilon}\cdot\frac{3}{R} k_2 C_P \tag{9-5}$$

where the subscripts of E, P, and N represent GPT, pyruvate, and NAD^+, respectively. Initial and boundary conditions are given as follows:

$$t = 0, \quad z > 0, \quad C_E = C_P = C_N = 0 \tag{9-6a}$$

$$0 \leq t \leq t_0, \quad z = 0, \quad C_E = C_{E0} \tag{9-6b}$$

$$t > t_0, \quad z = 0, \quad C_E = 0 \tag{9-6c}$$

$$t \geq 0, \quad z = 0, \quad C_P = C_N = 0 \tag{9-6d}$$

By applying the Laplace transform to these differential equations, the solutions of C_E, C_P, and C_N in the Laplace domain were obtained in the nondimensional forms of y_E, y_P, and y_N, where y_i (i = E, P, and N) is defined as C_i/C_{E0}. $\bar{y}_i$ represents the solution in the Laplace domain.

$$\bar{y}_E = [\{1-\exp(-s\theta_0)\}/s]\cdot\exp(\omega_1) \tag{9-7}$$

$$\bar{y}_P = [\{1-\exp(-s\theta_0)\}/s][\eta_1/(\eta_2 H)][\exp(\omega_1)-\exp(\omega_2)] \quad (9\text{-}8)$$

$$\bar{y}_N = [\{1-\exp(-s\theta_0)\}/s]\cdot\eta_1 \cdot[\{1/[1+4(1/\delta)s]^{1/2}-1/(\eta_2 H)\}\exp(\omega_1)+\{1/(\eta_2 H)\}\exp(\omega_2)] \quad (9\text{-}9)$$

where

$$\omega_1 = -s/[1/2+\{1/4+(1/\delta)s\}^{1/2}] \quad (9\text{-}10a)$$

$$\omega_2 = (-s-\eta_2 H)/[1/2+\{1/4+(1/\delta)(s+\eta_2 H)\}^{1/2}] \quad (9\text{-}10b)$$

and

$$\delta = Z/(D_z/u) \quad (9\text{-}11a)$$

$$\eta_1 = k_1\tau \quad (9\text{-}11b)$$

$$\eta_2 = 3k_2\tau/R \quad (9\text{-}11c)$$

$$H = (1-\varepsilon)/\varepsilon \quad (9\text{-}11d)$$

and τ is the average residence time with respect to void volume of the column. When the input of GPT can be considered to be a pulse, the term $[1-\exp(-s\theta_0)]/s$ can be approximated by θ_0.

Porous support. When LDH is immobilized to porous support and GPT cannot penetrate into the support, the mass balance equations for GPT, pyruvate, and NAD^+ are given by the following equations.

$$\frac{\partial C_E}{\partial t} = D_z \frac{\partial^2 C_E}{\partial z^2} - u\frac{\partial C_E}{\partial z} \tag{9-12}$$

$$\frac{\partial C_P}{\partial t} = D_z \frac{\partial^2 C_P}{\partial z^2} - u\frac{\partial C_P}{\partial z} - \frac{1-\varepsilon}{\varepsilon}\cdot\frac{3}{R}\cdot D_P \left.\frac{\partial C_{PS}}{\partial r}\right|_{r=R} + k_1 C_E \tag{9-13}$$

$$\frac{\partial C_{PS}}{\partial t} = D_P\left(\frac{\partial^2 C_{PS}}{\partial r^2} + \frac{2}{r}\cdot\frac{\partial C_{PS}}{\partial r}\right) - k_2 C_{PS} \tag{9-14}$$

$$\frac{\partial C_N}{\partial t} = D_z \frac{\partial^2 C_N}{\partial z^2} - u\frac{\partial C_N}{\partial z} - \frac{1-\varepsilon}{\varepsilon}\cdot\frac{3}{R}\cdot D_N \left.\frac{\partial C_{NS}}{\partial r}\right|_{r=R} \tag{9-15}$$

$$\frac{\partial C_{NS}}{\partial t} = D_N\left(\frac{\partial^2 C_{NS}}{\partial r^2} + \frac{2}{r}\cdot\frac{\partial C_{NS}}{\partial r}\right) + k_2 C_{PS} \tag{9-16}$$

where C_{iS} represents the concentration of component i at the gel phase. D_P and D_N are the gel-phase diffusion coefficients of pyruvate and NAD^+, respectively. Initial and boundary conditions are given as follows:

$$t = 0, \quad z > 0, \quad C_E = 0 \tag{9-17a}$$

$$C_P = C_{PS} = 0 \tag{9-17b}$$

$$C_N = C_{NS} = 0 \tag{9-17c}$$

$$t > 0, \quad r = R, \quad C_{PS} = K_P \cdot C_P \tag{9-17d}$$

$$C_{NS} = K_N \cdot C_N \tag{9-17e}$$

$$t > 0, \quad r = 0, \quad \partial C_{PS}/\partial r = 0 \tag{9-17f}$$

$$\partial C_{NS}/\partial r = 0 \tag{9-17g}$$

$$0 \leq t \leq t_0, \qquad z = 0, \qquad C_E = C_{E0} \tag{9-17h}$$

$$t > t_0, \qquad z = 0, \qquad C_E = 0 \tag{9-17i}$$

$$t \geq 0, \qquad z = 0, \qquad C_P = 0 \tag{9-17j}$$

$$C_N = 0 \tag{9-17k}$$

The solutions of y_E, y_P, and y_N in the Laplace domain are given by Eqs. (9-18) to (9-20).

$$\bar{y}_E = [\{1-\exp(-s\theta_0)\}/s]\cdot\exp(\omega_3) \tag{9-18}$$

$$\bar{y}_P = [\{1-\exp(-s\theta_0)\}/s]\cdot[\eta\phi_P^2/(3HK_P\lambda_P)] \cdot[\exp(\omega_3)-\exp(\omega_4)] \tag{9-19}$$

$$\bar{y}_N = \frac{1-e^{-s\theta_0}}{s}\cdot\frac{\eta\phi_N^2\phi_M^2}{(\phi_P^2-\phi_N^2)+\phi_M^2}\cdot\frac{\lambda_N-\lambda_P}{\lambda_P} \cdot\left\{\frac{3HK_P\lambda_P}{3HK_N\lambda_N}\cdot\frac{1}{3HK_P\lambda_P-(\phi_P^2/\phi_N^2)3HK_N\lambda_N}\cdot\exp(\omega_5)\right. - \frac{1}{3HK_N\lambda_N}\cdot\exp(\omega_3) - \left.\frac{1}{(\phi_N^2/\phi_P^2)3HK_P\lambda_P-3HK_N\lambda_N}\cdot\exp(\omega_4)\right\} \tag{9-20}$$

where

$$\omega_3 = \frac{-s}{1/2+[1/4+(1/\delta)s]^{1/2}} \tag{9-21a}$$

$$\omega_4 = \frac{-s-3HK_P\lambda_P/\phi_P^2}{1/2+[1/4+(1/\delta)(s+3HK_P\lambda_P/\phi_P^2)]^{1/2}} \tag{9-21b}$$

$$\omega_5 = \frac{-s - 3HK_N\lambda_N/\phi_N^2}{1/2+[1/4+(1/\delta)(s+3HK_N\lambda_N/\phi_N^2)]^{1/2}} \quad (9\text{-}21c)$$

$$\lambda_P = (s\phi_P^2+\phi_M^2)^{1/2}\coth(s\phi_P^2+\phi_M^2)^{1/2} - 1 \quad (9\text{-}22a)$$

$$\lambda_N = (s\phi_N^2)^{1/2}\coth(s\phi_N^2)^{1/2} - 1 \quad (9\text{-}22b)$$

and

$$\eta_1 = k_1 \quad (9\text{-}23a)$$

$$\phi_M = R(k_2/D_P)^{1/2} \quad (9\text{-}23b)$$

$$\phi_P = R[1/(D_P\tau)]^{1/2} \quad (9\text{-}23c)$$

$$\phi_N = R[1/(D_N\tau)]^{1/2} \quad (9\text{-}23d)$$

$$HK_P = (1 - \varepsilon)K_P/\varepsilon \quad (9\text{-}23e)$$

$$HK_N = (1 - \varepsilon)K_N/\varepsilon$$

Although the solutions can be found where GPT can penetrate into the gel phase, they become much more complex. The solutions shown here are obtained under the assumption that GPT cannot permeate into the gel phase. This assumption may be reasonable when LDH is immobilized to acrylamide gel, κ-carraginane, etc.

9. 4. Results and Discussion

Theoretical elution profiles of NAD^+. Elution profiles of NAD^+ were theoretically calculated for columns packed with LDH immobilized on non-porous support and into porous carrier. Figure 9-1 shows the elution profiles of NAD^+ in the column packed with

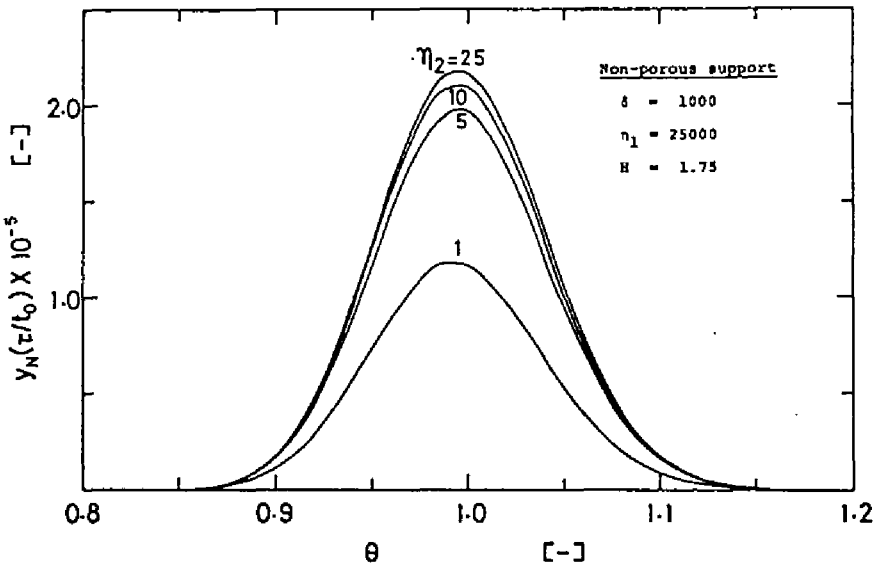

Fig. 9-1. Elution profiles of NAD^+ in a column packed with LDH immobilized onto non-porous support.

LDH immobilized onto non-porous support. The curves are calculated for various η_2 values. The large η_2 value means that the amount of LDH immobilized is much. Symmetrical curves are obtained without distinction of the η_2 value. The more the amount of LDH immobilized is, the larger the response is. The response, however, is not in proportion to the amount of LDH immobilized.

Figure 9-2 shows the elution profiles of NAD^+ in the column in which LDH immobilized into porous support is packed. The profiles are calculated for various ϕ_M values. As the ϕ_M value becomes larger, the response becomes larger. Asymmetrical curves, however, are observed with an increase of the ϕ_M value. The elution curves calculated for porous support are much broader than those obtained

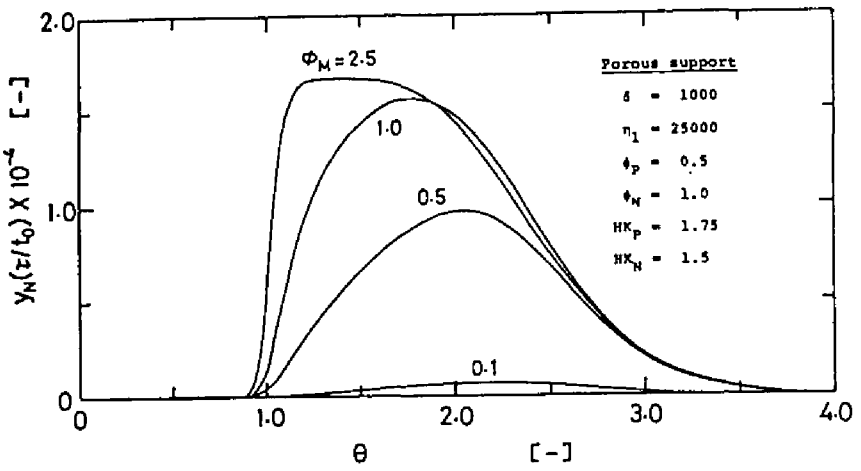

Fig. 9-2. Elution profiles of NAD^+ in a column in which LDH immobilized into porous support is packed.

for non-porous support. These figures show that the use of LDH immobilized onto non-porous support gives symmetrical elution curves and reduces the spreading of the curves if the immobilized enzyme has enough activity.

Elution profile of a pulse input of GPT solution. A pulse of GPT solution applied to the immobilized-LDH column was eluted with 0.1 mol/l potassium phosphate buffer (pH 7.4) containing NADH, α-ketoglutarate, DL-alanine, and BSA. When the eluent included no BSA, an asymmetrical elution curve with a long tail was observed. The tail could not curtailed by increasing the ionic strength of the eluent by the addition of NaCl. A relatively sharp elution curve was obtained when BSA was added to the eluent, although the reason for the decrease of tail is not evident. Fig-

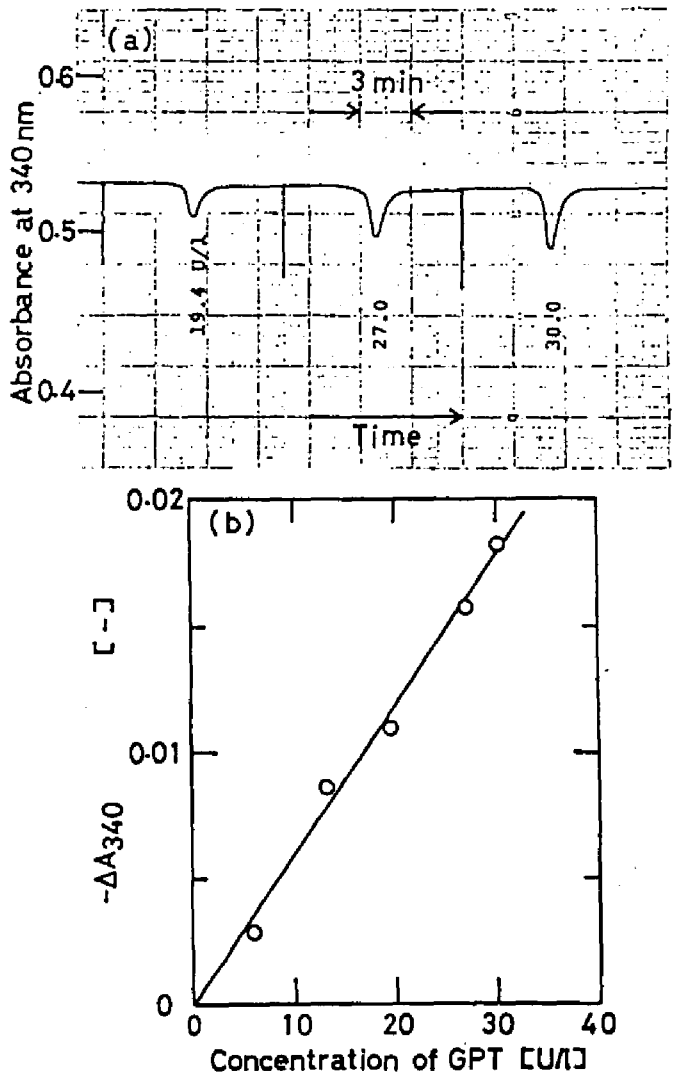

Fig. 9-3. Pulse response of GPT solution. (a) Elution profiles of pulse inputs of GPT. (b) Relation between $-\Delta A_{340}$ and the concentration of GPT applied.

ure 9-3(a) shows the elution profiles of pulse inputs of GPT solutions. Each peak is labelled with the concentration of GPT applied, as determined by the GPT Test. As shown in Fig. 9-3(b), the maximum decrease in absorbance at 340 nm was linearly related to

Table 9-1. Comparison of the Pulse Response Technique with the Usual One for Analysis of GPT.

	Sample volume [ml]	Time [min]
Pulse response technique	0.1	3
Usual technique	0.5	5

the concentration of GPT applied. This relationship can be used for analyzing GPT in serum. However, any pyruvate in the serum must be removed before the analysis of GPT.

Discussion. Table 9-1 illustrates the comparisom of this technique with the usual one for determination of GPT. This technique requires smaller amount of sample and shorter time than the usual one.

Former studies on applications of immobilized enzymes to analysis[1-6] are mainly concerned with determination of substrates. Determination of enzyme activity also, however, is important in clinical chemistry. The pulse response technique is very useful for analysis of enzymes as well as for analysis of substrates.

This technique might be useful for the analysis of another enzyme. For example, use of immobilized malate dehydrogenase may achieve the determination of glutamic oxaloacetic transaminase as well as L-malate and oxaloacetate.

9. 5. Summary

Pulse response technique was extended to analysis of an enzyme. An indicator enzyme was immobilized and packed into a column. A pulse of the enzyme to be analyzed was introduced to the top of the column and eluted with an adequate solution. The elution curve of a component which could be measured easily was observed and the activity of the enzyme was determined from the intensity of the curve. The method for predicting the elution profile of the component was presented. Use of enzyme immobilized onto non-porous support gives symmetrical elution profiles at short retention time. The pulse response technique was applied to determination of glutamic pyruvic transaminase (GPT) by using lactate dehydrogenase immobilized onto non-porous glass beads. The peak height of elution profile of NADH was in proportion to the GPT concentration loaded. The technique could reduce the amount of sample and time required to analyze GPT compared with the usual technique.

Nomenclature

C_{E0}	total concentration of enzyme	[mol/l], [U/l]
C_i	concentration of component i at mobile phase	[mol/l]
C_{iS}	concentration of i at gel phase	[mol/l]
D_i	gel-phase diffusion coefficient of i (i = P and N)	[cm^2/s]

D_z	axial dispersion coefficient	[cm^2/s]
H	$= (1 - \varepsilon)/\varepsilon$	[-]
K	distribution coefficient	[-]
k_1	first-order rate constant of the first-step reaction	[s^{-1}]
k_2	first-order rate constant of the reaction catalyzed by the indicator enzyme	[cm/s], [s^{-1}]
R	particle radius	[cm]
r	radial distance	[cm]
s	Laplace variable	[-]
t	time	[s]
t_0	sample injection time	[s]
u	linear interstitial velocity	[cm/s]
y_i	$= C_i/C_{E0}$	[-]
$\bar{y}_i$	solution of y_i in Laplace domain	[-]
Z	bed height	[cm]
z	axial distance	[cm]
δ	$= Z/(D_z/u)$	[-]
ε	void fraction of bed	[-]
η_1	$= k_1\tau$	[-]
η_2	$= 3k_2\tau/R$	[-]
θ	$= t/\tau$	[-]
θ_0	$= t_0/\tau$	[-]

τ	average residence time	[s]
ϕ_j	$= R[1/(D_j\tau)]^{1/2}$	[-]
ϕ_M	$= R(k_2/D_P)^{1/2}$	[-]

Literature Cited

1) K. Mosbach, B. Danielsson, A. Borgerud, and M. Scott, *Biochim. Biophys. Acta*, 403, 256 (1975).

2) B. Danielsson, K. Gadd, B. Mattiasson, and K. Mosbach, *Clin. Chim. Acta*, 81, 163 (1977).

3) B. Mattiasson, B. Danielsson, and K. Mosbach, *Anal. Lett.*, 9, 217 (1976).

4) G. P. Hicks and S. J. Updike, *Nature*, 214, 986 (1967).

5) L. B. Wingard, C. C. Liu, and N. L. Nagda, *Biotechnol. Bioeng.*, 13, 269 (1971).

6) S. Suzuki, I. Karube, and I. Satoh, "*Biochemical Application of Immobilized Enzymes and Proteins*," ed. by T. M. S. Chang, Plenum, New York, 1977, Vol. 2, p.177.

PART III

PRODUCTION OF HIGHER FRUCTOSE SYRUP

PART III

PRODUCTION OF HIGHER FRUCTOSE SYRUP

Introduction

Fructose syrup is a concentrated aqueous solution of fructose, glucose, and oligasaccharides. The most common type of fructose syrup contains 42% fructose, 52% glucose, and 6% oligosaccharides on dry basis.[1] This type of syrup is usually called high fructose syrup. It is a new type of sweetner and used in place of sucrose in some foods and beverages. Since fructose is sweeter and more soluble into water at low temperatures than glucose, it is desired to raise the content of fructose in the syrup to the level of 55 to 90%. This type of syrup is called higher fructose syrup.

Isomerization of glucose to fructose catalyzed by an enzyme (glucose isomerase) is a reversible reaction with the eqilibrium constant of 1.0 at 50°C,[2] and finally gives an equilibrium mixture containing about 50% glucose and 50% fructose. In order to produce higher fructose syrup containing fructose more than 50%, a process to separate fructose from the mixture is required. Some processes to separate fructose from the mixture are known.[3,4] These require the solid separation and desalination processes, and hence are complicated and unsuitable for a commercial process. A powerful process used at the present time is a selective adsorp-

tion method using Ca^{2+} ion forms of ion exchangers.[5] These may be classified into the chromatographic and simulated moving-bed operations. In the adsorptive separation process, water is used as a desorbent. The water must be evaporated in the succeeding process. With a rise of energy cost, it is desired to develop a new process for producing higher fructose syrup, which can reduce the amount of water and save the energy cost.

In this part, some types of adsorptive separation methods of glucose and fructose from their mixture are discussed. Chapter 10 deals with the adsorbent to separate glucose and fructose and with a chromatographic separation in a fixed-bed adsorber.

In Chapter 11, we explain in detail on glucose/fructose separation utilizing a simulated moving-bed adsorber[6] and present the analytical methods for calculating the concentration profiles in the adsorber and their validities are confirmed experimentally.

In Chapter 12, we develop a new process to produce higher fructose syrup using a system which includes the adsorption process and the immobilized-glucose isomerase reaction.

In Chapter 13, three processes for producing higher fructose syrup, that is, the chromatographic process, the process utilizing the simulated moving-bed adsorber, and the process developed in Chapter 12, are compared. It is shown that the third process can save the quantity of desorbent compared with other processes.

Literature Cilted

1) K. Yoritomi, "*Hand Book of Starch Science*," ed. by J. Nikuni, M. Nakamura, and S. Suzuki, 1977, Asakurashoten, Tokyo, p.489.

2) Y. Takasaki, *Agric. Biol. Chem.*, 31, 309 (1967).

3) Japanese patent, 45-26048.

4) Japanese patent, 43-16799.

5) R. W. Goulding, *J. Chromatogr.*, 103, 229 (1975).

6) U. S. patent, 2985589.

Chapter 10

Chromatographic Separation of Glucose and Fructose

10. 1. Introduction

The chromatographic separation of glucose and fructose requires a great amount of water as desorbent compared with the processes described in Chapters 11 and 12. This process is, however, suitable for a small scale separation because the equipment is simple and the operation is easy.

In this chapter, we consider the design problem of the chromatographic separation of glucose and fructose from their mixture. The adsorbent which has an adsorption selectivity for fructose is looked for. The adsorption isotherms of glucose and fructose for two adsorbents are obtained. Methods for predicting the chromatographic elution profiles and the breakthrough curves in a fixed-bed adsorber are presented.

10. 2. Materials and Methods

Adsorbents and Chemicals. Amberlite IR-120B and Dowex 50W were purchased from Organo and Muromachi Chemical Industries, respectively. Ion-exchangers S-07 and S-22 were kindly supplied by Organo. These ion exchangers were prepared in Ca^{2+} or Mg^{2+} ion form. Ca^{2+} ion is known to be an effective cation to adsorb fructose.[1)] The reason why the Mg^{2+} ion form is examined is as follows: In Chapter 12, we will propose a new system for producing

higher fructose syrup in which the glucose/fructose mixture is alternately passed through cation exchanger columns and immobilized-glucose isomerase reactors. The glucose isomerase requires Mg^{2+} ion for exhibiting its activity.[2] The use of any adsorbent in its Mg^{2+} form is advisable from both points of adsorption and the reaction if the form is effective for the glucose/fructose separation. Therefore, Mg^{2+} ion forms of ion exchangers were examined. Ca^{2+} and Mg^{2+} ion forms of Y zeolites were kindly supplied by Toyo Soda Mfg. Co., Ltd.

Glucose and fructose were purchased from Nakarai Chemicals. Other reagents were of analytical grade.

Determination of glucose and fructose. Glucose and fructose were mainly analyzed using a high-performance liquid chromatograph (Shimadzu, LC-3A) equipped with a separation column (Shimadzu, SCR-101N) and a differential refractometer (Showa Denko, Shodex RI SE-11). The glucostat method[3] and the method of Roe *et al.*[4] were secondarily used to determine glucose and fructose, respectively.

Screening of adsorbents. Liquid column chromatography, also known as a pulse test in the field of chemical engineering,[5] was conveniently used to screen various adsorbents. Adsorbent particles were packed in a column (1.485 cmϕ X 35.0 cm) kept at 50°C by circulating the thermostated water. A sample solution (1.0

cm^3) consisting of glucose and fructose (each component, 0.3 mol/l) was carefully added to the top of the bed. The moment the sample solution had been soaked into the bed, the eluent was started to be fed with a constant-feeding pump (Tokyo Rikakikai, MP-101). Distilled water or 0.02 mol/l Trsi-HCl buffer containing 0.01 mol/l magnesium sulfate was used as the desorbent. The buffer will be used for the glucose isomerase-catalyzed reaction in Chapter 12. The flow rate of the eluent was 0.5 cm^3/min. The eluate emerging from the column was collected at a regular interval. The concentrations of glucose and fructose in the eluate were determined and plotted against the elapsed time to yield the elution profiles.

On the assumption that the adsorption isotherm of a component k is linear and independent of the adsorption isotherms of other components, the mean residence time of the component k, $\bar{t}_k$, is calculated through the moment analysis of the elution curve, yielding Eq.(10-2).[6,7]

$$\bar{t}_k = \int_0^\infty t \cdot C_{kl} dt / \int_0^\infty C_{kl} dt \tag{10-1}$$

$$= (L/v)[\varepsilon_b + (1 - \varepsilon_b) m_k] \tag{10-2}$$

where C_{kl} is the concentration of the component k in the eluate, t the elapsed time, L the column length, v the linear superficial velocity of liquid flow, ε_b the void fraction of the bed, and m_k the distribution coefficient. The high value of m_k indicates that

the amount of the component k adsorbed is large.

The value of ε_b was determined by measuring $\bar{t}_k$ of soluble starch, because soluble starch connot penetrate into adsorbent, *i.e.*, $m_k = 0$, due to its high molecular weight. Soluble starch in the eluate was completely hydrolyzed to glucose by addition of glucoamylase and the resulting glucose was analyzed by the glucostat method.

The apparent densities of adsorbents were pycnometrically measured.

Adsorption isotherms. The adsorption isotherms of glucose and fructose onto Y zeolite (Ca^{2+} form) and Ion-exchanger S-07 (Ca^{2+} form) were obtained by using a batch desorption method together with an analysis of breakthrough curve in a packed-bed column. As a solvent, distilled water was used for Ion-echanger S-07, whereas 0.02 mol/l Tris-HCl buffer containing 0.01 mol/l magnesium sulfate was used for Y zeolite.

(a) *A batch desorption method.* About 0.5 g of an adsorbent weighed accurately was put into an Erlenmyer flask. Each 20 cm^3 of glucose-, fructose-, or the mixture solution was added to the flask. The flask with a silicane stopper to avoid evaporation of liquid was kept at 50°C for 36 hr under stirring condition. The concentration of the adsorbate in the liquid phase was measured. The adsorbent was removed from the solution, blotted with a piece

of filter paper to eliminate excess liquid on the surface, and put into 50 cm^3 of the pure solvent. After 36 hr, the concentration of the adsorbate in the liquid phase, C_{kd}, was measured. The amount adsorbed initially, q_k, was calculated by using Eq.(10-3) under the approximation that the amount of adsorbate remaining in the adsorbent was negligibly small.

$$q_k = V \cdot C_{kd}/w \tag{10-3}$$

where V and w are the volume of pure solvent and the weight of adsorbent, respectively.

(b) *A breakthrough method.* Adsorbent particles were packed in a column equipped with a water jacket. A solution of glucose, fructose, or their mixture was continuously introduced to the top of the bed. The solution was continued to be fed until the effluent concentration C_{kl} becomes almost equal to the influent concentration C_{k0}. The solute emerging from the bed was fractionated at a regular interval and was assayed to obtain the breakthrough curve of the adsorbate. The amount adsorbed was calculated from Eq.(10-4).

$$w \cdot q = C_{k0} \cdot Q \cdot t_E - C_{k0} \cdot \varepsilon_b \cdot \bar{V} - Q \cdot \int_0^{t_E} C_{kl}\, dt \tag{10-4}$$

where Q is the volumetric flow rate, $\bar{V}$ the bed volume, and t_E the elapsed time at which the concentration of adsorbate at the outlet reaches almost that at the inlet.

Estimation of overall volumetric mass transfer coefficient.

In this study, the approximation of a linear-driving-force was adopted to express simly the adsorption rate process. The overall volumetric mass transfer coefficient, $K_f a_v$, was determined so that the calculated breakthrough curve may fit to the experimental one.

Chromatographic separation of glucose and fructose. Ion-exchanger S-07 (Ca^{2+} form) was packed into a column of 1.485 cm in diameter and 36.8 cm in length. The bed was kept at 50°C. Distilled water was used as the eluent, and the flow rate was 1.19 cm^3/min. The mixture of glucose and fructose (each component, 0:1 mol/l) was introduced to the top of the bed for 10 min and the eluent was fed for 20 min. These operations were repeated three times. The eluate was fractionated every 2 min. The concentrations of glucose and fructose in the fractions were analyzed.

Modified procedure for chromatographic separation of glucose and fructose. Twelve columns, in which the Ca^{2+} ion form of Ion-exchanger S-07 was packed, were connected in circular series as shown in Fig. 10-1. Though the modified chromatographic procedure needs only three columns, twelve columns were used to obtain the concentration profiles in the adsorber. The size of each column was 1.36 cmϕ X 10.2 cm. The columns were kept at 50°C by circulating the thermostated water. The adsorber was divided into three zones by the inlets of feed and desorbent solutions. Each

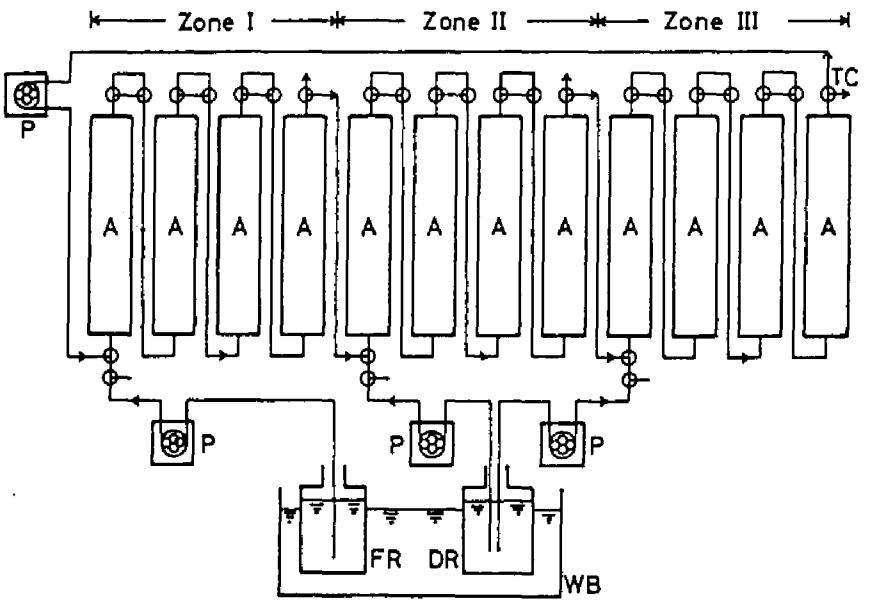

Fig. 10-1. Experimental apparatus used in a modified procedure for chromatographic separation of glucose and fructose from their mixture. A, adsorption column; DR, desorbent reservoir; FR, feed reservoir; P, constant-feeding pump; TC, three way stopcock; and WB, water bath.

zone contained four columns.

The feed solution, which included 1.0 mol/l glucose and 1.0 mol/l fructose, was continuously introduced to the inlet of zone I at the flow rate of 1.80 cm^3/min. The solution emerging from zone I was fractionated every 2 min and the concentrations of glucose and fructose in the fractions were analyzed. After 23 min, the flow was stopped. The solutions among the columns were sampled and analyzed to obtain the concentration profiles in zone I.

The solution in zone I, which included glucose and fructose,

was circulated at the flow rate of 1.41 cm^3/min to separate glucose and fructose for 142 min. By this operation, fructose and glucose were localized in zones II and III, respectively. The concentrations of glucose and fructose in the solutions among columns were measured to yield the concentration profiles in the adsorber.

Fructose and glucose located in zones II and III were separately eluted with water (desorbent) for 40 min. The flow rates of water in zones II and III were 1.45 and 1.43 cm^3/min, respectively. The elution profiles of glucose and fructose were obtained by measuring the concentrations in the eluates fractionated every 2 min.

10. 3. Theoretical Considerations

Prediction of elution curve in chromatography. In a conventional chromatographic separation, a solution of adsorbates to be separated and a desorbent solution are mutually introduced to a fixed-bed adsorber. Mass balance equations referring to the concentrations of the component k at the mobile phase, C_k and at the stationary phase, C_k^* are given by Eqs.(10-5) and (10-6) under the following assumptions; (i) the adsorption isotherm is linear and independent, (ii) the adsorption rate process is represented by a linear-driving-force approximation, and (iii) the axial dispersion can be ignored:

$$\varepsilon_b \frac{\partial C_k}{\partial t} = -v\frac{\partial C_k}{\partial z} - K_f a_v (C_k - C_k^*) \tag{10-5}$$

$$(1 - \varepsilon_b) m_k \frac{\partial C_k^*}{\partial t} = K_f a_v (C_k - C_k^*) \tag{10-6}$$

where K_f is the overall mass transfer coefficient and a_v is the specific surface area of adsorbent based on the bed volume. Initial and boundary conditions are given as follows:

$$z > 0, \qquad t = 0 \qquad ; \quad C_k = 0 \tag{10-7a}$$

$$C_k^* = 0 \tag{10-7b}$$

$$z = 0, \qquad 0 \leq t \leq t_0 \qquad ; \quad C_k = C_{k0}$$

$$t_0 < t < t_0 + t_d \qquad ; \quad C_k = 0$$

$$\cdots\cdots\cdots\cdots\cdots\cdots \qquad \cdots\cdots \tag{10-7c}$$

$$(n-1)(t_0+t_d) \leq t \leq t_0 + (n-1)t_d \; ; \quad C_k = C_{k0}$$

$$t_0 + (n-1)t_d < t < n(t_0+t_d) \qquad ; \quad C_k = 0$$

where t_0 and t_d represent the sample and desorbent injection times, respectively. n refers to the number of sample injection times. The variables are transformed into the dimensionless forms defined by Eqs.(10-8).

$$y_k = C_k/C_{k0} \tag{10-8a}$$

$$y_k^* = C_k^*/C_{k0} \tag{10-8b}$$

$$x = z/L \tag{10-8c}$$

$$\theta = t/\tau \tag{10-8d}$$

where τ is the residence time based on the void volume of the bed and is defined by

$$\tau = L/(v/\varepsilon_b) \tag{10-9}$$

By applying the Laplace transform to these differential equations, the solution of y_k in the Laplace domain, $\bar{y}_k$ was obtained.

$$\bar{y} = \frac{1-e^{-s\theta_0}}{s}\left\{\sum_{j=1}^{n}\exp[-(j-1)(\theta_0+\theta_d)s]\right\} \cdot\exp\left\{-\frac{[s+\alpha_c(1+\beta_{ck})]s}{s+\alpha_c\beta_{ck}}x\right\} \tag{10-10}$$

where s is the Laplace variable and the dimensionless parameters are defined by Eq.(10-11). The overall mass transfer coefficient, K_f, was assumed to be the same for glucose and fructose, because their molecular weights are identical and both are electrically neutral.

$$\alpha_c = K_f a_v \cdot L/v \tag{10-11a}$$

$$\beta_{ck} = \varepsilon_b/[(1-\varepsilon_b)m_k] \tag{10-11b}$$

$$\theta_0 = t_0/\tau \tag{10-11c}$$

$$\theta_d = t_d/\tau \tag{10-11d}$$

The solution in the time domain was obtained by the numerical inversion of $\bar{y}_k$ by the Fourier series approximation of the following

equation.[8]

$$y = (e^{a\theta}/T^*)\,[\bar{y}_k(a)/2 + \sum_{j=1}^{\infty} \{Re[\bar{y}_k(a+j\pi i/T^*)]\cdot\cos(j\pi i/T^*) - Im[\bar{y}_k(a+j\pi i/T^*)]\cdot\sin(j\pi i/T^*)\}] \quad (10\text{-}12)$$

where *Re* and *Im* indicate the real and imaginary parts of $\bar{y}_k$, respectively. T* and *a* are the arbitrary constants.

Calculation of breakthrough curve in a fixed-bed adsorber.

In a fixed-bed adsorber, the mass balnce equations for the concentrations of component *k* at the mobile and stationary phases are equal to Eqs.(10-5) and (10-6), respectively. Initial and boundary conditions are written as follows:

$$z > 0, \quad t = 0, \quad C_k = 0 \quad (10\text{-}13a)$$

$$C_k^* = 0 \quad (10\text{-}13b)$$

$$z = 0, \quad t \geq 0, \quad C_k = C_{k0} \quad (10\text{-}13c)$$

An analytical solution for C_k has been presented by Rosen.[9] The solution, however, is relatively complicated. Therefore, the numerical method was applied. Eqs.(10-5) and (10-6) are discretized forward for time and backward for distance to give the following equations.

$$C_k(x_i,\theta_{j+1}) = (1-\Delta\theta/\Delta x-\alpha_c\cdot\Delta\theta)\cdot C_k(x_i,\theta_j) + \alpha_c\cdot\Delta\theta\cdot C_k(x_i,\theta_j) + (\Delta\theta/\Delta x)\cdot C_k(x_{i-1},\theta_j) \quad (10\text{-}14)$$

$$C_k^*(x_i,\theta_{j+1}) = (1-\alpha_c\cdot\beta_{ck}\cdot\Delta\theta)\cdot C_k^*(x_i,\theta_j) + \alpha_c\cdot\beta_{ck}\cdot\Delta\theta\cdot C_k(x_i,\theta_j) \quad (10\text{-}15)$$

Initial and boundary conditions are as follows:

$$C_k(x_i,\theta_0) = 0 \quad (10\text{-}16a)$$

$$C_k^*(x_i,\theta_0) = 0 \quad (10\text{-}16b)$$

$$C_k^*(x_0,\theta_j) = C_{k0}[1 - \exp(\alpha_c\cdot\beta_{ck}\cdot\theta_j)] \quad (10\text{-}16c)$$

where Δx and $\Delta\theta$ are the increments for x- and θ-directions. The subscripts i and j represent i-th and j-th grid points for x- and θ-directions, respectively. $C_k(x_i,\theta_{j+1})$ and $C_k^*(x_i,\theta_{j+1})$ are calculated explicitly, and hence the calculation method described here may be simple.

10. 4. Results and Discussion

Screening of adsorbents. The adsorbent which has a high selectivity for fructose was looked for by using the pulse test. As an example, Fig. 10-2 shows the elution profiles of fructose, glucose, and soluble starch at the outlet of the bed of Ion-exchanger S-07 (Ca^{2+} form). In the figure, the abscissa represents the elapsed time normalized by the residence time based on the total bed volume, τ_0 (= L/v). The distribution coefficients of fructose and glucose for the adsorbent were calculated from Eqs. (10-1) and (10-2). In Table 10-1, the values of m_G and m_F for

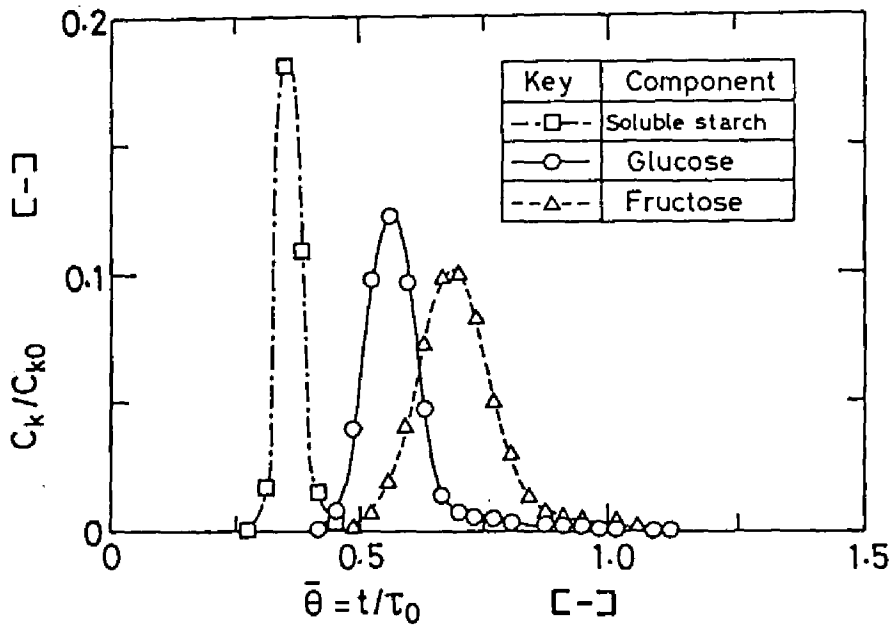

Fig. 10-2. Elution profiles of fructose, glucose, and soluble starch obtained by using Ion-exchanger S-07 (Ca^{2+} form)-packed column. Distilled water was used as eluent. The elution profiles of soluble starch was measured to estimate the void fraction of the bed. The concentration of component k in the eluate is normalized by that in the sample solution, whereas the elapsed time is normalyzed by the residence time with respect to the bed volume.

various adsorbents are listed together with the apparent densities of adsorbents. The larger the difference between m_G and m_F, the better the efficiency of the separation. From these observations, we picked up Ion-exchanger S-07 (Ca^{2+} form) and Y zeolite (Ca^{2+} form) as adsorbents with high separability.

Adsorption isotherms of glucose and fructose. The adsorption

Table 10-1. Apparent Density, ρ_p, Void Fraction of Bed, ε_b, and Distibution Coefficients of Glucose and Fructose, m_G and m_F, for Adsorbents.

Eluent	Water				0.02mol/l Tris-HCl buffer,pH 8.0 (including 0.01 mol/l $MgSO_4$)			
Adsorbent	ρ_p [g/cm^3]	ε_b [-]	m_G [-]	m_F [-]	ρ_p [g/cm^3]	ε_b [-]	m_G [-]	m_F [-]
Amberlite IR-120B(Ca)	1.274	0.364	0.099	0.164	-	0.362	0.058	0.157
Amberlite IR-120B(Mg)	-	0.339	0.047	0.095	-	-	-	-
Dowex 50W(Ca)	1.323	0.313	0.017	0.080	-	-	-	-
Y-Zeolite(Ca)	-	-	-	-	0.855*	0.388	0.586	0.686
Y-Zeolite(Mg)	-	-	-	-	1.096	0.379	0.423	0.488
S-07(Ca)	1.252	0.381	0.231	0.464	-	0.360	0.253	0.423
S-22(Ca)	1.254	0.352	0.326	0.518	-	0.368	0.335	0.506

* This value was obtained by using a mercury porosimeter. Another values were pycnometrically determined.

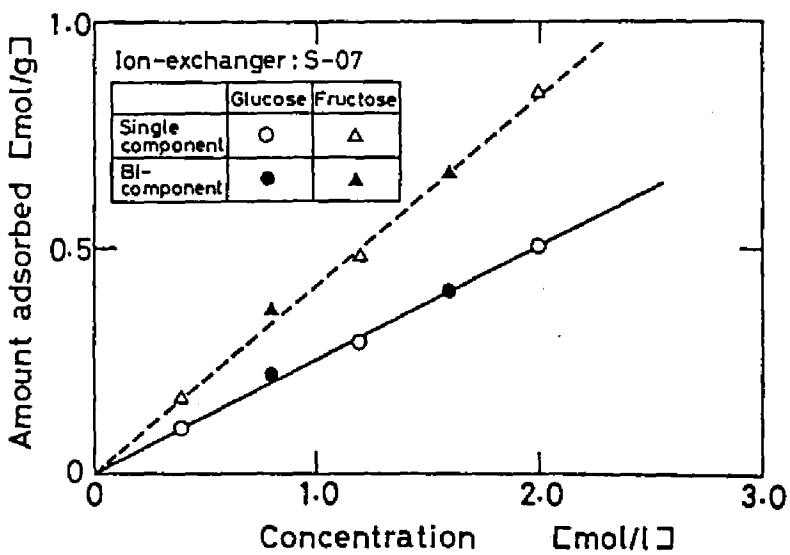

Fig. 10-3. Adsorption isotherms of glucose and fructose on Ion-exchanger S-07 (Ca^{2+} from) at 50°C. Distilled water was used as a solvent. The amounts of glucose and fructose adsorbed were obtained by analyzing the break-through curves.

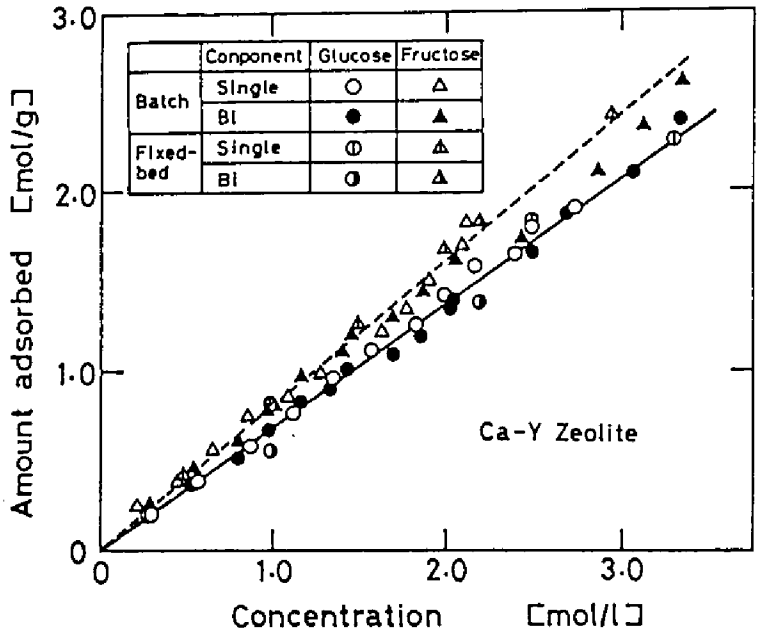

Fig. 10-4. Adsorption isotherms of glucose and fructose on Y zeolite (Ca^{2+} form) at 50°C. The amounts of glucose and fructose adsorbed were estimated by using both the batch desorption method and the analysis of breakthrough curves in fixed-bed adsorber. As a solvent, 0.02 mol/l Tris-HCl buffer containing 0.01 mol/l magnesium sulfate was used.

isotherms of glucose and fructose for Ion-exchanger S-07 (Ca^{2+} form) and Y zeolite (Ca^{2+} form) were obtained at 50°C. They are shown in Figs. 10-3 and 10-4. For Ion-exchanger S-07 and Y zeolite, distilled water and 0.02 mol/l Tris-HCl buffer containing 0.01 mol/l $MgSO_4$ were used as solvents, respectively. The reason to use the buffer solution was previously mentioned. In the experiments using the mixture of glucose and fructose, the concentrations of both glucose and fructose are initially taken to be

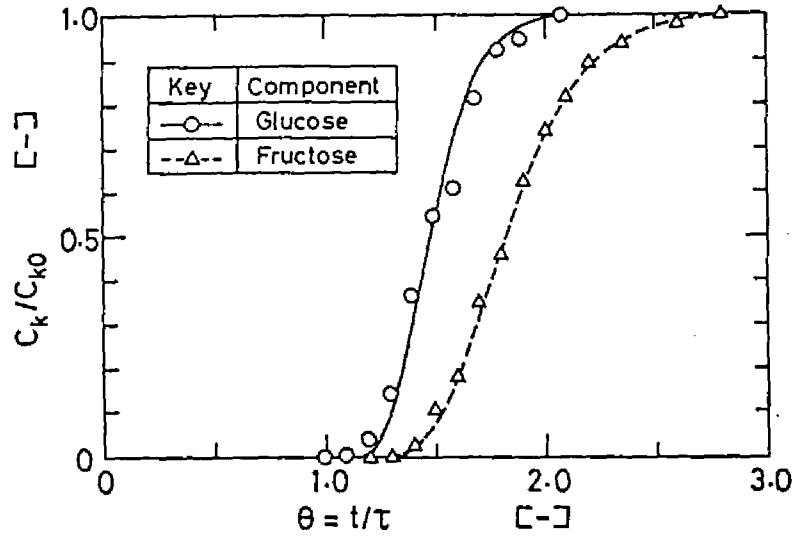

Fig. 10-5. Breakthrough curves of glucose and fructose in the Ion-exchanger S-07 (Ca^{2+} form)-packed column at 50°C. The solid and broken curves were calculated ones for glucose and fructose, respectively. The $K_f a_v$ value was set to be 6.18 X 10^{-3} s^{-1} for both curves.

equal. Linear isotherms were obtained for both glucose and fructose over a wide concentration range. The amount of fructose adsorbed was independent of that of glucose adsorbed.

Determination of overall volumetric mass transfer coefficient.

The overall volumetric mass transfer coefficient, $K_f a_v$, was determined so that the calculated breakthrough curve may fit to the experimental one. In the case of Ion-exchanger S-07, the $K_f a_v$ values for both glucose and fructose were 6.18 X 10^{-3} s^{-1}. Figure 3-5 shows the breakthrough curves of glucose and fructose obtained in the Ion-exchanger S-07 (Ca^{2+} form)-packed column. The solid

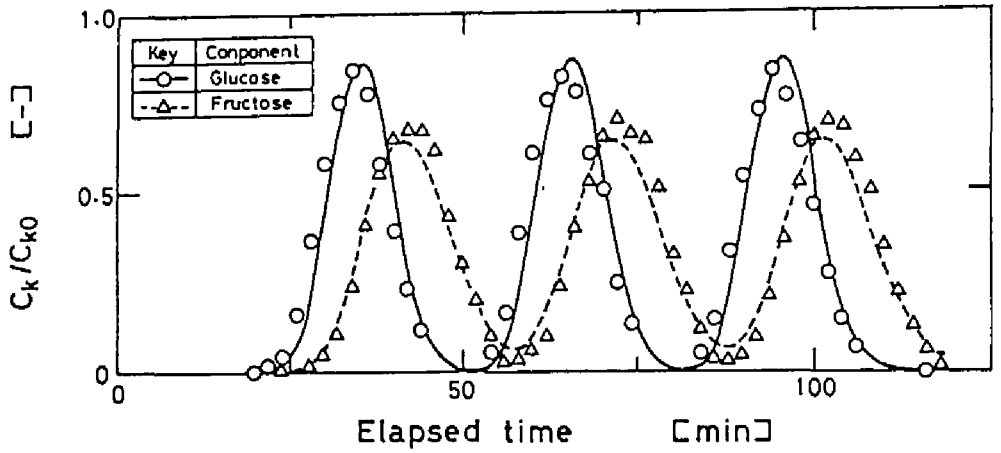

Fig. 10-6. Elution profiles of glucose and fructose in chromatography. The mixture of the components and distilled water were alternately introduced three times to the bed of Ca^{2+} ion form of Ion-exchanger S-07. The solid and broken curves are calculated ones for glucose and fructose, respectively.

and broken curves in the figure are the calculated ones for glucose and fructose, respectively. When Y zeolite was used as the adsorbent, the $K_f a_v$ values for both components were 6.84×10^{-3} s^{-1}. The $K_f a_v$ values scarecely depended on the flow rate of the eluent. This suggests that the resistance of interphase mass transfer is negligibly small.

Elution profiles of glucose and fructose in a conventional chromatography. The mixture of glucose and fructose was introduced to the bed of Ion-exchanger S-07 (Ca^{2+} form, 1.485 cmϕ X 36.8 cm) for 10 min and then distilled water was supplied to the bed for 20 min at the flow rate of 1.19 cm^3/min. This alternate feeding was

repeated three times. After the third supply of the mixture, distilled water was successively fed.

Figure 10-6 shows the elution profiles of glucose and fructose. The solid and broken curves represent the calculated ones for glucose and fructose, respectively. The theoretical elution profiles coincide well with the experimental ones, indicating that both the method for predicting the elution curves and the parameters determined are valid.

Separation of glucose and fructose by modified chromatography.

Figure 10-7(a) shows the time dependencies of glucose and fructose concentrations at the outlet of zone I. The solid and broken curves in the figure were calculated from Eqs.(10-14) and (10-15). Glucose with small distribution coefficient was eluted eariler than fructose as predicted from the theoretical calculation. Figure 10-7(b) illustrates the concentration profiles of glucose and fructose in zone I.

Figure 10-7(c) shows the concentration profiles in the adsorber at the time when the circulation of the liquid in the adsorber was stopped. Fructose and glucose were successfully localized in zones II and III, respectively. The two components in zones II and III were separately eluted by distilled water.

Figure 10-7(d) shows the elution profiles obtained at the outlet of zone II. Figure 10-7(e) illustrates the profiles of glucose and fructose concentrations in the solution emerging fron

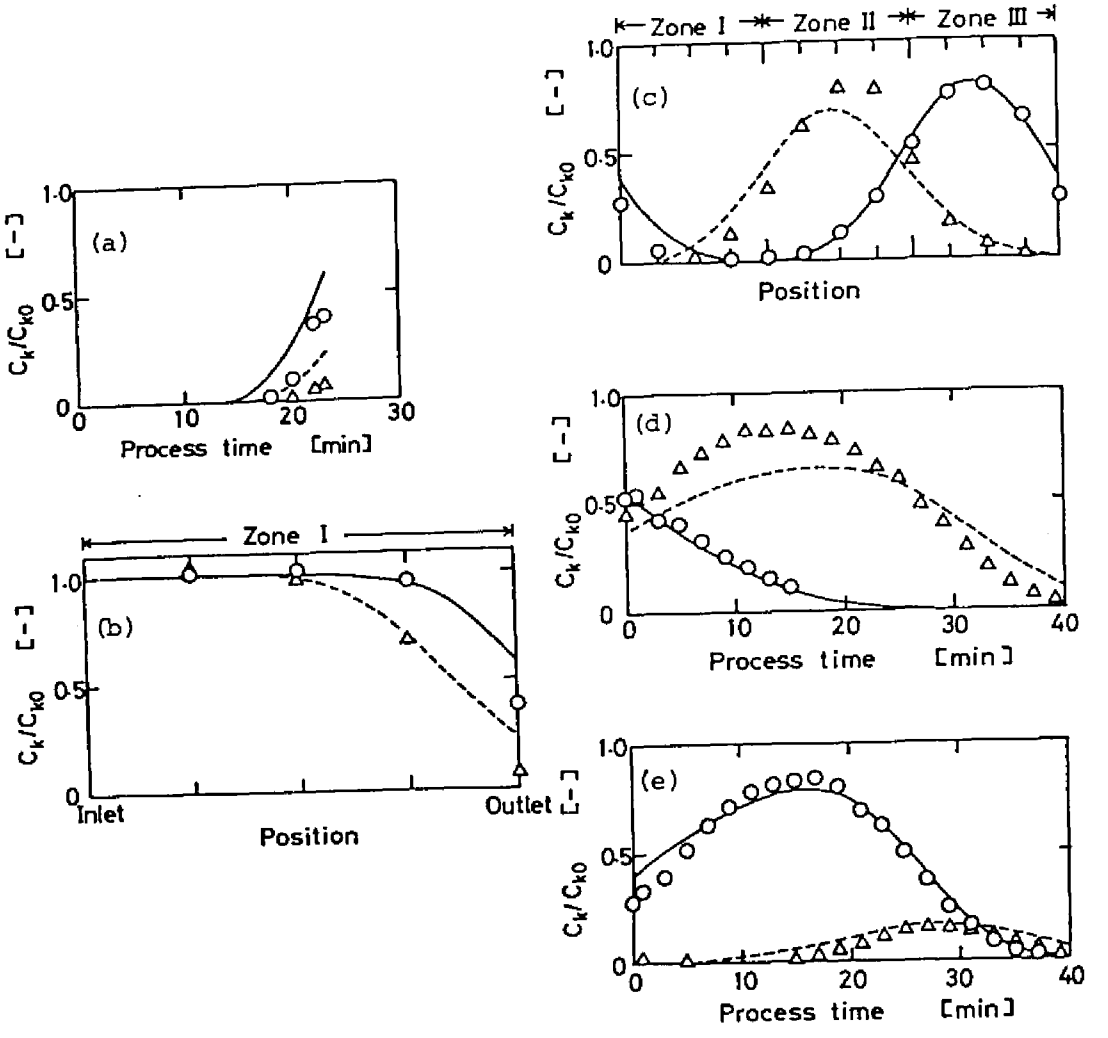

Fig. 10-7. Separation of glucose and fructose by a modified chromatographic process. The keys (○) and (△) represent glucose and fructose, respectively. The solid and broken curves are calculated ones for glucose and fructose. (a) Breakthrough curves of glucose and fructose observed at the outlet of zone I. (b) Concentration profiles in zone I at the end of the first operation. (c) Concentration profiles of glucose and fructose in the adsorber after circulation of the two components remained in zone I. (d) Elution profiles of glucose and fructose obtained at the outlet of zone II. (e) Elution profiles at the outlet of zone III.

zone III. Fructose and glucose were eluted mainly from zones II and III, and hence the separation of the two components was achieved.

Though the modified procedure for chromatographic separation is a little complicated, the procedure has some merits. Since the separation of two components was achieved in the procedure by circulating the liquid in the adsorber, both the size of the bed and the amount of desorbent introduced can be reduced compared with the conventional chromatographic procedure. When the mechanical intensity of the adsorbent is weak, or when the adsorbent is expensive, the modified procedure would be effective. Though the adsorbates in zone II were eluted with water introduced at the inlet of zone II in this study, the amount of water consumed in the procedure would be reducible if the operations mentioned above are regularly repeated and the water emerging from zone I at the first operation is utilized for desorption of fructose in zone II.

10. 5. Summary

The capabilities of some adsorbents for separating glucose and fructose were examined. Two adsorbents, Ion-exchanger S-07 (Ca^{2+} form) and Y zeolite (Ca^{2+} form), were found to adsorb more favorably fructose than glucose. The adsorption isotherms of glucose and fructose were obtained at 50°C. The isotherms of the two components were linear over a wide range of each concentration and

were independent each other. The validities of methods for predicting the elution profiles in chromatography and the breakthrough curves in a fixed-bed adsorber were experimentally verified. A modified procedure for chromatographic separation of the two components was successfully developed.

Nomenclature

a	arbitrary constant	[-]
a_v	specific surface area	[cm^2/cm^3-bed]
C	concentration in the liquid phase	[mol/l]
C*	concentration within the particle	[mol/l]
K_f	overall mass transfer coefficient	[cm/s]
L	column length	[cm]
m	distribution coefficient	[-]
n	number of sample injection times	[-]
Q	volumetric flow rate	[cm^3/s]
q	amount adsorbed	[mol/g]
s	Laplace variable	[-]
T*	arbitrary constant	[-]
t	time	[s]
$\bar{t}$	mean residence time of adsorbate in the fixed-bed adsorber	[s]
t_d	desorbent injection time	[s]
t_0	sample injection time	[s]

V	volume of solvent	[cm^3]
$\bar{V}$	bed volume	[cm^3]
v	linear superficial velocity of liquid flow in the fixed-bed adsorber	[cm/s]
w	weight	[g]
x	$= z/L$	[-]
y_k	$= C_k/C_{k0}$	[-]
y_k^*	$= C_k^*/C_{k0}$	[-]
$\bar{y}_k$	solution of y_k in Laplace domain	[-]
z	axial distance	[cm]
α_c	$= K_f a_v \cdot L/v$	[-]
β_{ck}	$= \varepsilon_b/[(1 - \varepsilon_b)m_k]$	[-]
ε_b	void fraction of the bed	[-]
θ	$= t/\tau$	[-]
θ_d	$= t_d/\tau$	[-]
θ_0	$= t_0/\tau$	[-]
ρ_p	apparent density	[cm^3/g]
τ	residence time of eluent based on the void volume of the bed	[s]
τ_0	residence time of eluent based on the total bed volume	[s]

Subscripts

E	end point

F fructose

G glucose

k component

l effluent

0 influent

Literature Cited

1) R. W. Goulding, *J. Chromatogr.*, 103, 229 (1975).

2) Y. Takasaki, Y. Kosugi, and A. Kanbayashi, *Agric. Biol. Chem.*, 33, 1527 (1969).

3) E. C. Toren, Jr., *J. Chem. Educ.*, 44, 172 (1967).

4) J. H. Roe, J. H. Epotein, and N. P. Goldstein, *J. Biol. Chem.*, 178, 839 (1949).

5) A. J. deRosset, R. W. Neuzil, and D. J. Korous, *Ind. Eng. Chem. Process Des. Dev.*, 15, 2 (1976).

6) M. Suzuki, *Seisankenkyu*, 24, 187 (1972).

7) K. Nakanishi, S. Yamamoto, R. Matsuno, and T. Kamikubo, *Agric. Biol. Chem.*, 17, 1515 (1975).

8) K. S. Crump, *J. ACM*, 23, 89 (1976).

9) J. B. Rosen, *J. Chem. Phys.*, 20, 387 (1952).

Chapter 11

Separation of Glucose and Fructose by Using a Simulated Moving-Bed Adsorber

11. 1. Introduction

The common type of high fructose syrup is produced by an enzymatic isomerization of glucose to fructose. The isomerization is a reversible reaction and its equilibrium constant is 1.0 at 50°C. Therefore, to produce the higher fructose syrup, the separation step is indispensable. The conventional chromatographic separation is a simple process. This process, however, has the following demerits;[1] (i) an adsorbent is not always utilized effectively, (ii) a large amount of desorbent is consumed, (iii) a large difference in the distribution coefficient between glucose and fructose is necessary, and (iv) the operation is discontiuous.

Another type of separation process, which can improve some of the demerits in the chromatographic process, is a process utilizing a simulated moving-bed adsorber. This was originally developed by UOP.[2] This chapter deals with a glucose/fructose separation process utilizing the simulated moving-bed adsorber. The design problems of the process will be discussed. Two methods for calculating the concentration profiles in the adsorber are presented and their validities are experimentally examined.

11. 2. Theoretical Considerations

Basic idea behind the process utilizing a simulated moving-bed adsorber. Although the adsorbent particles do not move actually in the simulated moving-bed operation, the operation is more clearly understood by describing a hypothetical moving-bed operation and describing how similar results are obtained without actual bed movement. In the conventional chromatographic separation, two components are separated by the difference between their migration rates in the fixed-bed adsorber. Therefore, when a sample solution is fed to the middle point of the adsorption column and adsorbent particles are traveled counter to liquid flow at the rate between the migration rates of two components in chromatography, a component adsorbed weakly moves in the direction of liquid flow and another component adsorbed strongly travels in the direction of adsorbent flow. Thus, in the moving-bed adsorber where adsorbent particles and liquid are conveyed continuously and countercurrently to each other, the two components migrate in different directions and are separated.

Figure 11-1 illustrates schematically the process utilizing the simulated moving-bed adsorber. Adsorbent particles move continuously toward the right-hand side through the bed and returned to the left-hand side of the apparatus. Feed and desorbent solutions enter continuously, and flow toward the left-hand side and countercurrently to the adsorbent particles. Raffinate and extract

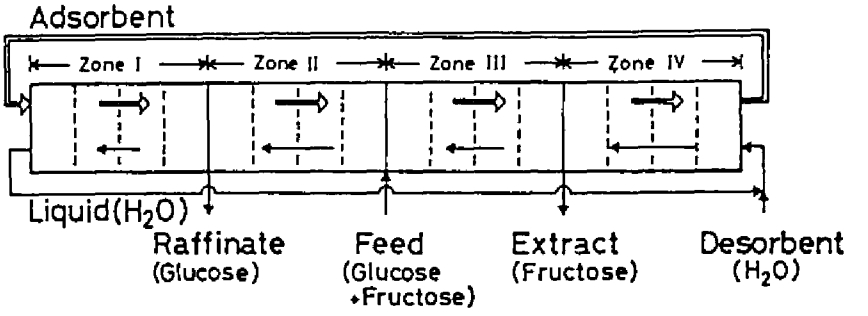

Fig. 11-1. Schematic representation of a hypothetical moving-bed adsorber. Adsorbent particles move continuously toward the right-hand side, while liquid flows toward the left-hand side. The adsorber is divided into four zones by the introduction and withdrawal points of liquid. A portion between two broken lines in the adsorber corresponds to a column in a simulated moving-bed adsorber.

solutions are withdrawn continuously. At both withdrawal points, a portion of the liquid flowing in the bed is withdrawn and the remainder continues to flow into the next zone. As shown in Fig. 11-1, the positions of introduction and withdrawal of liquid divide the bed into four zones, I to IV, each of which performs different function as described below.

We suppose here that fructose is adsorbed selectively in comparison with glucose. Fructose introduced by a feed stream is adsorbed mostly in zone II and carried to zones III and IV by the movement of adsorbent particles. Although glucose fed by the feed stream is weakly adsorbed, most of the glucose is passed through zone II and withdrawn by a raffinate stream. Glucose adsorbed

partially in zone II is desorbed in zone III to reduce the amount of glucose in an extract stream. Fructose adsorbed in zone II is desorbed in zone IV and recovered by the extract stream. The adsorbent particles are regenerated by the desorption of fructose in zone IV and flow to zone I. Zone I acts to adsorb glucose remaining in liquid, and hence the liquid emerging from zone I scarcely contains both the pomponents and can be utilized as a desorbent.

Compared with the conventional chromatographic separation process, the process using the moving-bed adsorber has some merits; (i) the quantity of desorbent used can be saved because the solution emerging from zone I is usable as a desorbent, (ii) the separation is effectively accomplished even if the difference in the distribution coefficient between glucose and fructose is small, and (iii) the operation is continuous.

The basic idea behind the process is explained by using a hypothetical moving-bed adsorber. However, the actual movement of adsorbent particles may cause the abrasion of adsorbent and the channelling of liquid flow. The smart process without the actual movement of adsorbent particles, which exhibits an function almost equal to that of the process mentioned above, has been developed. [2-4] By shifting the introduction and withdrawal points of liquid streams to the same direction as the liquid flow at regular intervals, the flow of adsorbent particles counter to liquid is achiev-

ed relatively.

Calculation of concentration profiles in simulated moving-bed adsorber. In order to calculate the concentration profiles in the simulated moving-bed adsorber, two models, namely, an intermitted moving-bed model and a continuous moving-bed model, are presented. An intermitted moving-bed model cosiders the real movement of adsorbent particles. The concentration profiles at the unsteady state can be calculated by using this model. In a continuous moving-bed model, it is assumed that the adsorbent particles hypothetically moves counter to the liquid flow. This model has a merit that the concentration profiles at the steady state can be calculated easily.

The followings are assumed in both models; (i) an approximation of linear-driving-force is satisfied in the adsorptive rate process, (ii) the liquid flow is a plug flow, and (iii) the overall mass transfer coefficients of glucose and fructose are the same and does not depend on the rate of liquid flow.

(a) *An intermitted moving-bed model.* The original process has accomplished the simulated movement of adsorbent particles by transferring the introduction and withdrawal points of liquid streams to the same direction as liquid flow. In this study, however, the counter-flow of adsorbent particles to liquid is achieved by conveying adsorption columns in the direction counter to the

liquid flow. In such a mode, adsorption columns are considered to be fixed-bed except for the moment of conveying the columns.

Mass balance equations referring to concentrations of component k at the mobile phase C_k and at the stationary phase C_k^* are given by Eqs.(11-1) and (11-2), setting to be positive for the direction of liquid flow.

$$\varepsilon_b \frac{\partial C_k}{\partial t} = -v_n \frac{\partial C_k}{\partial z} - K_f a_v (C_k - C_k^*) \tag{11-1}$$

$$(1 - \varepsilon_b) m_k \frac{\partial C^*}{\partial t} = K_f a_v (C_k - C_k^*) \tag{11-2}$$

where v_n is the linear superficial velocity of liquid flow in zone n, $K_f a_v$ the overall volumetric mass transfer coefficient, m_k the distribution coefficient of component k, and ε_b the void fraction of the bed. The process time t and axial distance z are normalized by the interval of transportation of adsorption columns T and the length of each column L_A, respectively.

$$\theta = t/T \tag{11-3a}$$

$$x = z/L_A \tag{11-3b}$$

Eqs.(11-1) and (11-2) are written as follows;

$$\frac{\partial C_k}{\partial \theta} = -\bar{\alpha}_n \frac{\partial C_k}{\partial x} - \bar{\beta}(C_k - C_k^*) \tag{11-4}$$

$$\frac{\partial C_k^*}{\partial \theta} = \overline{\gamma}_k (C_k - C_k^*) \tag{11-5}$$

where

$$\overline{\alpha}_n = v_n T/(\varepsilon_b L_A) \tag{11-6a}$$

$$\overline{\beta} = K_f a_v T/\varepsilon_b \tag{11-6b}$$

$$\overline{\gamma}_k = K_f a_v T/[(1 - \varepsilon_b) m_k] \tag{11-6c}$$

By discretizing Eqs.(11-4) and (11-5) forward for time and backward for distance, Eqs.(11-7) and (11-8) are obtained.

$$C_k(x_i,\theta_{j+1}) = (1-\overline{\alpha}_n \cdot \Delta\theta/\Delta x - \overline{\beta}\cdot\Delta\theta)\cdot C_k(x_i,\theta_j) + \overline{\beta}\cdot\Delta\theta\cdot C_k^*(x_i,\theta_j) + (\overline{\alpha}_n\cdot\Delta\theta/\Delta x)\cdot C_k(x_{i-1},\theta_j) \tag{11-7}$$

$$C_k^*(x_i,\theta_{j+1}) = \overline{\gamma}_k\cdot\Delta\theta\cdot C_k(x_i,\theta_j) + (1-\overline{\gamma}_k\cdot\Delta\theta)\cdot C_k^*(x_i,\theta_j) \tag{11-8}$$

There are the following boundary conditions between zones.

at the outlet of raffinate stream (between zones I and II)

$$C_{kII1} = C_{kI0} \tag{11-9a}$$

at the inlet of feed stream (between zones II and III)

$$v_f\cdot C_{kf} + v_{III}\cdot C_{kIII1} = v_{II}\cdot C_{k0} \tag{11-9b}$$

at the outlet of extract stream (between zones III and IV)

$$C_{kIV} = C_{kIII0} \tag{11-9c}$$

at the inlet of desorbent stream (between zones IV and I)

$$v_I\cdot C_{kI} = v_{IV}\cdot C_{kIV0} \tag{11-9d}$$

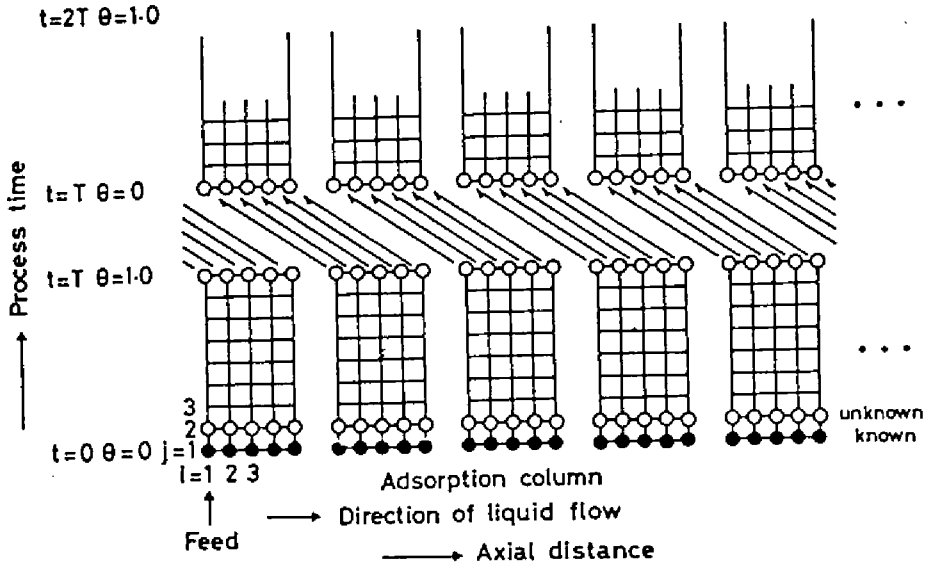

Fig. 11-2. Schematic explanation of the calculation method in an intermitted moving-bed model.

where the subscripts 0 and *1* denote the inlet and outlet of each zone, respectively. As shown in Fig. 11-2, $C_k(x_i,\theta_{j+1})$ and $C_k^*(x_i, \theta_{j+1})$ are calculated explicitly from Eqs.(11-7), (11-8), and (11-9). The calculations are repeated until $\theta = 1.0$. When $\theta = 1.0$, C_k and C_k^* are rearrenged in the direction of the arrows illustrated in the figure. The rearrangement corresponds to conveyance of adsorption columns.

(b) *A continuous moving-bed model.* It is assumed in this model that the adsorbent particles continuously at the rate of u_s. The u_s value is calculated to be L_A/T. Setting to be positive for the direction of the adsorbent movement, the mass balance equations at the steady state in terms of C_k and C_k^* are given by Eqs.

(11-10) and (11-11).

$$u_n \frac{dC_k}{dz} = K_f a_v (C_k - C_k^*) \tag{11-10}$$

$$(1 - \varepsilon_b) m_k u_s \frac{dC_k^*}{dz} = K_f a_v (C_k - C_k^*) \tag{11-11}$$

where u_n represents the linear superficial velocity of liquid flow in zone n in the hypothetical moving-bed adsorber and is related to v_n by the following equation.

$$u_n = v_n - \varepsilon_b L_A / T \tag{11-12}$$

Assuming that C_k and C_k^* at the inlet of each column are known, that is,

$$\text{at } z = 0, \qquad C_k = C_{k0} \tag{11-13a}$$

$$C_k^* = C_{k0}^* \tag{11-13b}$$

Eqs. (11-10) and (11-11) can be analytically solved to give

$$C_k = \frac{\exp[\alpha_n (1-\beta_{nk}) x] - \beta_{nk}}{1 - \beta_{nk}} C_{k0} + \frac{1 - \exp[\alpha_n (1-\beta_{nk}) x]}{1 - \beta_{nk}} C_{k0}^* \tag{11-14}$$

$$C_k^* = \frac{\beta_{nk} [\exp\{\alpha_n (1-\beta_{nk}) x\} - 1]}{1 - \beta_{nk}} C_{k0} + \frac{1 - \beta_{nk} \exp[\alpha_n (1-\beta_{nk}) x]}{1 - \beta_{nk}} C_{k0}^* \tag{11-15}$$

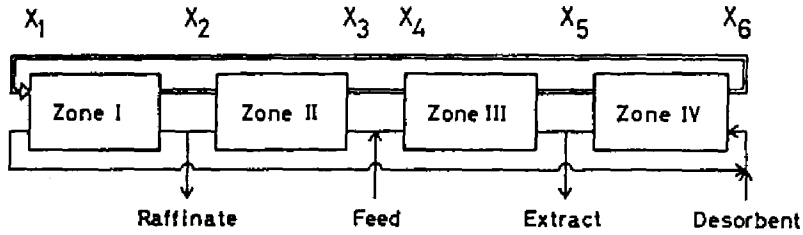

Fig. 11-3. Definition of variable vector X_i.

where

$$x = z/L_A \tag{11-3a}$$

$$\alpha_n = K_f a_v L_A / u_n \tag{11-16a}$$

$$\beta_{nk} = u_n / [u_s (1 - \varepsilon_b) m_k] \tag{11-16b}$$

By substituting N_n, which is the number of columns in zone n, for x, Eqs.(11-14) and (11-15) represent the relationships between C_k C_k^* at the inlet of zone and those at the outlet.

To make computational calculation suitable, we define a new variable $\bar{C}_k^*$ as follows:

$$\bar{C}_k^* = C_k - C_k^* \tag{11-17}$$

The variable vector X_i at any point in Fig. 11-3 is defined by

$$X_i = [C_{ki} \quad \bar{C}_{ki}^*]^T \tag{11-18}$$

The variable vectors X_i and X_{i+1} are related by the following equations.

$$x_1 = D \cdot x_6 \tag{11-19a}$$

$$x_2 = A_1 \cdot x_1 \tag{11-19b}$$

$$x_3 = A_2 \cdot x_2 \tag{11-19c}$$

$$x_4 = F \cdot x_3 - f \tag{11-19d}$$

$$x_5 = A_3 \cdot x_4 \tag{11-19e}$$

$$x_6 = A_4 \cdot x_5 \tag{11-19f}$$

where the constant matrices are given as follows:

$$A_n = \begin{bmatrix} 1 & \dfrac{1-\exp[\alpha_n(1-\beta_{nk})N_n]}{1-\beta_{nk}} \\ 0 & \exp[\alpha_n(1-\beta_{nk})N_n] \end{bmatrix} \tag{11-20a}$$

$$D = \begin{bmatrix} u_{IV}/u_I & 0 \\ 1 - u_{IV}/u_I & 1 \end{bmatrix} \tag{11-20b}$$

$$F = \begin{bmatrix} u_{II}/u_{III} & 0 \\ 1 - u_{II}/u_{III} & 1 \end{bmatrix} \tag{11-20c}$$

$$f = \begin{bmatrix} C_{kf} \cdot u_f/u_{III} \\ -C_{kf} \cdot u_f/u_{III} \end{bmatrix} \tag{11-20d}$$

By summarizing Eqs.(11-19), Eq.(11-21) is obtained. Eq.(11-21) is shown in the next page. E and 0 in Eq.(11-21) are defined by

$$E = \begin{bmatrix} 1 & 0 \\ 0 & 1 \end{bmatrix} \tag{11-22a}$$

$$0 = \begin{bmatrix} 0 \\ 0 \end{bmatrix} \tag{11-22b}$$

$$\begin{bmatrix} -E & & & & & D \\ A_1 & -E & & & & \\ & A_2 & -E & & & \\ & & F & -E & & \\ & & & A_3 & -E & \\ & & & & A_4 & -E \end{bmatrix} \cdot \begin{bmatrix} x_1 \\ x_2 \\ x_3 \\ x_4 \\ x_5 \\ x_6 \end{bmatrix} = \begin{bmatrix} 0 \\ 0 \\ 0 \\ f \\ 0 \\ 0 \end{bmatrix} \qquad (11\text{-}21)$$

The concentration profiles in the adsorber can be calculated by solving Eq.(11-21). This method is suitable for a computational calculation and for examing the operating conditions.

11. 3. Materials and Methods

Adsorbent and Chemicals. The Ca^{2+} ion form of Y zeolite kindly supplied by Toyo Soda Mfg. Co., Ltd. was used as an adsorbent. As shown in Chapter 10, the adsorption isotherms of glucose and fructose were linear over a wide concentration range and independent. The distribution coefficients of glucose and fructose were 0.586 and 0.686, respectively.

Glucose and fructose were purchased from Nakarai Chemicals. The other chemicals were of analytical grade.

Experimental apparatus. Figure 11-4 illustrates a schematic diagram of experimental apparatus. Sixteen columns, in which Y zeolite (Ca^{2+} form) was packed, were connected to a rotary valve. Four adsorption columns were assigned to each zone. The size of each column was 1.38 cm in diameter and 10.2 cm in length. The

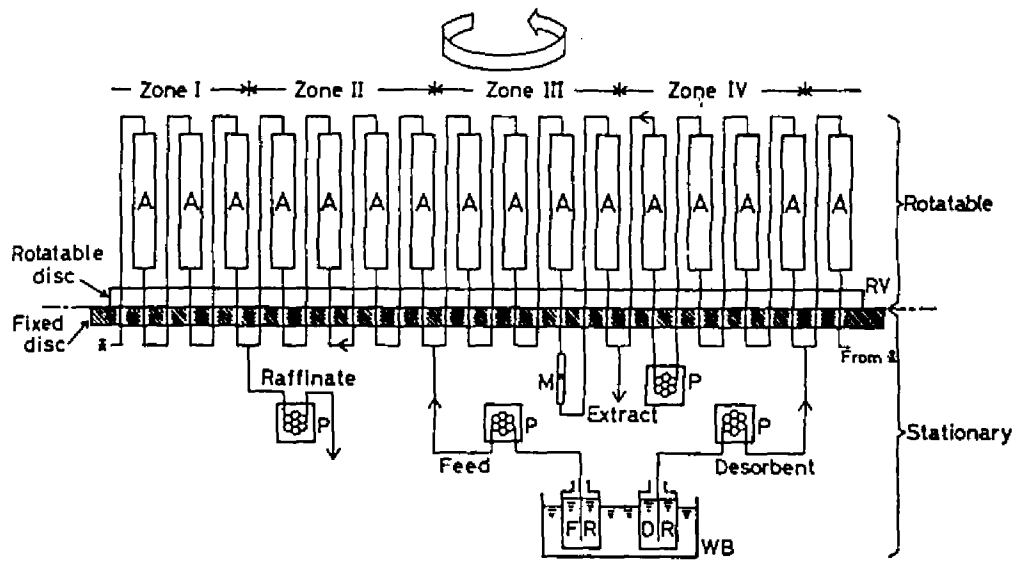

Fig. 11-4. Schematic diagram of experimental apparatus used in the glucose/fructose separation by utilizing a simulated moving-bed adsorber. The rotary valve consists of two discs. The lower disc is fixed, while the upper disc is rotatable. The simulated moving-bed operation was accomplished by rotating the upper disc at regular intervals. The adsorption columns were kept at 50°C by circulating the thermostated water, although the flow of the water is not painted in this figure. A, adsorption column; DR, desorbent reservoir; FR, feed reservoir; M, flow meter; P, constant-feeding pump; RV, rotary valve; WR, water bath.

columns with jackets were kept at 50°C by circulating the thermostated water. The valve consisted of two stainless steel discs. Some ingenuities were taxed to prevent escape of liquid from the boundary between the discs. The lower disc was fixed. The feed and desorbent reservoirs and the constant-feeding pumps to con-

trol the rate of liquid flow were arranged under the valve. The upper disc was mobile. In this study, the simulated movement of the adsorbent particles was accomplished by conveying periodically the adsorption columns in the direction counter to liquid flow.

Continuous separation of glucose and fructose. The feed solution contained glucose and fructose in the same concentration. They were dissolved in 0.02 mol/l Tris-HCl buffer containing 0.01 mol/l magnesium sulfate. The buffer solution was used as the desorbent. Prior to the experiment, the liquid in the adsorber was displayed by the solution containing glucose and fructose in the concentration equal to $C_{kf} \cdot Q_f/(Q_f + Q_d)$. C_{kf} represents the concentration of component k in the feed solution. Q_f and Q_d are the volumetric flow rates of feed and desorbent streams, respectively. The interval for conveying adsorption columns was set to be 2 to 5 min. The raffinate and extract streams were fractionated every 30 min and the concentrations of glucose and fructose in the fractions were measured. After establishment of the steady state was confirmed, the operation was stopped. The concentrations of glucose and fructose in each of tubes connecting the columns were measured. These data points give the concentration profiles of both the components in the adsorber.

Assay of glucose and fructose. The concentrations of glucose and fructose were analyzed by using a high-performance liquid

Table 11-1. Experimental Conditions for Separating Glucose and Fructose by Using the Simulated Moving-Bed Adsorber.

Run No.	S-1	S-2	S-3	S-4	S-5	S-6	S-7
C_{Gf} [mol/l]	0.1	0.1	0.1	0.1	0.5	0.5	1.0
C_{Ff} [mol/l]	0.1	0.1	0.1	0.1	0.5	0.5	1.0
Q_f [cm^3/min]	0.4	0.25	0.6	0.4	1.0	0.4	0.4
Q_d [cm^3/min]	1.6	0.75	1.8	1.2	3.0	1.6	2.0
Q_r [cm^3/min]	1.0	0.5	1.2	0.8	2.0	1.0	1.2
Q_e [cm^3/min]	1.0	0.5	1.2	0.8	2.0	1.0	1.0
T [min]	3	5	2	3	2	2	2
v_I [cm/min]	2.227	1.401	3.340	2.227	3.078	3.035	2.851
v_{II} [cm/min]	2.893	1.735	4.140	2.760	4.732	3.701	3.651
v_{III} [cm/min]	2.627	1.568	3.740	2.493	3.704	3.436	3.385
v_{IV} [cm/min]	3.293	1.901	4.540	3.027	5.038	4.102	4.185

chromatography (Shimadzu, LC-3A) equipped with a separation column (Shimadzu, SCR-101N) and a differential refractometer (Showa Denko, Shodex RI SE-11).

11. 4. Results and Discussion

Continuous separation of glucose and fructose. Seven runs of experiments were carried out under various operating conditions, which are listed in Table 11-1. Figure 11-5 shows the time courses of glucose and fructose concentrations in the extract and raffinate streams in run S-5. The curves in the figure were calculated by using the intermitted moving-bed model. Figure 11-6

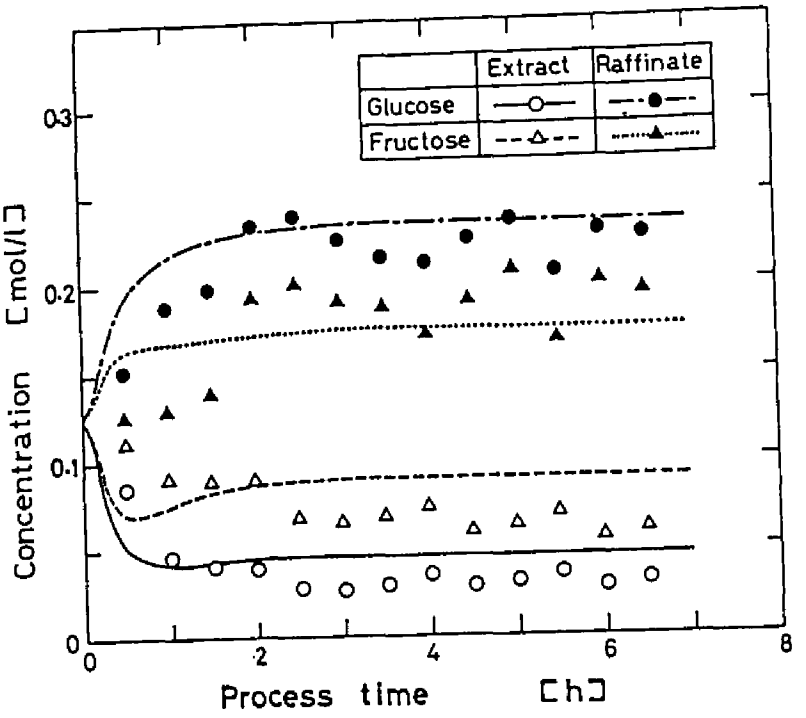

Fig. 11-5. Time courses of glucose and fructose concentrations in the extract and raffinate streams in run S-5. The theoretical curves in the figure were calculated by using the intermitted moving-bed model.

illustrates the concentration profiles at the steady state in run S-6. The theoretical profiles in Figs.11-6(a) and (b) were calculated by using the intermitted and continuous moving-bed models, respectively. The theoretical profiles by the continuous moving-bed model coincide with the experimental ones in the same degree as the theoretical ones by the intermitted moving-bed model. The concentration profiles at the steady state are simply calculated by the continuous moving-bed model and coincide fairly well with the experimental ones. Thus, the continuous moving-bed model is

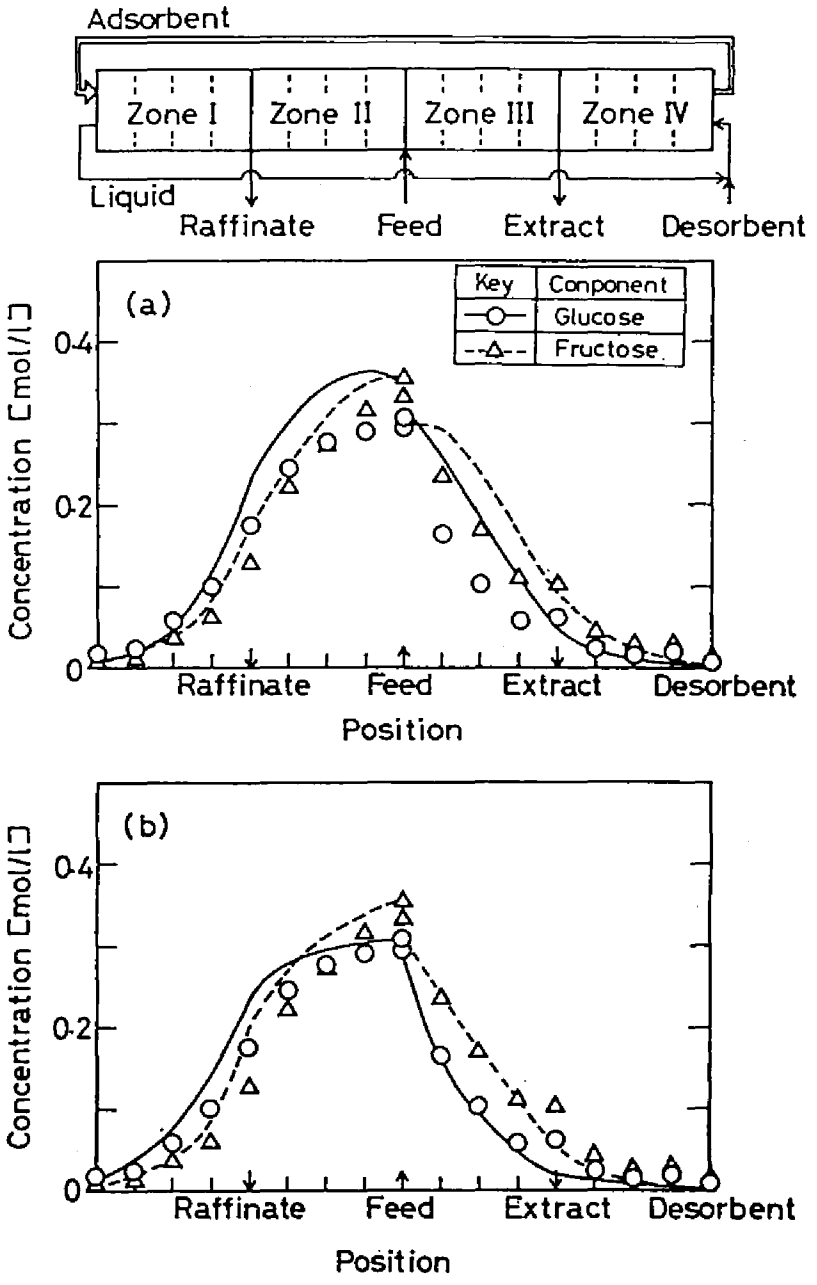

Fig. 11-6. Concentration profiles of glucose and fructose in the adsorber at the steady state. (a) The solid and broken curves for glucose and fructose were calculated from the intermitted moving-bed model. (b) The theoretical curves were obtained by using the continuous moving-bed model. The same experimental results are plotted in both (a) and (b).

Table 11-2. Set up of β_{nk} Values to Obtain High Separability.

Zone	I	II	III	IV
β_G	< 1	> 1	> 1	> 1
β_F	< 1	< 1	< 1	> 1

useful to determine the operating conditions and to examine the characteristics of the separation by using the adsorber.

Inportance of β_{nk} for determination of operating conditions.

The nondimensional parameter β_{nk} defined in the continuous moving-bed model denotes the ratio of the amount of adsorbate carried by the liquid flow against that carried by the flow of adsorbent particles. When β_{nk} is less than 1.0, the amount of adsorbate carried by the adsorbent flow is more than that carried by the liquid flow. In order to exhibit correctly the function of each zone, the values of β_{nk} must be set in the mode shown in Table 11-2.

The β_{nk} values were set up reasonably in run S-3. The concentration profiles obtained experimentally in run S-3 are illustrated in Fig.11-7(a) along with the theoretical ones calculated by using the continuous moving-bed model. Figure 11-7(b) shows the concentration profiles obtained in run S-7, where β_{nk} values do not satisfy the inequalities listed in Table 11-2. The separation of glucose and fructose could not be accomplished in run S-7.

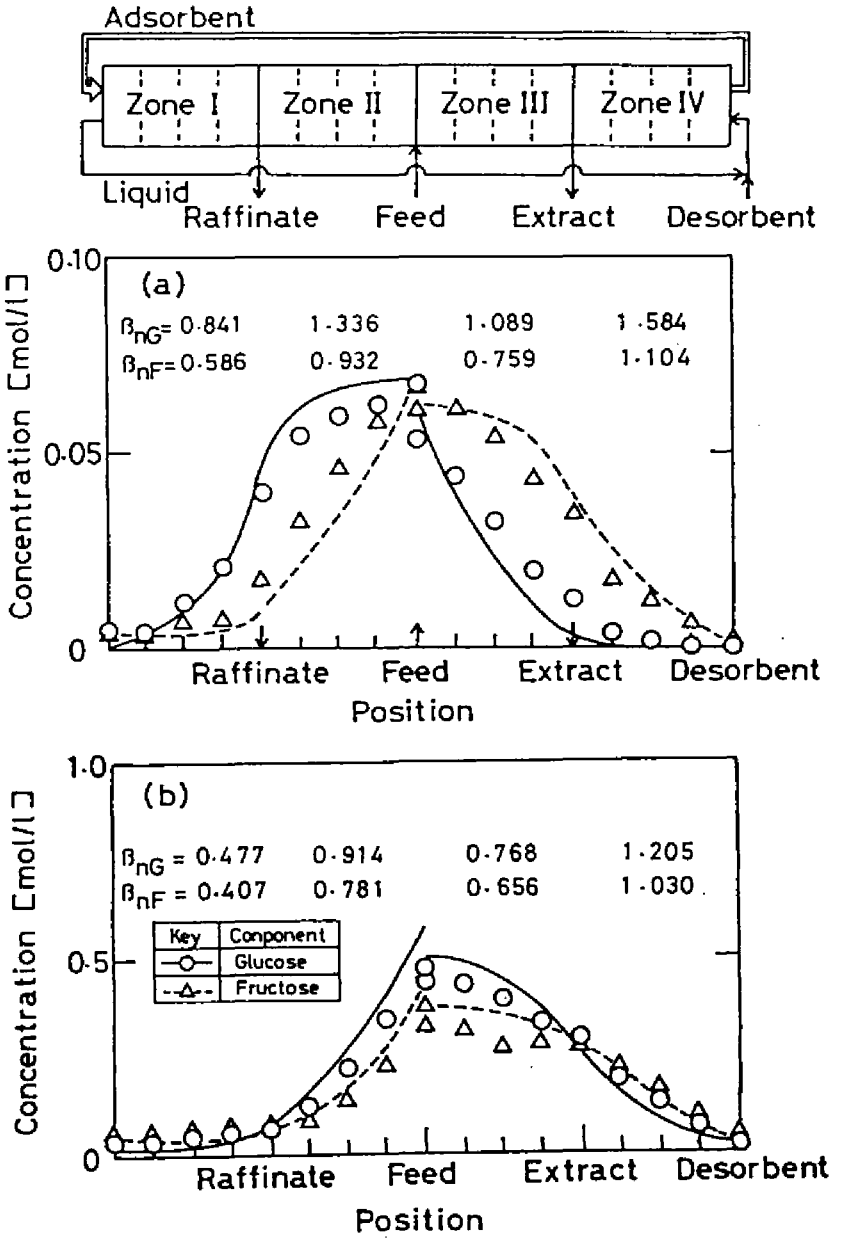

Fig. 11-7. Importance of β_{nk} values to obtain high separability. The curves in the figure were calculated from the continuous moving-bed model. The β_{nk} values are listed in the figure. (a) The concentration profiles at the steady state were obtained in run S-3, where the β_{nk} values were set up reasonably. (b) The profiles were measured in run S-7, where the set up of β_{nk} was not correct.

These experiments suggest that the β_{nk} is an important parameter for determing the operating conditions.

The importance of β_{nk} values is deduced from the intermitted moving-bed model. The migration rate of component k in zone n, $\bar{v}_{nk}$, is approximately given by the following equation.[5,6]

$$\bar{v}_{nk} = v_n/[\varepsilon_b + (1-\varepsilon_b)m_k] \qquad (II-23)$$

Now we consider the conditions that zone II plays the correct function. When zone II consists of N_{II} columns, the length of zone II is $N_{II}L_A$ and the interval renovating the zone is $N_{II}T$. The migrating distances of glucose and fructose through zone II in the renovation interval are represented by the right-hand sides of Eqs.(11-24) and (11-25). In order that zone II may act correctly, the following inequalities must be satisfied.

$$N_{II}L_A < N_{II}T \cdot v_{II}/[\varepsilon_b + (1-\varepsilon_b)m_G] \qquad (11-24)$$

$$N_{II}L_A > N_{II}T \cdot v_{II}/[\varepsilon_b + (1-\varepsilon_b)m_F] \qquad (11-25)$$

By using the relations of Eq.(11-12) and $u_s = L_A/T$, Eqs.(11-24) and (11-25) are rearranged to give

$$1 < u_{II}/[u_s(1-\varepsilon_b)m_G] \qquad (11-26)$$

$$1 > u_{II}/[u_s(1-\varepsilon_b)m_F] \qquad (11-27)$$

The right-hand sides of Eqs.(11-26) and (11-27) are equal to β_{nk}.

Similar considerations are taken for another zones and deduce the relationships in Table 11-2.

From the viewpoint of the rate of liquid flow, we can rearrange the relationships in Table 11-2 to yield the following inequality.

$$v_I < (L_A/T)[\varepsilon_b + (1-\varepsilon_b)m_G] < v_{III} < v_{II} < (L_A/T)[\varepsilon_b + (1-\varepsilon_b)m_F] < v_{IV} \qquad (11\text{-}28)$$

The rate of liquid flow in zone II, v_{II}, is different from that in zone III, v_{III}, due to the supply of feed stream. Both v_{II} and v_{III}, however, must be between $(L_A/T)[\varepsilon_b + (1-\varepsilon_b)m_G]$ and $(L_A/T)\cdot[\varepsilon_b + (1-\varepsilon_b)m_F]$, and hence the rate of feed stream, v_f, must be in a range of Eq.(11-29).

$$0 < v_f < (L_A/T)(1 - \varepsilon_b)(m_F - m_G) \qquad (11\text{-}29)$$

Similarly, the rate of desorbent stream, v_d, must satisfy the relation of Eq.(11-30).

$$v_d > (L_A/T)(1 - \varepsilon_b)(m_F - m_G) \qquad (11\text{-}30)$$

The inequalities (11-28) and (11-29) indicate that a large difference between m_G and m_F permits to treat a large amount of feed solution per unit operation time and gives a wide range of conditions where the adsorber can be operated reasonably.

11. 5. Summary

The continuous separation of glucose and fructose was experimentally performed by using the simulated moving-bed adsorber packed with Ca^{2+} ion form of Y zeolite. Two models, namely, an intermitted moving-bed model and a continuous moving-bed model, were presented for calculating the concentration profiles in the adsorber. The intermitted moving-bed model was useful to calculate the concentration profiles at the unsteady state, while the continuous moving-bed model was conveniently used to estimate the profiles at the steady state and to examine the operating conditions. It was also shown that the β_{nk} values defined in the continuous moving-bed model played a significant role in the determination of the operating conditions.

Nomenclature

a_v	specific surface area	[cm^2/cm^3-bed]
C	concentration at the mobile phase	[mol/l]
C*	concentration within the particle	[mol/l]
$\bar{C}^*$	= C - C*	[mol/l]
K_f	overall mass transfer coefficient	[cm/s]
L_A	length of each column	[cm]
m	distribution coefficient	[-]
N	number of adsorption columns	[-]
Q	volumetric flow rate	[cm^3/s]

T	interval of transportation of adsorption columns	[s]
t	time	[s]
u	linear superficial velocity of liquid flow in the hypothetical moving-bed adsorber	[cm/s]
u_s	linear velocity of adsorbent flow	[cm/s]
v	linear superficial velocity of liquid flow in the fixed-bed adsorber	[cm/s]
$\bar{v}$	approximate migration rate of adsorbate in the fixed-bed adsorber	[cm/s]
x	$= z/L_A$	[-]
z	axial distance	[cm]

α_n	$= K_f a_v L_A / u_n$	[-]
$\bar{\alpha}_n$	$= v_n T / (\varepsilon_b L_A)$	[-]
β_{nk}	$= u_n / [u_s (1 - \varepsilon_b) m_k]$	[-]
$\bar{\beta}$	$= K_f a_v T / \varepsilon_b$	[-]
$\bar{\gamma}_k$	$= K_f a_v T / [(1 - \varepsilon_b) m_k]$	[-]
ε_b	void fraction of the bed	[-]
θ	$= t/T$	[-]

Subscripts

d	desorbent
f	feed
k	component

1	outlet
n	zone number (= I to IV)
0	inlet

Literature Cited

1) D. B. Broughton, H. J. Bieser, M. C. Anderson, and R. A. Persak, the February number of *Kagakukeizai*, 1976, p.54.

2) U. S. patent, 2985589.

3) D. B. Broughton, *Chem. Eng. Progr.*, 64, 60 (1968).

4) D. B. Broughton, R. W. Neuzil, J. M. Pharis, and C. S. Brearly, *Chem. Eng. Progr.*, 66, 70 (1970).

5) K. Nakanishi, S. Yamamoto, R. Matsuno, and T. Kamikubo, *Agric. Biol. Chem.*, 17, 1515 (1975).

6) M. Suzuki, *J. Chem. Eng. Jpn*, 7, 262 (1974).

Chapter 12

Production of Higher Fructose Syrup by Using a System Including Adsorption Process and Immobilized-enzyme Reaction

12. 1. Introduction

A common type of high fructose syrup contains usually 42% fructose on the basis of dry materials. In terms of sweetness and solubility into water, the production of the syrup containing fructose more than 42% is desirable. Although several methods[1-3] have been presented to raise the fructose content in the syrup, at the present time the adsorption process is widely employed. The adsorption process, however, consumes a large amount of desorbent (water), which must be evaporated in a succeeding process. With an increase of energy cost, it is desired that a more efficient process is developed.

In this chapter, we develop a new process to produce higher fructose syrup. The process is constituted by a system in which packed-bed adsorbers and immobilized-glucose isomerase reactors are combined. Two models are presented to calculate the concentration profiles of glucose and fructose in the system.

12. 2. Theoretical Considerations

Basic idea behind the new process. Although in the system

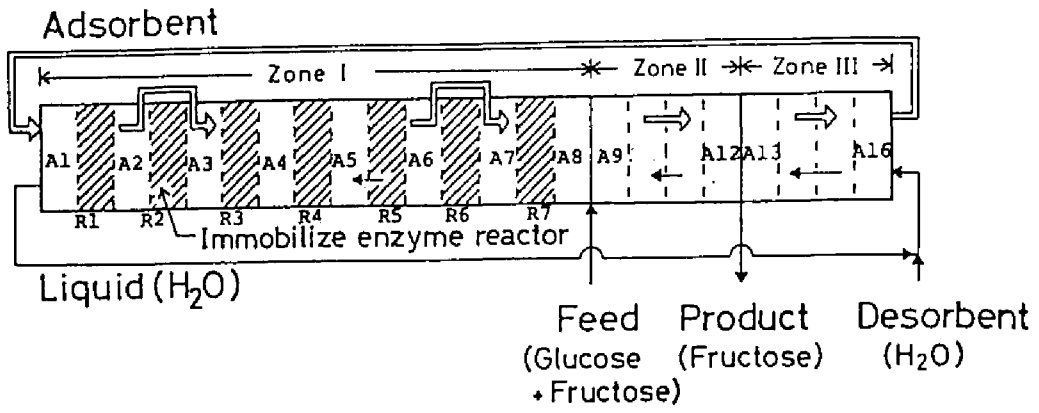

Fig. 12-1. Schematic representation of a system which combines adsorption columns and immobilized-glucose isomerase reactors for producing higher fructose syrup. The white sections (A1 to A16) bounded by two broken lines are adsorption columns. The shaded sections (R1 to R7) represent the immobilized-enzyme reactors.

the adsorbent particles does not actually move continuously, the basic character of the system is more clearly explained first by describing a hypothetical moving-bed adsorber including reactors. Figure 12-1 shows such a system consisting of adsorption columns (white sections bounded by broken lines) and immobilized-glucose isomerase reactors (shaded sections). The system is divided into three zones, I to III, by the introduction and withdrawal points of liquid streams. An adsorbent which adsorbs fructose selectively is packed in the adsorption columns. The reactors and adsorption columns are alternately arranged in zone I. Zones II and III consist of only the adsorption columns. The liquid flows through both the adsorption columns and the reactors. The adsorbent par-

ticles move toward the right direction skipping the reactors in zone I.

An equilibrated mixture of glucose and fructose fed to the system flows to the last adsorption columns (A8) in zone I. Fructose in the mixture is adsorbed on the adsorbent there, and a certain quantity of glucose is also adsorbed. Consequently, the glucose content of the solution leaving from the adsorption column (A8) becomes higher than the fructose content. The solution is introduced to the next reactor (R7), and the equilibrium between glucose and fructose is almost attained in the reactor. By passing through the adsorption columns and reactors alternately in zone I, glucose in the mixture is almost completely converted to fructose, all of which is adsorbed on the adsorbent particles. Therefore, the solution leaving from zone I contains neither glucose nor fructose, and can be utilized as a desorbent. Since all of the water in the feed solution can be used as the desorbent, the quantity of desorbent introduced to the system may be saved. This also means that the cost of evaporation of water in the product may be saved.

Fructose adsorbed on the adsorbent particles in zone I is conveyed to zone II and III by the movement of the adsorbent particles. The functions of zones II and III are the same as those of zones III and IV in the simulated moving-bed adsorber mentioned in Chapter 11. Zone II acts to desorb glucose adsorbed partially

in zone I and to reduce glucose in a product stream. Fructose adsorbed in zone I is desorbed in zone III and recovered from the product stream. Therefore, the solution leaving from the outlet of the product stream has a higher fructose content. The adsorbent particles are regenerated in zone III and conveyed to zone I.

Calculation of concentration profiles in a system including adsorption process and immobilized-enzyme reaction. Models similar to those proposed for the simulated moving-bed adsorber in Chapter 11 are presented to calculate the concentration profiles in the system. A model is an intermitted moving-bed model which expresses faithfully the real movement of adsorbent particles. Another model is a continuous moving-bed model where the continuous movement of adsorbent particles is hypothetically assumed. The assumptions made in Chapter 11 are also made in this chapter.

(a) *An intermitted moving-bed model.* The mass balance equations for the concentrations of component k at the liquid phase C_k and at the stationary phase C_k^* in the adsorption column are the same as Eqs. (11-1) and (11-2) in Chapter 11. The partial differential equations are discritized in the same way as mentioned in Chapter 11 to yield the following equations.

$$C_k(x_i,\theta_{j+1}) = (1-\bar{\alpha}_n\cdot\Delta\theta/\Delta x-\bar{\beta}\cdot\Delta\theta)\cdot C_k(x_i,\theta_j) + \bar{\beta}\cdot\Delta\theta\cdot C_k^*(x_i,\theta_j) + (\bar{\alpha}_n\cdot\Delta\theta/\Delta x)\cdot C_k(x_{i-1},\theta_j) \qquad (12\text{-}1)$$

$$C_k^*(x_i,\theta_{j+1}) = \bar{\gamma}_k \cdot \Delta\theta \cdot C_k(x_i,\theta_j) + (1-\bar{\gamma}_k \cdot \Delta\theta) \cdot C_k^*(x_i,\theta_j) \qquad (12\text{-}2)$$

The nondimensional parameters, $\bar{\alpha}_n$, $\bar{\beta}$, and $\bar{\gamma}_k$, are defined in Eq. (11-6) in the previous chapter.

The mass balance equations for glucose and fructose concentrations, C_G and C_F, in the immobilized-glucose isomerase reactor are expressed by Eqs.(12-3) and (12-4), respectively.

$$\varepsilon_{bR}\frac{\partial C_G}{\partial t} = -v_R\frac{\partial C_G}{\partial z} - (1-\varepsilon_{bR})\frac{Vm(C_G - C_F)}{Km + C_G + C_F} \qquad (12\text{-}3)$$

$$\varepsilon_{bR}\frac{\partial C_F}{\partial t} = -v_R\frac{\partial C_F}{\partial z} + (1-\varepsilon_{bR})\frac{Vm(C_G - C_F)}{Km + C_G + C_F} \qquad (12\text{-}4)$$

where ε_{bR} and v_R represent the void fraction of the immobilized-enzyme bed and the linear superficial velocity of liquid flow. By discritizing Eqs.(12-3) and (12-4) forward for time and backward for distance, the following equations are obtained.

$$C_G(x_i,\theta_{j+1}) = C_G(x_i,\theta_j) - (\alpha_R \cdot \Delta\theta/\Delta x)[C_G(x_i,\theta_j) - C_G(x_{i-1},\theta_j)] - \beta_R \cdot \Delta\theta \cdot \frac{Vm \cdot [C_G(x_i,\theta_j) - C_F(x_i,\theta_j)]}{Km + C_G(x_i,\theta_j) + C_F(x_i,\theta_j)} \qquad (12\text{-}5)$$

$$C_F(x_i,\theta_{j+1}) = C_F(x_i,\theta_j) - (\alpha_R \cdot \Delta\theta/\Delta x)[C_F(x_i,\theta_j) - C_F(x_{i-1},\theta_j)] + \beta_R \cdot \Delta\theta \cdot \frac{Vm \cdot [C_G(x_i,\theta_j) - C_F(x_i,\theta_j)]}{Km + C_G(x_i,\theta_j) + C_F(x_i,\theta_j)} \qquad (12\text{-}6)$$

where

$$\theta = t/T \tag{12-7a}$$

$$x = z/L_R \tag{12-7b}$$

$$\alpha_R = v_R T/(\epsilon_{bR} L_R) \tag{12-8a}$$

$$\beta_R = (1-\epsilon_{bR})T/\epsilon_{bR} \tag{12-8b}$$

and L_R is the length of an immobilized-enzyme column. The boundary conditions between zones are given as follows:

at the inlet of feed stream (between zones I and II)

$$v_f \cdot C_{kf} + v_{II} \cdot C_{kII1} = v_I \cdot C_{kI0} \tag{12-9a}$$

at the outlet of product stream (between zones II and III)

$$C_{kIII1} = C_{kII0} \tag{12-9b}$$

at the inlet of desorbent stream (between zones III and I)

$$v_I \cdot C_{kI1} = v_{III} \cdot C_{kIII0} \tag{12-9c}$$

where the subscripts 0 and 1 denote the inlet and outlet of each zone, respectively.

As shown in Fig.12-2, $C_k(x_i, \theta_{j+1})$ and $C_k^*(x_i, \theta_{j+1})$ for glucose and fructose can be calculated explicitly from Eqs.(12-1), (12-2), (12-5), and (12-6). The calculations of C_k and C_k^* are carried out until θ reaches to 1.0. When $\theta = 1.0$, C_k and C_k^* in the adsorption columns are transposed in the direction of the broken arrows, while C_k in the reactors are stayed in the same position as shown by the solid arrows. Then, the θ value is reset to be zero. These

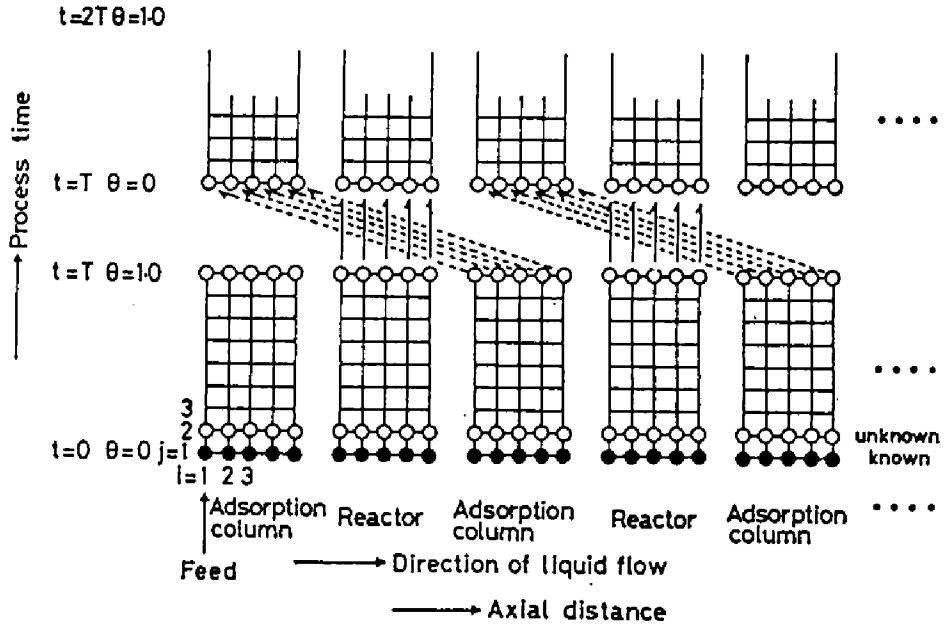

Fig. 12-2. Schematic representation of the procedure for calculating the concentration profiles in the system by using the intermitted moving-bed model. The solid and broken arrows indicate the directions of displacement of C_k and C_k^* when $\theta = 1.0$.

arrangements are repeated whenever θ reaches to 1.0. This model expresses faithfully the operating procedure of the system and can give the concentration profiles at the unsteady state. To obtain the concentration profiles at the steady state, however, the unsteady state process must be calculated in this model. Another model is presented to calculate conveniently the concentration profiles at the steady state.

(b) *A continuous moving-bed model.* A hypothetical and continuous movement of adsorbent particles is assumed in a continuous

moving-bed model. Considering the direction of adsorbent movement to be positive, the mass balance equations for C_k and C_k^* at the steady state are given by Eqs.(11-10) and (11-11) in Chapter 11 and solved analytically to yield Eqs.(12-10) and (12-11).

$$C_k = \frac{\exp[\alpha_n(1-\beta_{nk})x] - \beta_{nk}}{1 - \beta_{nk}} C_{k0} + \frac{1 - \exp[\alpha_n(1-\beta_{nk})x]}{1 - \beta_{nk}} C_{k0}^* \tag{12-10}$$

$$C_k^* = \frac{\beta_{nk}[\exp\{\alpha_n(1-\beta_{nk})x\} - 1]}{1 - \beta_{nk}} C_{k0} + \frac{1 - \beta_{nk}\exp[\alpha_n(1-\beta_{nk})x]}{1 - \beta_{nk}} C_{k0}^* \tag{12-11}$$

The dimensionless parameters, α_n and β_{nk}, are defined as follows:

$$\alpha_n = K_f a_v L_A / u_n \tag{12-12a}$$

$$\beta_{nk} = u_n / [u_s(1 - \varepsilon_b)m_k] \tag{12-12b}$$

When $x = 1$, Eqs.(12-10) and (12-11) express the relationships between the concentrations of component k at the inlet of adsorption column and those at the inlet.

The concentrations of glucose and fructose at the outlet of the reactor, C_G and C_F, are related to those at the inlet, C_{G0} and C_{F0}, by using the conversion of glucose to fructose x_G.

$$C_G = C_{G0} - x_G[C_{G0} - (C_{G0} + C_{F0})/(K + 1)] \tag{12-13}$$

$$C_F = C_{F0} + x_G[C_{F0} - K\cdot(C_{G0} + C_{F0})/(K + 1)] \tag{12-14}$$

where K is the equilibrium constant of the isomerizing reaction and is equal to 1.0 at 50°C. The conversion x_G is defined by Eq. (12-15) and expressed by Eq.(12-16).

$$x_G = [(C_{G0}-C_{Ge}) - (C_G-C_{Ge})]/(C_{G0}-C_{Ge}) \tag{12-15}$$

$$= 1 - \exp[-\frac{2(1-\varepsilon_{bR})Vm}{Km + C_{G0} + C_{F0}} \cdot \frac{L_R}{u_R}] \tag{12-16}$$

The euilibrium concentration of glucose is denoted by C_{Ge}. When the reaction can be approximated to be first-order, that is, $(C_{G0} + C_{F0})$ is much smaller than Km, the conversion x_G is fixed independently on the concentrations of glucose and fructose at the inlet of the reactor.

To avoid the overflow in calculation by a computer, we introduced a variable $\bar{C}_k^*$, which is used for calculating the concentration profiles in the moving-bed adsorber in Chapter 11.

$$\bar{C}_k^* = C_k - C_k^* \tag{12-17}$$

Taking the boundary conditions similar to Eqs.(12-9) into consideration, the simultaneous equations including C_k and $\bar{C}_k^*$ at the inlets and outlets of adsorption columns and reactors as unknown variables are set up. The variable vector X_i at any point in Fig.12-3 is defined by

$$X_i = [C_{Gi}\ \bar{C}_{Gi}^*\ C_{Fi}\ \bar{C}_{Fi}^*]^T \tag{12-18}$$

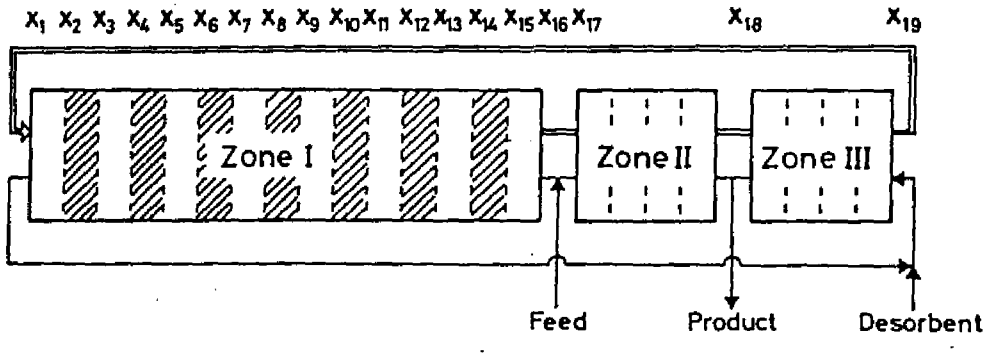

Fig. 12-3. Definition of variable vector X_i.

The variable vectors are related by the following simultaneous equations.

$$\begin{bmatrix} -E & & & & & & & D \\ A_I & -E & & & & & & \\ & R & -E & & & & & \\ & & \cdot & \cdot & & & & \\ & & & \cdot & \cdot & & & \\ & & & & A_I & -E & & \\ & & & & & F & -E & \\ & & & & & & A_{II} & -E \\ & & & & & & & A_{III} \quad -E \end{bmatrix} \cdot \begin{bmatrix} x_1 \\ x_2 \\ x_3 \\ \cdot \\ \cdot \\ x_{16} \\ x_{17} \\ x_{18} \\ x_{19} \end{bmatrix} = \begin{bmatrix} 0 \\ 0 \\ 0 \\ \cdot \\ \cdot \\ 0 \\ f \\ 0 \\ 0 \end{bmatrix} \qquad (12\text{-}19)$$

where

$$A = \begin{bmatrix} 1 & \dfrac{1-\exp[\alpha_n(1-\beta_{nG})N_n]}{1-\beta_{nG}} & 0 & 0 \\ 0 & \exp[\alpha_n(1-\beta_{nG})N_n] & 0 & 0 \\ 0 & 0 & 1 & \dfrac{1-\exp[\alpha_n(1-\beta_{nF})N_n]}{1-\beta_{nF}} \\ 0 & 0 & 0 & \exp[\alpha_n(1-\beta_{nF})N_n] \end{bmatrix} \qquad (12\text{-}20a)$$

$$R = \frac{1}{2(x_G-1)}\begin{bmatrix} x_G-2 & 0 & -x_G & 0 \\ x_G & 2(x_G-1) & -x_G & 0 \\ x_G & 0 & x_G-2 & 0 \\ -x_G & 0 & x_G & 2(x_G-1) \end{bmatrix} \qquad (12\text{-}20b)$$

$$D = \begin{bmatrix} u_{III}/u_I & 0 & 0 & 0 \\ 1-u_{III}/u_I & 1 & 0 & 0 \\ 0 & 0 & u_{III}/u_I & 0 \\ 0 & 0 & 1-u_{III}/u_I & 1 \end{bmatrix} \qquad (12\text{-}20c)$$

$$F = \begin{bmatrix} u_I/u_{II} & 0 & 0 & 0 \\ 1-u_I/u_{II} & 1 & 0 & 0 \\ 0 & 0 & u_I/u_{II} & 0 \\ 0 & 0 & 1-u_I/u_{II} & 1 \end{bmatrix} \qquad (12\text{-}20d)$$

$$E = \begin{bmatrix} 1 & 0 & 0 & 0 \\ 0 & 1 & 0 & 0 \\ 0 & 0 & 1 & 0 \\ 0 & 0 & 0 & 1 \end{bmatrix} \qquad (12\text{-}20e)$$

$$f = \begin{bmatrix} C_{Gf}\cdot u_f/u_{II} \\ -C_{Gf}\cdot u_f/u_{II} \\ C_{Ff}\cdot u_f/u_{II} \\ -C_{Ff}\cdot u_f/u_{II} \end{bmatrix} \qquad (12\text{-}20f)$$

and

$$0 = \begin{bmatrix} 0 \\ 0 \\ 0 \\ 0 \end{bmatrix} \qquad (12\text{-}20g)$$

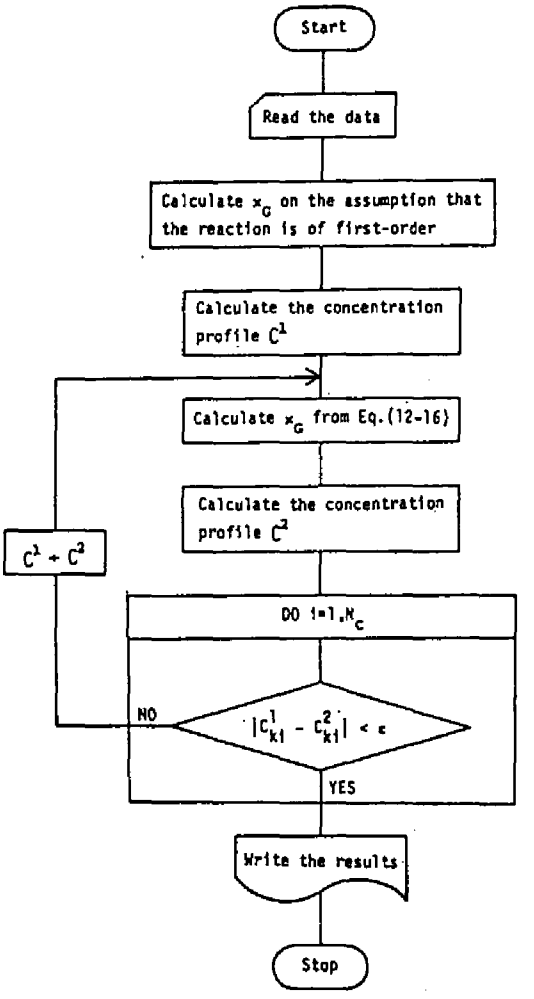

Fig. 12-4. Flow chart for calculating the concentrations of glucose and fructose in the system proposed by using the continuous moving-bed model.

In Eq.(12-20a), 1.0 is substituted into N_n only when n = I. The concentration profiles in the system are obtained by solving Eq. (12-19). Figure 12-4 shows the flow chart of calculation by a computer. First, assuming that the glucose isomerase-catalyzed reaction is first-order, the concentration vector C^1 is calculat-

ed.

$$C^1 = \begin{bmatrix} x_1 \\ x_2 \\ \cdot \\ \cdot \\ x19 \end{bmatrix} \qquad (12\text{-}21)$$

The x_G for each reactor is calculated by substituting the approximate C_{GO} and C_{FO} values into Eq.(12-16). The new concentration vector C^2 is obtained by using the x_G values. It is examined whether the difference between the new concentration profiles C^2 and the old ones C^1 is within a permissible range of error ε or not. If the difference is over the range, the profiles C^2 are substituted into C^1 and the more reasonable profiles C^2 are obtained. These calculations are repeated until the profiles C^2 coincide with the last ones C^1 within a given permissible error.

12. 3. Materials and Methods

Adsorbent, immobilized glucose isomerase, and chemicals.

The Ca^{2+} ion form of Y zeolite kindly supplied by Toyo Soda Mfg. Co. Ltd. was used as an adsorbent. The adsorbent adsorbs fructose selectively. The detailed properties of the adsorbent are described in Chapter 10.

The immobilized glucose isomerase (commercial name: Swetase, Nagase Sangyo) is, strictly speaking, an immobilized micoorganism, that is, *Streptomyces phaeochromogenes* is adsorbed on the quater-

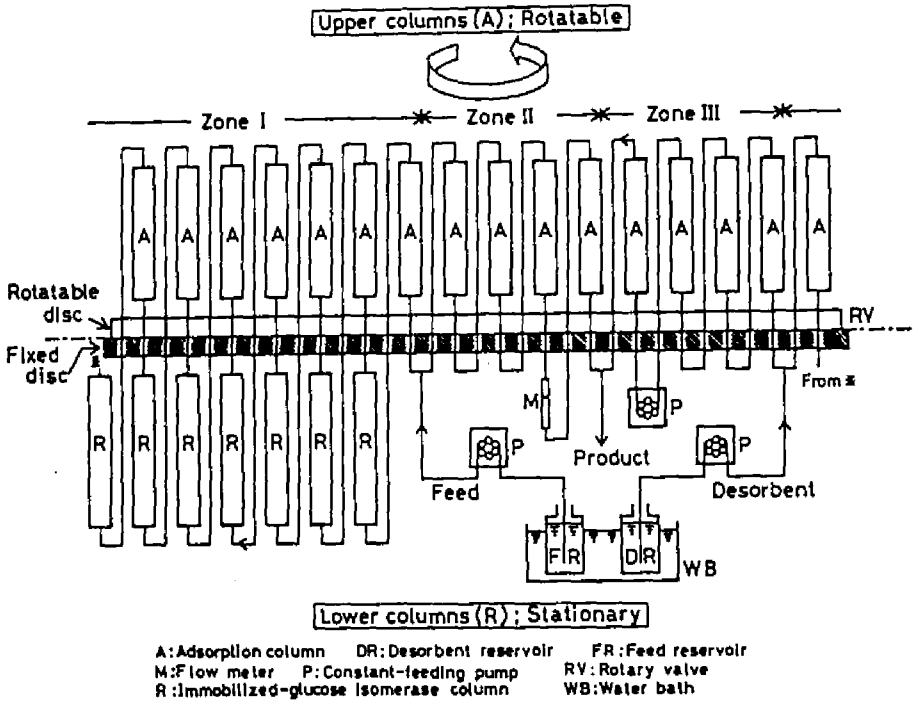

Fig. 12-5. Schematic diagram of experimental apparatus for producing higher fructose syrup by using the proposed system. The rotary valve consists of two stainless steel discs. The adsorption columns are connected to the upper disc. They are periodically moved to the direction counter to liquid flow. The reactors are connected to the lower disc and are stationary.

nary pyridine compound.

Glucose and fructose were purchased from Nakarai Chemicals. All other reagents were of analytical grade.

Experimental apparatus. Figure 12-5 shows the schematic diagram of experimental apparatus used in this study. The rotary valve is the same as that used in Chapter 11. Sixteen adsorption

columns packed with Y zeolite are connected to the upper disc. The size of each column is 1.38 cm in diameter and 10.2 cm in length. Seven reactors packed with the immobilized glucose isomerase are connected to the lower disc. The size of each reactor is 1.38 cmϕ X 18.0 or 10.2 cm. The lower disc is stationary, while the upper disc is rotated in the direction counter to the liquid flow at regular intervals. By the rotation of the upper disc, the simulated movement of only adsorbent particles is accomplished. The adsorption columns and reactors were kept at 50°C by circulating thermostated water in the jackets, although the flow of the water is omitted in Fig. 12-5.

Determination of kinetic parameters of immobilized glucose isomerase. The isomerization of glucose to fructose is a reversible reaction and its rate equation[4] may be expressed by

$$-r_G = r_F = \frac{Vm_1 Km_2 C_G - Vm_2 Km_1 C_F}{Km_1 Km_2 + Km_2 C_G + Km_1 C_F} \qquad (12\text{-}22)$$

where the subscripts 1 and 2 denote the forward and backward reactions, respectively.

The preliminary experiments showed that the Km and Vm values of the immobilized enzyme were identical for the forward and backward reactions at 50°C and were 0.36 mol/l and 1.99×10^{-3} mol/l·s, respectively. It was also suggested that the immobilized enzyme may possess weak activities of other enzymes.

Since it has been reported[5] that glucose isomerase from *Streptomyces sp.* has a relatively high thermal stability, the immobilized enzyme was heated at 70°C for 1 hr to denature impure enzymes. Since this thermal treatment may weaken slightly the activity of the immobilized enzyme, the activity was evaluated every experimental run.

The immobilized glucose isomerase was packed in a column (1.38 cmϕ X 10.2 or 18.0 cm) with water jacket. The reactor was kept at 50°C. A glucose solution of an appropriate concentration was continuously introduced to the bed. After the steady state was established, the conversion x_G was observed. The x_G values were obtained at various rates of feed. The conversion x_G is expressed by Eq.(12-24) under the assumptions of common Km and Vm values for the forward and backward reactions and of the plug flow of liquid.

$$x_G = 2\,C_F\,/C_{G0} \tag{12-23}$$

$$= 1 - \exp\{-(1-\varepsilon_{bR})\cdot[2Vm/(Km+C_{G0})]\cdot(L_R/v_R)\} \tag{12-24}$$

$\mathrm{Ln}(1 - x_G)$ was plotted against $(1 - \varepsilon_{bR})\cdot L_R/v_R$, yielding the slope *S*. The void fraction of the bed ε_{bR} was found to be 0.41. The values of slope *S* were obtained at some concentrations of glucose. The Km and Vm values were estimated from the plot of $2/S$ against C_{G0}. When the reaction could be approximated to be first-order, the first-order rate constant $\bar{k}$ (= Vm/Km) was estimated from the

plot of $\ln(1 - x_G)$ against $(1 - \varepsilon_{bR}) \cdot L_R / v_R$.

Production of higher fructose syrup. The Ca^{2+} ion form of Y zeolite (8 g on dry weight) was packed into each adsorption column. The immobilized glucose isomerase was swollen in distilled water, heated at 70°C for 1 hr, and packed into columns. The feed solution contained glucose and fructose at equivalent concentrations. They were dissolved in 0.02 mol/l Tris-HCl buffer (pH 8.0) containing 0.01 mol/l magnesium sulfate. The buffer was also used as a desorbent.

Before the operation being started, the liquid in the adsorption columns and the reactors was displaced by the solution containing glucose and fructose in the concentration of $C_{kf} \cdot Q_f / (Q_f + Q_d)$. By switching on three pumps, the experiment for producing higher fructose was started. The upper disc was rotated at 2 or 3 min intervals to accomplish the simulated movement of adsorbent particles counter to the liquid flow. The concentrations of glucose and fructose in the product stream were analyzed every 30 min. The operation was proceeded for 13 to 18 hr to establish the steady state. After the establishment of the steady state was confirmed, the operation was stopped. The solutions in the connecting tubes were sampled and the concentrations of glucose and fructose were measured. These measurements give the concentration profiles of both the components in the system.

Table 12-1. Experimental Conditions for Producing Higher Fructose Syrup by Using the System Combined Adsorption Process and Immobilized-Enzyme Reaction.

Run No.		R-1	R-2	R-3	R-4	R-5	R-6	R-7
C_{Gf}	[mol/l]	0.1	0.1	0.1	0.1	0.5	1.0	1.0
C_{Ff}	[mol/l]	0.1	0.1	0.1	0.1	0.5	1.0	1.0
Q_f	[cm^3/min]	0.4	0.4	0.4	0.357	0.187	0.143	0.187
Q_d	[cm^3/min]	2.0	2.0	2.0	1.950	0.744	0.439	0.378
Q_p	[cm^3/min]	2.4	2.4	2.4	2.307	0.931	0.582	0.565
T	[min]	2	2	2	2	3	3	3
x_G	[-]	0.70	0.67	0.63	0.51	-	-	-
Km	[mol/l]	-	-	-	-	0.48	0.14	0.37
Vm	[mol/l·min]	-	-	-	-	0.066	0.127	0.053
v_I	[cm/min]	3.654	3.144	3.780	3.978	2.658	2.640	2.670
v_{II}	[cm/min]	3.384	2.800	3.516	3.738	2.478	2.544	2.544
v_{III}	[cm/min]	4.986	4.482	5.112	5.280	3.096	2.934	2.922

The concentrations of glucose and fructose were determined by using high-performance liquid chromatography (Shimadzu, LC-3A).

12. 4. Results and Discussion

Production of higher fructose syrup. The experiments for producing higher fructose syrup were performed under various conditions. The operating conditions for the respective experimental runs are listed in Table 12-1. The kinetic parameters of the thermally treated immobilized-glucose isomerase are also listed in the table. The parameters were estimated from the procedure mentioned

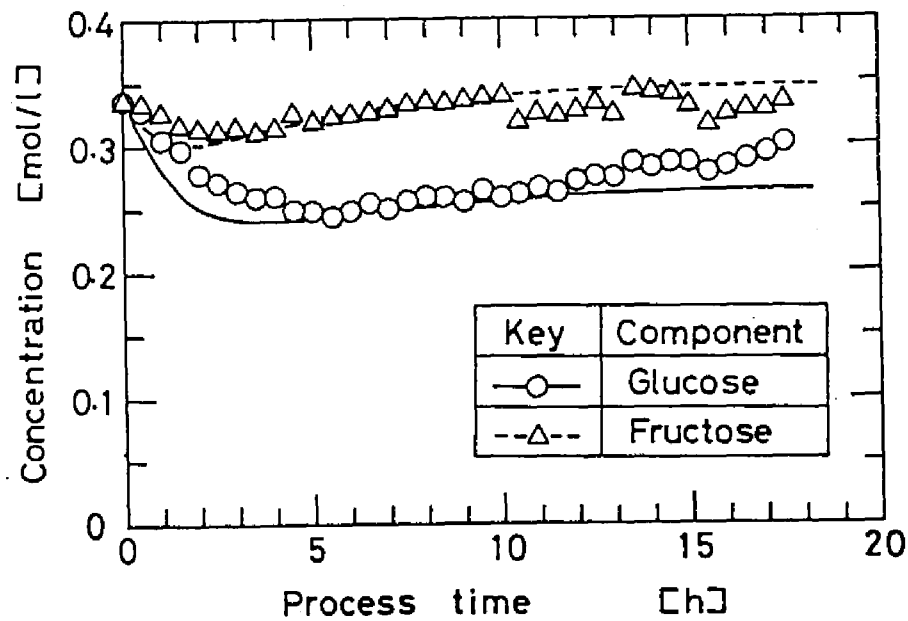

Fig. 12-6. Time courses of glucose and fructose concentrations in product stream in run R-7. The solid and broken curves were calculated for glucose and fructose, respectively, by using the intermitted moving-bed model.

above.

Figure 12-6 shows the time courses of glucose and fructose concentrations in the product stream, which were obtained for run R-7. The fructose content in the product stream became 52.6% after 17.5 hr and the higher fructose syrup could be obtained. The solid and broken curves in the figure were calculated for glucose and fructose by using the intermitted moving-bed model. The theoretical curves coincide with the experimental ones, indicating that the intermitted moving-bed model is useful to predict the unsteady state process in the system.

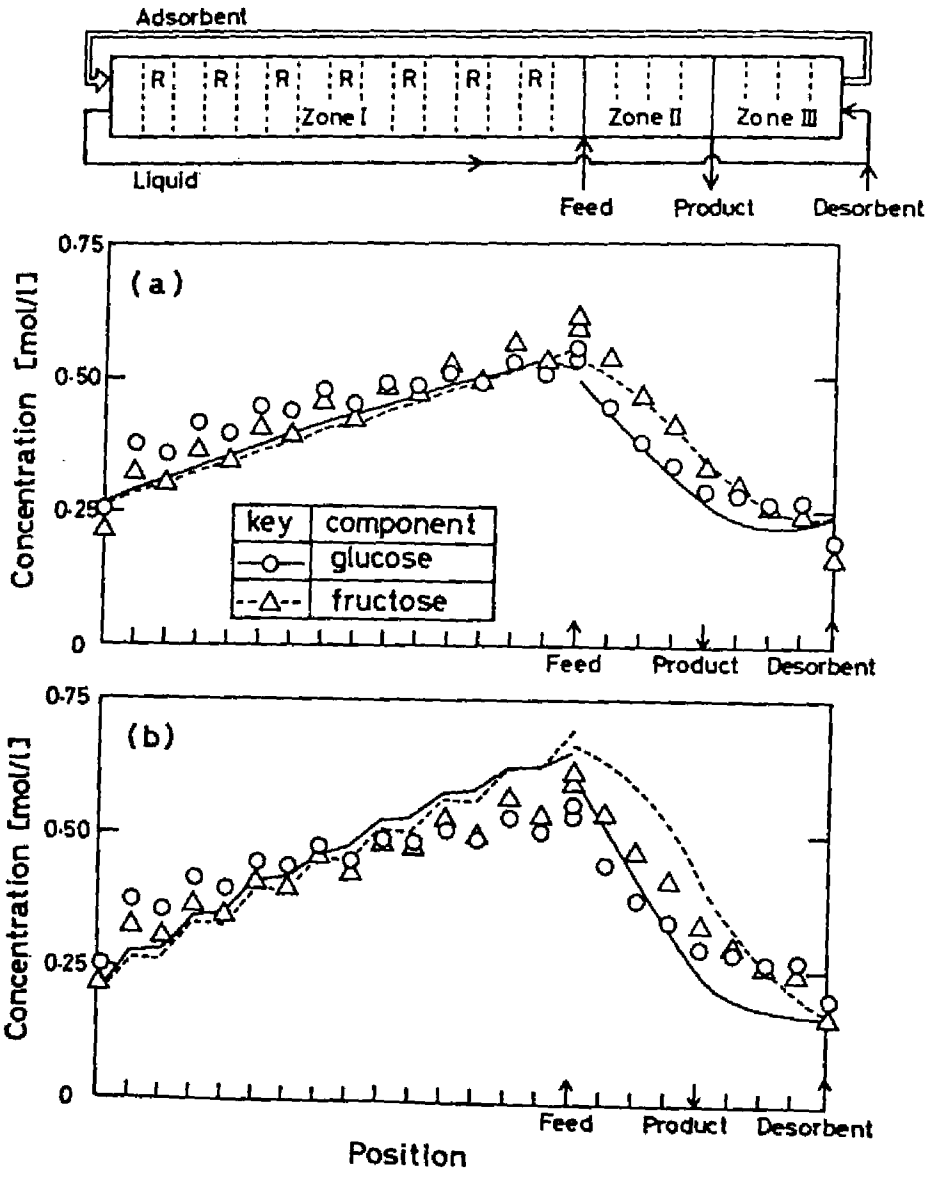

Fig. 12-7. Concentration profiles of glucose and fructose in the system for run R-7. The solid and broken curves are theoretical ones for glucose and fructose. The curves in the upper figure (a) were calculated by using the intermitted moving-bed model, while the curves in the lower figure (b) were obtained from the continuous moving-bed model.

Figure 12-7 shows the concentration profiles in the system for run R-7, which were measured at the end of operation. The solid and broken curves in Fig. 12-7(a) are the theoretical profiles of glucose and fructose concentrations in the system. The profiles were calculated by using the intermitted moving-bed model and coincide well with the experimental ones. The curves in Fig. 12-7 (b) were calculated by using the continuous moving-bed model. They express well the characteristics of concentration profiles.

In other runs, the theoretical profiles coincided with the experimental ones in the same degree as in run R-7. These observations mean that the intermitted moving-bed model is effective to predict precisely the concentration profiles in the system and that the continuous moving-bed model may be convieniently used to calculate roughly the profiles because of the easiness of calculation.

Determination of operating conditions. The nondimensional parameter β_{nk} defined in the continuous moving-bed model denotes the ratio of the amount of component k carried by the liquid flow to that conveyed by the flow of adsorbent particles. As mentioned in Chapter 11, the β_{nk} value has played an important role in the determination of the operating conditions for separating glucose and fructose by using the simulated moving-bed adsorber. In the proposed system, the β_{nk} value is also important for the determina-

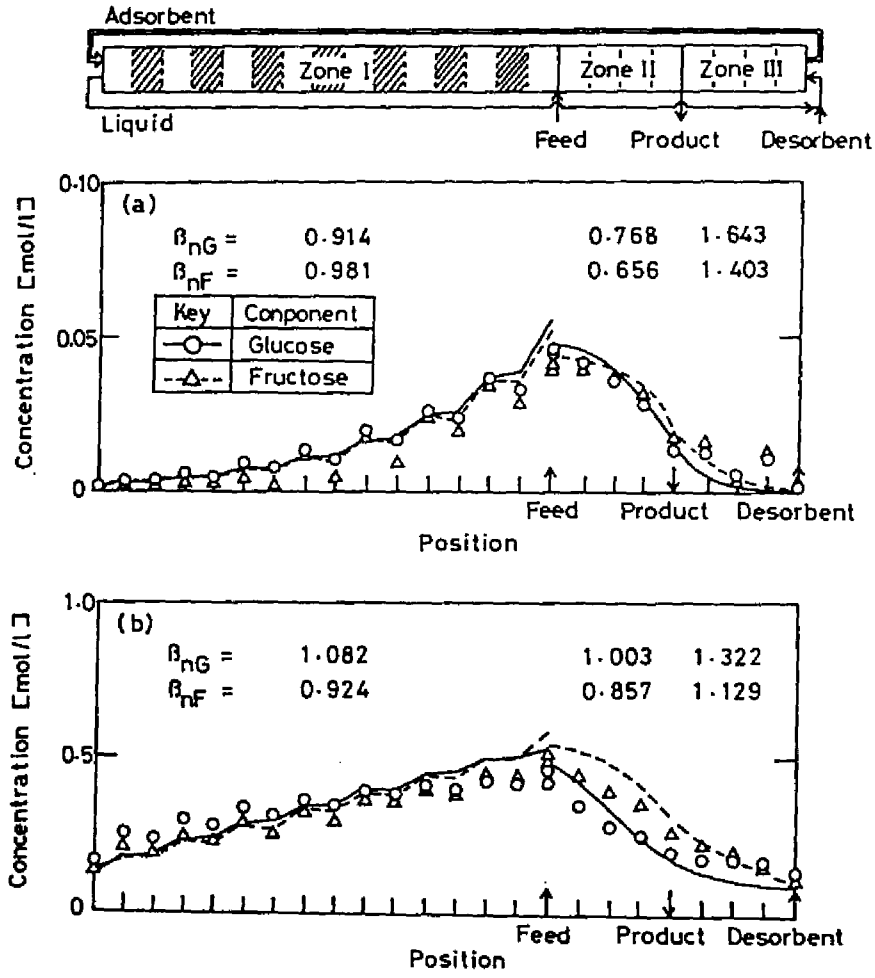

Fig. 12-8. Effect of β_{nk} values on the concentration profiles in the system. The β_{nk} values are listed in the figure. The profiles in the upper figure (a) and in the lower figure (b) were obtained in runs R-1 and R-6, respectively. The β_{nk} values were unreasonably set in run R-1. In run R-6, the β_{nk} values were in a proper manner and then higher fructose syrup could be produced.

tion of the operating conditions for producing the higher fructose syrup.

Fructose must be adsorbed in zone I, so that the β_{IF} value should be less that 1.0. The β_{IG} value should be more than 1.0 in order that zone I may fulfill its proper functions. Since zone II must function to recover only glucose adsorbed partially in zone I, the β_{IIG} and β_{IIF} values should be more and less than 1.0, respectively. Fructose adsorbed in zone I is desorbed in zone III and withdrawn by the product stream. Therefore, the β_{IIIF} should be set to be more than 1.0, and inevitably $\beta_{IIIG} > 1.0$.

Figures 12-8(a) and (b) illustrate the concentration profiles obtained in runs R-1 and R-6, respectively. The β_{nk} values are listed in the figure. The solid and broken curves are the theoretical concentration profiles of glucose and fructose. The curves were calculated by using the continuous moving-bed model. In run R-6 (Fig. 12-8(b)), the β_{nk} values were reasonably set so that the higher fructose syrup could be produced. On the other hand, in run R-1 (Fig. 12-8(a)), we failed to produce the higher fructose syrup because the β_{IG} and β_{IIG} values were set to be less than 1.0. These typical runs of experiments may suggest the β_{nk} values are important parameters to determine the operating conditions for producing the higher fructose syrup and that the β_{nk} values should be set in a manner mentioned above.

12. 5. Summary

An essential idea of the system developed in this chapter is promotion of the yield of the product in a reversible reaction by combining adsorption process and reaction. The idea of the system was realized by developing an apparatus consisting of adsorption columns and reactors. The system was applied to the process for producing higher fructose syrup. Two models to calculate the concentration profiles in the system were presented and their validities were experimentally confirmed.

The performance of the process using the system will be compared with the performances of the chromatographic separation process and the process using the simulated moving-bed adsorber in the next chapter. The process using the proposed system will be verified to be most effective of three processes.

Nomenclature

a_v	specific surface area	[cm^2/cm^3-bed]
C	concentration at the mobile phase	[mol/l]
C*	concentration within the particle	[mol/l]
$\bar{C}^*$	$= C - C^*$	[mol/l]
K	equilibrium constant	[-]
K_f	overall mass transfer coefficient	[cm/s]
Km	Michaelis constant	[mol/l]
$\bar{k}$	first-order reaction rate constant	[s^{-1}]

L_A	length of adsorption column	[cm]
L_R	length of immobilized-enzyme reactor	[cm]
m	distribution coefficient	[-]
N	number of adsorption columns	[-]
Q	volumetric flow rate	[cm^3/s]
r_k	formation rate of component k	[mol/l·s]
T	interval of transportation of adsorption column	[s]
t	time	[s]
u	linear superficial velocity of liquid flow in the hypothetical moving-bed	[cm/s]
u_s	linear velocity of adsorbent flow	[cm/s]
Vm	maximum reaction rate	[mol/l·s]
v	linear superficial velocity of liquid flow in the fixed-bed	[cm/s]
x	$= z/L_A$ or z/L_R	[-]
x_G	conversion	[-]
z	axial distance	[cm]

α_n	$= K_f a_v L_A/u_n$	[-]
α_R	$= v_R T/(\varepsilon_{bR} L_R)$	[-]
$\bar{\alpha}_n$	$= v_n T/(\varepsilon_b L_A)$	[-]
β_{nk}	$= u_n/[u_s(1 - \varepsilon_b)m_k]$	[-]
β_R	$= (1 - \varepsilon_{bR})T/\varepsilon_{bR}$	[s]
$\bar{\beta}$	$= K_f a_v T/\varepsilon_b$	[-]

$\overline{\gamma}_k$ = $K_f a_v T/[(1 - \varepsilon_b)m_k]$ [-]

ε_b void fraction of adsorbent bed [-]

ε_{bR} void fraction of immobilized-enzyme bed [-]

θ = t/T [-]

Subscripts

d desorbent

F fructose

f feed

G glucose

k component

l outlet

n zone number (= I to III)

0 inlet

1 forward reaction

2 backward reaction

Literature Cited

1) T. Fujii and B. Okamura, *Kagaku to Kogyo*, 31, 534 (1978).

2) Japanese patent, 45-26048.

3) Japanese patent, 43-16799.

4) D. Y. Ryu, S. H. Chung, and K. Katoh, *Biotechnol. Bioeng.*, 19, 159 (1977).

5) Y. Takasaki, Y. Kosugi, and A. Kanbayashi, *Agric. Biol. Chem.*, 33, 1527 (1969).

Chapter 13

Comparison of Processes for Production of Higher Fructose Syrup

13. 1. Introduction

Since isomerization of glucose to fructose is a reversible reaction, any separation process is necessary for production of higher fructose syrup, in which the fructose content exceed equilibrium point of the isomerization. Although some processes for separating glucose and fructose have been presented,[1-3] adsorption process may be the most promising of them. In prior chapters three processes for producing higher fructose syrup are presented, namely, a chromatographic separation process, a process using a simulated moving-bed adsorber, and a process using a system including adsorption process and immobilized-enzyme reaction. The last process is newly developed in this study. Although the basic idea behind two processes have been presented, calculation procedures for the processes have not published yet. This study has presented the procedures and given a chance of comparison of them.

As mentioned in Introduction of Part III, it is the most significant problem in the process for producing higher fructose syrup whether the amount of desorbent can be reduced or not. Therefore, we examine the performances of the three processes from the viewpoint of the amount of desorbent required. The comparison

will suggest that the process using the system including adsorption process and reactions is most effective for the production of higher fructose syrup containing 50 to 65% of fructose content.

The process proposed is a compound process using adsorption and enzyme reaction. Optimum operating conditions of adsorptive separation may be different from those of reaction. We will discuss in this chapter on the effects of operating conditions on performances of the process.

13. 2. Materials and Methods

Materials. Immobilized glucose isomerase (from *Streptomyces phaeochromogenes*) was a commercial preparation (Nagase Sangyo, commercial name: Swetase). Ca^{2+} ion form of Ino-echanger S-07 was used as an adsorbent. The ion exchanger was kindly supplied by Organo.

Standard conditions for comparison. Figure 13-1 illustrates three processes for producing higher fructose syrup. Process (a) is a chromatographic separation process. Process (b) indicates a separation process using a simulated moving-bed adsorber. Process (c) represents the process proposed. Glucose, a raw material for higher fructose syrup, is introduced to a main reactor packed with immobilized glucose isomerase and converted to fructose to the level of 90% of equilibrium point. The glucose/fructose mixture leaving from main reactor is fed to an adsorptive separator.

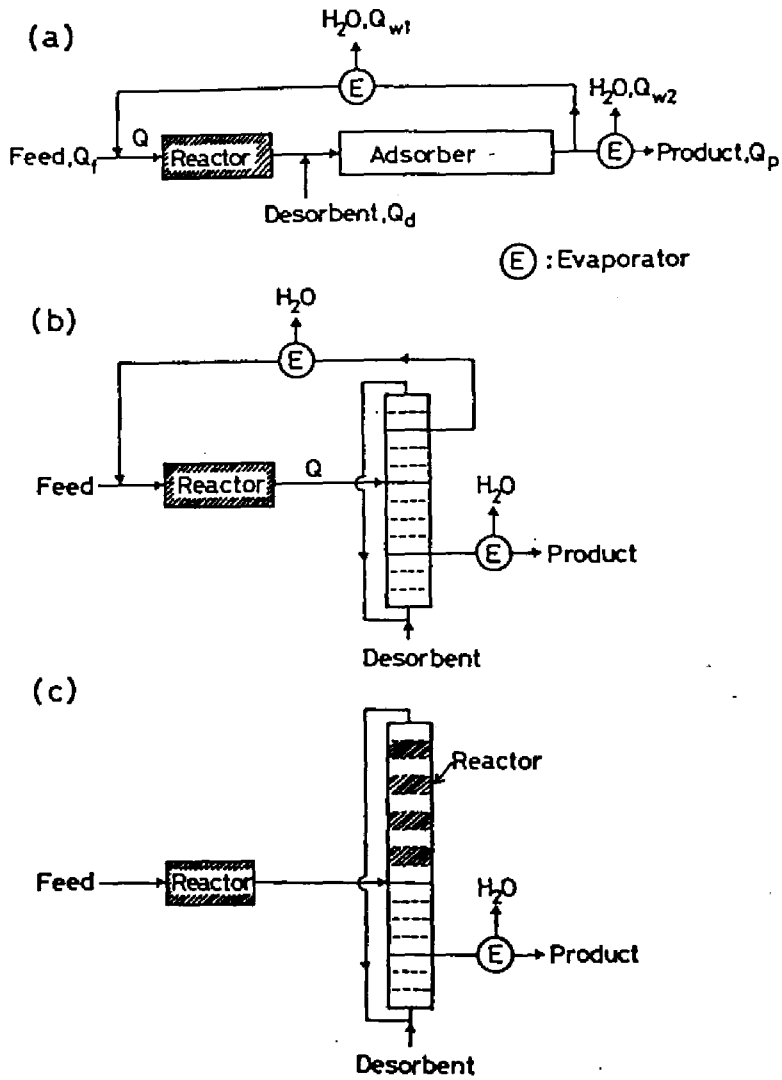

Fig. 13-1. Three processes for production of higher fructose syrup. (a) Chromatographic separation process. (b) Process using a simulated moving-bed adsorber. (c) Process proposed using a system including adsorption process and immobilized-glucose isomerase reaction.

In processes (a) and (b), a raffinate solution consisting mainly of glucose is introduced to an evaporator and then the condenced raffinate solution is recycled to the main reactor. Process (c)

Table 13-1. Standard Conditions for Comparison of Three Processes.

Feeding rate of glucose, Q_f	1.0 m^3/h
Glucose concentration in feed solution, C_{Gf}	2850 mol/m^3(= 45wt%)
Conversion in main reactor, x_G	0.9
Size of adsorber:	1.2 mϕ x 6.0 m
Production rate, Q_p	0.6 m^3/h
Concentration in product, C_{Gp}+ C_{Fp}	4750 mol/m^3(=75wt%)
Distribution coefficient, m_G	0.5
m_F	0.8
Overall volumetric mass transfer coefficient, $K_f a_v$	24.63 h^{-1}
Void fraction of adsorber, ε_b	0.40
Void fraction of reactor, ε_{bR}	0.41
Michaelis constant, Km	191 mol/m^3
Maximum reaction rate, Vm	5076 $mol/m^3 \cdot h$
Ratio of Q_r to Q_e in (a) and (b) process;	1 : 1
Number of divided adsorption column in (b) and (c) processes;	12
Construction of each zone in (b) and (c) processes;	
(b) process ; zone I - IV = 2, 3, 4, 3	
(c) process ; zone I - III = 5, 4, 3	
Number of reactor combined in (c) process:	4

has no recycle flow and produces only higher fructose syrup.

Standard conditions for comparing the three processes are listed in Table 13-1. Glucose solution of the concentration of 2850 mol/m^3 (= 45%(w/w)) is fed to each process at the rate of 1.0 m^3/hr. The size of each adsorber is 1.2 m in diameter and 6.0 m in

length. In processes (b) and (c), the adsorber is divided into twelve small columns. The ratio of withdrawal rate of raffinate stream to that of product stream is fixed to be 1 : 1. The distribution coefficients of glucose and fructose are assumed to be 0.5 and 0.8, respectively. Product solution is condenced until the concentration of the saccharides reaches to 4750 mol/m^3 (= 75 %(w/w)). The sizes of the main reactors used in processes (a) and (b) should be larger than the size of the main reactor used in process (c) because glucose separated is recycled to the reactors in processes (a) and (b). The amount of immobilized isomerase used in the system combining adsorption process and the enzyme reaction is made to be equal to the difference in the amount of the enzyme between the main reactors used in processes (b) and (c).

The comparison of performances of the three processes was made by examining the relation between the amount of desorbent introduced to each process and fructose content in the product solution. The concentration profiles of glucose and fructose in the simulated moving-bed adsorber of process (b) were calculated by using the continuous moving-bed model. The profiles in the system including adsorption and reaction of process (c) were also calculated by using the continuous moving-bed model.

Effect of Mg^{2+} concentration on kinetic parameters of immobilized glucose isomerase. Immobilized-glucose isomerase particles (20 to 24 mesh) were swollen in 0.02 mol/l Tris-HCl buffer (pH 8.0)

containing 0.01 mol/l magnesium sulfate and centrifuged for 2 min to eliminate excess solution on the surface by using a tube equipped with a glass filter. The particles were granulated in order that the reaction rate may be free from diffusion limitations. About 1.4 g of the granulated particles were accurately weighed and put into a flask. Fourteen ml of the buffer solution was added there and kept at 50°C. By adding 7 ml of fructose solution of an appropriate concentration to the flask, the reaction was allowed to start. The fructose concentration at the start of reaction was in the range of 0.1 to 0.8 mol/l. After 40 min, the catalyst particles in the reaction mixture were removed by filtration through a glass filter to stop the reaction. The glucose concentration in the filtrate was analyzed by using a glucostat method.[4)]

These measurements were performed for various concentrations of magnesium sulfate in 0.02 mol/l Tris-HCl buffer, pH 8.0.

Effect of Mg^{2+} concentration on thermal stability of immobilized glucose isomerase. About 1.5 g of immobilized glucose isomerase was accurately weighed and packed into a column equipped with a water jacket. As a substrate solution, 0.02 mol/l fructose or glucose solution was used. They were dissolved with 0.02 mol/l Tris-HCl buffer (pH 8.0) including 0.01 mol/l magnesium sulfate, the buffer containing no magnesium ion, or distilled water. Both the column and substrate reservoir were kept at 70°C. The substrate solution was continued to feed for 30 to 40 hr at the flow

rate of 1.0 cm^3/min. A solution emerging from the reactor was sampled at intervals. The glucose or fructose concentration in the solution was measured. These observations were also performed at 50°C and 60°C.

Under these conditions, the reaction catalyzed by glucose isomerase can be approximated to be a first-order reversible reaction.

$$-r_G = r_F = k_1[C_G - (1/K)\cdot C_F] \tag{13-1}$$

where k_1 is the first-order rate constant of forward reaction and K is the equilibrium constant. In such a case, a conversion x_G through the immobilized-enzyme column is expressed by Eq. (13-2) under the assumption of plug flow of liquid.

$$1 - x_G = \exp[-(1 - \varepsilon_{bR})(L_R/v_R)\{1 + (1/K)\cdot k_1\}] \tag{13-2}$$

When the denaturation of the immobilized enzyme can be expressed by a first-order irreversible process, that is,

$$dk_1/dt = -k_d\cdot k_1 \tag{13-3}$$

Eq. (13-4) is obtained approximately from Eqs. (13-2) and (13-3).

$$-\ln[-\ln(1-x_G)] = k_d\cdot t - \ln[-(1-\varepsilon_{bR})(L_R/v_R)(1+1/K)k_{10}] \tag{13-4}$$

where k_d is the denaturation rate constant and k_{10} is the rate constant of fresh catalyst. Plotting of the left-hand side of Eq.

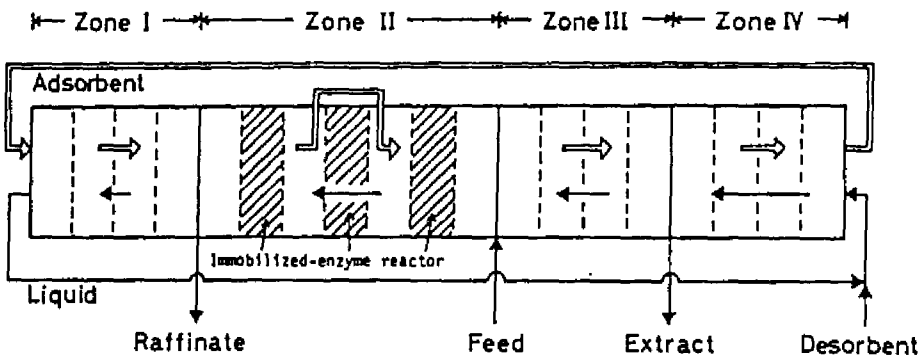

Fig. 13-2. Schematic representation of a modified system including adsorption and immobilized-glucose isomerase reaction.

(13-4) against operation time gives the k_d value. The half-life t_h of the catalyst is defined as the time elapsed until the k_l value becomes to a half of k_{l0}. The t_h value is given by the following equation.

$$t_h = (\ln 2)/k_d \qquad (13\text{-}5)$$

Modified system including adsorption process and immobilized-enzyme reaction. We developed a new system including adsorption process and immobilized-glucose isomerase reaction to produce higher fructose syrup with fructose content more than 70%. Figure 13-2 shows the system schematically. The system consists of four zones. Zone I functions to recover glucose remaining in the solution leaving zone II. The diagram of the experimental apparatus is shown in Fig. 13-3. The apparatus is almost similar to that used in Chapter 12. Different points are that the Ca^{2+} ion form

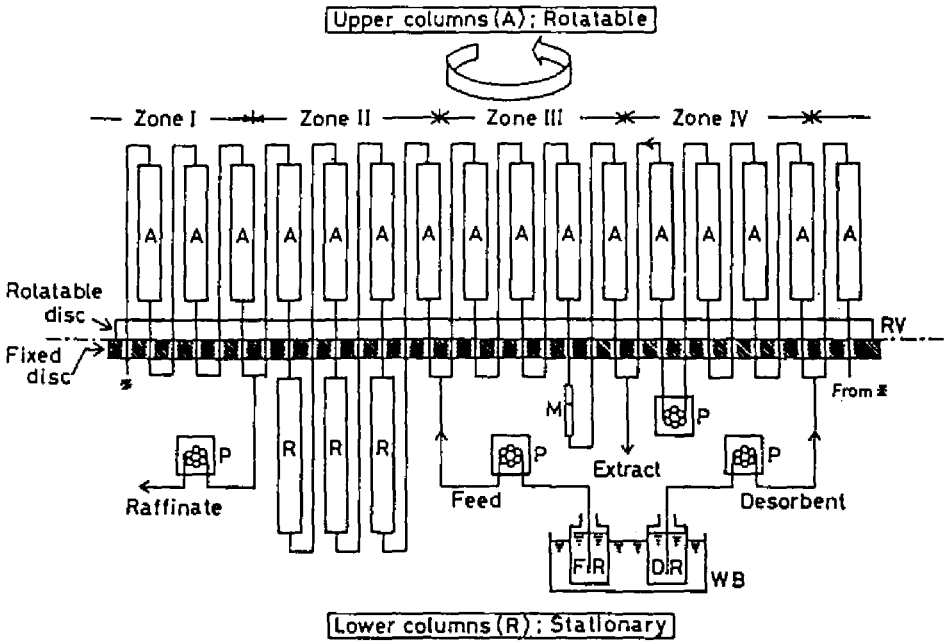

Fig. 13-3. Schematic diagram of experimental apparatus for a modified system. A, adsorption colum; DR, desorbent reservoir; FR, feed reservoir; M, flow meter; P, constant-feeding pump; RV, rotary valve; R, immobilized-glucose isomerase column; WB, water bath.

of Ion-exchanger S-07 was packed in adsorption columns and that distilled water was used as a solvent. A mixture of glucose and fructose was used as feed solution. The concentration of each component was 1.0 mol/l.

13. 3. Results and Discussion

Relation between amount of desorbent required and fructose content in product. Figure 13-4 shows the relationship between fructose content in higher fructose syrup and the quantity of de-

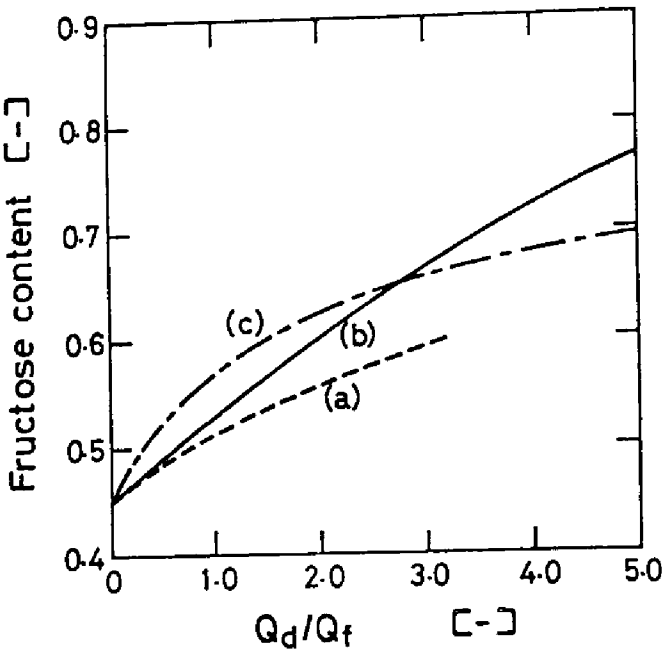

Fig. 13-4. Comparison of three processes for production of higher fructose syrup. Broken, solid, and dot-dash curves (curves (a), (b), and (c)) correspond with processes (a), (b), and (c) in Fig. 13-1. This figure shows that process (c) (the process proposed) requires the smallest amount of desorbent to produce higher fructose syrup with 45 to 65% fructose content.

sorbent required for production of the syrup. The abscissa in the figure represents the introduction rate of desorbent normalized by that of feed. The chromatographic separation process (process (a)) requires a large amount of desorbent to produce higher fructose syrup and has the lowest performance of the three processes. The process using the simulated moving-bed adsorber (process (b)) can achieve the higher fructose content. The amount of desorbent is, however, large in the relatively low fructose content. The fruc-

Table 13-2. Compositions of Fresh and Employed Zeolites.

Zeolite	Composition (wt%)						Exchange ratio (%)	
	CaO	Na_2O	MgO	SiO_2	Al_2O_3	ig. loss	Ca^{2+}	Mg^{2+}
Fresh	5.6	2.3	0.1	49.0	19.9	21.4	71.8	1.8
Employed	4.0	2.3	1.0	48.8	19.9	22.4	53.5	18.6

tose content in the syrup, which is desirable at the present time in food manufactures, is 55 to 75%. To produce the syrup of such a high fructose content, the process proposed (process (c)) requires the smallest amount of desorbent. The reduction of desorbent required in the process for production of higher fructose syrup means that the energy spent in the succeeding evaporation process can be saved. Therefore, the process proposed (c) may be the most efficient of three processes to produce higher fructose syrup with 55 to 65% fructose content.

Some problems included in proposed process. The system developed in Chapter 12 has included two different processes, namely, adsorption process and immobilized-enzyme reaction process. The optimum operating conditions for adsorption process may be different from those of reaction process. The Ca^{2+} ion form of ion exchanger is effective for glucose/fructose separation. On the other hand, it has been reported[5] that glucose isomerase from *Streptomyces sp.* requires Mg^{2+} ion to accelerate its activity. In the experimental studies performed in Chapter 12, the op-

erating conditions of reaction process preceded and 0.02 mol/l Tris-HCl buffer (pH 8.0) containing 0.01 mol/l magnesium sulfate was used as a solvent. Since it is suggested that the use of the buffer containing Mg^{2+} may lead an exchange of Ca^{2+} on Y zeolite with Mg^{2+} to decrease the separability, we analyzed the compositions of fresh Y zeolite and the zeolite employed. Table 13-2 shows the compositions. The Ca^{2+} on fresh Y zeolite is obviously exchanged with Mg^{2+} in the buffer. The exchange of Ca^{2+} with Mg^{2+} is inevitable as far as a solution containing Mg^{2+} is used as a solvent.

The immobilized glucose isomerase used in this study is an immozilized microorganism, that is, *Streptomyces phaeochromogenes* is adsorbed on the quaternary pyridine compound. Therefore, there is a possibility that the properties of immobilized glucose isomerase are different from those of the enzyme purified.

The relationship between the conversion x_G through a reactor in the system proposed and the fructose content in the syrup produced was examined on the assumption that the isomerization is a first-order reversible reaction. Figure 13-5 illustrates the relationship. The figure shows that the fructose content in the syrup is not proportional to the conversion and reaches the top with a certain extent of conversion.

In the following sections we will examine the effects of Mg^{2+} concentration on the kinetic parameters and thermal stability of

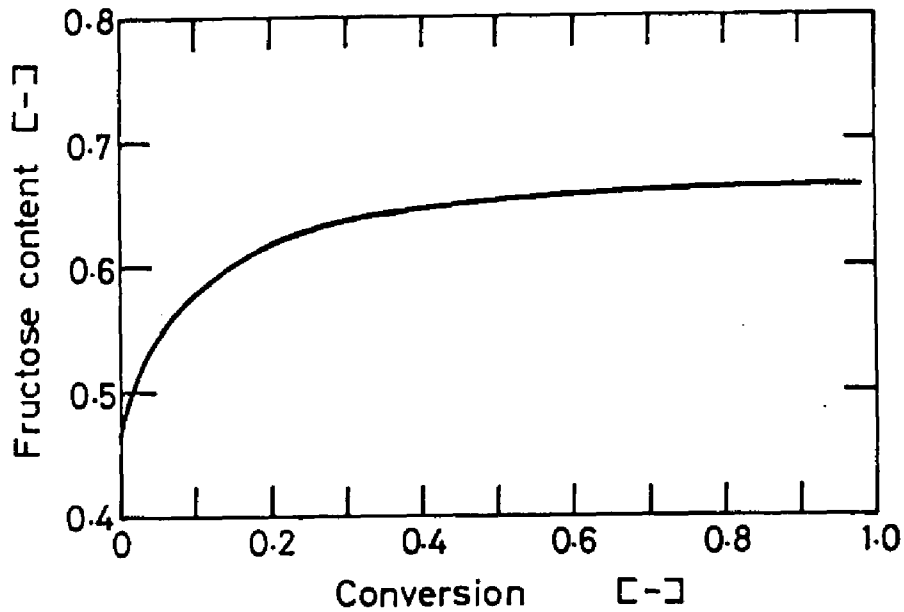

Fig. 13-5. Relationship between the conversion through a reactor in the system proposed and the fructose content in the syrup produced.

the immobilized enzyme.

Another problem is that the system proposed can not produce higher fructose syrup containing more than 70% of fructose. The reason for relatively low fructose content may be ascribed to the fact that the system has no zone to recover glucose remaining in the solution. Then, we have developed a modified system which consists of four zones. The modified system is schematically shown in Fig. 13-2. It will be verified experimentally and theoretically that the system can produce higher fructose syrup containing more than 70% of fructose.

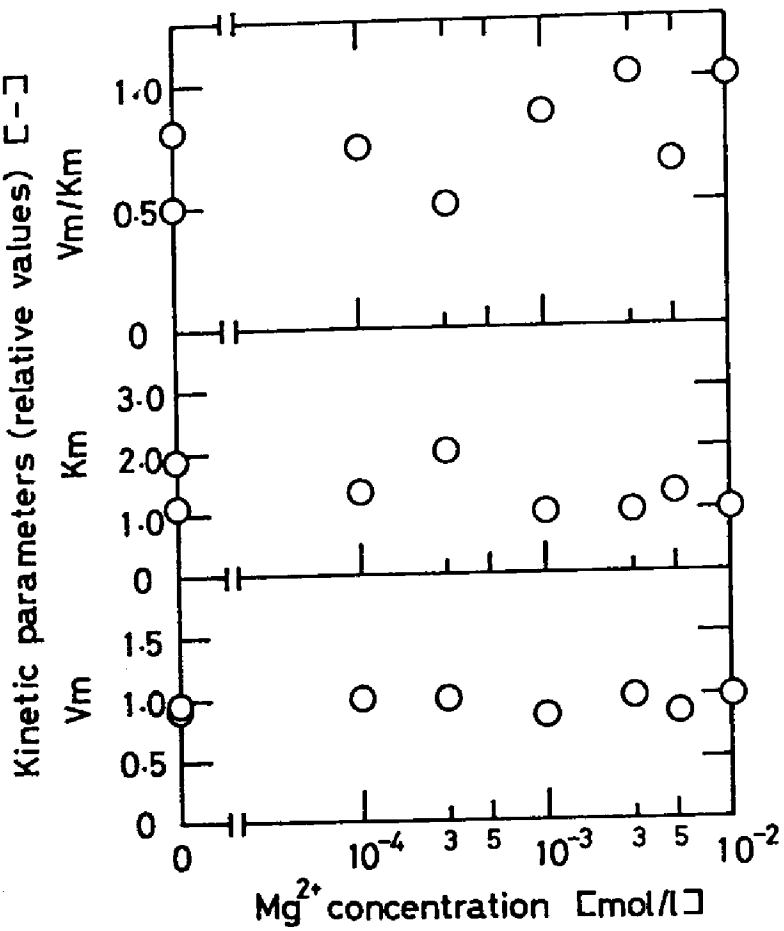

Fig. 13-6. Effect of Mg^{2+} concentration on the kinetic parameters of immobilized glucose isomerase at 50°C. The Km, Vm, and Vm/Km values are normalized by those observed when $C_{Mg}2+ = 0.01$ mol/l.

Effect of Mg^{2+} concentration on kinetic parameters of immobilized glucose isomerase. The kinetic parameters, Km and Vm, of immobilized glucose isomerase were observed in 0.02 mol/l Tris-HCl buffer (pH 8.0) containing various levels of magnesium sulfate. Figure 13-6 shows the plots of Vm, Km, and Vm/Km values against

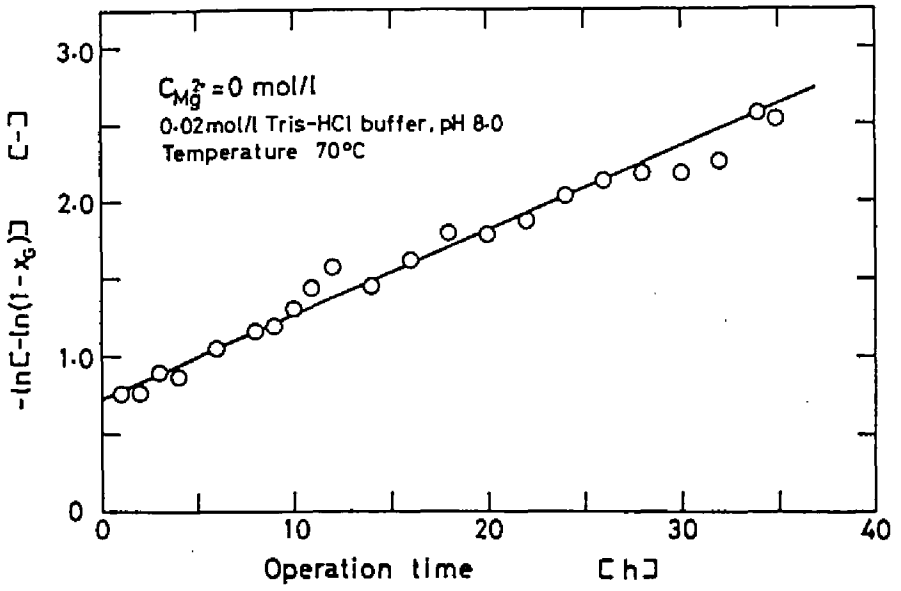

Fig. 13-7. Estimation of the denaturation rate constant k_d of immobilized glucose isomerase. The k_d value was observed at 70°C by using 0.02 mol/l Tris-HCl buffer without magnesium ion.

the concentration of magnesium ion. The vertical coordinates represent Vm, Km, and Vm/Km values normalized by the values observed when $C_{Mg}{}^{2+}$ = 0.01 mol/l. Figure 13-6 indicates that the kinetic parameters of immobilized glucose isomerase scarecely depend on Mg^{2+} concentration. These findings may suggest that *Streptomyces phaeochromogenes* possesses a certain level of Mg^{2+} in the cells. These findings may also suggest that the isomerization by immobilized glucose isomerase can be allowed to proceed by using a solution without magnesium ion.

Effect of Mg^{2+} ion on thermal stability of immobilized glucose

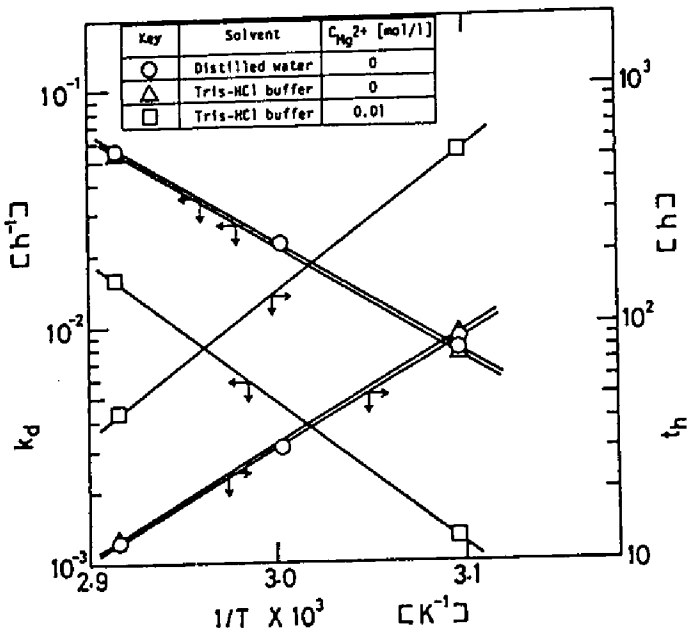

Fig. 13-8. Plots of the denaturation rate constant and the half-life against the reciprocal of absolute temperature. The keys are shown in the figure.

isomerase. The denaturation rate constant k_d of immobilized glucose isomerase was observed in distilled water, 0.02 mol/l Tris-HCl buffer (pH 8.0) without magnesium ion, and the buffer containing 0.01 mol/l magnesium sulfate.

Figure 13-7 shows a plot of $-\ln[-\ln(1 - x_G)]$ against process time. The slope of the plot gives the denaturation rate constant of the immobilized glucose isomerase. Figure 13-8 shows Arrhenius plot of k_d. The half-life t_h values are also plotted in the figure. The thermal stability of the immobilized enzyme obviously depends on Mg^{2+} concentration, while the control of pH value scarcely affects the thermal stability.

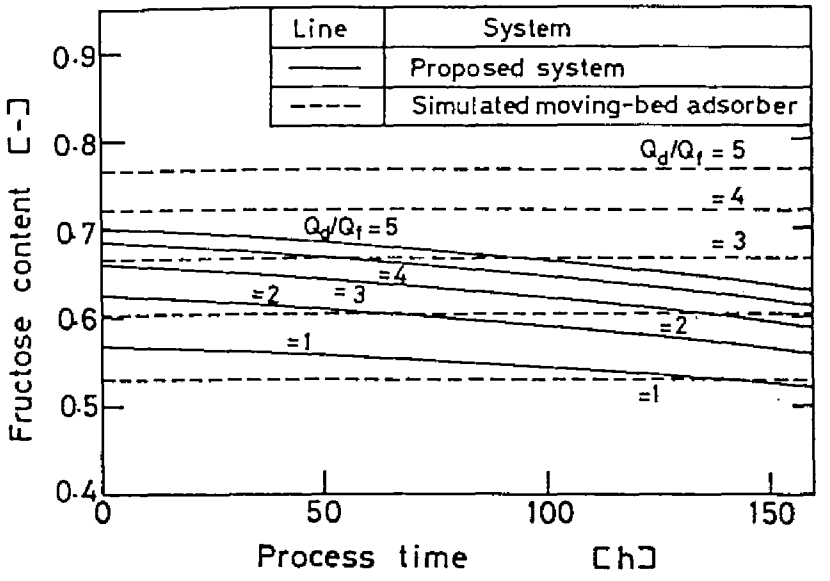

Fig. 13-9. Comparison of performance of the process using the system including adsorption and glucose isomerase reaction with that using the simulated moving-bed adsorber during continuous operation by taking the decay of immobilized glucose isomerase into cosideration. Solid and broken curves correspond with the process using the system and with the process using the simulated moving-bed adsorber, respectively. The curves were calculated for various Q_d/Q_f values under the conditions similar to those in Table 13-1.

The change of fructose content in the syrup produced by the process proposed during continuous operation was calculated by using the k_d value observed when distilled water was used as the solvent. Figure 13-9 illustrates the change of fructose content in various ratios of introduction rate of desorbent to that of feed, Q_d/Q_f, as a parameter. Standard conditions of calculation are similar to those listed in Table 13-1. The fructose content in

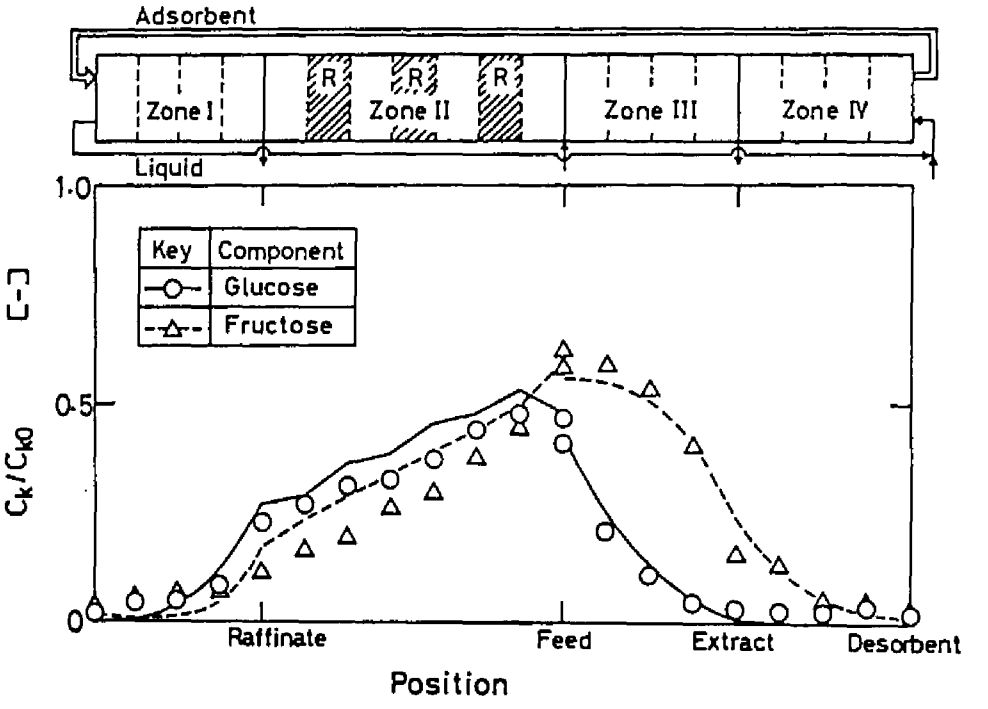

Fig. 13-10. Concentration profiles of glucose and fructose in the modified system including adsorption process and immobilized-glucose isomerase reaction at the steady state. Feed solution was a mixture of glucose and fructose. The concentration of each component was 1.0 mol/l. Distilled water was used as a solvent. Adsorption columns packed with Ca^{2+} ion form of Ion-exchanger S-07 were conveyed in the direction counter to liquid flow at 5 min intervals. The experiment was performed at 50°C.

the syrup produced by the process using the simulated moving-bed adsorber (process (b) in Fig. 13-1) is also shown in Fig. 13-9. The figure shows that the fructose content in the syrup produced by the process proposed decreases gradually with the denaturation of the immobilized enzyme. Therefore, it may depend on the rela-

Table 13-3. Standard Conditions for Comparison of the Modified System with the System using the Simulated Mobing-Bed Adsorber.

Flow rate of feed stream, Q_f	1.0 m^3/h
Glucose concentration in feed, C_{Gf}	1567.5 mol/l
Fructose concentration in feed, C_{Ff}	1282.5 mol/l
Concentration of saccharides in raffinate, $C_{Gr}+C_{Fr}$	2850 mol/l (= 45 wt%)
Concentration of saccharides in extract, $C_{Ge}+C_{Fe}$	4750 mol/l (= 75 wt%)
Construction of each zone	
Simulated moving-bed adsorber:	
Zone I - IV = 2, 3, 4, 3 adsorption columns	
Modified system	
Zone I - IV = 2, 3, 4, 3 adsorption columns	
Number of reactor in zone II = 2 (1.2 mϕ X 0.5 m X 2)	

tion between the evaropartion cost of water and the cost of the immobilized enzyme, whether distilled water can be utilized as a solvent or not.

Separation of glucose and fructose by modified system. To produce experimentally higher fructose syrup with fructose content more than 70%, the glucose/fructose separation was performed using the modified system including adsorption process and immobilized-enzyme reaction. Figure 13-10 illustrates the concentration profiles of glucose and fructose in the system, which were observed after the steady state was established. The fructose content in the extract solution is over 80%. The experimental results indicate that the modified system can produce higher fructose syrup

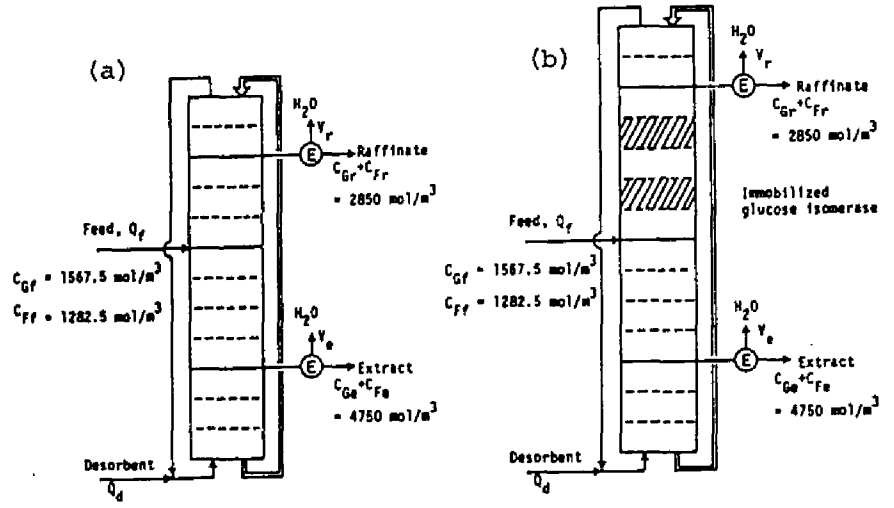

Fig. 13-11. Schematic representation of the processes for separation of glucose and fructose. (a) Process using the simulated moving-bed adsorber. (b) Process using the modified system including adsorption process and immobilized-glucose isomerase reaction.

with higher fructose content more that 70%.

Performance of modified system. Performance of the modified system was compared with that of the simulated moving-bed adsorber. Standard conditions for comparison are listed in Table 13-3. The two systems are schematically illustrated in Fig. 13-11. Figure 13-12 shows the results of comparison. Figure 13-12(a) represents that the fructose content in extract solution of the modified system is over the content in extract solution of the simulated moving-bed adsorber at any Q_d/Q_f value. As shown in Fig. 13-12(b), the modified system can recover more mass than the simulated mov-

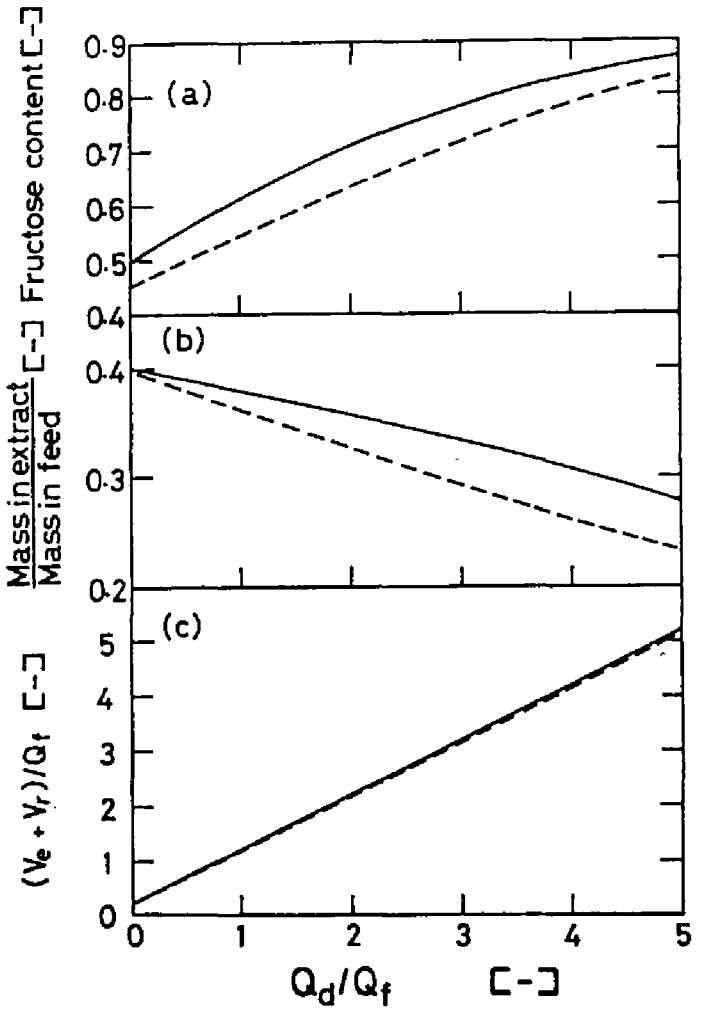

Fig. 13-12. Comparison of performance of the modified system including adsorption process and immobilized-glucose isomerase reaction with that of the simulated moving-bed adsorber. The solid and broken curves denote the modified system and the simulated moving-bed adsorber, respectively. (a) Fructose content in extract solution. (b) Ratio of mass in extract solution to that in feed solution. (c) ratio of amount of water evaporated per unit time to the volumetric flow rate of feed solution. The standard conditions for comparison are shown in Table 13-3.

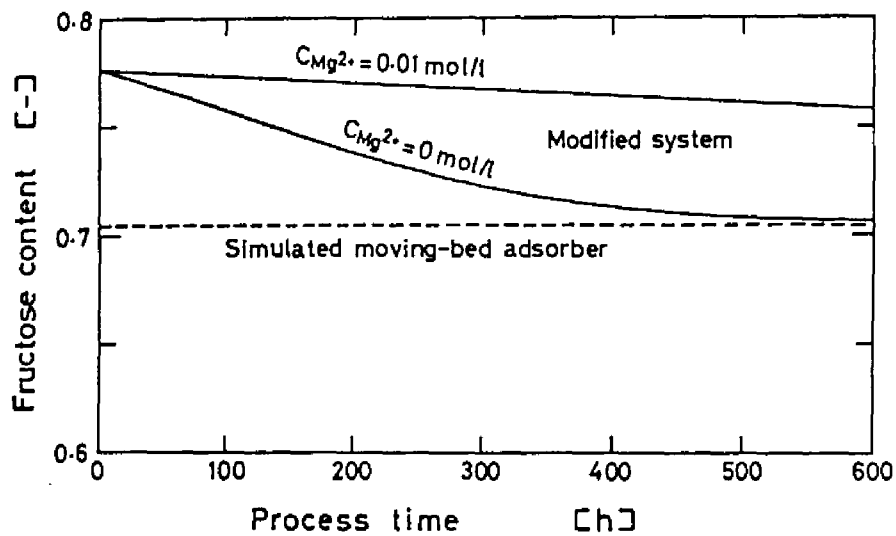

Fig. 13-13. Changes of fructose content in extract solutions emerging from the modified system and the simulated moving-bed adsorber during continuous oparation. The solid and broken curves correspond to the modified system and the simulated moving-bed adsorber, respectively. The solid curves were calculated by taking the denaturation of immobilized glucose isomerase into consideration.

ing-bed adsorber. Figure 13-12(c) shows that the amount of desorbent evaporated is scarcely different between the two systems.

Figure 13-13 shows the theoretical change of fructose content in extract solution during continuous operation. Although the fructose content in the extract solution produced by the modified system decreases gradually, the performance of the system never falls behind that of the simulated moving-bed adsorber even if the glucose isomerase decays.

These observations indicate that the modified system is supe-

rior to the simulated moving-bed adsorber to produce higher fructose with a fructose content more than 70%. The modified system requires a recycle flow of raffinate solution to main reactor and may be relatively complicated in operation. On the other hand, the system proposed originally possesses no recycle flow and the operation of the system may be easy. Therefore, the system proposed originally may be suitable for production of higher fructose syrup containing 50 to 65% fructose.

13. 4. Summary

Performances of three process for production of higher fructose syrup, namely, the chromatographic process, the process using the simulated moving-bed adsorber, and the process using the system including adsorption process and enzyme reaction, were compared each other in terms of the amount of desorbent required. The comparison indicated that the process using the system including adsorption process and enzyme reaction was most efficient of all to produce the syrup with 50 to 65% of fructose content under certain conditions.

The effect of Mg^{2+} concentration on the kinetic parameters and thermal stability of immobilized glucose isomerase was examined. Although Mg^{2+} ion affected the thermal stability, the kinetic parameters scarcely depended on Mg^{2+} concentration. These findings suggest that distilled water can be utilized as a solvent.

A modified system including adsorption process and immobilized enzyme reaction was developed for production of higher fructose syrup with fructose content more than 70%. The syrup with fructose content over 80% was produced experimentally using the modified system.

Nomenclature

C	concentration	[mol/l]
K	equilibrium constant	[-]
Km	Michaelis constant	[mol/l]
k_1	first-order rate constant of forward reaction	[s^{-1}]
k_d	denaturation rate constant	[s^{-1}]
L_R	length of immobilized-enzyme reactor	[cm]
m	distribution coefficient	[-]
Q	volumetric flow rate	[cm^3/s]
r_k	formation rate of component k	[mol/l·s]
T	absolute temperature	[K]
t	time	[s]
t_h	half-life of immobilized enzyme	[s]
Vm	maximum reaction rate	[mol/l·s]
v_R	linear superficial velocity of liquid in immobilized-enzyme reactor	[cm/s]
x_G	conversion	[-]

ε_{bR} void fraction of immobilized-enzyme reactor [-]

Subscripts

d desorbent

e extract

F fructose

f feed

G glucose

p product

r raffinate

0 initial

Literature Cited

1) T. Fujii and B. Okamura, *Kagaku to Kogyo*, 31, 534 (1978).

2) Japanese patent, 45-26048.

3) Japanese patent, 43-16799.

4) E. C. Toren, Jr., *J. Chem. Educ.*, 44, 172 (1967).

5) Y. Takasaki, Y. Kosugi, and A. Kanbayashi, *Agric. Biol. Chem.*, 33, 1527 (1969).

Acknowledgements

This study has been carried out in Laboratory of Manufacturing Technology of Agricultural Products, Department of Food Science and Technology, Faculty of Agriculture and in Laboratory of Chemical Reaction Engineering, Department of Chemical Engineering, Faculty of Engineering, Kyoto University.

The author wishes to express his sincere gratitude to Dr. Tadashi Kamikubo, Professor of Kyoto University, for his kind guidance and encouragement throughout the course of this study and for his critical reading of the manuscript.

The author would like to express his sincere appreciation to Dr. Kenji Hashimoto, Professor of Kyoto University, for his unfailing guidance and encouragement throughout this study.

The author is greatly indebted to Dr. Ryuichi Matsuno, Associate Professor of Kyoto University, for his valuable suggestions and discussions and for his invitation to a field of enzyme engineering.

The author is deeply grateful to Dr. Kazuhiro Nakanishi for his helpful advice and discussion, and to Dr. Kouichi Miura, Associate Professor of Kyoto University, for his encouragement and advice.

The author tenders his gratitude to Toyo Soda Mfg. Co. Ltd., Organo Co. Ltd., and Nagase Sangyo Co. Ltd. for their supply of Y zeolite, Ion-exchangers S-07 and S-22, and immobilized glucose isomerase, respectively.

Acknowledgements are made to Messrs. Jun Inoue, Kiyosato Miyai, Takahiro Ikeda, Hiromitsu Noujima, Hiroki Maruyama, Masaharu Shimono, Shin Tanabe, Yasuo Ueda, Minoru Miyahara, and Michitaka Matsuo, and Miss Yasuko Kawamura for their assistances in the experimental works.

Thanks are due to all the members of Laboratory of Manufacturing Technology of Agricultural Products and Laboratory of Chemical Reaction Engineering for their helpful discussion and supports.

Some parts of this work were supported by a Grant-in-Aid for Scientific Research from the Ministry of Education, Science, and Culture. The author has been supported economically by Sakkokai since 1981.

The author is grateful to his parents, brothers, and sisters for their encouragements and economical supports. He also wants to express his deep appreciation to his darling wife and beloved son, who patiently endured the many weekends and evenings that were devoted to studying and writting and who gave encouragement when it was most need.

List of Publications

1) S. Adachi, K. Nakanishi, R. Matsuno, and T. Kamikubo: Effect of Dextran and Dextran Sulfate on the Glucoamylase-catalyzed Reaction; *Agric. Biol. Chem.*, 41, 1673 (1977).

2) K. Nakanishi, S. Adachi, S. Yamamoto, R. Matsuno, and T. Kamikubo: Diffusion of Saccharides and Amino Acids in Cross-linked Polymer; *Agric. Biol. Chem.*, 41, 2455 (1977).

3) S. Adachi, Y. Kawamura, K. Nakanishi, R. Matsuno, and T. Kamikubo: Kinetics of Glucoamylase Immobilized by Ionic Linkage and Analysis of Its Adsorption and Desorption Processes; *Agric. Biol. Chem.*, 42, 1707 (1978).

4) S. Adachi, K. Hashimoto, R. Matsuno, K. Nakanishi, and T. Kamikubo: Pulse Response in an Immobilized-Enzyme Column: Theoretical Method for Predicting Elution Curves; *Biotechnol. Bioeng.*, 22, 779 (1980).

5) S. Adachi, K. Hashimoto, K. Miyai, H. Kurome, R. Matsuno, and T. Kamikubo: Pulse Response in an Immobilized-Enzyme Column: Elution Profiles in Reversible and Consecutive Reactions; *Biotechnol. Bioeng.*, 23, 1961 (1981).

6) S. Adachi, S. Tanabe, and K. Hashimoto: Determination of pyruvate, L-Lactate, and Glutamic Pyruvic Transaminase by Using an Immobilized-Lactate Dehydrogenase Column; submitted to *Anal. Biochem.*.

7) K. Hashimoto, S. Adachi, H. Noujima, and H. Maruyama: Separa-

tion of Glucose and Fructose by Using a Simulated Moving-Bed Adsorber; submitted to *Biotechnol. Bioeng.*.

8) K. Hashimoto, S. Adachi, H. Noujima, Y. Ueda, M. Shimono, and M. Miyahara: A New Process for Producing Higher Fructose Syrup by Using a System Combined Adsorption Process and Enzyme Reaction; submitted to *Biotechnol. Bioeng.*.